Pulses in singularly perturbed reaction-diffusion systems

PROEFSCHRIFT

Promotiecommissie

Promotor: prof. dr. Arjen Doelman (Universiteit Leiden)

Co-Promotor: dr. Vivi Rottschäfer (Universiteit Leiden)

Overige leden: prof. dr. Tasso Kaper (Boston University, VS)

                 dr. Jens Rademacher (Universität Bremen, Duitsland)

                 prof. dr. Peter Stevenhagen (Universiteit Leiden)

                 em. prof. dr. Ferdinand Verhulst (Universiteit Utrecht)

Cover idea and design Dimitris R. Havlidis

Tjielp tjielp - tjielp tjielp tjielp
tjielp tjielp tjielp - tjielp tjielp
tjielp tjielp tjielp tjielp tjielp tjielp
tjielp tjielp tjielp

Tjielp
etc.

Jan Hanlo, *De Mus*

Table of contents

1

Introduction and Summary

This introduction is written for non-scientists; its aim is to present the subject and research in this thesis in a way which is understandable for a broad audience. If you are a scientist, or even a mathematician, you might find this introduction lacking a certain depth. In that case, I recommend reading the introductory sections of the subsequent chapters – their content is specifically aimed at scientists, mathematicians in particular.

1.1 How should I read this?

There are a couple of reasons why a thesis in mathematics is hard to read for non-mathematicians. First, of course, there are the formulas. A mathematician conveys a large part of his message using symbols, and the connections between them by formulas. If you haven't got that much experience in using symbols and reading formulas, texts which heavily rely on them are notoriously hard, or even impossible, to read.

Having said this, the use of symbols to convey mathematics is not only convenient, but also necessary. It allows the researcher to represent certain ideas (which might be quite abstract) using a few symbols, thereby keeping his or her reasoning accessible and clear to follow – for the fellow mathematician, of course. If you would try to reconvert all the symbols in this thesis into words, the text would very quickly spiral into incomprehensibility: the sentences would span several pages, it would be impossible to structure them in a clear way, giving up any hope for conveying the ideas you want your reader to understand. The conciseness and clarity of symbols, and their use in mathematics, have proved beneficial for many, many centuries. Symbols

and formulas allow you to discover new connections and relations, which opens the door to abstract thinking and deeper understanding of the subject you're considering – and that's not only true for mathematicians, but also for other scientists who use the 'language of mathematics' to summarise their findings.

When you start to work with symbols and formulas, and thereby gain some experience in reading them, you'll notice that these symbols (and the ideas they represent) become more tangible. More and more, you get an idea of what that symbol stands for. You get a feeling of how a symbol behaves, how it reacts to other symbols, what it does. Then, you can start to shove them around, manipulate them, and introduce new symbols because that's the best way to explain what you found – and suddenly, you're doing mathematics.

The second reason why mathematics is hard to read, is the language that is being used. Your goal as a mathematician is to convey objective truths, to tell a coherent and logically sound story. That means the language becomes objective as well: there is no 'I' or 'you' in mathematics, you can hope for a 'we' at best. In a mathematical text, you're taken along a route towards understanding a mathematical topic, guided by the author. Anything which might reek like subjectivity is to be avoided at all costs, is the opinion of many. Mathematical truth does (or should) after all not depend on who's presenting it. Phrasing your sentences in subjective form also makes you more vulnerable to criticism: *you* might say it is so, but that doesn't mean *I* have to believe it.

Although often deemed necessary, this practice doesn't do the readability of the mathematical text any good. As you might have already noticed, I've chosen a different style for this introduction. At a risk of being 'not scientific enough', i.e. not objective enough, I think it is necessary, if you want your ideas to be understood by a wider audience, to present ideas through a text which is accessible to the non-mathematical, non-scientific reader. That is exactly what I try to accomplish with this introduction. Sometimes the nature of the subject I'm describing is such that using an objective style is unavoidable; however, I'll try to refrain from doing so. Once the 'real' content starts in chapter 2, you'll notice a change in style from the somewhat direct, subjective style wielded in this introductory chapter, to the objective and somewhat indirect 'mathematical' style. As argued above, this is a necessary feature of mathematical research texts.

Text isn't everything. As a mathematician, I've noticed that deeper understanding of a phenomenon through symbol manipulation goes hand in hand with the development of a certain mental picture. Since the objects you're working with are often of an abstract nature, this mental picture cannot be more than approximately accurate.

In that respect, I consider myself lucky that I'm an applied mathematician. More often than in other, more pure branches of mathematics, I've got the possibility to accurately visualise the objects I'm analysing. Since the excessive use of symbols holds the danger of obscuring the analysis, the use of pictures can be beneficiary to understanding the topic at hand. One of my goals is therefore to give the reader some idea what the pictures in this thesis mean. If you're browsing through the mathematical chapters, you encounter a figure and think 'Ah! I've seen something like that before, could this be related?', that goal is achieved.

This introduction is structured as follows. Based on the consideration 'if you've got a thesis in your hand, you should at least be able to understand its title', I will first explain some concepts which are central to the research area in which the topic of this thesis falls (section 1.2). Along the way, all the words which make up the title will be introduced. This part is specifically written for non-mathematicians, even for non-scientists. As you can see while skimming through the introduction, there aren't as many formulas as you would expect from a mathematics thesis – especially in comparison with the next chapters, where the 'real' content can be found.

Once I've told enough to explain the title, it's time to dive a little more into the research itself. If you've become interested at that point – and I hope you are –, I'll explain what the research presented in this thesis entails, since that is, purely based on the title, not at all clear. I'll explain in general the research methods and ideas used in this thesis (section 1.3). Also, I'll shed light on some research results, and tell you why they are important and why they are new. Although this part will unavoidably be a little bit more technical, it's still possible to get the message across without going into too much detail. In the end (section 1.4), I'll summarize the content of each chapter, giving you an overview of the content of this thesis.

1.2 Concepts

1.2.1 Patterns

What is a pattern? In the broadest sense, you could characterise a pattern as an 'observable regularity'. In nature, patterns are all over the place. The most obvious ones are stripes or spots on animal skins as found on zebras, leopards, cats, boar piglets; more elaborate spiral patterns occur as fingerprints, sea shells or snail shells. Once you start looking for patterns, 'there's something, then there's nothing, then there's
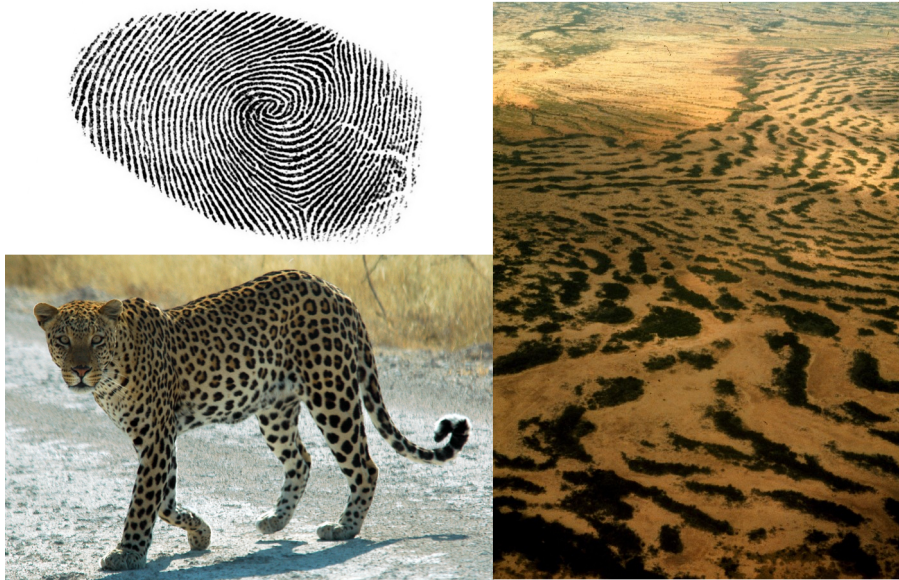
Figure 1.1: Some examples of patterns in nature: a leopard, a finger print, and vegetation patterns at the edge of the desert.

something again, etc.', you'll discover they are all around you. Think of a tree: its branches, twigs on the branches, leaves on those twigs are all roughly equally spaced – even the transport canals visible in the leaves exhibit a tree-like structure. On larger scales, examples of patterns are ubiquitous, even at arid places like the desert: think of wave patterns on sand dunes, or even the more or less equally spaced dunes themselves. At the edge of the desert, you can find vegetation patterns as spots and stripes. Similar spots and stripes can in turn be observed in the sky as cloud patterns.

All these patterns have an element of repetition; they can be characterised by the recurrence of a certain element. Nature is full of repeating processes: the daily cycle of the sun, the tides, the phases of the moon, the changing of the seasons. While you might be tempted to call these phenomena 'patterns' as well (which in a sense, of course, they are), the repetition in these phenomena is temporal rather than spatial. This distinguishes them from the patterns considered above: indeed, what mathematicians call a 'pattern', and we'll stick to that from now on, is a spatial pattern. Of course, this does not mean that (temporal) change will not play a role – far from it. We'll come to speak about 'the dynamics of patterns' later.
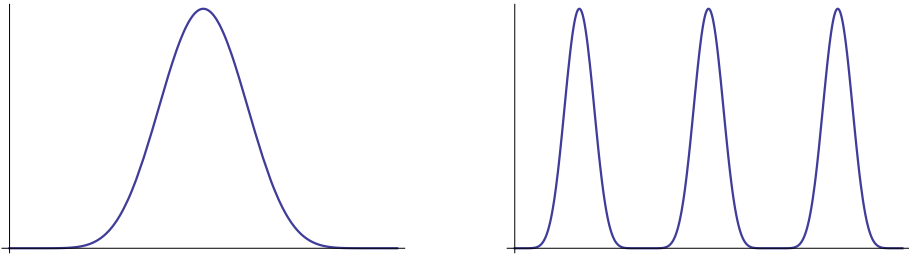
Figure 1.2: An example of a pulse and a pulse pattern.

As mentioned earlier, patterns can be characterised as the recurrence of a certain structural element, be it a spot, a stripe, a twig, a ripple, a leaf, or something else. In this thesis, the object of study is precisely such a structural element, a so-called '***pulse***'. This pulse can be viewed as a building block for more complicated patterns, see Figure 1.2. It is a natural idea to start the analysis of a pattern at its foundation, that is, by analysing its elementary building block. Once you know something (or, hopefully, a lot) about this building block, you can start to answer questions about the pattern as a whole, by looking at the ways this structural element can repeat itself. The latter, though being the obvious next step, is beyond the scope of this thesis.

Natural questions to answer when studying a pattern are: What is the repeating structural element? And how does it repeat? You can use both questions to approach the more encompassing problem of how a certain pattern is formed. The research presented in this thesis therefore falls naturally within the mathematical research area of 'pattern formation' – and in that area, within the analysis of 'localised structures'. The aforementioned pulse is an example of such a localised structure.

Depending on the pattern in question, the structural element, or localised structure, can be of more or less interest. Concerning the fingerprint, the spiral pattern itself is far more important than the narrow skin ridges of which it consists, especially in forensic analysis. In plant growth, on the other hand, the structural elements (leaves, twigs) are much more interesting. A related example is the process of embryonic limb development, which can be studied in the context of pattern formation: here, the localised structures (the arm, the fingers) are the key elements of interest. The process which causes a growing organism to develop its shape, morphogenesis, can therefore be studied in the mathematical context of pattern formation – and this is just one example of its many uses.

1.2.2 Dynamical systems

The mathematical techniques employed in this thesis are rooted in the field of dynamical systems, in particular that of differential equations. Without diving into the mathematics straight away, it is possible to give a flavour of how dynamical systems work, and which ideas can be used in the study of pattern formation.

A dynamical system describes the change of some quantity based on a certain system of rules. You can think of the changing position of the earth as it orbits around the sun, the concentration of chemicals when you put them together and let them react, the mass of a growing bacterial colony. There, rules governing the changes are the laws of gravity, the chemical reactions between the chemicals, and the way in which the bacterias use food and/or oxygen to reproduce. In particular, these rules can be given as a number of evolution equations. Given an initial state (a starting position, an initial concentration), an evolution equation describes how this initial state evolves in time; you might envision it like shown in Figure 1.3. Such an evolution equation is, mathematically speaking, a differential equation. An evolution equation for a quantity ϕ will therefore be an equation for its time derivative $\frac{d}{dt}\phi$, i.e. the change of ϕ in time at a certain moment:

$$\frac{d}{dt}\phi = \text{something (involving } \phi \text{ and/or } t\text{)}.$$

Here, ϕ plays the role of whatever your evolution equation is describing, be it temperature, an animal population, the concentration of a certain chemical, etcetera.
Of course, the 'something' part is where the fun begins. Once you make a choice for the 'something'-terms on the righthand side of the equation, you prescribe a certain behaviour, fixing the evolution of ϕ. Different choices for the righthand side terms will lead to different dynamical behaviour of the quantity ϕ – even small changes can have large consequences, as we will see in section 1.2.4.

Evolution equations are used as a model for phenomena in nature where the time evolution of certain quantities play a role, for instance the growth and decay of populations. Often, it is needed to describe in the model how the quantity in question is spread out – in space, that is. If the evolution of a quantity also depends on the way it is spread out, the space variable x plays an important role in the evolution equation describing such a process. The time evolution of a quantity ϕ will depend on x, and on spatial derivatives like $\frac{d}{dx}\phi$ and $\frac{d^2}{dx^2}\phi$. Therefore, such a model looks like

$$\frac{\partial}{\partial t}\phi = \text{something involving } \phi, \frac{\partial}{\partial x}\phi, \frac{\partial^2}{\partial x^2}\phi, x \text{ and/or } t.$$
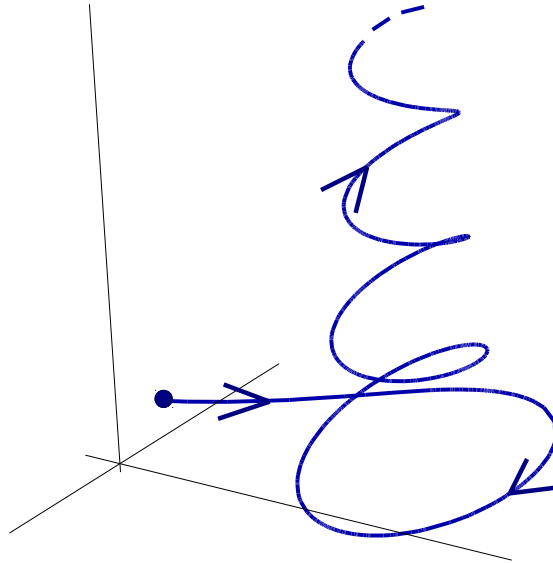
Figure 1.3: A visualisation of a dynamical system: a certain initial state evolves in time.

You may have noticed that the notation of the derivatives has slightly changed: we use '∂' instead of 'd'. This notation is commonly used to emphasise that the quantity ϕ depends on two variables, in this case x and t: in other words, ϕ is a function of both x and t. Also, for simplicity, we stick to just one spatial variable x; for phenomena occurring in more than one dimension, where it is for instance useful to distinguish length, width and height, more spatial variables are needed. However, the approach is often completely analogous to the one-variable case.

An important class of evolution equations where spatial spreading influences the evolution of a quantity is the class of ***reaction-diffusion equations***. These reaction-diffusion equations clearly distinguish the role of the spatial derivatives of ϕ ($\frac{\partial}{\partial x}\phi$, $\frac{\partial^2}{\partial x^2}\phi$, etc.) from other terms. That is, reaction-diffusion equations are structured as

$$\frac{\partial}{\partial t}\phi = \frac{\partial^2}{\partial x^2}\phi + \text{something involving } \phi.$$

This structure can be used to explain where the name 'reaction-diffusion' originates. The term 'diffusion' means the process of spreading in space: think of a drop of milk spreading in a cup of coffee. Another everyday example is heat conduction: if you heat a pan on the stove, the heat spreads to the pan (and, more importantly, the food) due to diffusion. Mathematically, you can model diffusion most straightforwardly by a second order spatial derivative, in this case $\frac{\partial^2}{\partial x^2}\phi$. This term in the reaction-diffusion equation dictates how the quantity ϕ spreads into space as it evolves over time.

The other terms, 'something involving ϕ', are called the reaction terms. The reason for using this terminology is most clear if you consider not one, but two reaction-diffusion equations, i.e. a 'reaction-diffusion system' (or, equivalently, you can consider a quantity ϕ which has two separate components). An example is the Gierer-Meinhardt system [22], describing the evolution of the quantities U and V:

$$\frac{\partial}{\partial t}U \quad = \quad \frac{\partial^2}{\partial x^2}U \quad + \quad V^2 - U$$

$$\frac{\partial}{\partial t}V \quad = \quad \frac{\partial^2}{\partial x^2}V \quad + \quad \frac{V^2}{U} - V$$

You can clearly see that the evolution of U, prescribed by the first equation, is influenced by the value of V through the term V^2. The second equation, describing the evolution of V, has in turn a term $\frac{V^2}{U}$ which depends on U. This mutual influence can be interpreted as a reaction between U and V, which clarifies calling these terms in the evolution equation 'reaction terms'.

Reaction-diffusion equations can therefore be characterised as evolution equations describing the spatial spreading and mutual interaction of certain quantities.

1.2.3   Patterns in reaction-diffusion systems

In phenomena described by reaction-diffusion models, all kinds of patterns frequently occur. This is no coincidence: the appearance of some kind of pattern in a natural phenomenon is often the incentive for researchers to try to model this phenomenon using a reaction-diffusion model. Alan Turing –the very same Alan Turing who's famous for his groundbreaking work in computer science and for deciphering the Enigma code– was the first to postulate that (and explain why) systems of reaction-diffusion equations naturally allow the formation of patterns [50]. Patterns formed in this way are often called Turing patterns.

The most common description of the Turing patterning principle uses a so-called

Figure 1.4: Examples of diffusion: a splash of milk in coffee, a pan on the stove.

activator-inhibitor pair. Given two species (say, chemicals), we call one the 'activator' and the other one the 'inhibitor': the activator makes both species grow, while the inhibitor tries to decrease the growth of both species. This activation/inhibition description can be modelled by the reaction terms of a reaction-diffusion equation. Turing found out that if the inhibitor spreads (diffuses) much easier than the activator, a certain feedback mechanism occurs. Because of this feedback mechanism, the activator and inhibitor are not evenly spread out. Their concentration fluctuates in a very regular way, creating a pattern.

This activator-inhibitor mechanism, modelled by a system of reaction-diffusion equations, is widely believed to be the cause of a broad range of patterns in nature, such as spots and stripes on animal skins, or vegetation patterns at the edge of the desert. In Figure 1.6, you can see some examples of patterns found in a specific reaction-diffusion system (the Gray-Scott model).

What is a pattern? In the context of reaction-diffusion equations, you could say that a pattern has a clear spatial structure, so it depends on the spatial variable x in some specific way. Moreover, as in the many examples of patterns seen in section 1.2.1, you could argue that something like a pattern should not, or not really, change in time. This last condition, although it seems natural, is quite restrictive. There are clear examples of things which you undoubtedly would call a 'pattern', but which do move. Travelling waves (such as water waves or radio waves, or light) are examples of this: they have a periodic (spatial) structure, but move as well. Of course, you could say that when you move along with the wave, it seems to be standing still –and that's exactly how these travelling waves are analysed in general– but that doesn't change the fact that these waves are moving.

Figure 1.5: Alan Turing (1912-1954), pattern formation pioneer.

However, focusing on stationary patterns has some major advantages: since the pattern you're looking for is independent of time, you can imagine that its analysis in the context of reaction-diffusion equations becomes somewhat easier: there is no interplay between space and time, the pattern won't evolve. Also, this can be considered as a starting point for the analysis of patterns which do change in time. You can start to phrase questions like 'If I change some conditions, will the pattern I established start to change? Will it start to move? Will it change its shape?' In section 1.3.3, some of these questions will be addressed.

Summing up, the search for a pattern in a reaction-diffusion model may start with finding a stationary, i.e. time independent solution with a specific spatial structure to the associated system of reaction-diffusion equations. Indeed, that's exactly what part of this thesis is about: to find patterns (in particular, pulses) in reaction-diffusion systems.
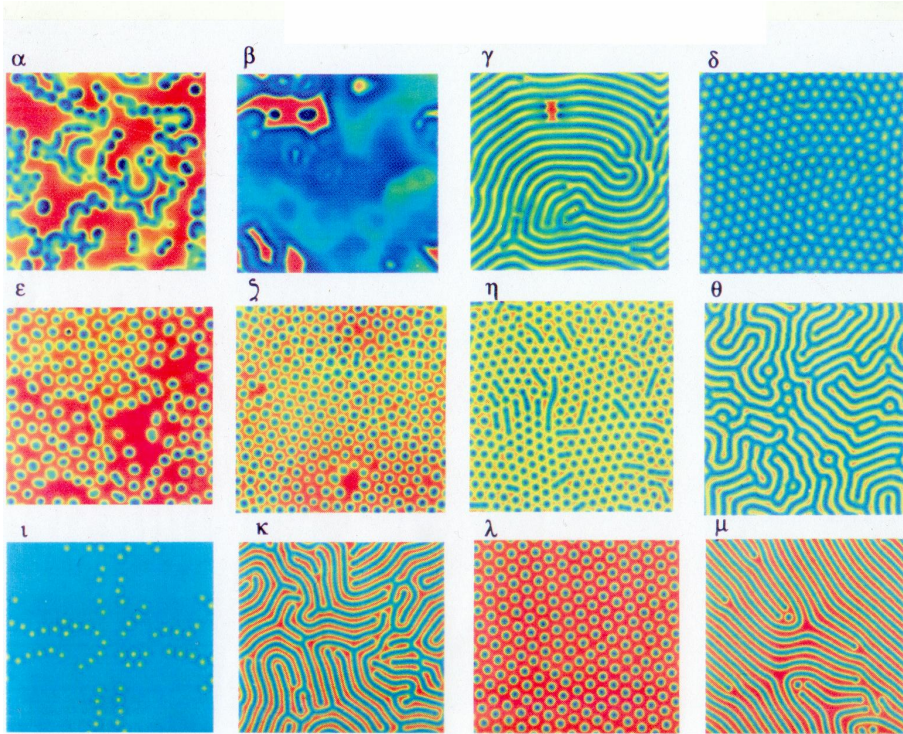
Figure 1.6: Several types of patterns in the Gray Scott model [43].

1.2.4 Perturbations

Let's do a little experiment. We want to study what happens to a ball when we let it drop from a certain height, say 2 metres. We can, for instance, measure how long it takes before the ball hits the ground. You can imagine that, when you perform this experiment multiple times, you won't always get the same answer. This variation in measurements can be caused by a lot of things: maybe you didn't drop the ball each time from exactly the same height, maybe you weren't always on time with your stopwatch. Those things have to do with the fallibility of the experimentalist: of course, the actual phenomenon you're investigating, the falling of a ball, isn't influenced by your incapability of measuring things exactly. Since this is a thought experiment, let's assume you are able to measure the falling time of the ball exactly.

Still, you won't get exactly the same measurement results. Maybe the ball was a little bit blown to the side by the wind, maybe the ground was somewhat uneven, maybe the atmospheric pressure changed a little, as well as the air humidity, changing the air resistance; maybe a dust speck stuck to the ball and changed its total weight, maybe the ball collided mid-air with an unsuspecting little fly, slowing it down. These are things you can't control, but which might influence the measurement results. You could argue that if you do a lot of experiments, under tightly controlled conditions, you can minimise and average out the influence of these disturbances. In the end, to explain the phenomenon of the falling ball (since we know that's just due to gravity), it shouldn't matter who's doing the experiment, or what time of day it is, or whether it's raining or not, or whether I perform the experiment in Oslo or Jakarta – but wait. That last condition actually *does* matter, although a little. We know, since the days of Newton, that the ball falls due to the mutual gravitational attraction between the ball and the Earth. When you start to measure the gravitational acceleration at different places on Earth (for instance, by performing our falling ball experiment), you'll find out that this gravitational acceleration g differs a little bit from place to place. Approximately, $g = 9.8$ m/s^2; in Oslo, we have $g_{\text{Oslo}} = 9.825$ m/s^2, while in Jakarta, we have $g_{\text{Jakarta}} = 9.777$ m/s^2. While the other small influences on the falling ball were random, and didn't have anything to do with the physics underlying the phenomenon of the falling ball, the location on Earth introduces a systematic, though small, change.

When a researcher studies a natural phenomenon, he or she tries to establish which processes or laws are really instrumental to understanding the phenomenon, and which processes are just noise, disturbances. If you would write down a model, i.e. an equation for the falling ball, you wouldn't incorporate the time of day or the color of your eyes, since you know those don't matter. Also, you wouldn't incorporate the wind or the air humidity, since you know those aspects of nature are not underlying the phenomenon of the falling ball. Although they might influence its movement a little, that's not what you want to study in the end. In other words, you want your equations (your model, your physical laws) to be as clean, as simple, as possible. This is one of the reasons why it's hard to write down a good model as a scientist: you need a lot of knowledge and experience to single out the processes that really matter for the phenomenon you're studying.

As for the falling ball, we can write down a formula for its falling time using Newton's second law, incorporating only gravity. If we call the falling time t and the gravitational acceleration g, this gives (for a falling height of 2 metres, and forgetting

about units)

$$t = \frac{2}{\sqrt{g}}$$

Since the value of gravitational acceleration g differs from place to place, the falling time differs from place to place. Of course, if we would just want an approximate result for the falling time, we could always use the approximate value for g – even though it's not exact, the 'real' value of g (and therefore the real value of t) is not far from it. Using the average value $g_{average} = 9.81$ m/s^2, we obtain $t_{average} = 0.64$ s. Now we can compare the actual values of the gravitational constant at Oslo and Jakarta with the average value: $g_{Oslo} = g_{average} + 0.015$ m/s^2 and $g_{Jakarta} = g_{average} - 0.033$ m/s^2. In this way, we can write the gravitational acceleration anywhere on Earth as $g = g_{average} + \varepsilon$, where the value of ε depends on where you are. Also, as we've already seen, ε is quite small compared to $g_{average}$. If we incorporate this in our equation for the falling time, we get

$$t = \frac{2}{\sqrt{g_{average} + \varepsilon}}$$

This formula, giving the falling time of a ball dropped from a height of 2 metres anywhere on Earth, is an example of a model with a ***perturbation***. In this way, you can immediately read off a number of aspects characteristic to the falling ball phenomenon. For instance, if you ignore the small variations in g, setting $\varepsilon = 0$, you can immediately see how to calculate the approximate, average falling time $t_{average}$, namely as

$$t_{average} = \frac{2}{\sqrt{g_{average}}}$$

Moreover, you can see that, as long as the perturbation ε is small, the falling time won't differ very much from the average falling time, see Figure 1.7. This last characteristic, that small changes in the model have small effects on its outcomes, is the defining property of so-called *regular* perturbations.

The opposite is true for ***singular perturbations***, where small perturbations in the model can have large effects on the quantities described by the model. This sounds somewhat counterintuitive, but there are everyday examples where singular perturbations play an important role.

Singular perturbations are almost always associated with sudden changes, or fast transitions. A good example is heat conduction, which we've encountered before in section 1.2.2, where it was intimately connected to the term 'diffusion'.

If you put a pan on the stove, the heat from the stove spreads very quickly through the
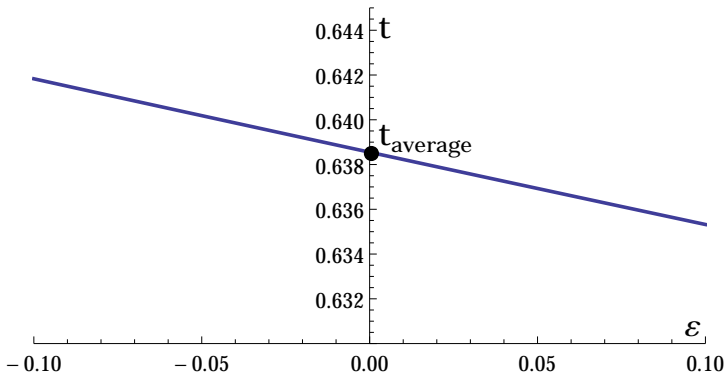
Figure 1.7: The value of the falling time *t* for small perturbations *ε*. As you can see from the axis scaling, the falling time doesn't change that much when *ε* is small.

metal of the pan: this metal conducts heat very well. If the pan would be ceramic, this would be completely different: since ceramic materials are quite good at insulating heat, the pan would heat up very slowly, since the heat from the stove would hardly spread through the ceramic material. The difference between metal and a ceramic material such as porcelain in terms of heat conduction can be seen clearly by comparing Figures 1.8 and 1.9. In the ceramic material, the heated spot in the middle does not spread out like in the metal. Therefore, there is a sharp transition between the heated region and its surroundings: at the edge of the heated region, there is a sudden drop in temperature. That this phenomenon is intimately related to singular perturbations, becomes clear once you consider the model underlying the phenomenon of heat flow through materials.

Heat spreads through materials due to diffusion. Indeed, the spread of heat through a material can be modelled by a very simple evolution equation known as the 'heat equation':

$$\frac{\partial}{\partial t}\phi = \alpha \, \frac{\partial^2}{\partial x^2}\phi$$

where, in this case, ϕ is the temperature at a given place in the material at a certain time. This is a very basic reaction-diffusion equation, or rather just a diffusion equation since there are no reaction terms present (see section 1.2.2). Here, α is called the thermal diffusivity: it is a constant, and its value depends on the material considered. A material which doesn't transfer heat very well has a very small thermal diffusivity. To make a connection with the previous example, let's call this small thermal diffu-
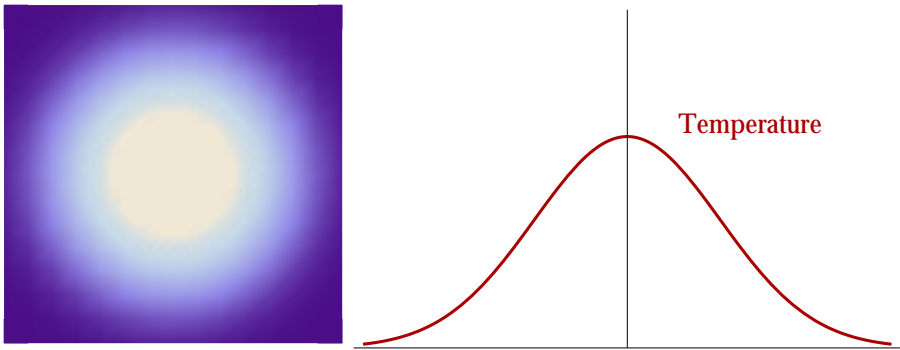
Figure 1.8: A heated spot on a metal pan: you can clearly see that the heat diffuses very well.
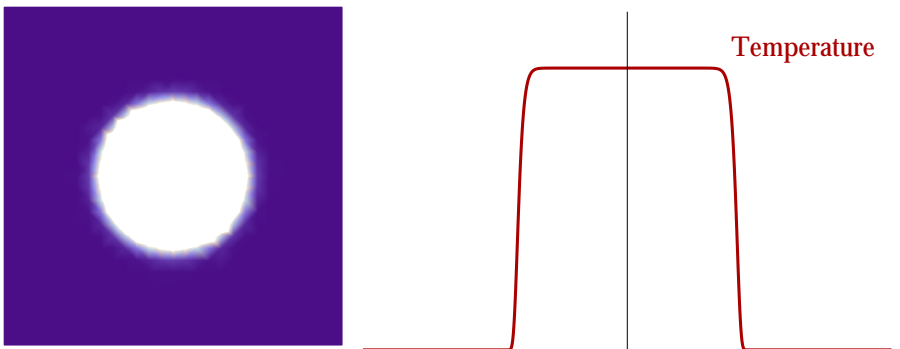
Figure 1.9: A heated spot on a porcelain pan: the heat hardly diffuses, and there is a sharp temperature transition from the heated spot to the outside.

sivity constant 'ε', such that the heat equation for such a highly insulating material becomes

$$\frac{\partial}{\partial t}\phi = \varepsilon\, \frac{\partial^2}{\partial x^2}\phi$$

Like in the falling ball example, you can ask yourself what happens when we neglect the small ε term, i.e. set $\varepsilon = 0$. In this case, something very drastic happens: the heat equation simplifies to

$$\frac{\partial}{\partial t}\phi = 0$$

In other words, the temperature ϕ does not change. This means that the transition

between the heated spot and the surrounding areas really is a sharp transition: the heated spot stays heated, since it's insulated by the surrounding material, and the surrounding material stays cold. Of course, this doesn't give a completely realistic description of the situation: in reality, the heat will slowly spread and the heated spot will cool down slowly. However, this so-called 'singular limit' gives a quite conveni-ent approximation of the real phenomenon, as long as you're willing to overlook the fact that a perfectly insulating material can hardly be expected to exist.

The limit $\varepsilon = 0$ is called 'singular', because it throws away a term in the model which is crucial to the description of the phenomenon, in this case heat diffusion. This tendency of singular limits to dispose of instrumental terms is a recurring theme in the study of singular perturbations, and can often be used to the advantage of the researcher, since it leads to a vast simplification of a possibly complicated model. You can think of it as a trade-off: by setting $\varepsilon = 0$ in a singular limit, it suddenly becomes possible to solve some equations, since the complicated system is severely reduced. On the other hand, you've thrown away quite a lot: it is often unclear how the analysis in the singular limit can tell you something about the case when ε is not equal to zero (but still very small). In the above example of heat diffusion, we already understood the phenomenon which was being modelled by the 'full' heat equation, so we could interpret the singular limit. In other applications, this is often not so easy.

We've seen that, in the case of very slow heat diffusion, there is a sharp transition between the heated spot and the surrounding areas. In reality, this transition is not discrete as in the singular limit, but occurs very fast. To obtain a better understanding of what's happening at the transition, it's a good idea to zoom in on that transition zone. If you do that, you'll see a gradual change from high to low temperature, but now gradual on a very small spatial scale. The best way to describe the temperature distribution in the porcelain pan is as follows:

1. Start far away from the heated spot. There, the temperature is low. If you start to 'walk' towards the heated spot, nothing much happens: the temperature stays the same.

2. Suddenly, there is a huge jump in temperature. You're now at the edge of the heated spot. To obtain a better view of what's happening here, you will have to slow down and zoom in at the transition zone: you'll see that, on this small scale, the temperature steadily rises.

3. After the jump, you're in the heated zone. Again, nothing much happens: the high temperature is everywhere more or less the same.

This phenomenon of scale separation, where the best way to describe a situation is to analyse different parts of it at different scales, occurs naturally when singular perturbations are present. The general approach in such situations is therefore to separate the problem into different scales, analyse each scale separately, and then try to paste these descriptions together to obtain a consistent global picture. This idea of separating scales, analysing reduced problems and trying to combine the results will be explained in more detail in section 1.3.1.

1.2.5 What is this thesis about?

We've come to a point in this introduction where it's possible to understand the title of this thesis: 'Pulses in singularly perturbed reaction-diffusion systems'. This thesis is about the analysis of a certain pattern, namely a single pulse, in the context a certain class of models, namely reaction-diffusion systems. Moreover, these reaction-diffusion systems possess a certain very useful quality: they are singularly perturbed. In section 1.2.1, we've seen what patterns are and how mathematicians think of them; in section 1.2.2, it was explained what we mean by 'reaction-diffusion systems', and in section 1.2.3, it was indicated why patterns can occur in these reaction-diffusion systems, and how they are characterised mathematically. The concept of 'perturbations', and in particular 'singular perturbations', has been introduced in section 1.2.4.

The concepts introduced in the previous sections will be used to clarify the research methods presented in the upcoming sections. I'll give an overview of the methods used in my research, and present the general approach to analysing patterns in reaction-diffusion systems.

1.3 Methods

When you start to analyse pulses (or any pattern, for that matter) in reaction-diffusion systems, you start by asking the question 'Does a pulse exist at all?'. In other words, you start to investigate whether the reaction-diffusion system you're considering admits something like a pulse solution. This is the question of *existence*, which will be addressed in section 1.3.1. If the system doesn't admit a pulse solution, there's not much to investigate. On the other hand, if the system does admit the pulse solution you're looking for, you're not done yet. The next obvious question is (and I'll explain why this question is obvious) 'Is this pulse stable?'. The notion of *stability* has not been introduced, but will be explained in detail in section 1.3.2. The short answer to

the question why stability is important, is that if a pulse exists but is unstable, you often won't observe it in 'real life' applications. Therefore, a priori, the stable pulses are the ones you're looking for.

However, that's not the whole story. Disregarding unstable pulse solutions as wholly uninteresting doesn't do them justice in all cases. There are numerous examples of exciting phenomena which can unfold when you look at an unstable pulse. Therefore, you should ask the question 'If the pulse is unstable, what will happen?'. This will open the gateway to a vast realm of possibilities in the field of pulse *dynamics*, i.e. the motion of a pulse. I'll explain how you could go about analysing one of those many possibilities in section 1.3.3. This is also the subject of the last chapter of this thesis, chapter 4.

In Figure 1.10, you can find an overview of this research approach.
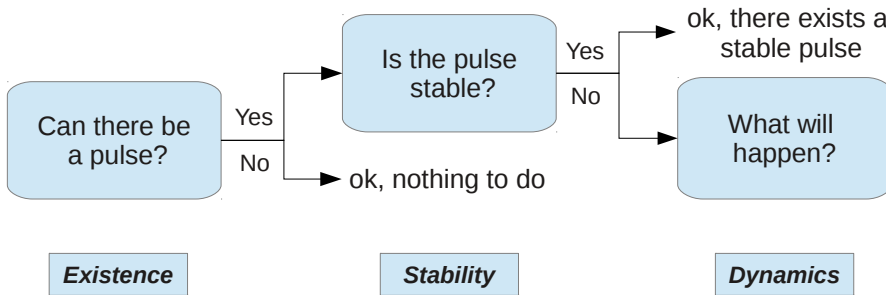
Figure 1.10: General research approach.

Parameters

In most cases, the answer to both the existence and stability question is a lot more subtle than just yes or no. This is the case when the reaction-diffusion system you're looking at depends on *parameters*. Parameters are constants, which in other words don't change in time or in space, which you can therefore choose freely. Parameters often tell you something about the environment in which the phenomenon you're modelling takes place, about the conditions you're dealing with. A good example is the heat equation from section 1.2.4,

$$\frac{\partial}{\partial t}\phi = \alpha \frac{\partial^2}{\partial x^2}\phi$$

The thermal diffusivity constant α, which depends on the material you're looking at, is an example of a parameter. The advantage of using parameters is that you don't have to redo your entire analysis if you decide to switch from analysing one material to analysing another. Since the parameter α is fixed from the model point of view (although its precise value may not be specified), you can do your analysis for all values of α in one go. You'll obtain an answer (for instance, to the question whether a pulse exists) which still depends on α, of course; then, you can see how that answer changes when you pick different values of the parameter α.

In general, a reaction-diffusion system always has some parameters, whose value you can pick at your own leisure, depending on the context you're working in. Therefore, the existence question then is not really *if* but *when* there exists a pulse, or 'For which parameter values does a pulse exist?'. Exactly the same situation occurs for the stability question. Say you've chosen suitable parameter values such that a pulse exists (you can still have a large number of ways to do that), then the question arises *when* your pulse is stable, i.e. for which parameter values. Within the set of parameter values for which your pulse exists, you can make a division between parameter values for which the pulse is stable, and for which it is unstable; see Figure 1.11 for a visualisation.
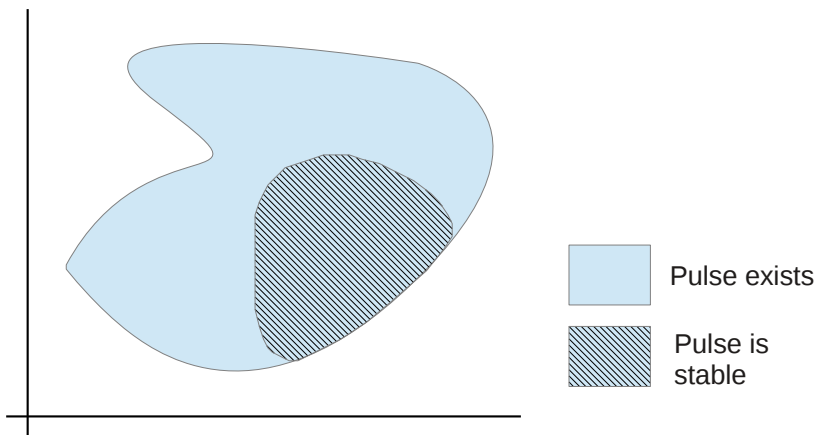
Figure 1.11: The existence and stability regions in parameter space.

The parameter ε

In this thesis, you'll come across a large number of parameters. There's one parameter that is the most important of them all, and that's ε. Everywhere in this thesis, ε is a very small parameter. It acts as a perturbation, just as in section 1.2.4, and is instrumental in obtaining virtually all results in this thesis. Without the help of the small parameter ε, the research presented in this thesis couldn't have been carried out. The reason why ε is so helpful in the analysis of the existence and stability of pulses was already revealed a little bit in the context of singular perturbations. In the following sections, the fact that ε is very small is used extensively.

Of course, how small 'small' actually is, depends on the situation. In the example of the falling ball, the deviation of the gravitational acceleration in Oslo and Jakarta from its global average value was very small – that is, very small when compared to that average value: the deviations were something like ± 0.03 m/s^2, while the global average gravitational acceleration was $g_{\text{average}} = 9.81$ m/s^2.
Since we're dealing in this thesis with quite general reaction-diffusion equations and, more importantly, with parameters whose value is not specified, the question how small ε needs to be to obtain sensible results is a hard one. However, once you've chosen your parameter values, you can often answer this question. Therefore, the most important results in this thesis, which are presented as Theorems, start with the phrase 'Let ε be small enough'.

The general idea is that, when ε is small enough, you can use the information obtained for the case $\varepsilon = 0$ to prove results about the case when ε is not zero, but small. This often works very well because the analysis for case $\varepsilon = 0$ is most of the time much simpler than for nonzero ε. Again, you can prove several results when ε is small enough. Although this can sound restrictive, experience tells us that in practice, these results continue to hold for surprisingly large values of ε.

In the following sections, you'll see how ε is being used to obtain results about the existence, stability and dynamics of pulses in singularly perturbed reaction-diffusion equations.

1.3.1   Existence and construction

As we already noted, the first question you ask yourself when analysing pulse solutions is 'Do these pulses exist at all?'. Questions about existence of certain things are not uncommon in mathematics. However, when you're working in a very abstract context, it's often not possible to go very much beyond that. You might be able to prove that something (in our case, a pulse) has to exist, but where you can find it and

what it looks like is often not known, or even not knowable.

In the case of pulses in reaction-diffusion systems, that's very different. The way the existence of pulses in these models is proved is *constructive*. That means that we start looking for a pulse, and once we find it, we know what it looks like. In other words, we obtain an explicit expression which describes our pulse in an approximate way, and that's often more than you could hope for. If you've got an explicit expression, you can make plots, investigate the specific shape of the pulse and draw several conclusions. That's the clear advantage of a so-called constructive proof of existence. You not only know if (and when) a pulse exists, you have it at your fingertips at the same time.

Pulse shape

What is a pulse? The shortest answer is that it's a function whose graph looks like the one in Figure 1.2. It has a single hump, and gradually decreases to the left and to the right to a constant value, most often to zero. That last property shall be the key to identify pulses. You can see that, if you're far away from the hump, that the graph of the function is very flat and very close to zero. In other words, when you get further and further away from the hump, the function and its slope (its derivative) should get closer and closer to zero.

Let's draw the function in another way. In Figure 1.12, the function is graphed in such a way that you can see its function value and the value of its slope. The horizontal axis gives the function value, the vertical axis the slope of the function. In this picture, you can't really see the spatial variable x anymore. Therefore, at some points, I indicated what the corresponding x-value is.

There are some things to notice in this picture. First, the pulse is now a kind of loop which starts and ends where the axes meet, at the origin. Here, both the function value and the value of the derivative are zero. Also, you can see that the loop doesn't 'really' close: as x becomes larger and larger (or more and more negative), the function value and its derivative come closer and closer to zero, but they never really reach it. However, you can get as close to the origin as you want, by going to large enough values of x. Moreover, you can argue why a pulse should be equivalent to such a loop: when you start far to the left, the function value will increase, so its slope will be positive. As you come close to the top of the hump, the pulse becomes flatter and flatter, until you're at the top, where the derivative is zero. Then you start going down, i.e. the slope is negative, while the function value decreases towards zero. The function becomes increasingly flat, so the derivative, while still negative, also becomes very small.
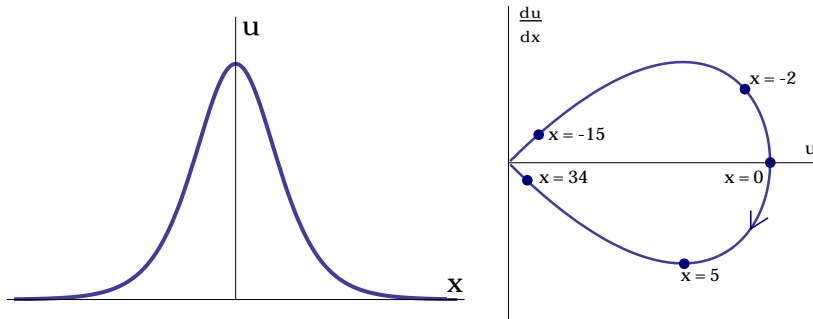
Figure 1.12: An example of a pulse: left, as a function of x; right, as a loop in the phase plane. The pulse height is given by u, its slope by $\frac{\mathrm{d}u}{\mathrm{d}x}$.

A plot such as shown in Figure 1.12 is called a phase plane plot, and is often used to clarify the behaviour of two-dimensional dynamical systems. The loop is an example of a so-called 'orbit' in such a dynamical system. If you pick a point on this loop as an initial value and let the dynamical system run, you'll start to move along this loop, thereby tracing out an orbit. This also holds when you move backwards, then you would trace the loop the other way around. In Figure 1.12, the direction you'll move in if you let x increase, is indicated by an arrow.

Four-dimensional problem

Back to our original problem, the construction of a pulse in a reaction-diffusion system. In this thesis, I look at reaction-diffusion systems which have two components, so which can be written as two reaction-diffusion equations. The components will influence each other through the reaction terms. An example of such a system is the Gierer-Meinhardt model, as mentioned in section 1.2.2. I'll also call these components U and V. Also, I'll introduce a small parameter ε in the evolution equation for V, which will come in handy at a later stage. A general reaction-diffusion system having these properties looks like

$$
\begin{aligned}
\frac{\partial}{\partial t} U &= \frac{\partial^2}{\partial x^2} U + F(U, V) \\
\frac{\partial}{\partial t} V &= \varepsilon^2 \frac{\partial^2}{\partial x^2} V + G(U, V)
\end{aligned}
$$

It doesn't really matter what the reaction terms $F(U, V)$ and $G(U, V)$ are; all that's important, is that they make sure that U influences the evolution of V and V influences

the evolution of U. In other words, these equations are coupled. You cannot solve one without the other, you'll have to analyse them simultaneously.

If we start looking for a pulse in this system, we're looking for a stationary solution of a particular form, i.e. something which does not change in time. That means that our equations simplify somewhat:

$$0 \ = \ \frac{\mathrm{d}^2}{\mathrm{d}x^2}u + F(u, v)$$

$$0 \ = \ \varepsilon^2 \frac{\mathrm{d}^2}{\mathrm{d}x^2}v + G(u, v)$$

You'll notice that I use lower case letters u and v instead of upper case ones: this is to emphasise that we're looking for something which does not depend on time, only on the spatial variable x. In other words, both u and v are functions of just x. For that reason, the notation of the derivative also changed a little: instead of '∂', there's now a 'd'. This indicates that the only variable we're need to worry about is x.

If we want to obtain a pulse solution for this system, we want *both* components u and v to look like Figure 1.2. If we draw them in one picture, this would look like Figure 1.13. Here, the u-component is indicated in blue and the v-component in red. We can try and draw this in terms of the 'loop' picture introduced earlier. However, that's a little problematic: since we've got two components, and for each component we need two axes (one for the component itself, one for its derivative), we'll need $2 \times 2 = 4$ axes in total. That means we'll have to work in a four-dimensional space. Mathematically, that's absolutely no problem: you just start to work with four different components. Visualisation-wise, this introduces large difficulties: how can you picture something in four dimensions? Well, in this case, I don't think you really can. However, I'll try to convey some ideas using three-dimensional plots, which should help you get the complete picture of what's happening.

In any case, we want to do something similar to the phase plane plot as shown in Figure 1.12. Our pulse in both components is now such a loop, but hanging in four-dimensional space instead of lying in the two-dimensional phase plane. Because the equations are still coupled to each other, we cannot analyse the equations for u and v separately: it's no use to draw to separate phase planes (one for u, one for v) and combine the results – at least, that's what you would think! It will turn out that, in our case, it *is* possible to separate the u- and v-components. The reasons why this wholly unexpected possibility arises will become clear in a moment.
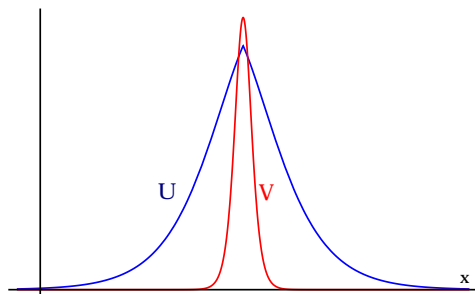
Figure 1.13: A pulse in both the *u*- and the *v*-component.

We're looking for a pulse in two components, *u* and *v*; for both components, it is true that their function values and their slope come close to zero when you're far away from their humps. That means that our loop hanging in four-dimensional space is connected with its tip to the place where all the four axes meet, i.e. where *u*, its derivative, *v* and its derivative are zero. Figure 1.14 gives an idea of what's happening. I omitted the axis for the derivative of *v* – when plotting a four-dimensional picture in three dimensions, you have to make some choices. Remember: we're still not sure if and when such a loop exists, that's exactly what we're trying to find out.

What are the defining characteristics of this loop? It starts at the origin of the axes, makes some excursion through the four-dimensional space, and then returns to the origin. This view is going to help us establishing the existence of such a loop. We're going to adapt a dynamical-systems point of view, and start looking for an orbit which:

a) goes towards the origin as *x* becomes very large, and

b) goes towards the origin as *x* becomes very negative.

We proceed as follows: let's look at *all* the orbits which a) go towards the origin as *x* becomes very large, and bundle them together. This bundle is an example of a manifold. For the purpose of this introduction, you can think of something resembling a sheet of paper. We do the same with all the orbits which b) go towards the origin as *x* become very negative; in this way, we obtain another bundle. Now, because the loop orbit we're looking for goes towards the origin both as *x* becomes very large and as *x* becomes very negative, we see that this orbit must belong to both bundles. If you
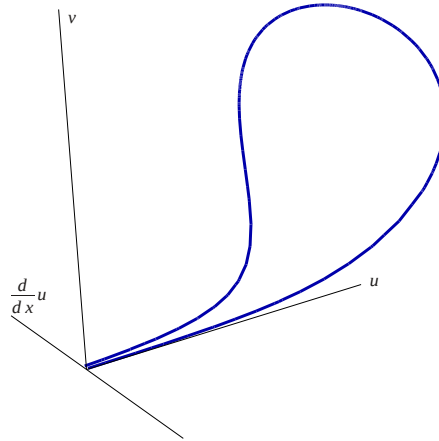
Figure 1.14: An impression of a loop hanging in four-dimensional space. The axis for the derivative of *v* is omitted.

picture these bundles as sheets, that means that such a loop must be in both sheets. This is only possible if these sheets intersect in some way. This situation is depicted in Figure 1.15.

We've now reformulated the question 'Does there exist a pulse solution?' as 'Do these two sheets intersect?'. Indeed, these two questions are equivalent: if there is a pulse, then the two sheets should intersect. Vice versa, if the two sheets intersect, then there must be a pulse. The problem of the existence of the pulse is now phrased in geometric terms. Apart from visualisation purposes, this approach has its advantages in other aspects of the problem. Combined with the fact that our problem is singularly perturbed, this will lead to a complete understanding of the pulse existence problem, and ultimately to its solution.

Scale separation

We now turn to the important property our reaction-diffusion system has: it is singularly perturbed. A small parameter ε can be found in the evolution equation for V:

$$\frac{\partial}{\partial t}V = \varepsilon^2 \frac{\partial^2}{\partial x^2}V + G(U,V)$$

25
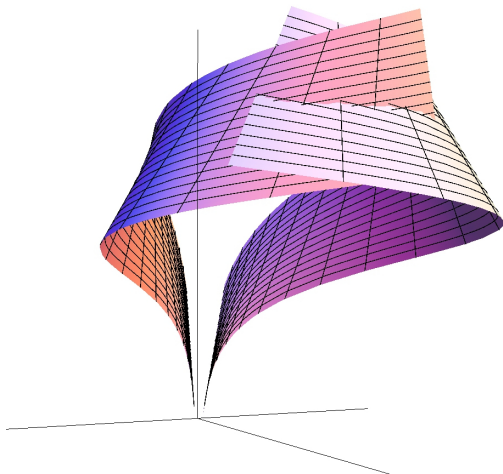
Figure 1.15: Intersecting sheets.

Just as in the example of the heat equation, this means that there will be a steep transition, in this case in the *V*-component. For the pulse we're looking for, this means that the pulse in the *v*-component will become very narrow and very steep, as you can see in Figure 1.16. In other words, the *v*-component of the pulse is practically everywhere just flat, almost equal to zero, except in a very small zone, where it's sharply peaked. That means that, apart from that very thin peak, we can just treat *v* as if it were zero. That means that everywhere except for that very small zone, the *u*-component can be described with

$$0 = \frac{\mathrm{d}^2}{\mathrm{d}x^2}u + F(u, 0)$$

This is much easier than before: the *u*-equation does not depend on *v* anymore, because *v* vanishes almost everywhere. In other words, the system decouples. We can analyse this system using the phase plane, where the horizontal axis gives the value of *u* and the vertical axis gives the value of its derivative $\frac{\mathrm{d}}{\mathrm{d}x}u$. Remember, we want to have a pulse in both components, so in particular in the *u*-component: that means that we're looking for orbits that go towards the origin as *x* becomes very large or very negative. Since *v* is already practically flat and close to zero except for a very small zone, we just need to focus on *u* and find orbits in the phase plane belonging to the
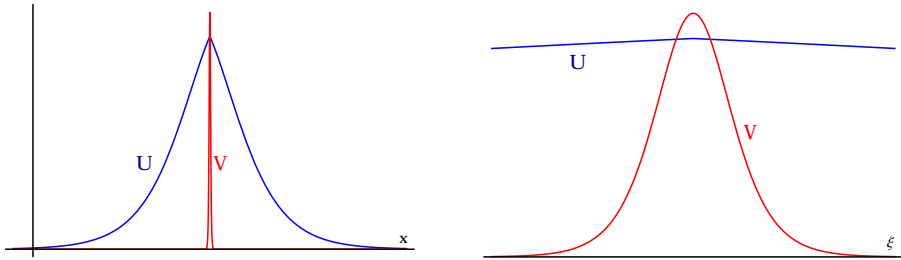
Figure 1.16: The *u*- and *v*-components of the pulse when ε is very small. The pulse in the *v*-component is very narrow and very steep. To the right, a zoom of the left picture near the narrow and steep *v*-pulse. Here, the *u*-component hardly changes at all.
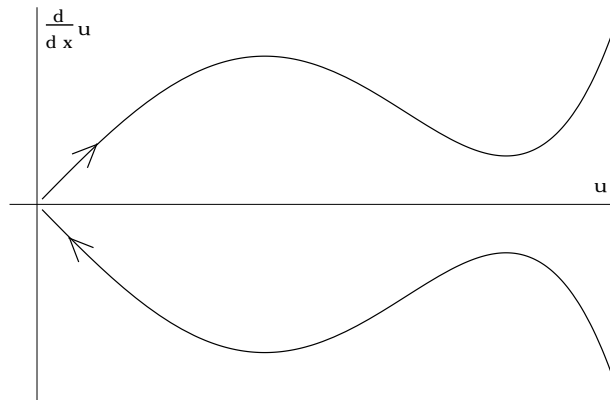
Figure 1.17: A possible phase plane, with orbits going towards and moving away from the origin.

u-equation which go towards the origin in that phase plane. A possible phase plane situation where this happens is sketched in Figure 1.17.

This reduction, where we can treat *v* as if it were zero, holds almost everywhere, except in a very small zone where the narrow *v*-peak is. Just as in the example of the heat equation, we'll try to zoom in on that small zone, to find out what's happening. That means we will try to use a very small spatial scale to rewrite our system. If

we were measuring space in metres, now we're going to millimetre scale, or even smaller. We can do that by rescaling our spatial variable x. We'll use our favourite small parameter ε for this, and introduce the new spatial variable ξ. This new spatial variable is just a rescaling of the old variable x, namely $\varepsilon\xi = x$. If $\varepsilon = 0.001$, this would indeed mean that if x is measured in metres, then ξ would be measured in millimetres.

Using this small scale variable to zoom in to the v-peak, we see that on this small spatial scale, the u-component hardly changes at all, see Figure 1.16. Just as we treated v as if it were zero outside this small zone, we can treat u as if it were constant inside this small zone. Then, the equation for v becomes

$$0 = \frac{\mathrm{d}2}{\mathrm{d}\xi^2}v + G(u = \text{some constant}, v)$$

You'll immediately notice that the small parameter ε is gone, this is incorporated in the fact that we're looking at a small ξ-scale now. Also, the v-equation does not really depend on u anymore – well, of course it still does, but not in a very complicated way, since we decided to treat u as if it were constant on this very small interval. In other words, we can treat the value of u as a *parameter* on this small interval. For whatever constant value of u is appropriate (we'll see how to choose that appropriate value later), we can now perform our phase plane trick on this v-equation. In our small spatial scale ξ, the sharp narrow v-peak looks like a 'regular' pulse, just like the one in Figure 1.2. Therefore, its phase plane, drawn in Figure 1.18, looks very much like that in Figure 1.12.

Geometric theory

It is clear that the small parameter ε has been very instrumental in pulling apart the u-equation and the v-equation, allowing us to analyse them separately. Now the question is: how do we combine these two pictures? How do we use our insight on the reduced system outside the very small area, where only u is interesting, and the other reduced system inside the very small area, where only v is interesting, to build up a complete picture for the complete system?

Here, the previously developed picture of the intersecting sheets returns. Without going into details, it turns out that you can use your knowledge about the reduced systems on the two different spatial scales to describe what these sheets look like. Since the extreme situation, where $\varepsilon = 0$, can be very well understood using both reduced equations (one for u on the 'normal' x-scale, one for v on the small ξ-scale), the sheets are also very well understood in this singular limit. Now it's time to in-
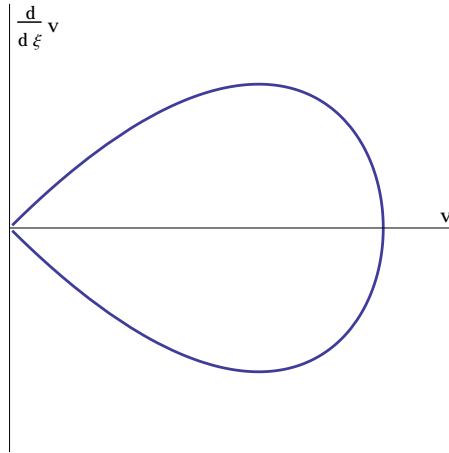
Figure 1.18: The *v*-peak, as depicted in the phase plane.

voke something called 'geometric singular perturbation theory', which was devised by Neil Fenichel in the 1970s [18, 19], to conclude something about the situation where ε is not zero, but very small.

Fenichel tells us that geometric objects like those sheets we introduced, change very little in shape when you go from the situation when $\varepsilon = 0$ to the situation where ε is not zero but small. In other words, when you 'turn on' the small parameter ε, the sheets will be a little bit perturbed, but not much. That means that if the sheets intersected properly (in technical terms: 'transversally') when $\varepsilon = 0$, they still intersect when ε is small but not zero. In other words, you can use the reduced equations for u and v to obtain a picture like Figure 1.15, which still holds when ε is small but not zero. You can imagine why ε must be small: if it becomes too large, the sheets will deform too much and therefore maybe not intersect anymore, see Figure 1.19.

By combining the information from the phase plane of the *u*-equation with information from the phase plane of the *v*-equation, it is possible to determine when the two sheets intersect. Since in the *v*-equation, the value of *u* was treated as a constant and therefore acted as a parameter, this 'intersection criterion' determines which values this *u*-value can take such that the sheets intersect. This determines the height of the tip of the *u*-pulse. Once you've chosen this (almost) constant value of *u*, the phase plane of the *v*-equation (see Figure 1.18) is fixed, and therefore the loop orbit in that phase plane (which represents the *v*-pulse) is also fixed.
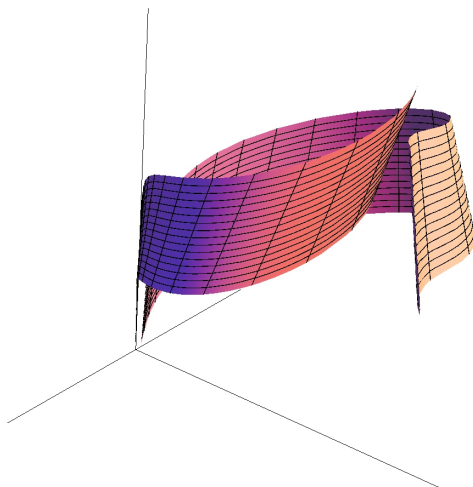
Figure 1.19: Non-intersecting sheets.

This way, a geometric approach can be used to construct a pulse in a singularly perturbed reaction-diffusion system, thereby establishing its existence. Moreover, we know approximately what it looks like: the *u*-pulse looks very much like the orbits in the phase plane for the *u*-equation, Figure 1.17, which go towards the origin as *x* becomes very large or very negative. In turn, the *v*-pulse looks very much like the loop orbit in the phase plane for the *v*-equation, Figure 1.18.

1.3.2 Stability

To introduce the concept of stability, let's return to our example of the falling ball. When you start to think about the experiment in practical terms, you'll find out that there are a large number of unwelcome circumstances which might, and often will influence your measurement of the falling time. Environmental disturbances like wind, changing air humidity and atmospheric pressure, and the occasional intervening fly will certainly influence the path of the ball by nudging it a little bit off course, slowing it down or speeding it up. Even though you can try to eliminate these disturbances by executing your experiment under tightly controlled conditions, you know these conditions will play a role once you start to consider falling balls or falling objects in nature.
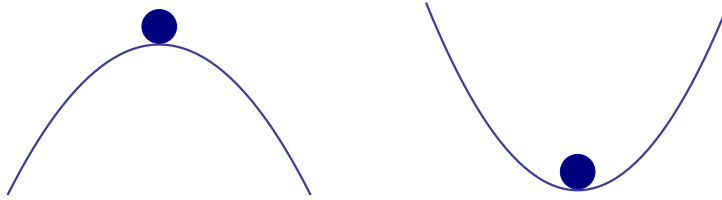
Figure 1.20: Stability visualised.

Evolution equations like reaction-diffusion systems are widely used in natural sciences like biology, chemistry, physics, geology and ecology to model natural phenomena. These models try to capture the 'essence' of the driving forces behind these phenomena, disregarding environmental noise. However, in the real world, such noise will always be present. Therefore, if you're looking for a pattern in your model of which you hope you'll observe that same pattern in nature, it's important to know whether this pattern is robust under such naturally occurring disturbances. If even the smallest nudge will cause the pattern to change into something else, you'll never have the chance to observe that pattern in nature.

The concept of stability is maybe best illustrated by a ball on top of a hill: if you give the ball a small nudge, it will start rolling down the hill. Therefore, the situation where the ball rests on top of the hill is unstable. On the other hand, if your ball lies at the bottom of a pit, giving the ball a small nudge won't change much: the ball will roll around a little bit, and after a while come to rest at the bottom of the pit again. Therefore, the situation where the ball rests at the bottom of a pit is stable. For an illustration, see Figure 1.20.

Both situations describe a certain equilibrium. The equilibrium of the ball on top of the hill is an unstable one, while the equilibrium of the ball at the bottom of the pit is stable. You can determine the stability of these equilibria by considering a situation where the ball has been given a small displacement. If that small displacement starts to grow (in the case of the ball rolling down the hill), the equilibrium is unstable; if the small displacement diminishes and eventually disappears, the equilibrium is stable. When you want to determine the stability of an equilibrium, you therefore always start by considering a situation 'nearby', and see what will happen.

How can we translate this to the stability of patterns, or in particular, the stability of our pulse? How can we take something to be 'nearby' our pulse, and how will we discover what will happen for such a 'nearby' configuration? To give you an idea how to approach this, I'll first have to say something about linearity.
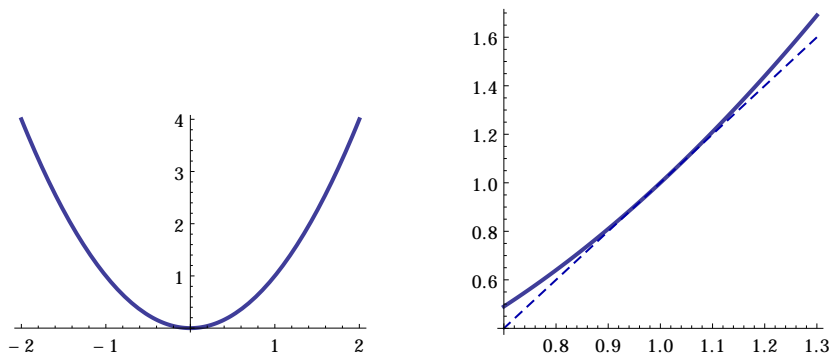
Figure 1.21: The graph of x^2, zoomed in near $x = 1$. As you can see, the dashed tangent line at $x = 1$ approximates the function very well near $x = 1$.

Linearity

Let's consider a simple function, like x^2. As you probably know, the graph of this function is curved; it's a parabola, see Figure 1.21. Suppose you want to know how the function behaves in the neighbourhood of a certain point, say at $x = 1$. If you zoom in at the graph of x^2 around that point, you'll notice that the graph near $x = 1$ looks remarkably like a line, see also Figure 1.21. Of course, the graph still curves a little bit, but you don't notice that when you're zoomed in that much. Therefore, if you stay close enough to $x = 1$, you can approximate the graph of x^2 very well by a line. This line is called the tangent line, and its slope is exactly equal to the slope of the graph of x^2 at $x = 1$. Because you can calculate the slope of a graph of a function by calculating its derivative at that point, you see that taking the derivative of a function has everything to do with obtaining 'local' information of that function, near a certain point. Of course, in our example, the choice of $x = 1$ as a point around which we wanted to obtain local information was completely arbitrary, we could have chosen any other point and taken a close look at the graph around that point. For that matter, we could have chosen a different function to investigate: the principle of obtaining local information by using the derivative stays the same.

How exactly do you use the derivative to obtain local information about a function around a certain point? Let's look at the example again, and let's zoom in again at $x = 1$. The slope of the graph at that point is 2: if you start at $x = 1$ and move a tiny bit to the right, the function value will increase twice that tiny bit, see Figure 1.22. If we call that tiny increment δ, we see that the tangent line around $x = 1$ is given by
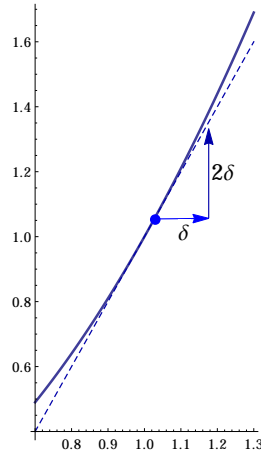
Figure 1.22: The linear approximation of x^2 near $x = 1$.

$1 + 2\delta$. Therefore, if δ is small, the real function value $(1 + \delta)^2$ is approximated very well by the value at the tangent line, $1 + 2\delta$. In other words,

$$(1 + \delta)^2 \approx 1 + 2\delta \text{ if } \delta \text{ is small.}$$

This is called a *linear approximation* of the function x^2 near $x = 1$. You can approximate any function at a certain point in this way, by using the slope of the function at that point. So, in general, if you have a certain function $f(x)$ which you want to approximate at a certain point, say $x = 1$, the linear approximation gives

$$f(1 + \delta) \approx f(1) + \left.\frac{\mathrm{d}f}{\mathrm{d}x}\right|_{x=1} \times \delta$$

where $\left.\frac{\mathrm{d}f}{\mathrm{d}x}\right|_{x=1}$ denotes the derivative of the function f, calculated at the point $x = 1$, i.e. the slope of the graph of the function f at $x = 1$.

Now it's time to make a conceptual jump. Imagine that the point $x = 1$ represents the pulse, and the function $f(x)$ represents the reaction-diffusion system. The idea is to use this principle of linear approximation to find out information about the behaviour of the reaction-diffusion system 'near' our pulse. Of course, it will not be possible to draw this anymore, or to visualise it properly in another way. However, the approach is exactly the same as in the previous example.
We take our pulse, and add a little disturbance to it. Since the pulse is a stationary

solution to the reaction-diffusion system, it will not change in time. However, the pulse with a little added disturbance *will* in general change in time if we look how it evolves according to our reaction-diffusion system. As explained above, we want to know if the little disturbance 'dies out', i.e. diminishes in time, or if it will grow in time. The behaviour of the little disturbance characterises the stability of our pulse. This disturbance has to be rather general, since we don't want the stability of our pulse to depend on the random choice of our disturbance. Maybe if you disturb the pulse a certain way, the disturbance will diminish, while if you disturb the pulse in a slightly different way, that disturbance will grow in time. If your pulse is to be stable, you want *all* disturbances to diminish in time, since in practice, you don't have control over the way your pulse is disturbed. Even if there's just one specific way to nudge the pulse such that that disturbance grows in time, you cannot say that the pulse is stable, so then the pulse is unstable.

Back to the pulse and its disturbance. The pulse is a stationary solution to our reaction-diffusion system, so it has a U-component and a V-component which are both independent of time but still depend on the spatial variable x. Let's call these pulse components $U_{\text{pulse}}(x)$ and $V_{\text{pulse}}(x)$. If we disturb the pulse, we disturb both components, maybe in different ways. Let's call the disturbance in the U-component 'u' and the disturbance in the V-component 'v'. Note that these lower case u and v have nothing to do with the same symbols which were introduced in section 1.3.1, in the context of the existence question. Although it can be a little bit confusing to re-use symbols in this way, it's often more convenient than introducing yet another symbol.

If we want to see whether the disturbances u and v grow or diminish in time under the evolution described by the reaction-diffusion system, we'll have to put them in there and see what happens. In other words, we make the substitution

$$U \to U_{\text{pulse}} + u, \quad V \to V_{\text{pulse}} + v$$

Here, the pair $(U_{\text{pulse}} + u, V_{\text{pulse}} + v)$ plays the role of '$1 + \delta$' in the previous example. By the principle of linear approximation, we can use the 'derivative' of the reaction-diffusion system calculated 'at the pulse $(U_{\text{pulse}}, V_{\text{pulse}})$'. It's too technical to go into details at this point, but the result is that we obtain two linear equations: one for u, one for v. Although they are still intertwined (the equation for u depends on v and vice versa), they are intertwined in a simple, linear way.

For such systems of linear equations, it's possible to isolate the growth rate of u and v. Remember, u and v were still very general disturbances, which are functions of the spatial variable x (since they deform the pulse) and the temporal variable t (since

34

they evolve in time). This growth rate is called λ, and its value determines the fate of the disturbances – both disturbances have the same growth rate, that's one of the advantages of having a set of linear equations. The way the growth rate determines the stability is very straightforward: if λ is negative (or, more specifically, if its real part is negative, but that's not really important here), the disturbances u and v will decay, so then the pulse is stable. If λ is positive, the disturbances will grow, so the pulse is then unstable.

If you introduce this growth rate λ and you start to shove terms around a little bit, you end up with a system of four linear equations, in this case a four-dimensional linear dynamical system. It's rather similar to the way we obtained a four-dimensional dynamical system in section 1.3.1: the four components are given by u, the derivative of u, v, and the derivative of v. That's just like in section 1.3.1: even the symbols are the same, even though they represent something else. Also, this dynamical system is linear, whereas the dynamical system in section 1.3.1 was not linear. Does that make things easier? Yes and no. Although our newly obtained linear dynamical system is linear, it has a peculiarity which makes it in principle hard to analyse: it depends explicitly on x. We can write the system down in a concise way as

$$\frac{\mathrm{d}}{\mathrm{d}x}\phi = A(x; \lambda)\,\phi$$

where we put all four components u, $\frac{\mathrm{d}}{\mathrm{d}x}u$, v and $\frac{\mathrm{d}}{\mathrm{d}x}v$ into one four-component vector ϕ. As you can clearly see, this is an example of a dynamical system, only in terms of x instead of t (see section 1.2.2). From a mathematicians' point of view, this makes absolutely no difference: it's just a symbol. This is an example of a situation where it's useful to 'forget' for a moment what x stands for, allowing you to recognise the system of equations for u, v and their derivatives as a dynamical system. This allows you to use techniques from the field of dynamical systems in a situation where you initially wouldn't have thought they could come in handy. The symbolic language of mathematics shows an unforeseen connection between this analysis of small disturbances and dynamical systems.

I mentioned that this dynamical system we've cooked up is hard to analyse since the system depends on x – in particular, the matrix $A(x; \lambda)$ (since that's what it is, a matrix) depends on x. Don't worry about matrices and vectors: the important thing is that this dynamical system looks different for different values of x. Why is this a problem? Well, remember that the variable x has taken over the role of 'time' in this dynamical system. A dynamical system which depends actively on time is constantly changing the evolution rules as you let an initial state evolve in time. It's like rolling

a ball over a table top, while constantly wiggling and moving the table itself. You can imagine that the path of the ball becomes very erratic, and will be highly influenced by the movements of the table.

Luckily, in our case, we have some knowledge of how A depends on x, in other words, we know something about the 'movements of the table'. The reason A depends on x is that we consider small disturbances u and v of our pulse solution, i.e. we've started to look 'nearby' our pulse. Therefore, we had to calculate the 'derivative' of the reaction-diffusion system 'at the pulse'. Regardless of its exact meaning, this 'derivative' of the reaction-diffusion system evaluated 'at the pulse' is exactly what defines A. Therefore, the spatial dependence of A is very closely related to the spatial structure of the pulse.

Remember, our pulse solution looks like the one in Figure 1.16. It has three important features:

a) The V-component of the pulse is very sharp and very narrow: except for a very small region in the middle, the V-component is practically flat and almost zero.

b) The U-component of the pulse is, except for the very small region in the middle, not really influenced by the V-component, since the V-component vanishes almost everywhere.

c) Both components decrease and become very flat and almost zero as you move further and further away from the pulse peak, i.e. if x becomes very large or very negative.

This spatial structure of the pulse has a direct influence on the way A depends on x. In the small central region, it is predominantly determined by the V-component of the pulse, whereas outside that region, the U-component of the pulse takes its role in determining the spatial dependence of A. Since both components become flat and almost zero when you are far away from the pulse peak, A loses its x-dependence and becomes very simple in that far-away limit. In Figure 1.23, the x-dependence of A is visualised based on the spatial structure of the pulse.

With all this talk about the dynamical system and A, it seems that we've drifted away from our original goal, which was to determine the growth rate λ of our disturbances u and v. How do we combine these two things?

First, it's good to notice that our dynamical system is an equation for u and v, and the dynamical system uses the variable x. Therefore, the dynamical system determines the spatial dependence of u and v, in other words, the way they deform the pulse. So,
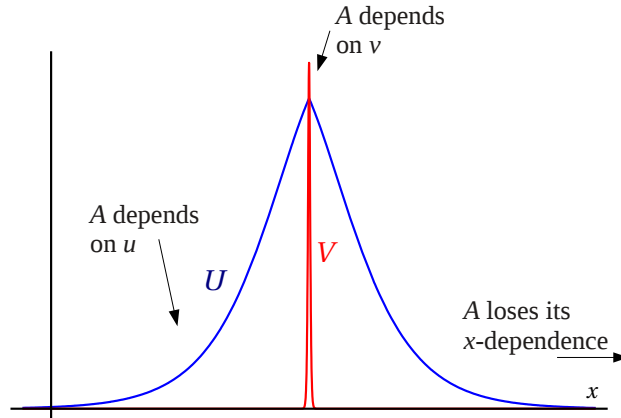
Figure 1.23: The *x*-dependence of *A*, based on the spatial structure of the pulse.

we're looking for small disturbances *u* and *v* which are at the same time solutions to the dynamical system $\frac{\mathrm{d}}{\mathrm{d}x}\phi = A(x; \lambda)\phi$. Are all possible solutions of this dynamical systems then disturbances? Certainly not. The reason for this is that disturbances are, by nature, small – that means, they are small *everywhere*, for all values of *x*. However, not every solution of the dynamical system stays small for all *x*. It's even worse: in general, a solution to such a dynamical system is 'unbounded'. That means that such a solution will increase as *x* increases, and it can become as large as you want if you go to higher and higher values of *x*. Analogously, things can go wrong at the other side: a solution can become as large as you want if you go to more and more negative values of *x*. A good example is the function x^2, see Figure 1.21: although it's fairly small near $x = 0$, it increases as *x* becomes larger or more negative, and this never stops. You can obtain arbitrarily high values if you just go far away enough from $x = 0$. Therefore, x^2 is unbounded, and that's the reason that it is not admissible as a small disturbance.

You can wonder if it's even possible at all to find bounded solutions for the dynamical systems, which are then admissible as small disturbances. The answer is yes, well, sometimes: it depends on $A(x; \lambda)$. Now we remember that *A* also depends on the growth parameter λ. Here, λ plays the role of a parameter: for different values of λ, the matrix $A(x; \lambda)$ will be different, and therefore the associated dynamical system will be different, and the possible solutions to that dynamical system will be different for different values of λ. You can imagine that for some values of λ, the dy-

namical system doesn't have any bounded solutions, while for other values of λ there are bounded solutions possible. Finding bounded solutions, and therefore obtaining admissible disturbances, is now a question of choosing the right values of λ.

Those 'right' values of λ are called 'eigenvalues', and since they were originally introduced as growth rates, they determine the stability of the pulse. The strategy to determine the stability of the pulse is therefore as follows: first, we determine for which values of λ the associated dynamical system admits bounded solutions. Then, we take a look at those eigenvalues: if all of them are negative, then the pulse must be stable. This is because every admissible disturbance is, since it is a solution to the dynamical system, associated to some eigenvalue. This eigenvalue is the growth rate of that disturbance. If you know all eigenvalues, you know the growth rates of all admissible disturbances. If all disturbances have a negative growth rate, then they will all diminish, and therefore the pulse is stable. However, if there is just one positive eigenvalue, the disturbance (or disturbances) associated to that eigenvalue will grow. Therefore, not every disturbance will diminish in time, and therefore the pulse is unstable.

In general, it's very hard to obtain such eigenvalues, let alone obtain them all. If we want to know whether a pulse is stable, we need to know all eigenvalues: we want to make sure that each and every one of them is negative, or else the pulse is not stable. On the other hand, once we found just one positive eigenvalue, we can immediately conclude that the pulse is unstable. Therefore, it's often much easier to prove statements like 'Under these and these circumstances, the pulse is unstable' than statements like 'Under these and these circumstances, the pulse is stable'. In chapters 2 and 3, you will therefore find more instability results than stability results. However, in some cases, it is possible to prove stability, especially in chapter 2 (section 2.4.2).

Our knowledge of the x-dependence of A can help us to obtain these eigenvalues. What's really helpful, is that we know that A becomes very simple in the far-away limit, if we take x to be very large or very negative. From this very simple 'limit'-version of A, which doesn't depend on x anymore, we can infer some properties of the solutions of the entire dynamical system. Since A becomes very simple as x becomes very large (or very negative), we know that the solutions of the dynamical systems should behave accordingly. From this 'limit'-version of A, there are just two possibilities: a solution either grows in an unbounded way as x becomes larger and larger, or it decays to zero as x becomes larger and larger. Therefore, we reason as follows. Whatever a solution to the dynamical system looks like 'in the middle', where A depends on some complicated way on x, if we want that solution to be bounded, i.e. to
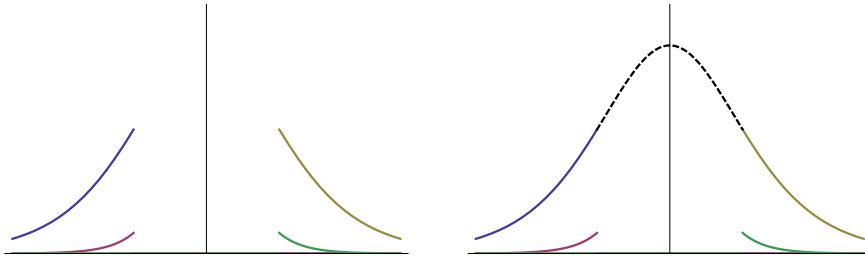
Figure 1.24: Matching solutions which decay to the left and to the right.

be an admissible disturbance, it has to decay to zero as x becomes very large or very negative. Because an admissible disturbance, i.e. a bounded solution has to decay to zero both as x becomes very large and as x becomes very negative, we try something similar as in section 1.3.1, where we tried to construct a pulse: we approach it from both sides. That is, we take a solution which decays as x becomes very negative (which behaves nicely at 'the left'); we take a solution which decays as x becomes very large (which behaves nicely at 'the right'), and we try to let them match. In Figure 1.24, this idea is illustrated.

In section 1.3.1, we tried to let two sheets intersect, see Figure 1.15. This 'intersection criterion' could be calculated, and it gave the value which the 'constant' component u should have in the very small zone where the sharp v-spike was. In other words, it gave the value of that parameter, such that the sheets would intersect. While matching these decaying solutions from both sides, something equivalent is going on. When trying to tune the value of λ such that these solutions can indeed be matched, you obtain a 'matching criterion', which gives you the 'right' values of λ, in other words, the eigenvalues. This 'matching criterion' can be reformulated in terms of a function, which is called the Evans function. This Evans function is particularly useful since the values for which the Evans function is zero are precisely the eigenvalues you're looking for. In short: if you know the Evans function, you know the eigenvalues, and therefore you know whether the pulse is stable or not. It turns out that the scale separation which is present in our pulse, and which had a direct influence on the x-dependence of A (see Figure 1.23), can be used to separate the equations for the disturbance u and the disturbance v, just as in the existence section 1.3.1. Analysing those equations separately, it is possible to obtain the Evans function explicitly in the end. It's too much to go into details, but the similarities between the approach of the existence problem and the stability problem are striking. In the

end, the process of 'matching' solutions to obtain admissible disturbances is just the problem of letting two sheets of properly chosen solutions intersect. Behind it all, there's the singularly perturbed nature of the reaction-diffusion system which causes the scale separation, which in turn allows us break up the large problem into smaller sub-problems. Then, you analyse these sub-problems separately and combine the results of these analyses at the end. Without the singular perturbation, none of this would be possible.

1.3.3 Dynamics

In the previous section, I've explained how you can analyse the stability of the pulse whose existence was established in section 1.3.1. It was already mentioned in section 1.3 that reaction-diffusion systems often depend on a number of parameters, which you can choose freely. Depending on the value of these parameters, a pulse might exist, and if it exists, it can be stable; see Figure 1.11. The 'existence zone' in parameter space can be found by the methods explained in section 1.3.1; the 'stability zone' inside the existence zone can be found by the methods explained in section 1.3.2.
In this section, I'll elaborate some more on the fate of the pulse when it is disturbed. If the pulse is stable, it's easy to see what will happen: the disturbance will fade away, and the pulse will stay where it is, in its original shape. However, if the pulse is unstable, it's not clear at all what will happen. Yes, the disturbance will grow, but how does that affect the pulse? Will the pulse grow as well? Will it deform? Will it start to move? In general, these questions are very hard to answer.

The easiest way to get an idea about what's going to happen with an unstable pulse is to do numerical simulations. You put your reaction-diffusion system in encoded form in a simulation program, you prescribe your pulse, disturb it a little, push the button, and see what happens. Since the computer does all the work, this seems like a very good approach – although the actual setup of such a simulation can be a lot harder than you might imagine. However, this approach has its limitations. You have to choose a value for each of your parameters, including ε; since the computer calculates things step by step, you have to tell the computer to take very small time steps – but not too small, otherwise the simulation takes too much time. Also, you have to divide the space into small parts, because the computer can only handle numbers, and not smooth things like functions. In the case of our pulse, where the V-component is very narrow and very sharp, you'll have to divide the space in that region into a large number of very, very small segments.
All these things introduce a certain aspect of trial and error. You have to make sure

that ε is 'small enough', whatever that may mean, and you will have to be lucky in picking the values of your parameters such that something interesting happens. If you've got a lot of parameters, this becomes increasingly difficult. Moreover, if something exciting happens, you often don't really know *why* this happens. There-fore, numerical simulations can act as a guide to interesting phenomena, but the real insight often has to come from 'proper' mathematical analysis.

There are situations where you can analytically investigate the fate of an unstable pulse. This is when a pulse *becomes* unstable: by that, I mean the following. Sup-pose you know that for a certain parameter choice, your pulse is stable, i.e. you're in the 'stable region' in parameter space, see Figure 1.11. Then, you start to change the value of one of the parameters, and see what will happen to the growth rates, the eigenvalues. At some point, one of your eigenvalues (which were all negative) will become positive. In other words, you'll cross the boundary of the 'stable region' in Figure 1.11. At the boundary of that region, where the pulse becomes unstable, it's possible to see what's happening in more detail, i.e. to analyse *how* the pulse becomes unstable.
Such a crossing of the boundary of a region in parameter space is an example of a 'bifurcation'. A 'bifurcation' is a rather general term to describe a situation where something genuinely changes. That's what happening at the boundary of the stable region: within that region, you can change your parameters around a little, but that doesn't have large effects: the pulse will change its shape a little, but it will still be stable. However, if you cross the stability boundary, this really makes a difference. If you pick two parameter values which are very close together but on opposite sides of the stability boundary, the two associated pulses will look very much alike; however, one pulse will be stable, while the other pulse is unstable. Something similar happens when you cross the boundary of the existence region: suddenly, the pulse that you had can no longer exist.

Our pulse can become unstable in a number of ways. For each way of becoming unstable, there is an associated bifurcation, where a parameter crosses the boundary of the stability region. It really depends where you cross the boundary: if you're unlucky, you'll be not only out of the stability region, but immediately out of the ex-istence region as well – see Figure 1.11. Other parts of the stability boundary are a lot less dangerous. For our kind of pulses, it turns out that there is a certain general way in which such a pulse loses its stability, and that's through a so-called oscillatory instability. It's not to say that this will *always* happen when you start playing with parameters and push the pulse out of the stability region, but it will happen most of
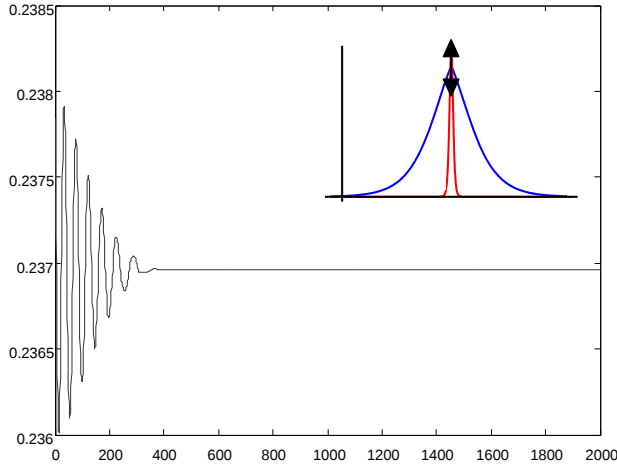
Figure 1.25: The movement of the tip of the pulse just before a Hopf bifurcation.

the time. It's even stronger: you'll have to choose your parameters very carefully to avoid this oscillatory instability while pushing the pulse out of the stability region.
This oscillatory instability bifurcation is also called a Hopf bifurcation, and it manifests itself as follows. If you've got a stable pulse and you're near the boundary of the stable region, and you give your pulse a little nudge, then it will start to oscillate, i.e. to wobble up and down. This oscillation will die out after some time, because the pulse is stable. In Figure 1.25, you can see the results of a numerical simulation of such a pulse near the stability boundary, i.e. near a Hopf bifurcation. Once you change your parameters such that you cross the stability boundary and then give your pulse again a little nudge, you'll see that the pulse will start oscillating again. Only now, because the pulse is unstable, the amplitude of the oscillation will grow, and the pulse will go up and down in an increasing way. This oscillation can become so wild that the pulse can slap itself flat, and disappear. This is indeed what you observe in simulations, see Figure 1.26.

However, when playing around with parameter values and simulating the resulting pulse, you will stumble upon something quite exciting. In Figure 1.27, you can see the result of such a simulation. What you see is a pulse which is disturbed and starts to oscillate. The amplitude of the oscillation starts to grow – nothing new so far, it means that we're outside the stability region. But then, after a while, you ob-
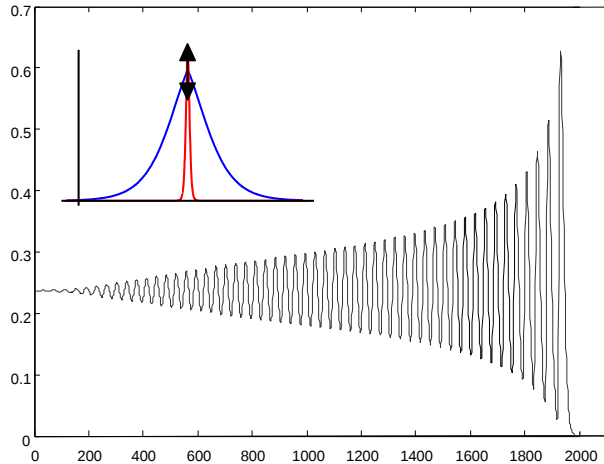
Figure 1.26: The movement of the tip of the pulse just after a Hopf bifurcation.

serve that the amplitude of the oscillating pulse stabilises, and that you're looking at a steadily oscillating, or 'breathing' pulse. This is quite something: we've discovered a pulse which moves up and down in time, a first step beyond the realm of stationary patterns. Moreover, the pulse seems to stay where it is: it wants to move up and down, but it apparently doesn't want to move to the side.

Those observations are a reason for further analysis, and a few questions arise: 'How can we go beyond the Hopf instability bifurcation and find a breathing pulse?' 'Can we predict when we will see a breathing pulse, and when we will just see an increasingly wild oscillation?'

These questions were the driving force behind the last, fourth chapter of this thesis. This chapter is also rather technical; however, it certainly is possible to give you an idea about the approach you can take to answer these questions.

In order to do that, we'll revisit the example concerning the linear approximation, section 1.3.2. There, I argued that when you zoomed in on the graph of a function, you could approximate that graph very well by its tangent line. That was called a linear approximation, see Figure 1.22. If you zoom out a little, you'll see that this linear approximation starts to differ from the 'real' graph of the function. Therefore, if you want to approximate this graph a little better, you will have to go beyond this linear approximation. This means you'll have to make a quadratic approximation.
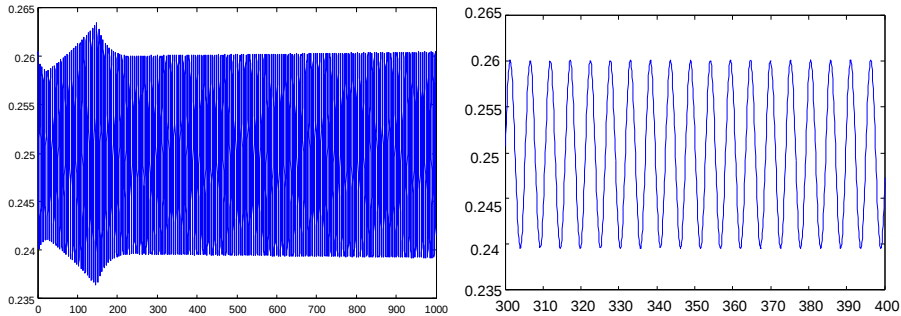
Figure 1.27: A breathing pulse. After a period of initial amplitude growth, the oscillation of the tip of the pulse settles down to a steady breathing motion, with constant amplitude. The right figure is a zoom of the left figure; here you can clearly see the periodic motion.

Formula-wise, this means that you approximate the function at a certain point (say, again, $x = 1$) as follows:

$$f(1 + \delta) \approx f(1) + \left.\frac{\mathrm{d}f}{\mathrm{d}x}\right|_{x=1} \times \delta + \frac{1}{2}\left.\frac{\mathrm{d}^2 f}{\mathrm{d}x^2}\right|_{x=1} \times \delta^2$$

If you compare this with the linear approximation in section 1.3.2, you'll see that there's just an extra term. In that extra term, $\left.\frac{\mathrm{d}^2 f}{\mathrm{d}x^2}\right|_{x=1}$ denotes the second derivative of f, calculated at $x = 1$.

Such a higher order approximation is also possible in the case of the pulse and the reaction-diffusion system. Just like in section 1.3.2, you have to make the conceptual jump where you imagine that the point $x = 1$ represents the pulse, while the function $f(x)$ represents the reaction-diffusion system. Just as it is possible to take the 'derivative' of this reaction-diffusion system, you can also take its 'second derivative'. It's all quite analogous, really. The only disadvantage of this higher order approximation is that your formulas become a lot, lot longer; you can see that when browsing through chapter 4. Therefore, it also becomes harder and harder to say something definite about the fate of the pulse, because your equations become increasingly complicated. Once again, the singular perturbation helps you out. Based on the results of the existence and stability of the pulse, it turns out that it is possible to obtain explicit formulas which tell you something about whether such a breathing pulse will or will not appear.
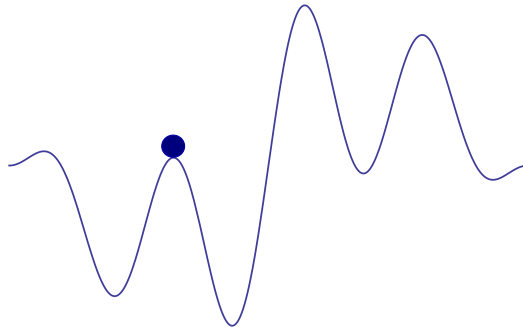
Figure 1.28: An example of a 'landscape'.

The reason why this higher order approximation can shed light on the appearance of a breathing pulse can be made clear by an example. In section 1.3.2, the concept of stability was illustrated by a ball on top of a hill versus a ball at the bottom of a pit. The first situation was unstable, the second was stable; see also Figure 1.20. In this case, the linear approximation only tells you if you're on top of a hill, or at the bottom of a pit. It doesn't tell you anything of what the rest of your surroundings look like. There might be other hills nearby, or other pits: see Figure 1.28. The higher order approximation lets you take a better look at the surrounding landscape.

In the case of a breathing pulse, the following situation occurs. Since you're in an unstable situation, you know that your ball (which represents the pulse) is on top of a hill. If the ball is given a little nudge, it will roll down. However, in some situations, your starting hill lies in between to larger hills. You might be able to roll down the hill, but you'll never escape the larger valley: see Figure 1.29. That means that, while the ball rolls around in the larger valley, it will never escape. The associated periodic motion of the ball is therefore bounded: its amplitude doesn't grow indefinitely.

Therefore, if you use higher order approximations and find out that the local 'landscape' is such as in Figure 1.29, then you know there has to exist a steadily oscillating, breathing pulse. Moreover, you can find that particular breathing pulse by giving an unstable stationary pulse nearby a little nudge, such that it starts to oscillate (see for example Figure 3.1). In chapter 4, the analysis tells us that such a situation can indeed arise, if you choose your parameters correctly. In more technical terms, that means that the Hopf bifurcation is called 'supercritical'. If there is no surrounding valley, and your ball keeps rolling down the hill with increasing speed, then the Hopf bifurcation is called 'subcritical'. Using these concepts, it is possible to prove the existence of a breathing pulse.
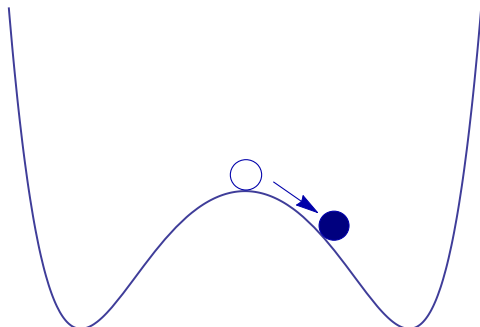
Figure 1.29: A hill in a valley: bounded periodic motion.

1.4 Thesis structure and main results

Now that you've encountered some central concepts and methods used in this thesis, it is time to explain how this thesis is structured, and which results have been obtained during the research leading to this thesis.

Let's focus first on chapters 2 and 3. I'll introduce them together, since they are rather similar in structure and content.
Chapter 2 treats pulse solutions in the 'slowly nonlinear Gierer-Meinhardt model'. The Gierer-Meinhardt model, mentioned in section 1.2.2, is one among many canonical models which have been studied in the last few decades in the context of pattern formation in reaction-diffusion systems. While the origin of the Gierer-Meinhardt model lies in developmental biology (it was developed in the context of morphogenesis), other sciences have contributed to the class of canonical reaction-diffusion models as well. The Gray-Scott model [23] has its basis in chemistry, while the Fitzhugh-Nagumo model [20, 40] describes the transmission of a electrical signal in a nerve.

The study of patterns in reaction-diffusion equations has largely been centered around the models just mentioned. One of the distinguishing features of the research presented in this thesis is the step beyond these canonical, quite specific models. Once you know how to find a pattern in a reaction-diffusion system, it doesn't matter that much what the system looks like. Of course, there are some mild restrictions on the reaction terms in the reaction-diffusion system under consideration, but those aren't really 'restrictive'; still, a wide range of systems falls into this admissible class.

The slowly nonlinear Gierer-Meinhardt model is such a step beyond the canonical models, in this case beyond the Gierer-Meinhardt model. In chapter 2, the existence and stability (in that order) of a pulse in this extended version of the Gierer-Meinhardt model is treated. It turns out that the extension of the Gierer-Meinhardt model with a slowly nonlinear term introduces a lot of new things: not only is it possible to construct a new, different type of pulse in comparison with the 'canonical' Gierer-Meinhardt model, the stability analysis of the constructed pulse shows that it can become unstable in a previously unobserved way. Another feature of this model is that, even though it is a nonlinear extension of the canonical model, you can still calculate everything you want in an explicit way: there is an explicit formula for the pulse, the stability analysis can be carried out explicitly, and even the Evans function can be determined in an explicit way. This is very useful for the stability analysis, in finding all the eigenvalues. For this model, it is possible to prove some results about the stability of the pulse.

Chapter 3 has the same structure as chapter 2. The main difference is that here we treat a wide range of possible reaction-diffusion systems instead of just one specific example. Since we showed in chapter 2 that such an extended system can give new results, it's interesting to see how far you can go with this. During the entire analysis in chapter 3, the reaction-diffusion system is kept at a very general form, almost like 'something involving ϕ' as in section 1.2.2 – well, it's a little more exact than that, but the main idea still is that it doesn't really matter that much what your reaction-diffusion system looks like. Once it obeys some very general conditions, it is possible to construct a pulse solution for it. Even the stability analysis can be carried out in the same way as for the explicit example of the slowly nonlinear Gierer-Meinhardt system of chapter 2. What's even more surprising, is that for such a very general system, you can still write down the Evans function explicitly. This is a really strong result, because it allows you to prove a number of (in)stability results for this very general class of systems. It even becomes clear that already during the construction process of the pulse, you can predict which pulse will certainly be unstable, and which pulse has a chance to be stable. The previous sentence already suggests that there's more than one possibility to construct a pulse (just like in chapter 2), which is indeed true in general. Chapter 3 shows you how to approach such a general system, and gives you the tools to construct and analyse a pulse yourself.
In this sense, chapters 2 and 3 are each other's mirror image. They follow exactly the same approach: chapter 2 for an explicit system, chapter 3 for a very wide class of systems of which the slowly nonlinear Gierer-Meinhardt system of chapter 2 is just an example.

While both chapters 2 and 3 treat existence and stability, the first two steps of the general research approach (Figure 1.10), the last chapter takes a first step into the largely unexplored world of pulse dynamics. Here, the higher order approximation of a destabilising Hopf bifurcation (which was found to exist in general in chapter 3, and was explicitly established in chapter 2) leads to the discovery of so-called breathing pulses, see section 1.3.3. In this fourth chapter, I present two equivalent methods to calculate these higher order approximations. These higher order approximations are applied to the slowly nonlinear Gierer-Meinhardt system, using the results of chapter 2. The numerical simulations which were presented at the end of chapter 2, section 2.5 already hinted at the existence of breathing pulses (see also Figure 1.27): in chapter 4, it is shown that these solutions can indeed exist, and when this is the case.

2

Pulses in a slowly nonlinear Gierer-Meinhardt equation

The content of this chapter was published as [54].

2.1 Introduction

The study of localised pulses in a two-component system of singularly perturbed reaction-diffusion equations has been a very active field of research since the nineties of the previous century. In its most general form, a system that may exhibit such a pulse reads – in one, unbounded, spatial dimension –

$$
\begin{cases}
U_t = U_{xx} + F(U, V) & \text{(2.1a)} \\
V_t = \varepsilon^2 V_{xx} + G(U, V) & \text{(2.1b)}
\end{cases}
$$

with $U, V : \mathbb{R} \times \mathbb{R}^+ \to \mathbb{R}$, and $0 < \varepsilon \ll 1$ asymptotically small. The nonlinear reaction terms $F, G : \mathbb{R}^2 \to \mathbb{R}$ are assumed to satisfy $F(\bar{U}, \bar{V}) = G(\bar{U}, \bar{V}) = 0$ for certain $(\bar{U}, \bar{V})$, such that the trivial background state $(U, V) \equiv (\bar{U}, \bar{V})$ is spectrally stable. However, research on pulses in equations of the type (2.1) has been restricted mostly to model equations. In particular two of these models have played a central role in the development of the theory: the (irreversible) Gray-Scott (GS) equation for a class of autocatalytic reactions [23] – that became the centre of research attention by the intriguing observations in [38, 43] – and the Gierer-Meinhardt (GM) equation [22] for (biological) morphogenesis – for which the existence problem has already been

considered in the mathematical literature for a somewhat longer time [48]. For both the GS and the GM model, quite precise insight has been obtained in the existence, stability and dynamics of localised (multi-) pulses, also in more than one spatial dimension – although one certainly cannot claim that the models are fully understood; see [5, 6, 7, 12, 13, 26, 32, 33, 34, 41, 42, 51, 58] and the references therein for the literature on one spatial dimension.

The 'fast' V-component of a localised (multi)pulse solution of a singularly perturbed model (2.1) is asymptotically localised: it decays exponentially to the V-component $\bar{V}$ of the background state on a spatial scale that is asymptotically shorter than the spatial scale associated to the 'slow' U-component. As a consequence, the two-component (U, V)-flow generated by (2.1) is governed by a scalar equation in the slow component U:

$$U_t = U_{xx} + F(U, \bar{V}) \tag{2.2}$$

except for the asymptotically small spatial regions in which the V-component is not exponentially close to $\bar{V}$. Clearly, this is in general a nonlinear equation. However, for the GS and GM models, this slow reduced scalar equation is linear:

$$
\begin{array}{llll}
\text{(GS)} & U_t = U_{xx} + A(1 - U), & A > 0 \text{ parameter}, & (\bar{U}, \bar{V}) = (1, 0) \\
\text{(GM)} & U_t = U_{xx} - \alpha U, & \alpha > 0 \text{ parameter}, & (\bar{U}, \bar{V}) = (0, 0)
\end{array}
\tag{2.3}
$$

In fact, as far as we are aware, this – the fact that the counterpart of (2.2) is linear – is the case for all singularly perturbed two-component reaction-diffusion equations with exponentially localised pulse solutions considered in the literature (including the Schnakenberg model [46, 56]). There are a number of papers in the literature in which more general classes of equations than the GS or GM models are considered – see [4, 6, 10]. In these papers the background state $(\bar{U}, \bar{V})$ is translated to $(0, 0)$ so that $F(\bar{U}, \bar{V}) = F(0, 0) = 0$ in (2.1). Moreover, the nonlinear part of $F(U, V)$ is assumed to be separable, i.e. $F(U, V)$ is written as $-\alpha U + F_1(U)F_2(V)$. Therefore $F_2(\bar{V}) = F_2(0) = 0$, and these more general systems also reduce to linear slow scalar equations like (2.3) outside the asymptotically small regions where V is not close to $\bar{V}$.

In this chapter, and in the subsequent chapter 3, we consider the potential impact of the nonlinearity of $F(U, \bar{V})$ as function of U in comparison with the literature on 'slowly linear' model systems such as GS and GM. Here, we consider a very explicit model problem, a Gierer-Meinhardt equation with a 'slow nonlinearity' (see (2.7) below), in full analytical detail; in chapter 3, we consider the existence and stability

of pulses in a general setting, i.e. as solutions of (2.1). We refer to Remark 2.1 for a more specific motivation of our choice to study equations with 'slow nonlinearities'.

In the standard form (2.1), the classical Gierer-Meinhardt equation [22] is given by

$$\begin{cases} U_t = \quad U_{xx} - \alpha\, U + \sigma\, V^2 & \text{(2.4a)} \\ V_t = \varepsilon^2 V_{xx} - V + \dfrac{V^2}{U} & \text{(2.4b)} \end{cases}$$

in which $\alpha > 0$ is the main bifurcation parameter and $\sigma > 0$ is most often scaled to 1. The pulse type solutions of (2.4) have an amplitude of $O\!\left(\frac{1}{\varepsilon}\right)$ [6, 26]. Therefore, we scale U and V and subsequently x and ε,

$$U \to \frac{U}{\varepsilon},\ V \to \frac{V}{\varepsilon},\ x \to \sqrt{\varepsilon}\, x,\ \varepsilon \to \varepsilon^2 \tag{2.5}$$

to bring (2.4) in its 'normal form' [6]

$$\begin{cases} \varepsilon^2 U_t = \quad U_{xx} - \varepsilon^2 \alpha\, U + \sigma\, V^2 & \text{(2.6a)} \\ V_t = \varepsilon^2 V_{xx} - V + \dfrac{V^2}{U}. & \text{(2.6b)} \end{cases}$$

In this chapter, we study a 'slowly nonlinearised' version of (2.6), that is obtained from (2.6) by adding a very simple nonlinear term to its 'slow' U-equation (2.6a):

$$\begin{cases} \varepsilon^2 U_t = \quad U_{xx} - \varepsilon^2 \left(\alpha\, U - \gamma\, U^d \right) + \sigma\, V^2 & \text{(2.7a)} \\ V_t = \varepsilon^2 V_{xx} - V + \dfrac{V^2}{U} & \text{(2.7b)} \end{cases}$$

with new parameters $\gamma \geq 0$, $d > 1$. Moreover, we now allow $\sigma \in \mathbb{R}\backslash\{0\}$. Systems incorporating such a slow nonlinearity were already encountered in [37] (although no pulse type solutions were considered in this paper). This equation indeed reduces to a nonlinear slow reduced scalar U-equation away from the regions in which V is not exponentially close to $\bar{V} = 0$:

$$U_t = U_{\chi\chi} - \alpha\, U + \gamma\, U^d \tag{2.8}$$

in which $\chi = \varepsilon x$ is a 'super-slow' spatial coordinate – see section 2.2. Note that scaling back the additional 'slowly nonlinear' term $\gamma\, U^d$ through (2.5) introduces an $O\!\left(\varepsilon^{d-1}\right)$, i.e an asymptotically small, additional term to the Gierer-Meinhardt equation in its classical form (2.4). We will see in the upcoming analysis that this term has
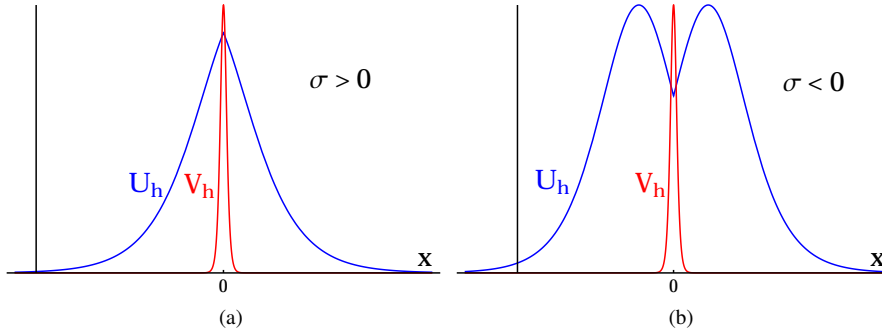
Figure 2.1: The stationary homoclinic pulse $(U_h(x), V_h(x))$ of (2.7); (a) $\sigma > 0$, (b) $\sigma < 0$.

a significant impact on the dynamics generated by (2.4). Thus, in a way, our work can also be interpreted as a study of the 'vulnerability' of the classical Gierer-Meinhardt model (2.4) to asymptotically small 'slowly nonlinear' changes to the model.

In recent years, the analysis of localised pulses in one-dimensional singularly perturbed reaction-diffusion equations has been focused mostly on pulse dynamics and interactions – see [5, 10, 12, 34] and the references therein. However – like the work on multi-pulse patterns [26, 32, 33, 51, 52, 56] – this analysis is based on fundamental insights on the existence and stability of stationary, solitary, pulses [6, 7, 13, 48, 58]. On the unbounded domain, i.e. for $x \in \mathbb{R}$, these pulses correspond to homoclinic solutions of the four-dimensional spatial dynamical system reduction of the partial differential equation. Here, we restrict our analysis to the existence and stability of homoclinic stationary pulse solutions $(U_h(x), V_h(x))$ to (2.7) that are bi-asymptotic to the background state $(0, 0)$, i.e. $\lim_{x \to \pm\infty} (U_h(x), V_h(x)) = (0, 0)$. Especially the issue of stability requires a significant extension of the methods developed in the literature for 'slowly linear' GS/GM-type models. The present results form the foundation for a subsequent analysis of the multi-pulse patterns – see remark 2.1 – and pulse interactions. Moreover, already at the level of these most basic pulse solutions, we encounter novel phenomena in the dynamics generated by (2.7) that have not yet been observed in the literature on 'slowly linear' models.

The existence problem – see section 2.2 – can be studied directly along the lines developed in [6] for 'slowly linear' normal form models of GM type with a separable

nonlinearity. Our main result on the existence of homoclinic pulses $(U_h(x), V_h(x))$, Theorem 2.2, can be established by a direct application of the methods of geometric singular perturbation theory [18, 19]. In other words, at the existence level the 'slow nonlinearity' in (2.7) does not require the development of novel theory. However, it is established by Theorem 2.2 that (2.7) does exhibit homoclinic pulse patterns that differ significantly from those found in 'slowly linear' GS/GM-type models. Unlike linear slow reductions such as (2.3), the planar stationary problem associated to reduction (2.8) has orbits homoclinic to its saddle point (that corresponds to the background state of (2.7)). As a consequence, unlike the classical GM model (2.4), system (2.7) has homoclinic pulse solutions $(U_h(x), V_h(x))$ for $\sigma < 0$. At leading order in ε, the slow U-component $U_h(x)$ follows a large part of the homoclinic orbit of (2.8), so that for $\sigma < 0$ the slow component of the solitary homoclinic 1-pulse solution has the leading order structure of two combined slow scalar pulses – see Figure 2.1b.

The spectral stability of $(U_h(x), V_h(x))$ is studied in section 2.3 by the Evans function $\mathcal{D}(\lambda)$ associated to the linearised stability problem, following the ideas developed in [6, 7]. As is to be expected from the general theory [3], $\mathcal{D}(\lambda)$ can be decomposed into a slow and a fast component, and all nontrivial eigenvalues are determined by the slow component. In [6, 7], i.e. for the GM and GS models, the zeroes of this slow component are determined analytically by 'the NLEP method'. The linearity of the slow scalar reduction (2.3) plays a central role in this approach – as it does in all analytical studies of the spectral stability of pulses in GS/GM-type models (see [5, 26, 32, 33, 34, 51, 58] and the references therein). More explicitly, the fact that the spectral stability problem is exponentially close to a constant coefficients eigenvalue problem outside the asymptotically small regions in which V is not close to $\bar{V}$ is a crucial ingredient of the stability analysis of GS/GM-type models. Due to the nonlinearity in the slow scalar reduction (2.8) this is not the case for (2.7): away from the fast V-pulse, the linear operator associated to the stability problem still has coefficients that depend explicitly (and slowly) on x (on χ – see (2.8)). Its solution space is therefore not governed by simple, pure exponentials (as for GS/GM-type models).

The key to the NLEP approach as developed in [6, 7] is constructing a set of basis functions for the linear operator/system associated to the stability of the pulse for which the Evans function $\mathcal{D}(\lambda)$ – the determinant of this set – can be evaluated, or better: approximated, explicitly. In chapter, and in the subsequent chapter 3, we show that the NLEP approach can be based on a set of basis functions that is determined by the slowly varying problem outside the fast V-pulse region, in such a way that it is still possible to determine an analytical approximation for the zeroes of $\mathcal{D}(\lambda)$.

Here, a central role is played by the χ-dependent Sturm-Liouville problem associated to the linearisation of (2.8) about its (stationary) homoclinic orbit, defined on a half-line. This problem has a two-dimensional set of slowly varying solutions. We show that these solutions can take over the role of the slow exponentials coming from the (slow) stability problem about the trivial state $U = 0$ of the linear constant coefficient GS/GM-type reductions (2.3). In the context of this chapter, these solutions can be expressed in terms of Legendre functions, due to the special/simple nature of the nonlinearity in (2.8). In the general setting of chapter 3, the construction of the Evans functions cannot be this explicit. The main novel analytical result of this chapter is given by Theorem 2.12, in which indeed an explicit expression is given for the zeroes of $\mathcal{D}(\lambda)$, which is a generalisation of the corresponding 'slowly linear' results in [6, 7].

In section 2.4, we analyse and interpret the expression obtained in Theorem 2.12. One of our first – and quite straightforward – results is Corollary 2.15: the $\sigma < 0$ 'double hump' pulses of Figure 2.1b cannot be stable. The $\sigma > 0$ pulses of Figure 2.1a, however, can very well be stable. In Figure 2.3, a graphical description is given of our two main stability results, Theorems 2.18 and 2.19. The stability of the pulse $(U_h(x), V_h(x))$ depends strongly on the character of the 'slow nonlinearity' in (2.7). As long as the exponent of the nonlinearity d is smaller than 3, the stability scenario is exactly like that of the 'slowly linear' GS/GM-type models: $(U_h(x), V_h(x))$ stabilises by a Hopf bifurcation for increasing α – even the shape of the orbit of the critical eigenvalues $\lambda(\alpha)$ through $\mathbb{C}$ is very similar to its counterparts in [6, 7]. However, this orbit changes drastically when d becomes larger than 3 – see Figure 2.3: for $d > 3$ there is a second Hopf bifurcation (as function of α) that destabilises $(U_h(x), V_h(x))$. Different from the results on GS/GM-type models, for $d > 3$, there is only a bounded α-region for which $(U_h(x), V_h(x))$ can be stable. In Theorem 2.20 this is established rigorously for $d > 3$ large enough.

Finally, in section 2.5, we present some simulations of (2.7). We have not attempted to perform a systematic (numerical bifurcation) analysis of the dynamics of (2.7). Apart from checking (and confirming) the outcome of our asymptotic stability analysis, our goal has been to obtain an indication of whether or not the 'slow nonlinearity' of (2.7) generates behaviour that is not known from the (vast) literature on GS/GM-type models.

We are not aware of any examples in the literature on GS/GM-type models of stable non-moving solitary pulses that are not completely stationary. A priori, one
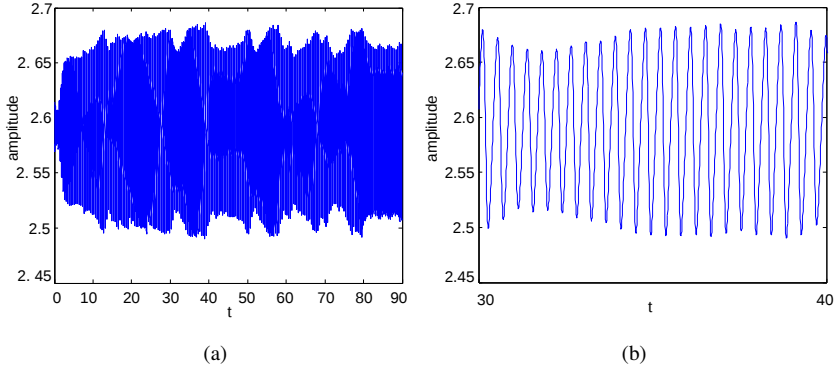
Figure 2.2: The dynamics of the maximum of the U-pulse as function of time in a simulation of (2.7) with $\gamma = 2$, $\sigma = 1$, $\varepsilon = 0.002$, $d = 5$ and $\alpha = 90.6$ for $x \in [-5000, 5000]$ with homogeneous Neumann boundary conditions – (b) zooms in on a small part (in time) of (a). The position of the maximum does not vary in time. The value of α is close to the second Hopf bifurcation at which $(U_h(x), V_h(x))$ destabilises – see Figure 2.3.

would expect that if a pulse is destabilised (for instance by decreasing α in the GM model (2.4)), it may bifurcate into a stable standing pulse with a periodically varying amplitude. However, this requires a supercritical Hopf bifurcation, and all Hopf bifurcations of stationary pulses in GS/GM-type models reported on in the literature seem to be subcritical: as α decreases through its critical Hopf bifurcation value, the standing pulse starts to oscillate up and down, but the amplitude of this oscillation grows and after a certain time the pulse is extinguished – see for instance Figure 2.11 (a) in section 2.5. It should be noted that this statement is based on numerical observations, the nature of the Hopf bifurcation of solitary, standing pulses in GS/GM-type models has not been analysed in the literature (for instance by a centre manifold reduction). Moreover, it should also be remarked that – for instance – the GS model does exhibit periodic and even chaotic pulse dynamics – see for instance [5, 42]. However, this richer type of behaviour occurs only in the context of pulse interactions, it is governed by the interactions between travelling pulses, and/or between pulses and the boundary of the domain. We have not considered this type of dynamics here, as we have completely focused on the behaviour of standing, solitary spatially homoclinic pulses. Nevertheless, we have observed very rich dynamics, much richer

than that exhibited by linear GS/GM-type models. In section 2.5 examples are given of periodically oscillating pulses, i.e. standing pulses with an amplitude that varies periodically in time; quasi-periodically oscillating pulses – the amplitude of the pulse oscillation is modulated periodically – and oscillating pulses of which the amplitude is modulated in an even more complex fashion. A simulation of such a 'chaotically oscillating pulse' is shown in Figure 2.2.

In this chapter, it is not investigated whether the pulse dynamics of Figure 2.2 is 'chaotic' or –for instance– is quasi-periodic with three or more independent frequencies. In other words, we do not study the details of the associated bifurcation scenario and do not compute any measure by which the (possible) chaotic nature of the pulse dynamics can be quantified. The analytic core of this chapter, the analysis of the spectrum associated to the stability of $(U_h(x), V_h(x))$, serves as an ideal starting point for a centre manifold analysis of the nature of the Hopf (and subsequent) bifurcations for pulses and/or multi-pulses occurring in this model (and/or generalisations of (2.7)). This will be the subject of chapter 4, where analytic insight in (the possible route leading to) the complex/chaotic behaviour observed in Figure 2.2 will be obtained.

Remark 2.1. Our research is strongly motivated by recent findings on the character of the destabilisation of spatially periodic multi-pulse patterns with long wavelength L. In [52] it is established for GM-type models that these patterns can only be destabilised by two distinct types of Hopf bifurcations as $L \to \infty$, one in which the linearly growing mode also has wavelength L – the most commonly encountered destabilisation in the literature – and another in which this mode has wavelength $2L$. Moreover, these destabilisations alternate countably many times as $L \to \infty$. This is called the 'Hopf dance' in [52]. This Hopf dance also occurs in the GS model, as indicated by the AUTO-simulations in [52]. The GM analysis in [52] shows that this 'dance' is completely driven by the exponential expression $E(L) = e^{-L\sqrt{\alpha + \lambda_h}}$ associated to the slow reduced eigenvalue equation $u_{xx} - \alpha u = \lambda_h u$ originating from (2.3), in which $\lambda_h \in \mathbb{C}$ is the (complex) eigenvalue of the homoclinic ($L \to \infty$) limit pattern. The rotation of $E(L) \in \mathbb{C}$ as $L \to \infty$ is the mechanism underpinning the Hopf dance. From a generic point of view, it is not at all clear why this 'linear' Hopf dance should take place (this is even more obvious for the subsequent 'belly dance' [52]). Hence, to really understand the subtleties involved in the destabilisation of long wavelength spatially periodic patterns, one needs to go beyond 'slowly linear' models for which the associated 'slow reduced' eigenvalue problems are not governed by expressions as $E(L)$. In other words, one needs to study systems of the type (2.1) with $F(U, \bar{V})$ not linear as a function of U.
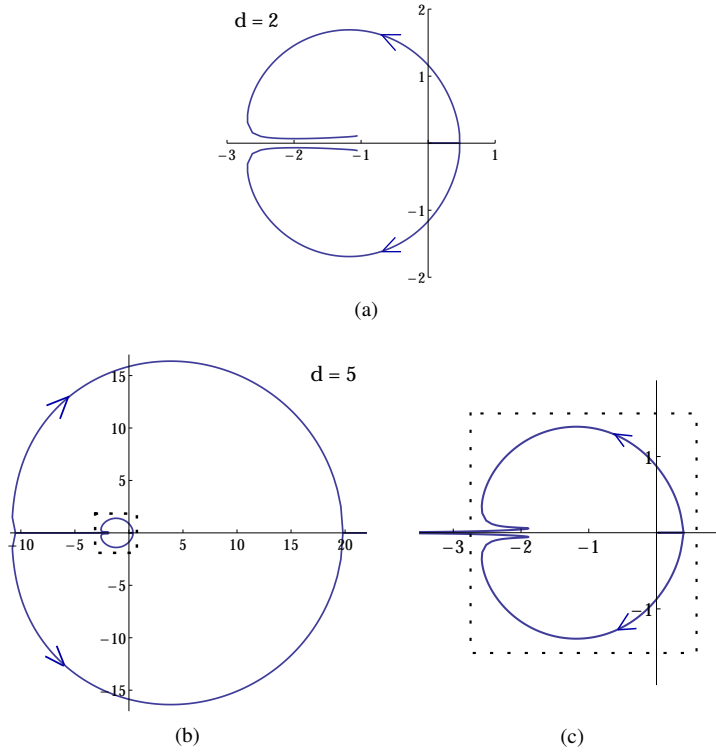
Figure 2.3: The orbits through $\mathbb{C}$ of the critical eigenvalue λ associated to the spectral stability of $(U_h(x), V_h(x))$ as function of increasing α ($\gamma = 2$, $\sigma = 1$), to leading order in ε. (a) $d = 2 < 3$: The same scenario as in the GS and the GM models [6, 7]. Two real positive eigenvalues merge and become a pair of complex conjugate eigenvalues that travels through the imaginary axis: the pulse is stabilised by a Hopf bifurcation at a critical value of α. (b) $d = 5 > 3$: A significantly different scenario. The eigenvalues initially display the same behaviour as in the case $d < 3$: the pulse is again stabilised by a Hopf bifurcation. However, for α increasing further, the orbits sharply turn around and follow the imaginary axis closely in the negative direction – see (c), a zoom of (b). Eventually, the orbits branch off, head back to the imaginary axis, and again cross the imaginary axis at a second critical – Hopf – value of α. Finally, the pair meets again at the positive real axis and splits up into two positive real valued eigenvalues.

2.2 Pulse construction

Our goal is to construct a stationary pulse solution which is homoclinic to the trivial background state $(U, V) = (0, 0)$. To achieve this goal, we use the singularly perturbed nature of the system. The spatial dynamics of the stationary pulse are given by the four-dimensional system

$$
\begin{cases}
u_x = p & \text{(2.9a)} \\
p_x = -\sigma v^2 + \varepsilon^2 \left(\alpha u - \gamma u^d \right) & \text{(2.9b)} \\
\varepsilon v_x = q & \text{(2.9c)} \\
\varepsilon q_x = v - \dfrac{v^2}{u} & \text{(2.9d)}
\end{cases}
$$

Along the lines of Fenichel theory, we can perform a slow-fast decomposition in the spatial variable x: recognising system (2.9) as the *slow* system, we can define the fast variable $\xi = \frac{x}{\varepsilon}$ to obtain the associated *fast* system

$$
\begin{cases}
u_\xi = \varepsilon p & \text{(2.10a)} \\
p_\xi = -\varepsilon \sigma v^2 + \varepsilon^3 \left(\alpha u - \gamma u^d \right) & \text{(2.10b)} \\
v_\xi = q & \text{(2.10c)} \\
q_\xi = v - \dfrac{v^2}{u} & \text{(2.10d)}
\end{cases}
$$

The trivial background state is in these systems represented by the origin $(u, p, v, q) = (0, 0, 0, 0)$. While the vector field which generates the flow of the system is not defined at the origin due to the singular $\frac{v^2}{u}$ term in the v-equation, the ratio $\frac{v^2}{u}$ will be well-defined for the constructed pulse.

2.2.1 Geometric analysis

When $\varepsilon \to 0$, the slow and fast systems (2.9) and (2.10) reduce to the *reduced slow system*

$$
u_{xx} = -\sigma v^2 \tag{2.11a}
$$

$$
q = v - \frac{v^2}{u} = 0 \tag{2.11b}
$$

and the *reduced fast system*

$$u_\xi = p_\xi = 0 \tag{2.12a}$$

$$v_{\xi\xi} = v - \frac{v^2}{u} \tag{2.12b}$$

We see that in this limit, the slow and fast dynamics decouple completely. We define $\mathcal{M}_0 = \{(u, p, v, q) \,|\, u > 0,\ v = q = 0\}$ as the two-dimensional normally hyperbolic invariant manifold that consists of hyperbolic equilibria of the reduced fast system (2.12); it has three-dimensional stable and unstable manifolds $\mathcal{W}^{s,u}(\mathcal{M}_0)$ which are the unions of the two-parameter families of one-dimensional stable and unstable manifolds (fibres) at the saddle points $(u_0, p_0, 0, 0) \in \mathcal{M}_0$. The reduced fast dynamics (2.12) allow a two-parameter family of homoclinic solutions $v_{0,h}$:

$$v_{h,0}(\xi; u_0, p_0) = \frac{3\, u_0}{2} \operatorname{sech}^2\left(\tfrac{1}{2}\xi\right) \tag{2.13}$$

The union over this family as a bundle over $\mathcal{M}_0$ forms the intersection $\mathcal{W}^s(\mathcal{M}_0) \cup \mathcal{W}^u(\mathcal{M}_0)$, see Figure 2.4a.

Fenichel persistence theory [18, 19, 29, 30] states that, for ε sufficiently small, the full system (2.10) has a locally invariant slow manifold $\mathcal{M}_\varepsilon$ which is $O(\varepsilon)$ close to $\mathcal{M}_0$. Since $\mathcal{M}_0$ is also invariant under the non-reduced (fast) flow of (2.10), we have already found $\mathcal{M}_\varepsilon = \mathcal{M}_0$. Moreover, Fenichel theory states the existence of three-dimensional stable and unstable manifolds $\mathcal{W}^{s,u}(\mathcal{M}_\varepsilon)$ which are $O(\varepsilon)$ close to their unperturbed counterparts $\mathcal{W}^{s,u}(\mathcal{M}_0)$. The intersection $\mathcal{W}^s(\mathcal{M}_\varepsilon) \cap \mathcal{W}^u(\mathcal{M}_\varepsilon)$ exists, is transversal and therefore determines a two-dimensional manifold. This existence and transversality is based on a Melnikov-type calculation in [6], which can be applied directly to system (2.10). Since the original model equations (2.7) are invariant under reflection in the spatial variable $x \to -x$, this reflection is in the four-dimensional system (2.9) equivalent to the momentum reflection $(p, q) \to (-p, -q)$. Because the coordinate reflection $\xi \to -\xi$ maps $\mathcal{W}^s(\mathcal{M}_\varepsilon)$ to $\mathcal{W}^u(\mathcal{M}_\varepsilon)$ and vice versa, it follows that the intersection of these two manifolds is symmetric in the invariant subset of the momentum reflection, the two-dimensional hyperplane $\{(u, p, v, q) \,|\, p = q = 0\}$. The transversality of this hyperplane to $\mathcal{M}_\varepsilon$ excludes the possibility that it has the intersection $\mathcal{W}^s(\mathcal{M}_\varepsilon) \cap \mathcal{W}^u(\mathcal{M}_\varepsilon)$ as a subset, from which we can conclude that $\mathcal{W}^s(\mathcal{M}_\varepsilon) \cap \mathcal{W}^u(\mathcal{M}_\varepsilon)$ intersects the hyperplane $\{(u, p, v, q) \,|\, p = q = 0\}$ transversally. This determines a one-parameter family of orbits bi-asymptotic to $\mathcal{M}_\varepsilon$. Since both $\mathcal{W}^s(\mathcal{M}_\varepsilon)$ and $\mathcal{W}^u(\mathcal{M}_\varepsilon)$ are $O(\varepsilon)$ close to $\mathcal{W}^{s,u}(\mathcal{M}_0)$ where the two-parameter family of homoclinic orbits was parametrised by u_0 and p_0 (see (2.13)), it is convenient to

(a)   (b)
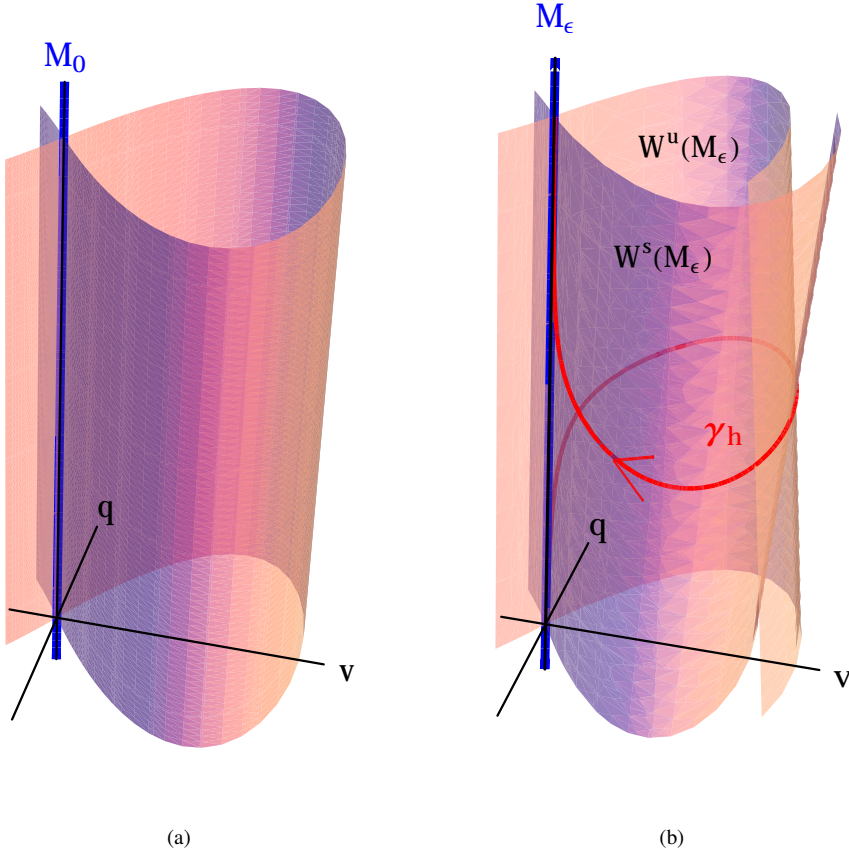
Figure 2.4: Transversal intersection of the stable and unstable manifolds. (a): The family of homoclinic orbits $v_{h,0}(\xi; u_0, p_0)$, viewed as a bundle over $\mathcal{M}_0$. Both u- and p-directions are along the vertical axis; $\mathcal{M}_0$ is indicated in blue. (b): For the perturbed system ($\varepsilon > 0$), $\mathcal{W}^s(\mathcal{M}_\varepsilon)$ and $\mathcal{W}^u(\mathcal{M}_\varepsilon)$ intersect transversally: γ_h (indicated in red) represents $\mathcal{W}^s(\mathcal{M}_\varepsilon) \cap \mathcal{W}^u(\mathcal{M}_\varepsilon)$, a one-parameter family of orbits homoclinic to $\mathcal{M}_\varepsilon$ – recall that $\dim(\mathcal{M}_\varepsilon) = 2$, $\dim(\mathcal{W}^{s,u}(\mathcal{M}_\varepsilon)) = 3$ so $\dim(\gamma_h) = 2$.

use u_0 to parametrise the one-parameter family of orbits bi-asymptotic to $\mathcal{M}_\varepsilon$ determined by $\mathcal{W}^s(\mathcal{M}_\varepsilon) \cap \mathcal{W}^u(\mathcal{M}_\varepsilon)$. For a sketch of the situation, see Figure 2.4b.

The next step is to use this structure to construct an orbit homoclinic to $(0, 0, 0, 0)$ in the full, perturbed system (2.9) / (2.10). For that purpose, it is necessary to consider the dynamics on $\mathcal{M}_\varepsilon$. The flow on $\mathcal{M}_\varepsilon$ can be determined by substituting $v = q = 0$ in (2.9) and yields

$$u_{xx} = \varepsilon^2 \left(\alpha u - \gamma u^d \right) \tag{2.14}$$

Introducing a super-slow coordinate $\chi = \varepsilon x$, this can be written as

$$u_{\chi\chi} = \alpha u - \gamma u^d \tag{2.15}$$

This equation allows a solution (bi)asymptotic to the trivial background state: since $\gamma > 0$, it is homoclinic to $(0, 0, 0, 0) \in \mathcal{M}_\varepsilon$ and explicitly given by

$$u_{h,0}(\chi) = \left[\frac{\alpha(d+1)}{2\gamma} \operatorname{sech}^2 \left(\tfrac{1}{2}(d-1) \sqrt{\alpha}\chi \right) \right]^{\frac{1}{d-1}} \tag{2.16}$$

The super-slow dynamics on $\mathcal{M}_\varepsilon$ allows us to get a grip on picking exactly that orbit bi-asymptotic to $\mathcal{M}_\varepsilon$ from the intersection $\mathcal{W}^s(\mathcal{M}_\varepsilon) \cap \mathcal{W}^u(\mathcal{M}_\varepsilon)$ which is also homoclinic to $(0, 0, 0, 0) \in \mathcal{M}_\varepsilon$, that is, which is -mostly- asymptotically close to $u_{h,0} \in \mathcal{M}_\varepsilon$. This orbit will make a *fast* excursion through the V-field, since this is where the fast dynamics take place (see (2.10), (2.12)). Since our goal is to construct a symmetric pulse, we can choose an interval symmetric around the origin in which the fast jump occurs. The interval needs to be asymptotically small with respect to the slow variable x, but asymptotically large with respect to the fast variable ξ: to be asymptotically close to $\mathcal{M}_\varepsilon$, the V-component of the pulse needs to be exponentially small. A standard [6] choice for this fast spatial region is

$$I_f = \left\{ \xi \in \mathbb{R} \,\middle|\, |\xi| < \frac{1}{\sqrt{\varepsilon}} \right\} \tag{2.17}$$

Indeed, $x \ll 1$ and $\xi \gg 1$ on ∂I_f. For a sketch of the orbit, see Figure 2.5.

Now, we define the *take-off* and *touchdown* sets $T_{o,d} \subset \mathcal{M}_\varepsilon$ to be the collection of base points of all Fenichel fibres in $\mathcal{W}^u(\mathcal{M}_\varepsilon)$ resp. $\mathcal{W}^s(\mathcal{M}_\varepsilon)$ that have points in the transverse intersection $\mathcal{W}^s(\mathcal{M}_\varepsilon) \cap \mathcal{W}^u(\mathcal{M}_\varepsilon)$. Detailed information on $T_{o,d}$ can be obtained by studying the fast system (2.10) on $\mathcal{M}_\varepsilon$. First, we observe that $p_\xi = O(\varepsilon^3)$ on $\mathcal{M}_\varepsilon$ so the p-coordinate on $\mathcal{M}_\varepsilon$ remains constant to leading order during the fast excursion through the V-field. Therefore, the change in the p-coordinate of the pulse is completely determined by its accumulated change during its excursion through the
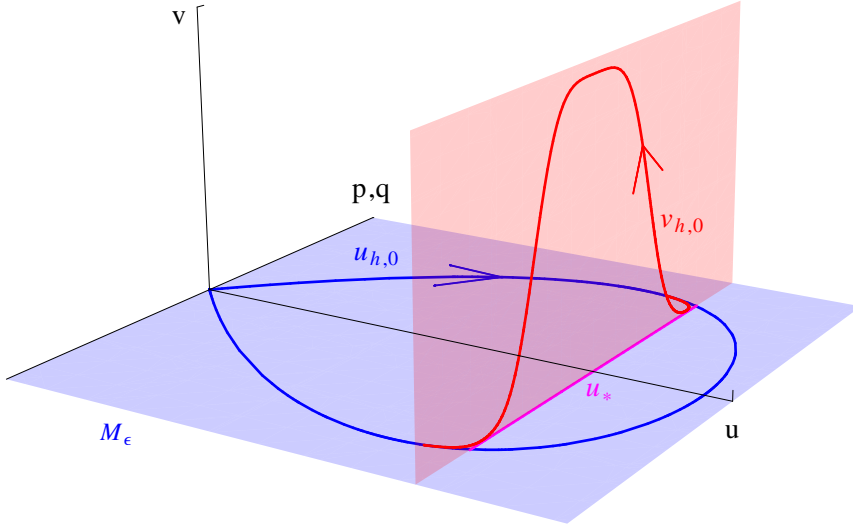
Figure 2.5: An asymptotic construction of the orbit $\gamma_h(\xi)$ of Theorem 2.2 drawn in three dimensions. The p- and q-directions are combined, since there is no direct interaction between them. The blue surface represents the persistent slow manifold $\mathcal{M}_\varepsilon$ while the fast dynamics take place on the red surface, which is spanned by the v and q directions. The slow homoclinic orbit $u_{h,0}(\chi)$ is drawn in blue, the fast homoclinic orbit $v_{h,0}(\xi; u_*, 0)$ is drawn in red. The jump through the fast field projected on $\mathcal{M}_\varepsilon$ is indicated by the purple line.

fast field, and is given by

$$
\Delta_\xi p = \int_{I_f} p_\xi \, d\xi = \int_{I_f} -\varepsilon \sigma v^2 + O(\varepsilon^3) \, d\xi = \int_{-\infty}^{\infty} -\varepsilon \sigma v_{h,0}(\xi; u_0, p_0)^2 \, d\xi + O(\varepsilon^2)
$$
$$
= -6 \varepsilon \sigma u_0^2 + O(\varepsilon^2) \tag{2.18}
$$

where we have used (2.10) and (2.13). Moreover, since $u_\xi = \varepsilon p$ and $p = O(\varepsilon)$ on I_f, we see that $\Delta_\xi u = O(\varepsilon^2)$. This means that during the jump through the fast field, the u-coordinate of the pulse does not change to leading order.

Since $\mathcal{W}^s(\mathcal{M}_\varepsilon) \cap \mathcal{W}^u(\mathcal{M}_\varepsilon)$ intersects the hyperplane $\{(u, p, v, q) \mid p = q = 0\}$ transversally, we can define the take-off and touchdown sets as curves

$$
T_o = \left\{ (u, p, 0, 0) \in \mathcal{M}_\varepsilon \,\middle|\, p = 3 \varepsilon \sigma u^2 \right\}, \ T_d = \left\{ (u, p, 0, 0) \in \mathcal{M}_\varepsilon \,\middle|\, p = -3 \varepsilon \sigma u^2 \right\} \tag{2.19}
$$

at leading order. Note that if σ changes sign, the take-off and touchdown curves are

(a) For $\sigma > 0$ the jump is downwards, the resulting pulse is shown in Figure 2.1a.

(b) For $\sigma < 0$ the jump is upwards, the resulting pulse is shown in Figure 2.1b.
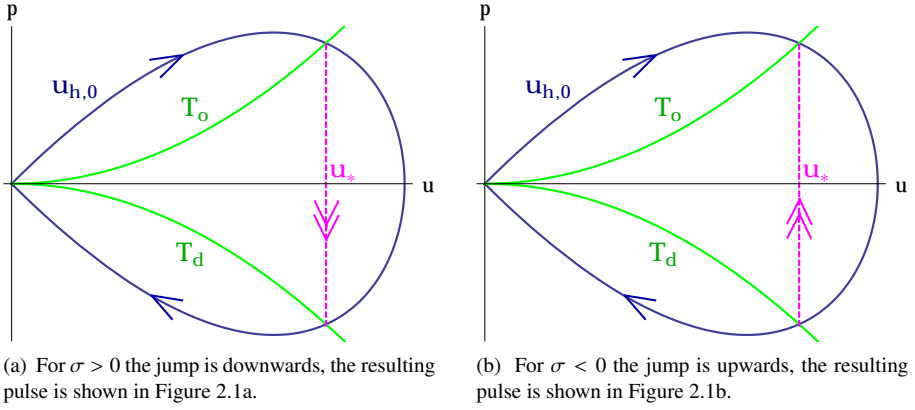
Figure 2.6: The homoclinic orbit $u_{h,0}(\chi)$ is drawn in blue in the (u, p)-plane. The take-off and touchdown curves $T_o = \left\{(u, p) \,\middle|\, p = 3\,\varepsilon\,\sigma u^2\right\}$ and $T_d = \left\{(u, p) \,\middle|\, p = -3\,\varepsilon\,\sigma u^2\right\}$ are drawn in green. The jump through the fast field at $u = u_*$ is indicated by the dashed purple line.

interchanged: for $\sigma > 0$ the take-off curve has positive p-values, while for $\sigma < 0$ the take-off curve has negative p-values. This also means the *direction* of the fast jump is reversed when σ changes sign, see (2.18) and Figure 2.6a.

An orbit of the system (2.9) / (2.10) is homoclinic to $(0, 0, 0, 0)$ if its Fenichel fibre basepoints in $T_{o,d}$ intersect the super-slow homoclinic orbit $u_{h,0} \in \mathcal{M}_\varepsilon$, see Figure 2.6a. This intersection can be determined by integrating (2.14) once,

$$\tfrac{1}{2}p^2 = \varepsilon^2\left(\tfrac{1}{2}\alpha\,u^2 - \frac{\gamma}{d+1}\,u^{d+1}\right) \tag{2.20}$$

and substituting $p = \pm 3\,\varepsilon\,\sigma u^2$ from (2.19) to obtain

$$\frac{2\gamma}{d+1}u^{d-1} = \alpha - 9\,\sigma^2 u^2 \tag{2.21}$$

which for $\alpha, \gamma, |\sigma| > 0$ and $d > 1$ always has a unique real positive solution, denoted by u_*. Furthermore, we define χ_* as the (unique) *positive* χ-value for which $u_{h,0}(\chi_*) = u_*$, the u-coordinate of the intersection. When $\sigma < 0$, we obtain a slightly different pulse since part of the slow homoclinic orbit $u_{h,0}$ is covered twice, see Figure 2.6b. This has its consequences for the formulation of our main existence result:

Theorem 2.2. *Let $\varepsilon > 0$ be sufficiently small. Then, for all values of the parameters $\alpha > 0$, $\gamma > 0$, $|\sigma| > 0$ and $d > 1$, there exists a unique orbit $\gamma_h(\xi) = (u_h(\xi), p_h(\xi), v_h(\xi), q_h(\xi))$ as a solution of system (2.10) which is homoclinic to $(0,0,0,0)$ and lies in the intersection $\mathcal{W}^s(\mathcal{M}_\varepsilon) \cap \mathcal{W}^u(\mathcal{M}_\varepsilon)$. Moreover,*

$$
\begin{aligned}
\|v_h(\xi) - v_{h,0}(\xi; u_*, 0)\|_\infty &= O(\varepsilon), \\
\|q_h(\xi) - \tfrac{\mathrm{d}}{\mathrm{d}\xi} v_{h,0}(\xi; u_*, 0)\|_\infty &= O(\varepsilon)
\end{aligned}
\tag{2.22}
$$

for all $\xi \in \mathbb{R}$ and

$$
\begin{aligned}
\|u_h(\chi) - u_{h,0}(\chi - \mathrm{sgn}(\sigma)\chi_*)\|_\infty &= O(\varepsilon), \\
\|p_h(\chi) - \varepsilon \tfrac{\mathrm{d}}{\mathrm{d}\chi} u_{h,0}(\chi - \mathrm{sgn}(\sigma)\chi_*)\|_\infty &= O(\varepsilon)
\end{aligned}
\tag{2.23}
$$

for all $\quad \chi < 0$, while

$$
\begin{aligned}
\|u_h(\chi) - u_{h,0}(\chi + \mathrm{sgn}(\sigma)\chi_*)\|_\infty &= O(\varepsilon), \\
\|p_h(\chi) - \varepsilon \tfrac{\mathrm{d}}{\mathrm{d}\chi} u_{h,0}(\chi + \mathrm{sgn}(\sigma)\chi_*)\|_\infty &= O(\varepsilon)
\end{aligned}
\tag{2.24}
$$

for all $\quad \chi > 0$.

The orbit γ_h corresponds to a homoclinic pulse solution (U_h, V_h) of system (2.7).

Proof. The missing details in the above geometric construction, especially in the precise estimates of (2.22), (2.23) and (2.24), can be obtained in a manner identical to the corresponding result on 'slowly linear' systems in [6]. □

2.3 Pulse stability: analysis

The linear stability of the stationary pulse solution (U_h, V_h) of (2.7) found in the previous section is determined by adding a perturbation of the form $(\bar{u}(x), \bar{v}(x))\, e^{\lambda t}$ and linearising equation (2.7) around the stationary solution, obtaining in the fast variable ξ,

$$
\begin{cases}
\bar{u}_\xi = \varepsilon\,\bar{p} & \text{(2.25a)} \\[4pt]
\bar{p}_\xi = -2\,\varepsilon\,\sigma\,V_h(\xi)\,\bar{v} + \varepsilon^3\left(\alpha + \lambda - \gamma\,d\,U_h(\xi)^{d-1}\right)\bar{u} & \text{(2.25b)} \\[4pt]
\bar{v}_\xi = \bar{q} & \text{(2.25c)} \\[4pt]
\bar{q}_\xi = \left(1 + \lambda - 2\dfrac{V_h(\xi)}{U_h(\xi)}\right)\bar{v} + \dfrac{V_h(\xi)^2}{U_h(\xi)^2}\,\bar{u} & \text{(2.25d)}
\end{cases}
$$

We write the fast system (2.25) in vector form

$$\frac{\mathrm{d}}{\mathrm{d}\xi}\phi = A(\xi; \lambda, \varepsilon)\phi \tag{2.26}$$

where $\phi(\xi) = ((\bar{u}(\xi), \bar{p}(\xi), \bar{v}(\xi), \bar{q}(\xi))^T$ and

$$A(\xi; \lambda, \varepsilon) = \begin{pmatrix} 0 & \varepsilon & 0 & 0 \\ \varepsilon^3 \left(\alpha + \lambda - \gamma\, d\, U_h(\xi)^{d-1}\right) & 0 & 2\,\varepsilon\,\sigma\, V_h(\xi) & 0 \\ 0 & 0 & 0 & 1 \\ \frac{V_h(\xi)^2}{U_h(\xi)^2} & 0 & 1 + \lambda - 2\frac{V_h(\xi)}{U_h(\xi)} & 0 \end{pmatrix} \tag{2.27}$$

Since the *V*-component of the stationary pulse decays much faster than its *U*-component, the ratio $\frac{V_h}{U_h}$ is well-defined and converges to zero as $\xi \to \pm\infty$. This results in the constant coefficient matrix

$$A_\infty(\lambda, \varepsilon) = \lim_{|\xi| \to \infty} A(\xi; \lambda, \varepsilon) = \begin{pmatrix} 0 & \varepsilon & 0 & 0 \\ \varepsilon^3 (\alpha + \lambda) & 0 & 0 & 0 \\ 0 & 0 & 0 & 1 \\ 0 & 0 & 1 + \lambda & 0 \end{pmatrix} \tag{2.28}$$

which has eigenvalues

$$\pm\, \Lambda_f = \pm\, \sqrt{1 + \lambda} \quad \text{and} \quad \pm\varepsilon^2 \Lambda_s = \pm\varepsilon^2\, \sqrt{\alpha + \lambda} \tag{2.29}$$

and associated eigenvectors

$$E_{f,\pm} = \left(0, 0, 1, \pm\sqrt{1 + \lambda}\right)^T \quad \text{and} \quad E_{s,\pm} = \left(1, \pm\varepsilon\, \sqrt{\alpha + \lambda}, 0, 0\right)^T. \tag{2.30}$$

The essential spectrum of the linear eigenvalue problem (2.25) therefore is

$$\sigma_{\text{ess}} = \{\lambda \in \mathbb{R}\,|\,\lambda \le \max(-\alpha, -1)\}, \tag{2.31}$$

see [45]. Since $\alpha > 0$, we can conclude that the stability of the pulse (U_h, V_h) is determined by its discrete spectrum.

2.3.1 The Evans function and its decomposition

The Evans function, which is complex analytic outside the essential spectrum – see [3, 45] and the references therein – associated to system (2.25) can be defined by

$$\mathcal{D}(\lambda, \varepsilon) = \det\left[\phi_i(\xi; \lambda, \varepsilon)\right] \tag{2.32}$$

where the functions ϕ_i, $i = 1, 2, 3, 4$ satisfy boundary conditions at $\pm\infty$ (see below) and span the solution space of (2.25). The eigenvalues of (2.26) outside σ_{ess} coincide with the roots of $\mathcal{D}(\lambda, \varepsilon)$, including multiplicities.

Definition 2.3. *A statement of the form '$f(x) \rightsquigarrow c\,g(x)$ as $x \to \infty$' is true whenever the limit $\lim_{x \to \infty} \frac{1}{g(x)} f(x) = c$ exists and is well-defined.*

Lemma 2.4. *For all $\lambda \in \mathbb{C} \setminus \sigma_{\mathrm{ess}}$, there are solutions $\phi_{f,\mathrm{L/R}}(\xi; \lambda, \varepsilon)$ and $\phi_{s,\mathrm{L/R}}(\xi; \lambda, \varepsilon)$ to (2.25) such that the set $\left\{ \phi_{f,\mathrm{L/R}}(\xi; \lambda, \varepsilon), \phi_{s,\mathrm{L/R}}(\xi; \lambda, \varepsilon) \right\}$ spans the solution space of (2.25) and*

$$\phi_{f,\mathrm{L}}(\xi; \lambda, \varepsilon) \rightsquigarrow E_{f,+}\, e^{\Lambda_f \xi} \quad as \quad \xi \to -\infty \tag{2.33a}$$

$$\phi_{f,\mathrm{R}}(\xi; \lambda, \varepsilon) \rightsquigarrow E_{f,-}\, e^{-\Lambda_f \xi} \quad as \quad \xi \to \infty \tag{2.33b}$$

$$\phi_{s,\mathrm{L}}(\xi; \lambda, \varepsilon) \rightsquigarrow E_{s,+}\, e^{\varepsilon^2 \Lambda_s \xi} \quad as \quad \xi \to -\infty \tag{2.33c}$$

$$\phi_{s,\mathrm{R}}(\xi; \lambda, \varepsilon) \rightsquigarrow E_{s,-}\, e^{-\varepsilon^2 \Lambda_s \xi} \quad as \quad \xi \to \infty \tag{2.33d}$$

Moreover, there exist analytic transmission functions $t_{f,+}(\lambda, \varepsilon)$ and $t_{s,+}(\lambda, \varepsilon)$ such that

$$\phi_{f,\mathrm{L}}(\xi; \lambda, \varepsilon) \rightsquigarrow t_{f,+}(\lambda, \varepsilon)\, E_{f,+}\, e^{\Lambda_f \xi} \quad as \quad \xi \to \infty \tag{2.34a}$$

$$\phi_{s,\mathrm{L}}(\xi; \lambda, \varepsilon) \rightsquigarrow t_{s,+}(\lambda, \varepsilon)\, E_{s,+}\, e^{\varepsilon^2 \Lambda_s \xi} \quad as \quad \xi \to \infty \tag{2.34b}$$

where $t_{s,+}(\lambda, \varepsilon)$ is only defined if $t_{f,+}(\lambda, \varepsilon) \neq 0$. These choices, when possible, determine $\phi_{f,\mathrm{L/R}}$ and $\phi_{s,\mathrm{L}}$ uniquely.

Proof. Although the linearised system 2.26 is not identical to its counterpart in [6], exactly the same arguments as in [6] can be applied here. Therefore, we refer to [6] for the details of the proof. □

The Evans function can be determined by taking the limit $\xi \to \infty$ of the determinant of the functions defined in Lemma 2.4, since the Evans function itself does not depend on ξ since the trace of $A(\xi; \lambda, \varepsilon)$ vanishes (Abel's theorem). This yields (see [6])

$$\mathcal{D}(\lambda, \varepsilon) = 4\varepsilon\, t_{f,+}(\lambda, \varepsilon)\, t_{s,+}(\lambda, \varepsilon)\, \sqrt{1 + \lambda}\, \sqrt{\alpha + \lambda} \tag{2.35}$$

Corollary 2.5. *The set of eigenvalues of (2.26) is contained in the union of the sets of roots of $t_{f,+}(\lambda, \varepsilon)$ and $t_{s,+}(\lambda, \varepsilon)$.*

Note that, due to the fact that $t_{s,+}(\lambda, \varepsilon)$ only defined when $t_{f,+}(\lambda, \varepsilon) \neq 0$, the Evans function $\mathcal{D}(\lambda, \varepsilon)$ does not necessarily vanish when $t_{f,+}(\lambda, \varepsilon) = 0$. This is called the 'resolution to the NLEP paradox' in [6, 7]. The roots of $t_{f,+}$ will be discussed later, in section 2.3.3.

2.3.2 The slow solution $\phi_{s,\mathrm{L}}$ outside I_f

To obtain more information about the roots of $t_{s,+}(\lambda, \varepsilon)$, it is necessary to determine the leading order behaviour of $\phi_{s,\mathrm{L}}(\xi; \lambda, \varepsilon)$ in the different coordinate regimes. From Lemma 2.4 we know that $\phi_{s,\mathrm{L}}$ is *slowly growing* in ξ, since its leading order behaviour for both $\xi \to \pm\infty$ is determined by the exponential growth factor $\varepsilon^2 \Lambda_s = O(\varepsilon^2)$. However, the dynamics governing $\phi_{s,\mathrm{L}}$ differ significantly inside and outside the fast spatial region I_f. Based on our knowledge of the homoclinic solution stated in Theorem 2.2, we can infer the form of the matrix $A(\xi; \lambda, \varepsilon)$ both inside and outside I_f:

$$
A_f(\xi; \lambda, \varepsilon) = \begin{pmatrix} 0 & \varepsilon & 0 & 0 \\ \varepsilon^3 \left(\alpha + \lambda - \gamma\, d\, u_*^{d-1} \right) & 0 & 2\,\varepsilon\,\sigma\, v_{h,0}(\xi; u_*, 0) & 0 \\ 0 & 0 & 0 & 1 \\ \frac{v_{h,0}(\xi; u_*, 0)^2}{u_*^2} & 0 & 1 + \lambda - 2\frac{v_{h,0}(\xi; u_*, 0)}{u_*} & 0 \end{pmatrix}
\tag{2.36}
$$

to leading order for $\xi \in I_f$ and

$$
A_s(\xi; \lambda, \varepsilon) = \begin{pmatrix} 0 & \varepsilon & 0 & 0 \\ \varepsilon^3 \left(\alpha + \lambda - \gamma\, d\, u_{h,0}(|\varepsilon^2 \xi| + \mathrm{sgn}(\sigma)\chi_*)^{d-1} \right) & 0 & 0 & 0 \\ 0 & 0 & 0 & 1 \\ 0 & 0 & 1 + \lambda & 0 \end{pmatrix}
\tag{2.37}
$$

for $\xi \notin I_f$ to leading order.

Note that it is the fact that this 'intermediate' slow matrix exists, or better: that it is not identical to $A_\infty(\lambda, \varepsilon)$ (2.28), that distinguishes the 'slowly nonlinear Gierer-Meinhardt problem' from 'slowly linear' problems as the classical Gierer-Meinhardt or Gray-Scott systems. Note also that a intermediate matrix as $A_s(\xi; \lambda, \varepsilon)$ was already encountered in [8], in the study of a system with non-exponential (algebraic) decay.

Lemma 2.6. *Consider the system*

$$
\frac{\mathrm{d}}{\mathrm{d}\xi}\psi = A_s(\xi; \lambda, \varepsilon)\psi
\tag{2.38}
$$

with $A_s(\xi; \lambda, \varepsilon)$ as given in (2.37). There exist solutions $\psi_{f,\pm}(\xi; \lambda, \varepsilon)$ and $\psi_{s,\pm}(\xi; \lambda, \varepsilon)$ which span the solution space of (2.38) for $\xi < -\frac{1}{\sqrt{\varepsilon}}$ and

$$
\psi_{f,+}(\xi; \lambda, \varepsilon) \rightsquigarrow E_{f,+}\, e^{\Lambda_f \xi}, \quad \psi_{s,+}(\xi; \lambda, \varepsilon) \rightsquigarrow E_{s,+}\, e^{\varepsilon^2 \Lambda_s \xi},
\tag{2.39a}
$$

$$
\psi_{f,-}(\xi; \lambda, \varepsilon) \rightsquigarrow E_{f,-}\, e^{-\Lambda_f \xi}, \quad \psi_{s,-}(\xi; \lambda, \varepsilon) \rightsquigarrow E_{s,-}\, e^{-\varepsilon^2 \Lambda_s \xi}
\tag{2.39b}
$$

as $\xi \to -\infty$.

Proof. The same arguments as in the proof of Lemma 2.4 can be used, because $\lim_{\xi \to -\infty} A_s(\xi; \lambda, \varepsilon) = A_\infty(\lambda, \varepsilon)$. □

Since $A(\xi; \lambda, \varepsilon)$ is to leading order equal to $A_s(\xi; \lambda, \varepsilon)$ for $\xi < -\frac{1}{\sqrt{\varepsilon}}$ and both $\phi_{s,L}$ and $\psi_{s,+} \leadsto E_{s,+} e^{\varepsilon^2 \Lambda_s \xi}$ as $\xi \to -\infty$, combining Lemma 2.4 and Lemma 2.6 yields the following Corollary:

Corollary 2.7. *For $\xi < -\frac{1}{\sqrt{\varepsilon}}$, we can write*

$$\phi_{s,L}(\xi; \lambda, \varepsilon) = \psi_{s,+}(\xi; \lambda, \varepsilon)$$

to leading order.

The slow evolution of the $\bar{u}$-component of $\psi_{s,\pm}$ can be written, again using $\chi = \varepsilon^2 \xi$, as

$$\bar{u}_{\chi\chi} - \left(\alpha + \lambda - \gamma d\, u_h(|\chi| + \text{sgn}(\sigma)\chi_*)^{d-1}\right) \bar{u} = 0 \tag{2.40}$$

We can introduce the coordinate transformation

$$
\begin{aligned}
z &= -\frac{1}{\sqrt{\alpha}} \frac{\frac{d}{d\chi} u_{h,0}(\chi - \text{sgn}(\sigma)\chi_*)}{u_{h,0}(\chi - \text{sgn}(\sigma)\chi_*)} \\
&= \frac{1}{\sqrt{\alpha}} \frac{d}{d\chi} \log \frac{1}{u_{h,0}(\chi - \text{sgn}(\sigma)\chi_*)} \\
&= \tanh\left(\tfrac{1}{2}(d-1)\sqrt{\alpha}\,(\chi - \text{sgn}(\sigma)\chi_*)\right)
\end{aligned}
\tag{2.41}
$$

(by (2.16)) for the region $\chi < 0$ to obtain

$$(1 - z^2)\,\bar{u}_{zz} - 2z\,\bar{u}_z + \left(\nu(\nu+1) - \frac{\mu^2}{1-z^2}\right)\bar{u} = 0 \tag{2.42}$$

where

$$\nu = \frac{d+1}{d-1} \tag{2.43a}$$

$$\mu = +\frac{2}{d-1}\sqrt{1 + \frac{\lambda}{\alpha}} \tag{2.43b}$$

where we have chosen the branch cut associated to σ_{ess} such that $\text{Re}\,\mu > 0$; note that $\nu > 1$. Equation (2.42) is the Legendre differential equation: its solutions are the associated Legendre functions $P_\nu^\mu(z)$ and $Q_\nu^\mu(z)$ [1, 2]. Given the symmetry $z \to -z$ of the equation, we choose the basis of the solution space to be $P_\nu^\mu(\pm z)$. The limit

$\chi \to -\infty$ corresponds to the limit $z \to -1$. Taking into account the normalisation of $\psi_{s,+}$ from Lemma 2.6, the correct expression for the $\bar{u}$-component of $\psi_{s,+}$ is

$$\bar{u}(\chi) = \Gamma(1 + \mu)\, e^{\Lambda_s \operatorname{sgn}(\sigma)\chi_*}\, P_\nu^{-\mu}\left(-z(\chi)\right) \tag{2.44}$$

such that

$$\lim_{\chi \uparrow 0} \bar{u}(\chi) = \Gamma(1 + \mu)\, e^{\Lambda_s \operatorname{sgn}(\sigma)\chi_*}\, P_\nu^{-\mu}\left(z_*\right) \tag{2.45}$$

where we define

$$z_* = \operatorname{sgn}(\sigma)\, \tanh\left(\tfrac{1}{2}(d - 1)\,\sqrt{\alpha}\,\chi_*\right) \tag{2.46}$$

We can express z_* in terms of u_* using equation (2.15): integrating once yields

$$u_\chi^2 = \alpha\, u^2 - \frac{2\gamma}{d + 1} u^{d+1} \tag{2.47}$$

so, by equation (2.41)

$$z^2 = \frac{1}{\alpha} \frac{u_\chi^2}{u^2} = 1 - \frac{2\gamma}{\alpha(d + 1)} u^{d-1} \tag{2.48}$$

hence

$$\alpha\left(1 - z_*^2\right) = \frac{2\gamma}{d + 1} u_*^{d-1} = \alpha - 9\sigma^2 u_*^2 \tag{2.49}$$

by equation (2.21); from this, we conclude that

$$z_* = \frac{3\,\sigma}{\sqrt{\alpha}}\, u_*. \tag{2.50}$$

Note that z_* inherits the sign of σ since χ_* is chosen to be positive, see section 2.2.1.

Lemma 2.8. *Let $\bar{u}_s(\xi; \lambda, \varepsilon)$ be the $\bar{u}$-component of $\phi_{s,\mathrm{L}}(\xi; \lambda, \varepsilon)$ as defined in Lemma 2.4. Then*

$$\bar{u}_s(\xi) = \Gamma(1 + \mu)\, e^{\Lambda_s \operatorname{sgn}(\sigma)\chi_*}\, P_\nu^{-\mu}\left(z_*\right) + O(\varepsilon\sqrt{\varepsilon}) \quad \text{for} \quad \xi \in I_f. \tag{2.51}$$

Moreover, there are two transmission functions $t_{s,+}(\lambda, \varepsilon)$ and $t_{s,-}(\lambda, \varepsilon)$ such that

$$\phi_{s,\mathrm{L}}(\xi; \lambda, \varepsilon) = t_{s,+}(\lambda, \varepsilon)\,\psi_{s,-}(-\xi; \lambda, \varepsilon) + t_{s,-}(\lambda, \varepsilon)\,\psi_{s,+}(-\xi; \lambda, \varepsilon) \quad \text{for} \quad \xi > \frac{1}{\sqrt{\varepsilon}} \tag{2.52}$$

up to exponentially small terms in ξ, where $t_{s,+}$ was already introduced in Lemma 2.4.

Proof. The $\bar{u}$-component of $\phi_{s,\mathrm{L}}$ is constant on I_f, since both $\frac{\mathrm{d}}{\mathrm{d}\xi}\bar{u}_s$ and $\frac{\mathrm{d}}{\mathrm{d}\xi}\bar{p}_{s,+}$ are asymptotically small on I_f. Therefore, we can determine its leading order value using Corollary 2.7 and (2.45). The matrix A_s as defined in (2.37) is symmetric in ξ. For the region $\xi > \frac{1}{\sqrt{\varepsilon}}$ we can therefore use the same $\psi_{f,\pm}$ and $\psi_{s,\pm}$ from Lemma 2.6 as a basis for the solution space in this region, under the reflection $\xi \to -\xi$. The role of $\psi_{s,+}$ and $\psi_{s,-}$ is reversed compared to the interval $\xi < -\frac{1}{\sqrt{\varepsilon}}$: we see that $\psi_{s,-}(-\xi)$ grows (slowly) exponentially as $\xi \to \infty$, whereas $\psi_{s,+}(-\xi)$ has an exponential (slow) decay under the same limit. The normalisation of $\phi_{s,\mathrm{L}}$ for $\xi \to \infty$, which by Lemma 2.4 introduces $t_{s,+}(\lambda,\varepsilon)$ in (2.52), does not exclude the possibility that for $\xi > \frac{1}{\sqrt{\varepsilon}}$, $\phi_{s,\mathrm{L}}$ has components which *decay* (slowly) as $\xi \to \infty$. Therefore, we write the leading order expression of $\phi_{s,\mathrm{L}}$ in this region as a linear combination of a slowly increasing and a slowly decreasing component, and introduce $t_{s,-}(\lambda,\varepsilon)$ to measure the decreasing component. A term containing the fast decreasing component is omitted, since for $\xi > \frac{1}{\sqrt{\varepsilon}}$ this would only give an exponentially small correction to the result in (2.52). $\qquad\square$

Based on the results of Lemma 2.8, we have

$$\lim_{\chi\downarrow 0}\bar{u}_s(\chi) = \Gamma(1+\mu)\left[t_{s,+}(\lambda,\varepsilon)\,P_\nu^{-\mu}(-z_*) + t_{s,-}(\lambda,\varepsilon)\,P_\nu^{-\mu}(z_*)\right] \qquad (2.53)$$

to leading order.

Corollary 2.9. *Combining equations* (2.51) *and* (2.53) *yields*

$$t_{s,+}(\lambda,\varepsilon)\,P_\nu^{-\mu}(-z_*) + t_{s,-}(\lambda,\varepsilon)\,P_\nu^{-\mu}(z_*) = P_\nu^{-\mu}(z_*) + O(\varepsilon\sqrt{\varepsilon}) \qquad (2.54)$$

to leading order.

This gives a (first) relation between $t_{s,+}(\lambda,\varepsilon)$ and $t_{s,-}(\lambda,\varepsilon)$.

2.3.3 The fast components of $\phi_{s,\mathrm{L}}$ inside I_f

Since $\bar{u}_s(\xi;\lambda,\varepsilon)$ is constant to leading order for $\xi \in I_f$ (see Lemma 2.8), we can represent it by its value at $0 \in I_f$. Moreover, the equation for the $\bar{v}$-component in (2.25) decouples and yields an inhomogeneous Sturm-Liouville problem,

$$\bar{v}_{\xi\xi} - \left((1+\lambda) - \frac{2}{u_*}v_{h,0}(\xi;u_*,0)\right)\bar{v} = \frac{1}{u_*^2}v_{h,0}(\xi;u_*,0)^2\,\bar{u}_s(0) \qquad (2.55)$$

where we used that $u_h(\xi) = u_*$ and $v_h(\xi) = v_{h,0}(\xi;u_*,0)$ for $\xi \in I_f$ to leading order (see Theorem 2.2). Based on the slow behaviour of $\phi_{s,\mathrm{L}}$ determined in Lemmas 2.4

and 2.8, we observe that the solution $\bar{v}$ of (2.55) must extinguish as $\xi \to \partial I_f$, which implies that $\bar{v}$ must decay exponentially fast in ξ.

By the nature of the Gierer-Meinhardt equation (2.4) and its 'slow nonlinearity' the problem can be solved exactly along the same lines as done in section 2.3.2 for the slow problem. First, we introduce a coordinate transformation similar to (2.41),

$$\zeta = -\frac{\frac{d}{d\xi} v_{h,0}(\xi; u_*, 0)}{v_{h,0}(\xi; u_*, 0)} = \frac{d}{d\xi} \log \frac{1}{v_{h,0}(\xi; u_*, 0)} = \tanh\left(\tfrac{1}{2}\xi\right) \tag{2.56}$$

using (2.13). In this coordinate, v_h can be written as

$$v_h(\zeta; u_*, 0) = \frac{3 u_*}{2}\left(1 - \zeta^2\right) \tag{2.57}$$

and equation (2.55) is transformed to

$$(1 - \zeta^2)\,\bar{v}_{\zeta\zeta} - 2\,\zeta\,\bar{v}_\zeta + \left(12 - \frac{4(1 + \lambda)}{1 - \zeta^2}\right) \bar{v} = 9\,\bar{u}_s(0)\,(1 - \zeta^2) \tag{2.58}$$

and $I_f = \{\zeta \in \mathbb{R} \,|\,|\zeta| < 1\,\}$ up to exponentially small terms, compare (2.17). Its homogeneous reduction

$$(1 - \zeta^2)\,\bar{v}_{\zeta\zeta} - 2\,\zeta\,\bar{v}_\zeta + \left(12 - \frac{4(1 + \lambda)}{1 - \zeta^2}\right) \bar{v} = 0 \tag{2.59}$$

can again be solved using associated Legendre functions; it is a special case ($\alpha = 1$, $d = 2$) of the slow eigenvalue problem (2.42).

It should be noted that there is a crucial difference between (2.42) and (2.58). The slow equation (2.42) is only defined on part of the 'full' domain: $z \in (-1, z_*) \subset (-1, 1)$. Therefore, the eigenvalues of (2.42) do not yield direct implications for the stability of the pulse (U_h, V_h). This is very different from the fast system (2.58). It has three eigenvalues; its corresponding eigenfunctions are

$$\lambda_f^{(0)} = \frac{5}{4}, \quad \bar{v}_f^{(0)}(\zeta) = \left(1 - \zeta^2\right)^{\frac{3}{2}} \tag{2.60a}$$

$$\lambda_f^{(1)} = 0, \quad \bar{v}_f^{(1)}(\zeta) = \zeta\left(1 - \zeta^2\right) = -\frac{2}{3u_*}\frac{d\zeta}{d\xi}\frac{d}{d\zeta}v_h(\zeta; u_*, 0) \tag{2.60b}$$

$$\lambda_f^{(2)} = -\frac{3}{4}, \quad \bar{v}_f^{(2)}(\zeta) = \left(\zeta^2 - \tfrac{1}{5}\right)\sqrt{1 - \zeta^2} \tag{2.60c}$$

Referring to [6], we recall that the roots of $t_{f,+}(\lambda, \varepsilon)$ are to leading order given by the eigenvalues of (2.59), so we have the following Lemma:

Lemma 2.10. *There are unique $\lambda^{(i)}(\varepsilon) \in \mathbb{R}$ such that $\lim_{\varepsilon \to 0} \lambda^{(i)}(\varepsilon) = \lambda_f^{(i)}$ and $t_{f,+}(\lambda^{(i)}(\varepsilon), \varepsilon) = 0$ with multiplicity 1 for $i = 0, 1, 2$.*

Proof. See [6]. $\square$

Hence, the eigenvalues of (2.59) are to leading order zeroes of the fast component of the Evans function $\mathcal{D}(\lambda, \varepsilon)$ given in (2.35) and thus in principle candidates for being zeroes of the full Evans function.

For all $\lambda \in \mathbb{C} \setminus \sigma_{\text{ess}}$, the solution space of (2.59) is spanned by the associated Legendre functions

$$\bar{v}_\pm(\zeta; \lambda) = c_\pm(\lambda) P_3^{-2\sqrt{1+\lambda}}(\pm\zeta); \qquad \lim_{\zeta \to \pm 1} \bar{v}_\pm(\zeta; \lambda) = 0 \tag{2.61}$$

where we normalise $\bar{v}_\pm$ (i.e. choose $c_\pm$) such that their Wronskian is given by

$$W(\bar{v}_-, \bar{v}_+)(\zeta; \lambda) = \frac{1}{1 - \zeta^2} \tag{2.62}$$

which implies that

$$c_+(\lambda) c_-(\lambda) = -\frac{1}{2} \Gamma\left(4 + 2\sqrt{1+\lambda}\right) \Gamma\left(-3 + 2\sqrt{1+\lambda}\right) \tag{2.63}$$

Indeed, the expression in (2.63) has poles at $\lambda = \lambda_f^{(i)}$, $i = 0, 1, 2$. This is due to the fact that $\bar{v}_\pm(\zeta; \lambda)$ cannot span the two-dimensional solution space for $\lambda = \lambda_f^{(i)}$. Since we have normalised the Wronskian (2.62), this is now encoded in the values of $c_\pm(\lambda)$.

We know that the inhomogeneous equation (2.58) has a unique bounded solution $\bar{v}_{\text{in}}(\xi; \lambda)$ for all $\lambda \in \mathbb{C} \setminus \sigma_{\text{ess}}$ and $\lambda \neq \lambda_f^{(0,1,2)}$. It can be determined using the Green's function

$$G(\zeta, s; \lambda) = \begin{cases} \dfrac{\bar{v}_-(s; \lambda)\,\bar{v}_+(\zeta; \lambda)}{W(\bar{v}_-, \bar{v}_+)(s; \lambda)\,(1 - s^2)} & s < \zeta \\[3mm] \dfrac{\bar{v}_-(\zeta; \lambda)\,\bar{v}_+(s; \lambda)}{W(\bar{v}_-, \bar{v}_+)(s; \lambda)\,(1 - s^2)} & s > \zeta \end{cases} \tag{2.64}$$

so that

$$\bar{v}_{\text{in}}(\zeta; \lambda) = \int_{-1}^{1} 9\,\bar{u}_s(0)\,(1 - s^2)\,G(\zeta, s; \lambda)\,\mathrm{d}s \tag{2.65}$$

$$= 9\,\bar{u}_s(0)\left[\bar{v}_+(\zeta; \lambda)\int_{-1}^{\zeta}(1 - s^2)\,\bar{v}_-(s; \lambda)\,\mathrm{d}s + \bar{v}_-(\zeta; \lambda)\int_{\zeta}^{1}(1 - s^2)\,\bar{v}_+(s; \lambda)\,\mathrm{d}s\right]$$

Note that the inhomogeneous term in (2.58) is only orthogonal to the eigenfunction corresponding to $\lambda_f^{(1)} = 0$; for the other two eigenvalues the solvability condition

$$\int_{-1}^{1} 9\,\bar{u}_s(0)\,(1 - \zeta^2)\,\bar{v}_f^{(i)}(\zeta)\,\mathrm{d}\zeta = 0 \quad i = 0, 1, 2 \tag{2.66}$$

is not satisfied since both $\bar{v}_f^{(0,2)}(\zeta)$ and $9(1 - \zeta^2)$ are even functions in ζ. This means that $\bar{v}_{\mathrm{in}}$ as a function of λ has a simple pole at $\lambda_f^{(0)}$ and $\lambda_f^{(2)}$, and is smooth at $\lambda_f^{(1)} = 0$.

To summarise this section, the resulting expression of $\bar{v}_{\mathrm{in}}$ is restated in the following Lemma:

Lemma 2.11. *The unique solution* $\bar{v}_{in}(\zeta; \lambda)$ *to equation* (2.58) *is given by*

$$\bar{v}_{\mathrm{in}}(\zeta; \lambda) = 9\,\bar{u}_s(0) \left[\bar{v}_+(\zeta; \lambda) \int_{-1}^{\zeta} (1 - s^2)\,\bar{v}_-(s; \lambda)\,\mathrm{d}s + \bar{v}_-(\zeta; \lambda) \int_{\zeta}^{1} (1 - s^2)\,\bar{v}_+(s; \lambda)\,\mathrm{d}s \right] \tag{2.67}$$

with $v_\pm(\zeta; \lambda)$ *as defined in* (2.61) *and subject to condition* (2.63).

2.3.4   The slow transmission function $t_{s,+}(\lambda, \varepsilon)$

In section 2.3.2 we studied $\phi_{s,\mathrm{L}}$ outside I_f and in section 2.3.3 we considered its fast dynamics inside I_f. However, we did not yet combine these results.
Using (2.25), we see that

$$\begin{aligned}
\bar{u}_{\xi\xi} &= -2\,\varepsilon^2 \sigma\, V_h(\xi)\,\bar{v} + O(\varepsilon^4) \\
&= -2\,\varepsilon^2 \sigma\, v_{h,0}(\xi; u_*, 0)\,\bar{v}_{\mathrm{in}}\,(\zeta(\xi); \lambda)
\end{aligned} \tag{2.68}$$

to leading order in I_f. Thus, the total change of $\bar{u}_\xi$ over I_f is given by

$$\begin{aligned}
\Delta_\xi \bar{u}_\xi &= \int_{I_f} u_{\xi\xi}\,\mathrm{d}\xi \\
&= -2\,\varepsilon^2 \sigma \int_{-\infty}^{\infty} v_{h,0}(\xi; u_*, 0)\,\bar{v}_{\mathrm{in}}\,(\zeta(\xi); \lambda)\,\mathrm{d}\xi \\
&= -2\,\varepsilon^2 \sigma \int_{-1}^{1} v_{h,0}\,(\xi(\zeta); u_*, 0)\,\bar{v}_{\mathrm{in}}\,(\zeta; \lambda)\,\frac{2\,\mathrm{d}\zeta}{1 - \zeta^2} \\
&= -2\,\varepsilon^2 \sigma \int_{-1}^{1} \frac{3\,u_*}{2}\,(1 - \zeta^2)\,\bar{v}_{\mathrm{in}}\,(\zeta; \lambda)\,\frac{2\,\mathrm{d}\zeta}{1 - \zeta^2} \\
&= -6\,\varepsilon^2 \sigma\,u_* \int_{-1}^{1} \bar{v}_{\mathrm{in}}\,(\zeta; \lambda)\,\mathrm{d}\zeta := \Delta_f
\end{aligned} \tag{2.69}$$

all to leading order. Using the expression for $\bar{v}_{\text{in}}(\zeta; \lambda)$ from Lemma 2.11 and the symmetry in ζ between $\bar{v}_+$ and $\bar{v}_-$, this can be rewritten as

$$\Delta_f = -108\,\varepsilon^2 \sigma\, u_* \,\bar{u}_s(0) \int_{-1}^{1} \int_{-1}^{\zeta} \bar{v}_+(\zeta; \lambda)\, \bar{v}_-(s; \lambda)(1 - s^2)\, \mathrm{d}s\, \mathrm{d}\zeta \tag{2.70}$$

The desired coupling between the slow and fast dynamics can now be obtained by realising that this change in $\bar{u}_\xi$ should match with the slow behaviour of $\phi_{s,\mathrm{L}}$ outside I_f. Using Corollary 2.7 and Lemma 2.8,

$$\begin{aligned}
\Delta_f = \Delta_\xi \bar{u}_\xi &= \bar{u}_\xi\left(\frac{1}{\sqrt{\varepsilon}}\right) - \bar{u}_\xi\left(-\frac{1}{\sqrt{\varepsilon}}\right) \\
&= \varepsilon^2\,\Gamma(1 + \mu)\frac{\mathrm{d}z}{\mathrm{d}\chi}\frac{\mathrm{d}}{\mathrm{d}z}\left[t_{s,+}\,P_\nu^{-\mu}(-z) + t_{s,-}\,P_\nu^{-\mu}(z)\right]_{z=z_*} \\
&\quad - \varepsilon^2\Gamma(1 + \mu)\frac{\mathrm{d}z}{\mathrm{d}\chi}\frac{\mathrm{d}}{\mathrm{d}z}\left[P_\nu^{-\mu}(-z)\right]_{z=-z_*} \\
&= \varepsilon^2\,\Gamma(1 + \mu)\frac{\mathrm{d}z}{\mathrm{d}\chi}\frac{\mathrm{d}}{\mathrm{d}z}\left[t_{s,+}\,P_\nu^{-\mu}(-z) + (t_{s,-} + 1)\,P_\nu^{-\mu}(z)\right]_{z=z_*} \tag{2.71}
\end{aligned}$$

to leading order. Together, expressions (2.69) and (2.71) can be used to obtain a second relation between the two transmission functions $t_{s,\pm}(\lambda, \varepsilon)$, see Corollary 2.9. Thus, we can eliminate $t_{s,-}$ and obtain a leading order expression for $t_{s,+}$:

$$t_{s,+}\,\varepsilon^2\frac{\mathrm{d}z}{\mathrm{d}\chi}\frac{\mathrm{d}}{\mathrm{d}z}\left[P_\nu^{-\mu}(-z) - \frac{P_\nu^{-\mu}(-z_*)}{P_\nu^{-\mu}(z_*)}P_\nu^{-\mu}(z)\right]_{z=z_*} = \frac{\Delta_f}{\Gamma(1 + \mu)} - 2\,\varepsilon^2\frac{\mathrm{d}z}{\mathrm{d}\chi}\frac{\mathrm{d}}{\mathrm{d}z}\left[P_\nu^{-\mu}(z)\right]_{z=z_*}$$

so that, using the Wronskian $W\left(P_\nu^{-\mu}(z), P_\nu^{-\mu}(-z)\right)(z_*)$,

$$t_{s,+} = P_\nu^{-\mu}(z_*)\frac{\frac{\Delta_f}{\Gamma(1+\mu)} - 2\,\varepsilon^2\frac{\mathrm{d}z}{\mathrm{d}\chi}\frac{\mathrm{d}}{\mathrm{d}z}\left[P_\nu^{-\mu}(z)\right]_{z=z_*}}{\varepsilon^2\frac{\mathrm{d}z}{\mathrm{d}\chi}W\left(P_\nu^{-\mu}(z), P_\nu^{-\mu}(-z)\right)(z_*)} \tag{2.72}$$

which, using (2.69) and (2.50), leads to the following Theorem:

Theorem 2.12. *Let $\varepsilon > 0$ be sufficiently small. The function $t_{s,+}(\lambda, \varepsilon)$ is meromorphic as a function of λ outside σ_{ess}. It has simple poles at $\lambda^{(0)}(\varepsilon)$ and $\lambda^{(2)}(\varepsilon)$ and is analytic elsewhere. The leading order behaviour of $t_{s,+}$ is given by*

$$t_{s,+}(\lambda, 0) = P_\nu^{-\mu}(z_*)\frac{\frac{\sqrt{\alpha}\,z_*}{\Gamma(1+\mu)}\int_{-1}^{1}\bar{v}_{\text{in}}(\zeta; \lambda)\,\mathrm{d}\zeta + \frac{\mathrm{d}z}{\mathrm{d}\chi}\frac{\mathrm{d}}{\mathrm{d}z}\left[P_\nu^{-\mu}(z)\right]_{z=z_*}}{-\frac{1}{2}\frac{\mathrm{d}z}{\mathrm{d}\chi}W\left(P_\nu^{-\mu}(z), P_\nu^{-\mu}(-z)\right)(z_*)} \tag{2.73}$$

The nontrivial roots of the Evans function $\mathcal{D}(\lambda, \varepsilon)$ coincide with the roots of $t_{s,+}(\lambda, \varepsilon)$. These roots determine the stability of the pulse $(U_h(\xi), V_h(\xi))$.

Note that it is clear from (2.73) that $t_{s,+}$ inherits the poles of $\bar{v}_{\text{in}}$ at $\lambda = \lambda_f^{(0,2)}$.

The roots of the Evans function $\mathcal{D}(\lambda, \varepsilon)$ outside σ_{ess} are given by the roots of the product $t_{f,+}(\lambda, \varepsilon) \, t_{s,+}(\lambda, \varepsilon)$. Based on orthogonality arguments, we have established that $t_{s,+}(\lambda, 0)$ has simple poles at $\lambda = \lambda_f^{(0,2)}$, see the solvability condition (2.66). These coincide with the (simple) roots of $t_{f,+}(\lambda, 0)$ (see Lemma 2.10), so the Evans function will *not* necessarily be zero at these values of λ. Moreover, since the Evans function is analytic, this statement continues to hold for $\varepsilon > 0$. Note that $\lambda = 0$ is always a trivial eigenvalue for system (2.25), with eigenfunction $\frac{d}{d\xi}(U_h(\xi), V_h(\xi))$; it does not appear as a zero of $t_{s,+}(\lambda, 0)$.

2.4 Pulse stability: results

The purpose of this section is to analyse the roots of $t_{s,+}(\lambda, 0)$ as given in Theorem 2.12. The Wronskian in the denominator is always finite for $-1 < z_* < 1$ because the underlying differential equation (2.42) is only singular at $z = -1, 1$. We can therefore focus at the numerator, which is zero whenever $P_\nu^{-\mu}(z_*) = 0$ or

$$\frac{\sqrt{\alpha}\, z_*}{\Gamma(1+\mu)} \int_{-1}^{1} \bar{v}_{\text{in}}\,(\zeta; \lambda)\ \mathrm{d}\zeta + \frac{\mathrm{d}z}{\mathrm{d}\chi} \frac{\mathrm{d}}{\mathrm{d}z}\left[P_\nu^{-\mu}(z)\right]_{z=z_*} = 0 \qquad (2.74)$$

Using

$$\left[\frac{\mathrm{d}z}{\mathrm{d}\chi}\right]_{z=z_*} = \frac{1}{2}(d-1)\sqrt{\alpha}(1-z_*^2) \qquad (2.75)$$

and

$$\frac{\mathrm{d}}{\mathrm{d}z}\left[P_\nu^{-\mu}(z)\right]_{z=z_*} = \frac{1}{1-z_*^2}\left((\nu-\mu)P_{\nu-1}^{-\mu}(z_*) - z_*\nu P_\nu^{-\mu}(z_*)\right) \qquad (2.76)$$

equation (2.74) can be rewritten into

$$18\, z_*\, P_\nu^{-\mu}(z_*) \int_{-1}^{1} \int_{-1}^{\zeta} \bar{v}_+(\zeta; \lambda)\, \bar{v}_-(s; \lambda)(1-s^2)\,\mathrm{d}s\,\mathrm{d}\zeta$$

$$+ \frac{1}{2}(d-1)\left((\nu-\mu)P_{\nu-1}^{-\mu}(z_*) - z_*\nu P_\nu^{-\mu}(z_*)\right) = 0, \qquad (2.77)$$

using (2.70) and recalling that $\bar{u}_s(0) = \Gamma(1+\mu)\, P_\nu^{-\mu}(z_*)$ to leading order by Lemma 2.8. Since this equation is only relevant if $P_\nu^{-\mu}(z_*) \neq 0$, we divide by $z_*\, P_\nu^{-\mu}(z_*)$ (note that $z_* \neq 0$ since $u_* \neq 0$, see (2.50)) to obtain the following:
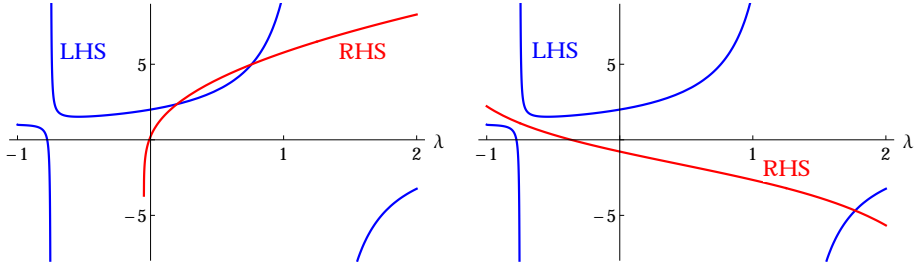
Figure 2.7: Here, LHS(λ) is plotted in blue for $\lambda \in (-1, 2)$; the red line is the graph of RHS($\frac{\lambda}{\alpha}; \nu, z_*$). In the left plot $\alpha = 0.05$, $\nu = 2$ and $z_* = 0.75$. In the right plot $\alpha = 1.5$, $\nu = 2$ and $z_* = -0.60$; the right plot is a illustration of the statement in Theorem 2.14.

Corollary 2.13. *If $P_\nu^{-\mu}(z_*) \neq 0$, the nontrivial roots of the Evans function $\mathcal{D}(\lambda, \varepsilon)$ as defined in* (2.35) *are given to leading order by the solutions of the equation*

$$18 \int_{-1}^{1} \int_{-1}^{\zeta} \bar{v}_+(\zeta; \lambda) \, \bar{v}_-(s; \lambda)(1 - s^2) \, \mathrm{d}s \, \mathrm{d}\zeta = \frac{1}{\nu - 1} \left(\nu - (\nu - \mu) \frac{P_{\nu-1}^{-\mu}(z_*)}{z_* \, P_\nu^{-\mu}(z_*)} \right), \quad (2.78)$$

with μ, ν, z_* as given in (2.43) *and* (2.50).

The left-hand side of this equation is a function of λ only; all parameters are contained in the right-hand side. Moreover, we have restricted our parameter space $(\alpha, \gamma, \sigma, d) \in \mathbb{R}_{>0} \times \mathbb{R}_{>0} \times \mathbb{R} \setminus \{0\} \times (1, \infty)$, a union of two orthants in $\mathbb{R}^4$ to $(\alpha, \nu, z_*) \in \mathbb{R}_{>0} \times (1, \infty) \times (-1, 0) \cup (0, 1)$, the union of two (semi-compact) slabs in $\mathbb{R}^3$.

It is useful to define the left- and right-hand sides of equation (2.78) separately:

$$\text{LHS}(\lambda) = 18 \int_{-1}^{1} \int_{-1}^{\zeta} \bar{v}_+(\zeta; \lambda) \, \bar{v}_-(s; \lambda)(1 - s^2) \, \mathrm{d}s \, \mathrm{d}\zeta \qquad (2.79)$$

$$\text{RHS}(\tfrac{\lambda}{\alpha}; \nu, z_*) = \frac{1}{\nu - 1} \left(\nu - (\nu - \mu(\tfrac{\lambda}{\alpha}; \nu)) \frac{P_{\nu-1}^{-\mu(\frac{\lambda}{\alpha};\nu)}(z_*)}{z_* \, P_\nu^{-\mu(\frac{\lambda}{\alpha};\nu)}(z_*)} \right) \qquad (2.80)$$

In Figure 2.7, the graphs of LHS(λ) and RHS($\frac{\lambda}{\alpha}; \nu, z_*$) are plotted for real values of λ. It is worthwhile to note that LHS(λ) $= 288 \, \mathcal{R}(P = \sqrt{1 + \lambda}; 2, 2)$ as used in [6].

2.4.1 Immediate results: $\sigma < 0$ and $\gamma \downarrow 0$

In this subsection we present the first 'immediate' implications of the developed theory for the stability of the pulse (U_h, V_h).

Theorem 2.14. *Let $\varepsilon > 0$ be sufficiently small. For all $\sigma < 0$, there is a real zero $\lambda_{\text{pos}} > \lambda_f^{(0)} > 0$ of the Evans function associated with the stability problem* (2.25).

Proof. As $\lambda \to \infty$, from (2.43) we infer that $\mu \gg \nu$ such that the ratio $\frac{P_{\nu-1}^{-\mu}(z_*)}{P_\nu^{-\mu}(z_*)} \to 1$. Therefore, RHS$(\frac{\lambda}{\alpha}; \nu, z_*) \rightsquigarrow \frac{\mu}{\nu-1} \frac{1}{z_*} \rightsquigarrow \frac{1}{3\sigma u_*} \sqrt{\lambda}$ as $\lambda \to \infty$. Using an equivalent argument to that in [15], Lemma 4.1 (ii), one can show that LHS(λ) increases monotonically (from $-\infty$) to zero for $\lambda > \lambda_f^{(0)}$. Therefore, there is a $\lambda > \frac{5}{4}$ for which LHS and RHS intersect and which therefore solves (2.78) for all parameter values when $\sigma < 0$, see Figure 2.7. $\qquad\square$

Corollary 2.15. *A pulse with a double hump in the U-component, as shown in Figure 2.1b, is always unstable.*

A direct consequence of the above Corollary is that in order to obtain any stability result, we have to confine ourselves to the interval $0 < z_* < 1$ since sgn$(z_*) = $ sgn(σ), see (2.50). It would be beneficial to a complete understanding of the linear stability of the constructed pulse if more would be known about the zeroes of $P_\nu^{-\mu}(z_*)$. However, while some information can be obtained regarding the number of zeroes of $P_\nu^{-\mu}(z_*)$ for real values of μ (see [1], the general case will be treated in chapter 3, section 3.5.1), the authors are not aware of any general analytic expressions concerning zeroes of $P_\nu^{-\mu}(z_*)$ for complex μ. Notwithstanding, direct numerical evaluation of $P_\nu^{-\mu}(z_*)$ for a broad parameter range has led to the following Conjecture:

Conjecture 2.16. *For all $\lambda \in \mathbb{C}$ for which* Re $\lambda > 0$, $P_\nu^{-\mu}(z_*) \neq 0$ *for all $0 < z_* < 1$. Moreover, for* Im $\lambda \neq 0$, $P_\nu^{-\mu}(z_*) \neq 0$ *for all $0 < |z_*| < 1$.*

Based on this observation, the study of linear stability of the pulse can be confined to the study of solutions of (2.78). Moreover, any additional eigenvalues originating from zeroes of $P_\nu^{-\mu}(z_*)$ would occur on the real line and be negative. Note that in the following results, this Conjecture is not needed.

Equation (2.80) can be studied for different parameter values (and limits thereof) to obtain information about the pulse spectrum. Another direct result can be obtained by taking the limit $\gamma \downarrow 0$ to remove the influence of the slow nonlinearity in (2.7) and obtain the classical Gierer-Meinhardt equations. As $\gamma \downarrow 0$, $u_* \to \frac{\sqrt{\alpha}}{3|\sigma|}$ (see (2.21)) so $z_* \to$ sgn(σ) using (2.50). Note that, while the limit $\gamma \downarrow 0$ reduces equation (2.7) to the 'classical' Gierer-Meinhardt equation –where the slow evolution in U is linear, yielding a 'simple' exponential instead of an associated Legendre function– the coordinate z is ill-defined for $\gamma = 0$, see (2.41) in relation to (2.40). Therefore,

some of the expressions in the following will still depend on ν, while ν disappears from (2.7) as $\gamma \downarrow 0$. Since

$$P_\nu^{-\mu}(z_*) \rightsquigarrow \frac{1}{\Gamma(1+\mu)} \left(\frac{1-z}{2}\right)^{\frac{\mu}{2}} \quad \text{as} \quad z_* \to 1 \tag{2.81a}$$

$$P_\nu^{-\mu}(z_*) \rightsquigarrow \frac{\Gamma(\mu)}{\Gamma(\mu-\nu)\Gamma(1+\mu+\nu)} \left(\frac{1+z}{2}\right)^{-\frac{\mu}{2}} \quad \text{as} \quad z_* \to -1 \tag{2.81b}$$

(see [1, 2]), this means that

$$\lim_{\gamma \downarrow 0} \text{RHS}(\tfrac{\lambda}{\alpha}; \nu, z_*(\alpha, \gamma, \sigma, d)) = \lim_{z_* \to \text{sgn}(\sigma)} \text{RHS}(\tfrac{\lambda}{\alpha}; \nu, z_*) = \text{sgn}(\sigma) \frac{\mu}{\nu - 1}$$

$$= \text{sgn}(\sigma) \sqrt{1 + \frac{\lambda}{\alpha}} \tag{2.82}$$

Moreover, $P_\nu^{-\mu}(z_*)$ can be written as $P_\nu^{-\mu}(z_*) = \left(\frac{1-z_*}{2}\right)^{\frac{\mu}{2}} F(z_*)$ where $F(z)$ has a regular expansion (see [1, 2]). Near $z = 1$, $F(z)$ can be expanded as $F(z) = \sum_{k=0}^{\infty} a_k \left(\frac{1-z}{2}\right)^k$, with

$$a_k = \sum_{j=0}^{\infty} \frac{\left(\frac{\mu}{2}\right)_{k-j} (-\nu)_j (\nu + 1)_j}{\Gamma(1 + j + \mu)(k - j)! \, j!} \tag{2.83}$$

Since $a_0 = \frac{1}{\Gamma(1+\mu)} \neq 0$ for all μ considered since $\text{Re}\,\mu > 0$ and the limit $\gamma \downarrow 0$ only influences the value of z_*, it follows that $P_\nu^{-\mu}(z_*)$ does not have any zeroes asymptotically close to, but different from $z_* = 1$. The same reasoning applies for $z_* \to -1$. Therefore, in this particular limit, we do not need to appeal to Conjecture 2.16. This yields the following Lemma:

Lemma 2.17. *For $\gamma \downarrow 0$, the nontrivial pulse spectrum is to leading order given by the roots of the equation*

$$18 \int_{-1}^{1} \int_{-1}^{\zeta} \bar{v}_+(\zeta; \lambda) \, \bar{v}_-(s; \lambda)(1 - s^2) \, ds \, d\zeta = \text{sgn}(\sigma) \sqrt{1 + \frac{\lambda}{\alpha}} \tag{2.84}$$

which, for $\sigma > 0$, coincides with the corresponding expression found in [6] for the classical Gierer-Meinhardt equations.

2.4.2 Varying α and investigating the role of d

As the parameter α occurs in both the expression for μ and z_* (see (2.43) and (2.50)), it is worthwhile to study the behaviour of $\text{RHS}(\lambda)$ as α changes to obtain α-parametrised

eigenvalue orbits. Moreover, the parameter α is the classical parameter to be varied, as α plays the role of μ in the classical Gierer-Meinhardt equations. In Figure 2.3, left, the (complex) solutions to equation (2.78) are plotted as a function of increasing α for $d = 2$, $\gamma = 2$ and $\sigma = 1$. The eigenvalues cross the imaginary axis for $\alpha \approx 0.83083$ and converge to $\lambda \approx -0.990268 \pm 0.147318\,i$ as $\alpha \to \infty$. The same plot, now for $d = 5$, is given in Figure 2.3, middle and right. The eigenvalues initially display the same behaviour as in the case $d = 2$; here, the imaginary axis is crossed for $\alpha \approx 0.36654$. A clear change of behaviour can be seen for increasing α; whereas the orbit seems to converge to a complex conjugate pair of stable limit points for $d = 2$, for $d = 5$ the orbits crosses the imaginary axis again for $\alpha \approx 90.634$ and yields a pair of unstable eigenvalues as $\alpha \to \infty$. Note that this behaviour is essentially different from the equivalent analysis found in [6], Figure 5.3 therein.

The behaviour for $\alpha \to \infty$ can be determined explicitly: since only the right-hand side of (2.78) is parameter dependent, it suffices to calculate $\lim_{\alpha \to \infty} \mathrm{RHS}(\frac{\lambda}{\alpha}; \nu, z_*)$. Since

$$\lim_{\alpha \to \infty} \mu(\lambda; \alpha, d) = \frac{2}{d - 1} = \nu - 1 \tag{2.85}$$

by (2.43) and

$$\lim_{\alpha \to \infty} z_*(\alpha, \gamma, \sigma, d) = \left\{ \begin{array}{ll} 0 & \text{if} \quad d > 3 \Leftrightarrow \nu < 2 \\ \mathrm{sgn}(\sigma) & \text{if} \quad d < 3 \Leftrightarrow \nu > 2 \end{array} \right. \tag{2.86}$$

by (2.21) and (2.50), we see that a dichotomy occurs at $d = 3$ or equivalently $\nu = 2$. For $\nu > 2$, the right-hand side of (2.78) converges as $\alpha \to \infty$ to

$$\lim_{\alpha \to \infty} \mathrm{RHS}\left(\frac{\lambda}{\alpha}; \nu > 2, z_*(\alpha)\right) = \lim_{\mu \to \nu - 1} \lim_{z_* \to \mathrm{sgn}(\sigma)} \mathrm{RHS}(\lambda; \mu, \nu > 2, z_*) = \mathrm{sgn}(\sigma) \tag{2.87}$$

using (2.81).

Following the same reasoning preceding Lemma 2.17, there are no additional zeroes of $P_\nu^{-\mu}(z_*)$ to be taken into account since the same limit behaviour $z_* \to \pm 1$ takes place here. The fact that a simultaneous limit is taken for $\mu(\lambda; \alpha, d)$ does not change this, since the coefficients of the expansion of $F(z)$, given in (2.83), have a regular expansion in orders of $\frac{1}{\alpha}$. Again, $a_0 = \frac{1}{\Gamma(1+\mu)} = \frac{1}{\Gamma(\nu)} + O\left(\frac{1}{\alpha}\right)$ is not equal to zero since $\nu > 1$. Therefore, it is not necessary to appeal to Conjecture 2.16 in this limit, since again it follows that $P_\nu^{-\mu}(z_*)$ does not have any zeroes asymptotically close to, but different from $z_* = \pm 1$.
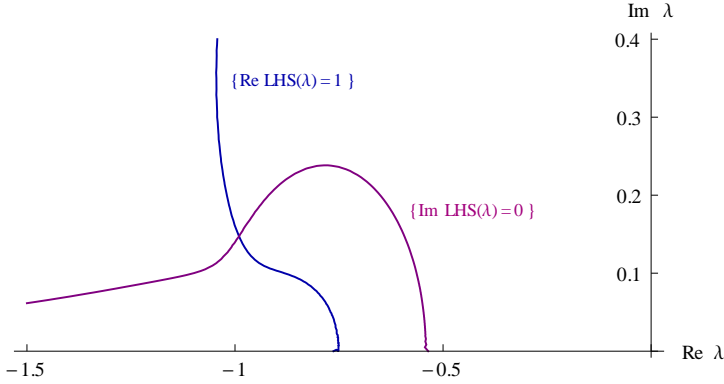
Figure 2.8: The equation $\text{LHS}(\lambda) = \text{sgn}(\sigma)$ is solved graphically for $\sigma > 0$. Plotted in blue is the level curve $\{\text{Re LHS}(\lambda) = 1\}$, which intersects the purple level curve $\{\text{Im LHS}(\lambda) = 0\}$ in the left half-plane for $\sigma > 0$ at $\lambda \approx -0.990268 \pm 0.147318\,i$. Since the level curves are symmetric, only the upper half-plane is shown.

The solution to $\text{LHS}(\lambda) = \text{sgn}(\sigma)$ is determined by direct evaluation of the integral (2.79), see Figure 2.8 for a graphic illustration. For $\sigma > 0$, this equation has a conjugate pair of complex solutions in the left half-plane; for $\sigma < 0$, there is a real positive solution, see Theorem 2.14. Of course the existence of these isolated solutions can be confirmed by a rigorous numerical winding number calculation (see [7]). Note that this both corroborates and extends the corresponding result in [6], giving a method to calculate the 'endpoints' of the eigenvalue orbits. The above leads to the following Theorem:

Theorem 2.18. *Let $\varepsilon > 0$ be sufficiently small. For all $1 < d < 3$, there is an $\alpha_*(\gamma, \sigma, d) > 0$ such that for all $\alpha > \alpha_*$, the nontrivial zeroes of the Evans function associated with the stability problem* (2.25) *are to the left of, and bounded away from the imaginary axis.*

When $\nu < 2$, we need to investigate $\lim_{z_* \to 0} \lim_{\mu \to \nu - 1} \text{RHS}(\frac{\lambda}{\alpha}; \nu < 2, z_*)$. Since $P_\nu^{-(\nu-1)}(z) = z\, P_{\nu-1}^{-(\nu-1)}(z)$ [1, 2], we see that $\text{RHS}(\frac{\lambda}{\alpha}; \nu < 2, z_*(\alpha)) \rightsquigarrow \frac{1}{z_*^2}$ while $z_* \to 0$ as $\alpha \to \infty$. This means that the solutions of equation (2.78) will either converge to the poles of $\text{LHS}(\lambda)$, which lie at $\lambda = \lambda_f^{(2)} = -\frac{3}{4}$ and $\lambda = \lambda_f^{(0)} = \frac{5}{4}$, or take off to infinity – see Figure 2.7, right. From this, it is clear that the pulse becomes unstable for $\nu < 2 \Leftrightarrow d > 3$ when α is large enough; see again Figure 2.3 for an example.

Theorem 2.19. *Let $\varepsilon > 0$ be sufficiently small. For all $d > 3$, there are $\alpha_{*,1}(\gamma, \sigma, d) > 0$ and $\alpha_{*,2}(\gamma, \sigma, d) > 0$ such that for all $\alpha < \alpha_{*,1}$ and all $\alpha > \alpha_{*,2}$, the nontrivial zeroes of the Evans function associated with the stability problem* (2.25) *are to the right of the imaginary axis.*

Proof. The above arguments show that the pulse becomes unstable when α is large enough. For $0 < \alpha \ll 1$, we see that the same approximations apply as for the case $\lambda \to \infty$, see the proof of Theorem 2.14. Moreover, combining (2.21) and (2.50) we see that $z_* \to \mathrm{sgn}(\sigma)$ as $\alpha \downarrow 0$. Therefore, RHS $\rightsquigarrow \mathrm{sgn}(\sigma) \frac{\sqrt{\lambda}}{\sqrt{\alpha}}$ as $\alpha \downarrow 0$. As for the case $\alpha \to \infty$, RHS thus has to blow up, which yields the existence of a positive real solution close to $\lambda_f^{(0)}$ for (2.78). $\qquad\square$

However, the eigenvalue orbit for $d > 3$ traverses the left half plane for a particular α-interval, as shown in Figure 2.3. That is, direct evaluation of (2.78) indicates that there also is a non-empty region $\alpha \in (\alpha_{*,1}, \alpha_{*,2})$ for which the pulse is stable. To investigate this behaviour analytically, we focus on the parameter d.

Consider the limit $d \gg 1$. This is equivalent with the limit $\nu - 1 \ll 1$. Therefore, we introduce an asymptotically small parameter δ and set $\nu = 1 + \delta$, so that $\mu = \delta \sqrt{1 + \frac{\lambda}{\alpha}}$ (see (2.43)). The equation for z_*, combining (2.21) and (2.50), is

$$\frac{\gamma(\nu - 1)}{\nu} \left(\frac{\alpha}{9\sigma^2}\right)^{\frac{1}{\nu-1}} \left(z_*^2\right)^{\frac{1}{\nu-1}} = \alpha(1 - z_*^2) \tag{2.88}$$

which, when $\nu = 1 + \delta$, yields

$$\frac{\gamma \delta}{1 + \delta} \left(\frac{\alpha}{9\sigma^2}\right)^{\frac{1}{\delta}} \left(z_*^2\right)^{\frac{1}{\delta}} = \alpha(1 - z_*^2) \tag{2.89}$$

Substituting $z_*^2 = e^{-y}$, $y > 0$, we obtain

$$\frac{\gamma \delta}{1 + \delta} \left(\frac{\alpha}{9\sigma^2}\right)^{\frac{1}{\delta}} e^{-\frac{y}{\delta}} = \alpha(1 - e^{-y}); \tag{2.90}$$

writing

$$\frac{\alpha}{9\sigma^2} = e^{\beta} \tag{2.91}$$

this becomes

$$\frac{\gamma \delta}{\alpha(1 + \delta)} \frac{e^y}{e^y - 1} = e^{\frac{y - \beta}{\delta}} \tag{2.92}$$

When $\beta > 0$, we can rewrite this as

$$y = \beta + \delta \, \log \left[\frac{\gamma \, \delta}{\alpha(1 + \delta)} \frac{e^y}{e^y - 1} \right] \tag{2.93}$$

yielding $y = \beta + \delta \log \left(\delta \frac{\gamma e^\beta}{\alpha(e^\beta - 1)} \right) +$ h.o.t.. When $\beta < 0$ and not asymptotically small, equation (2.92) is solved by $y = -\log \left(1 - \delta \frac{\gamma}{\alpha} e^{\frac{\beta}{\delta}} \right) +$ h.o.t.. This means that when $\frac{\alpha}{9\sigma^2} > 1$, then $z_*^2 = \frac{9\sigma^2}{\alpha} \left(\frac{\alpha - 9\sigma^2}{\delta \gamma} \right)^\delta +$ h.o.t, while $z_*^2 = 1 - \delta \frac{\gamma}{\alpha} \left(\frac{\alpha}{9\sigma^2} \right)^\delta +$ h.o.t. when $\frac{\alpha}{9\sigma^2} < 1$. Thus, for $d \gg 1$ a sharp transition in the value of z_* occurs as α passes through $\alpha = 9\sigma^2$.

We will now show that at this 'transition', all zeroes of the Evans function, i.e. all solutions of (2.78) (Corollary 2.5), must have negative real part. Using the same decomposition $P_\nu^{-\mu}(z_*) = \left(\frac{1 - z_*}{2} \right)^{\frac{\mu}{2}} F(z_*)$ as before, with $F(z)$ having a regular expansion near $z_* = 1$ with coefficients given by (2.83), we see that for $\mu = \delta \mu_0$, $\nu = 1 + \delta$ and $z_* = 1 - \frac{1}{2} y_1 \delta$ to leading order, both the term $\left(\frac{1 - z_*}{2} \right)^{\frac{\mu}{2}}$ and the coefficients in (2.83) can be expanded in δ, yielding $P_{1+\delta}^{-\delta \mu_0}(1 - \frac{1}{2} y_1 \delta) = 1 + \frac{1}{2} \mu_0 \delta \log(\delta) + O(\delta)$. From this, we can conclude that it is not possible to choose y_1 such that $P_{1+\delta}^{-\delta \mu_0}(1 - \frac{1}{2} y_1 \delta) = 0$ for asymptotically small δ, so Conjecture 2.16 is not needed.

First we set $\nu = 1 + \delta$ in RHS (2.80):

$$\text{RHS}(\tfrac{\lambda}{\alpha}; 1 + \delta, z_*) = \frac{1}{\delta} \left(1 + \delta - (1 + \delta - \delta \sqrt{1 + \frac{\lambda}{\alpha}}) \frac{P_\delta^{-\delta \sqrt{1 + \frac{\lambda}{\alpha}}}(z_*)}{z_* P_{1+\delta}^{-\delta \sqrt{1 + \frac{\lambda}{\alpha}}}(z_*)} \right) \tag{2.94}$$

The above approximations yield, with the same asymptotically small parameter δ as introduced above,

$$\text{RHS}(\tfrac{\lambda}{\alpha}; 1 + \delta, z_*) = \begin{cases} -\frac{\gamma}{\alpha} + \sqrt{1 + \frac{\lambda}{\alpha}} + O(\delta) & \text{if} \quad \alpha < 9\sigma^2 \\ \frac{1}{\delta} \left(1 - \frac{\alpha}{9\sigma^2} \right) + 1 + \frac{-1 + \sqrt{1 + \frac{\lambda}{\alpha}}}{z_*^3} + O(\delta) & \text{if} \quad \alpha > 9\sigma^2 \end{cases} \tag{2.95}$$

From this result, we see that for $\alpha < 9\sigma^2$, the behaviour of RHS is similar to the behaviour treated in Theorem 2.18. Moreover, for $\gamma \downarrow 0$, we obtain the same result as in Lemma 2.17.

However, when α crosses the threshold $\alpha \approx 9\sigma^2$, the behaviour of RHS radically changes. This accounts for the sharp 'turning' behaviour observed in Figure 2.3b. The expression for $\alpha > 9\sigma^2$ only accounts for the limiting behaviour yielding unstable eigenvalues as described in Theorem 2.19, since RHS blows up: to study the intermediate regime, we must zoom in on the situation when $\alpha \approx 9\sigma^2$. By (2.91), we thus set $\beta = \delta B + \text{h.o.t.}$, we see that equation (2.92) can be solved by $y = \delta y_1 + \text{h.o.t.}$, with y_1 determined by

$$\frac{\gamma}{\alpha} e^B = y_1 e^{y_1} \tag{2.96}$$

so $y_1 = W(\frac{\gamma}{\alpha} e^B)$, where $W(z)$ is the Lambert W-function. Since $z_*^2 = e^{-y} = 1 - \delta y_1$ at leading order, the same approximation as for $\alpha < 9\sigma^2$ can be used, yielding

$$\text{RHS}(\tfrac{\lambda}{\alpha}; 1 + \delta, z_*) = -B + \sqrt{1 + \frac{\lambda}{\alpha}} + \text{h.o.t.} \quad \text{if} \quad \frac{\alpha}{9\sigma^2} = 1 + \delta B + O(\delta^2) \tag{2.97}$$

Using the previous analysis, we can go beyond the previous instability result for $d > 3$ and find an interval for α where the pulse is stable, and state the following:

Theorem 2.20. *Let $\varepsilon > 0$ be sufficiently small. There is a $d_* > 3$ such that for all $d > d_*$, there is an open set Ω_* in (α, γ, σ)-parameter space such that for all $(\alpha, \gamma, \sigma) \in \Omega_*$, the nontrivial zeroes of the Evans function associated with the stability problem (2.25) are to the left of, and bounded away from the imaginary axis.*

Proof. For $d \gg 1$, the above analysis can be applied. Taking $\alpha = 9\sigma^2$, we obtain from (2.97) $\text{RHS}(\frac{\lambda}{\alpha}) = \sqrt{1 + \frac{\lambda}{\alpha}}$ as a leading order expression for RHS. Taking $\sigma = 1$, solving LHS$(\lambda) = \sqrt{1 + \frac{\lambda}{\alpha}}$ numerically yields Re $\lambda = -1.2 < 0$ for these parameter values. Note that in this asymptotic approximation, the value of γ does not play a role. Therefore, for fixed $\gamma = \gamma_*$, there is a $d \gg 1$ such that there is an open neighbourhood of $(\alpha, \gamma, \sigma) = (9, \gamma_*, 1)$ where the statement of the Theorem holds. As observed above, since this only concerns the numerical evaluation of a meromorphic, coefficient free expression, this result can be confirmed rigorously by a winding number calculation. $\square$

For fixed values of the parameter d, accurate numerical simulations and rigorous numerical winding number calculations similar to those used in the proof of the main stability theorem in [7] can be used. For $(\alpha, \gamma, \sigma) = (\frac{1}{2}, 2, 1)$, such numerical calculations show that for d between 3 and 21, there is a pair of complex conjugate eigenvalues with real part < -0.02, where the real part decreases as d increases. Based on these numerical calculations, we believe Theorem 2.20 holds for all $d > 3$.
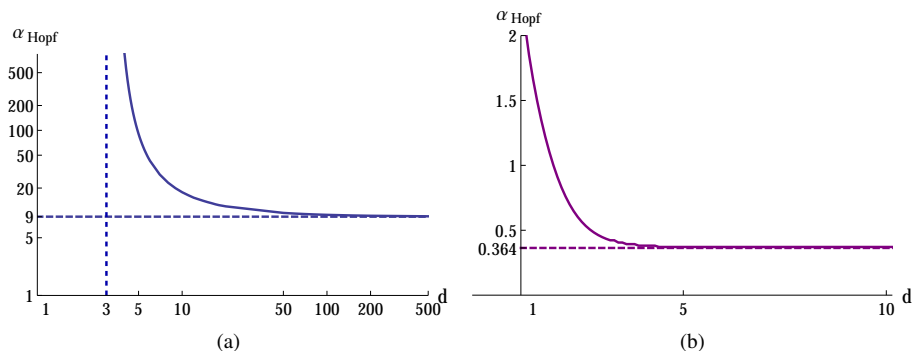
Figure 2.9: The stabilising (a) and destabilising (b) Hopf bifurcation values α_{Hopf} as a function of d.
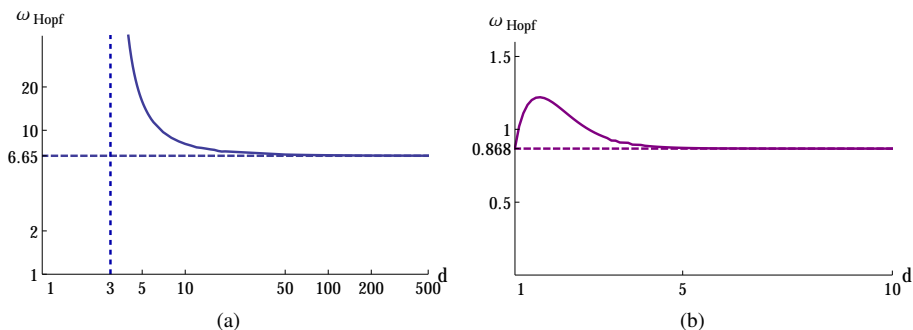
Figure 2.10: The stabilising (a) and destabilising (b) Hopf frequencies ω_{Hopf} as a function of d.

2.5 Numerical simulations

A Hopf bifurcation occurs when the eigenvalues cross the imaginary axis; this happens once for $d < 3$ (see Figure 2.3a) and twice for $d > 3$ (see Figure 2.3b). A plot of the bifurcation value α_{Hopf} as a function of d for both stabilising and destabilising Hopf bifurcations is given in Figure 2.9 for $\gamma = 2$ and $\sigma = 1$. The Hopf frequency $\omega_{\text{Hopf}} = \text{Im}\,\lambda_{\text{Hopf}}$ for both Hopf bifurcations as a function of d is given in Figure 2.10; again, $\gamma = 2$ and $\sigma = 1$. As the destabilising Hopf bifurcation only occurs for $d > 3$, a vertical asymptote at $d = 3$ can be found at both Figures 2.9b and 2.10b. For large

values of d, the functions seem to converge to the indicated horizontal asymptotes. Based on the asymptotic $d \gg 1$ analysis of the previous subsection, the asymptote $\lim_{d \to \infty} \alpha_{\text{Hopf}} = 9$ of Figure 2.9b can be understood by looking at the asymptotic expansion of RHS for $\nu = 1 + \delta$, see (2.95). If α crosses the threshold $\alpha = 9\sigma^2$, RHS blows up yielding unstable eigenvalues, in a manner equivalent to the situation described in Theorem 2.14. Since RHS blows up for asymptotically small δ, the unstable regime lies asymptotically close to $\alpha = 9\sigma^2$, which explains the horizontal asymptote $\alpha_{\text{Hopf}} = 9$ in Figure 2.9b.

The super- or subcriticality of both stabilising and destabilising Hopf bifurcations has been checked by direct numerical simulation of the constructed pulse. The pulse was simulated on the domain $x \in [-10\,\varepsilon^{-1}, 10\,\varepsilon^{-1}]$ with homogeneous Neumann boundary conditions. Note that in all these direct numerical pulse simulations, the position of the pulse was seen to remain completely fixed. This phenomenon will be treated in detail in chapter 4, section 4.3.2.
In Figure 2.11, the tip of the U-component of the simulated pulse is plotted as a function of time for $d = 2$. Here, $\gamma = 2$, $\sigma = 1$ and $\varepsilon = 0.02$. For these parameter values, the Hopf bifurcations occurs at $\alpha_{\text{Hopf}} = 0.83 + O(\varepsilon)$. Figure 2.11 shows that for these parameter values, the Hopf bifurcation is subcritical. For $d = 5$, the equivalent stabilising Hopf bifurcation occurs at $\alpha_{\text{Hopf}} = 0.37 + O(\varepsilon)$ for the same values of the other parameters. As can be seen in Figure 2.12, this Hopf bifurcation is subcritical as well.

The destabilising Hopf bifurcation occurs for $d = 5$ at $\alpha_{\text{Hopf}} = 90.634 + O(\varepsilon)$. In this simulation, $\varepsilon = 0.002$ while still $\gamma = 2$ and $\sigma = 1$. In Figure 2.13 it can be seen that upon destabilisation, the pulse tip initially exhibits typical 'subcritical' growth behaviour. However, for longer times, a bounded temporally oscillating pulse is observed. Nearby the other Hopf bifurcations, such 'breathing' pulses can also be observed. For $d = 2$ and stable values of α, i.e. for α within the region in which the pulse is stable (here, $\alpha = 0.9 > \alpha_{\text{Hopf}}$), Figure 2.14 shows an oscillating pulse.

In Figures 2.15, 2.16 and 2.2, the oscillating behaviour of the pulse near the destabilising Hopf bifurcation for $d = 5$ is studied in more detail. For parameter values relatively far in the stable regime (here, $\alpha = 85 < \alpha_{\text{Hopf}} = 90.634 + O(\varepsilon)$), simulations reveal bounded temporally periodic behaviour with a slowly periodically modulated amplitude, see Figure 2.15. When α is increased towards α_{Hopf}, the frequency of the modulation increases; see Figure 2.16 for the pulse behaviour when $\alpha = 90.5$. For parameter values even closer to α_{Hopf}, the irregular behaviour as shown in Figure 2.2 is observed.
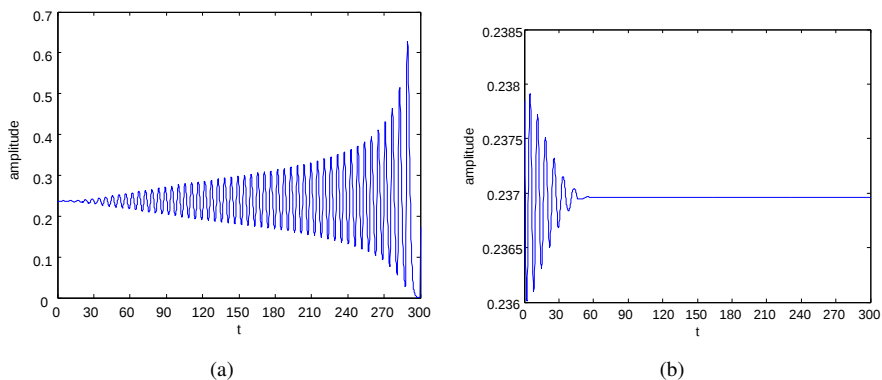
Figure 2.11: The tip of the U-pulse as a function of time for $\alpha = 0.827$ (a) and $\alpha = 0.829$ (b). Here, $d = 2$.
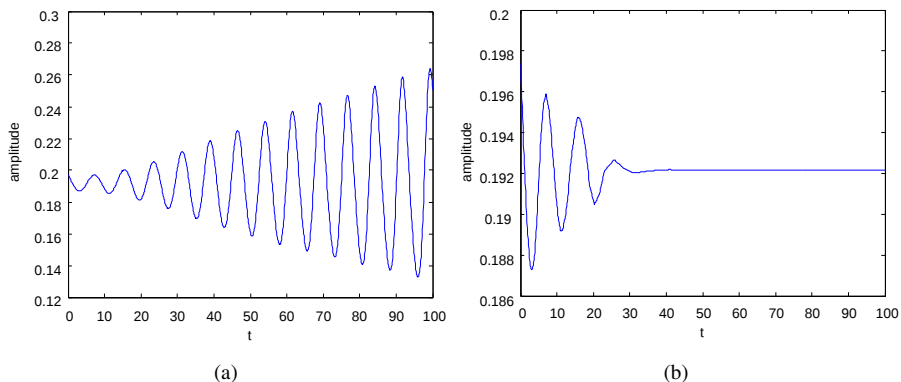
Figure 2.12: The tip of the U-pulse as a function of time for $\alpha = 0.352$ (a) and $\alpha = 0.353$ (b). Here, $d = 5$.

This pulse behaviour has not been observed in the literature on GS/GM-type models. In the fourth chapter of this thesis, the nature of the Hopf bifurcation of pulses in system (2.7) is studied. It is established that this Hopf bifurcation can be both sub- and supercritical, see chapter 4, Theorem 4.16.

(a)

(b)
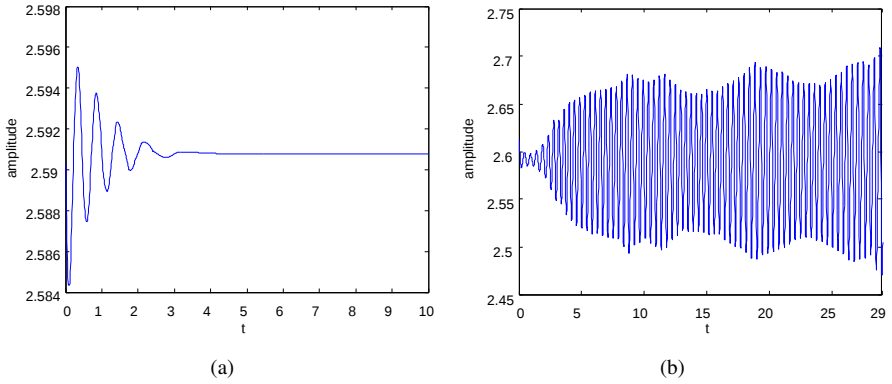
Figure 2.13: The tip of the U-pulse as a function of time for $\alpha = 90.61$ (a) and $\alpha = 90.69$ (b).

(a)

(b)
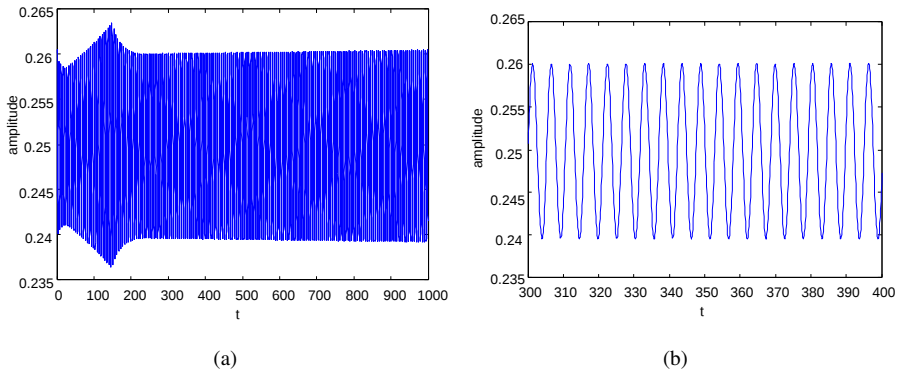
Figure 2.14: The tip of the U-pulse as a function of time for $\alpha = 0.9$, $d = 2$. Figure (a) shows the entire simulated time domain, while (b) zooms in on a part of the time domain, showing the regularity of the pulse tip movement.
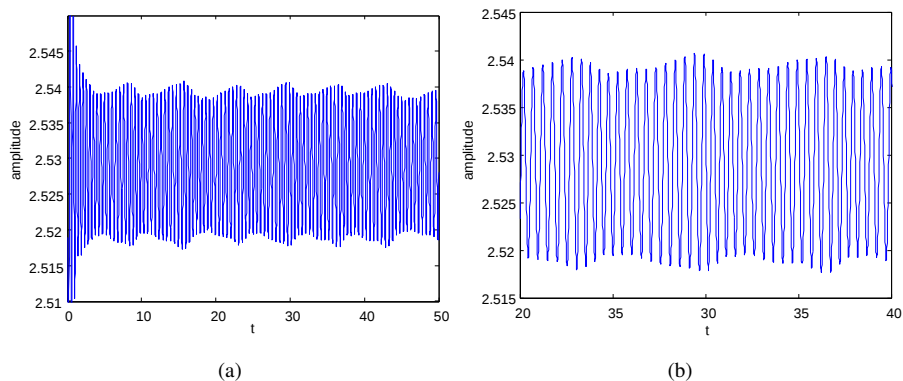
Figure 2.15: The tip of the *U*-pulse as a function of time for $\alpha = 85$, $d = 5$. Figure (a) shows the entire simulated time domain, while (b) zooms in on a part of the time domain.
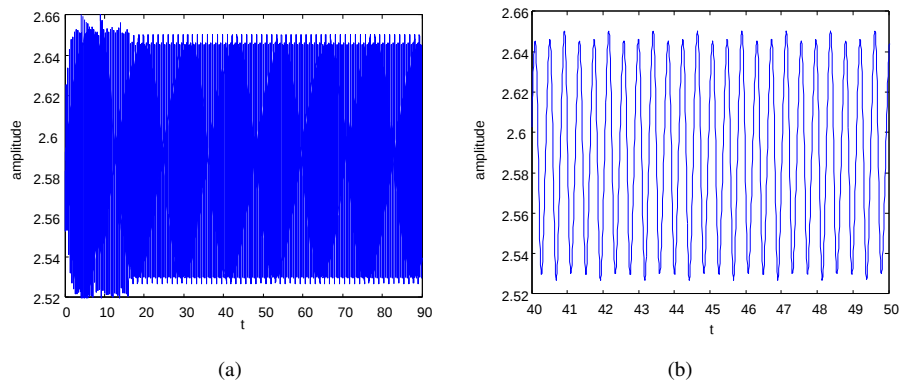
Figure 2.16: The tip of the *U*-pulse as a function of time for $\alpha = 90.5$, $d = 5$. Figure (a) shows the entire simulated time domain, while (b) zooms in on a part of the time domain.

3

Pulses in a general reaction-diffusion system

The content of this chapter was accepted for publication as [16].

3.1 Introduction

The existing theory for the existence and stability of symmetric, stationary pulse solutions to two-component singularly perturbed reaction-diffusion equations has in essence been developed in the context of two explicit models, the Gray-Scott (GS) model for autocatalytic reactions [23, 13] and the Gierer-Meinhardt (GM) system modelling morphogenesis [22]. The (generalised) GM equation is directly included in the general class of two-component, singularly perturbed systems considered here,

$$
\begin{cases}
U_t = U_{xx} - [\mu U - \nu_1 F_1(U; \varepsilon)] + \frac{\nu_2}{\varepsilon} F_2(U, V; \varepsilon) \\
V_t = \varepsilon^2 V_{xx} - V + G(U, V; \varepsilon),
\end{cases}
\tag{3.1}
$$

the particular structure of which emphasises the new, generalised aspects of this system compared to the specific well-studied GS/GM-type models. More details on this specific form can be found in section 3.1.1.

In this chapter, we consider equation (3.1) on the unbounded domain $\mathbb{R}$, so $U(x, t)$, $V(x, t) : \mathbb{R} \times \mathbb{R}_{>0} \to \mathbb{R}_{>0}$; we restrict ourselves to positive solutions. Moreover, we assume that $\mu > 0$, $\nu_{1,2} \in \mathbb{R}$ and $F_1 : \mathbb{R}_{>0} \to \mathbb{R}$, $F_2, G : \mathbb{R}_{>0} \times \mathbb{R}_{\geq 0} \to \mathbb{R}$ are nonlinear functions obeying mild regularity assumptions, see section 3.1.1. The parameter

$0 < \varepsilon \ll 1$ is assumed to be asymptotically small, i.e. the results established in this chapter will be valid for '$\varepsilon > 0$ small enough'. While strictly speaking not part of the domain of F_2 and G, the trivial background state $(U, V) \equiv (0, 0)$ is assumed to be asymptotically stable, see also Remark 3.6. The Gray-Scott equation can also be brought into the form (3.1) by a number of transformations that scale the magnitude of the patterns to $O(1)$ with respect to ε and that shift the Gray-Scott background state $(1, 0)$ to the normalised state $(0, 0)$ in (3.1) [6, 14].

The model problem (3.1) can be considered as the most general (semilinear) two component, singularly perturbed reaction-diffusion system –see equations (3.3) and (3.4)– that may exhibit $O(1)$ pulse patterns (Remark 3.2), *apart from an explicit codimension* 1 *condition on the structure of the linearised model near the trivial background state that determines the limiting behaviour of the pulse.* This condition –that roughly states that near this background state the 'slow' U-component only couples into the 'fast' V-equation in a nonlinear way– has mainly been imposed for technical reasons; see however Remark 3.5. A derivation and more precise motivation of the model will be given in section 3.1.1, together with a list of specific assumptions on the parameters and nonlinearities in (3.1).

The class of equations covered by (3.1) significantly extends the GS and GM type models. In this chapter, we will develop an explicit theory for the existence and the stability of symmetric, stationary pulse solutions to (3.1) that have positive U and V-components and that have $O(1)$ (sup-)norm with respect to ε (Remark 3.2). We will especially highlight the effect of generalising two –as it will turn out– quite restrictive properties shared by the GS and GM models. Firstly, these models do not allow for nonlinear behaviour in U in the slow U-equation outside the fast pulse region, i.e. the slow U-equations of the GS/GM models are linear in U for $V = 0$. In other words, both the GS and the (generalised) GM equations correspond to system (3.1) with $\nu_1 = 0$ – the nonlinearity in the U-equation is decomposed in a V-independent term (F_1) and a term that vanishes at $V = 0$, hence $F_2(U, 0) = 0$ (see section 3.1.1 and especially assumption (A3)). In the literature, this linearity in the slow U-system is crucially exploited in the stability analysis of pulse solutions to both GS- and GM-type models: this analysis relies heavily on the fact that the stability problem can be solved explicitly in terms of exponential functions in the slow U-fields [6, 7, 26, 32, 33, 58]. Note that systems incorporating a slow nonlinearity ($\nu_1 \neq 0$) were already encountered in [37], although no pulse-type solutions were considered in this paper. Secondly, in almost all previous studies the nonlinear term $G(U, V)$ in (3.1) is a simple, explicit power of V as function of V (it is in fact quadratic

in V in the GS and the standard GM equation) – see [59, 39] for some exceptions involving saturation terms. This also forms an essential ingredient of the analysis, since it enables one to explicitly solve the fast reduced stability problem (see [6, 7] and section 3.3).

One can thus say that the existing methods for the explicit analysis of homoclinic pulses in two component, singularly perturbed reaction-diffusion equations are applicable to the subclass of (3.1) in which $v_1 = 0$ and $G(U, V) = g(U)V^d$ for $d > 1$ and some function $g(U)$ – see also Remark 3.2. The theory to be developed in this chapter goes beyond these rather severe restrictions. Moreover, the richness of the novel phenomena introduced by the extended class (3.1) is shown by way of an explicit example in chapter 2 – see also Remark 3.1.

In section 3.2, the existence of stationary singular pulses for system (3.1) is established by the methods of geometric singular perturbation theory, under mild and natural assumptions; in particular, we assume that the fast V-system admits a homoclinic pulse solution. Similar to related results in [6, 13], pulses correspond to intersections of the slow unstable manifold $W_s^u((0,0))$ and a take off curve T_o in the half-plane $\{(u, p) : u > 0\}$ associated to the reduced slow existence problem (i.e. $V \equiv 0$, $\varepsilon = 0$ and $U = u(x)$ in (3.1). As a consequence, system (3.1) may in general exhibit various homoclinic pulse solutions – see Figure 3.2 in section 3.2. The precise existence result is summarised in Theorem 3.7. From section 3.3 onwards, the (linear) stability of a homoclinic pulse is analysed using Evans function techniques. The slow reduced linear stability problem is no longer of constant coefficient type, as is the case in the GS/GM type models studied in the literature: both the slow and fast reduced linear problems have the structure of classical Sturm-Liouville problems. This fact is strongly used in the analysis. It is shown that the Evans function associated to the (spectral) stability of the pulse can be decomposed into a fast and a slow component. The main result of this analysis –which is obtained through a nonlocal eigenvalue problem (NLEP)– is Theorem 3.21, which provides an explicit expression for the slow component $t_{s,+}$ of the Evans function in terms of the nonlinearities $F_{1,2}$, G of (3.1) and the leading order approximation of the pulse (as established by Theorem 3.7). Since it is established in Corollary 3.24 that all nontrivial eigenvalues correspond to zeroes of $t_{s,+}$, Theorem 3.21 thus provides an explicit analytical control over the stability of the pulses given by Theorem 3.7.
Even though the pulse is constructed in a most general setting under mild assumptions on the nonlinearities $F_{1,2}$ and G, a number of (relatively) simple instability results is obtained by detailed analysis of the function $t_{s,+}$ in the neighbourhood of known ei-

genvalues of the fast reduced problem, these results are presented in section 3.5. The instability of the homoclinic pulse can be established by determining the sign of certain explicit expressions (Corollary 3.29, Theorem 3.35). Some of these expressions can be interpreted and determined directly in terms of the existence problem, or more specifically, by considering the slow unstable manifold $W_s^u((0,0))$ and the take off curve T_o that establish the existence of the pulses (Theorem 3.7). In the linear $\nu_1 = 0$ case, $W_s^u((0,0))$ always has positive $p(= u_x)$-coordinate so that $W_s^u((0,0)) \cap T_o$ must lie in the positive quadrant of the slow reduced $\{(u,p) : u > 0\}$ half-plane. In general, $W_s^u((0,0)) \cap T_o$ may have negative p-coordinates – in such cases the U-component of the pulse has a maximum on both sides the fast V-pulse, see Figure 3.4c. It is established in Corollary 3.29 that these pulses are unstable. Moreover, the sign of the relative slopes of the take-off curve T_o with respect to the slow unstable manifold $W_s^u((0,0))$ at their intersections also gives a direct instability criterion: this sign changes at successive intersections, but only those intersections with negative sign can be stable – see Lemma 3.34, Theorem 3.35 and Figure 3.8. Analysis of the slow component of the Evans function near the trivial eigenvalue $\lambda = 0$ reveals close relations between bifurcations in the existence problem and pulse instabilities, see Corollary 3.30 and Corollary 3.32. Finally, in section 3.6, we discuss some implications of the general approach developed here.

Remark 3.1. The present general results are both inspired by and reflected in the analysis in chapter 2, where the theory is developed in the explicit setting of a Gierer-Meinhardt problem with a 'slow nonlinearity':

$$\begin{cases} U_t &= U_{xx} &- [\mu U - \nu_1 U^d] &+ \frac{\nu_2}{\varepsilon} V^2 \\ V_t &= \varepsilon^2 V_{xx} &- V &+ \frac{V^2}{U}. \end{cases} \tag{3.2}$$

For a specific system like this, it is possible to go beyond the previously mentioned instability results, especially since it is possible to get an even more explicit 'analytical control' over the reduced Sturm-Liouville problems associated to the stability of the pulses – in chapter 2, a crucial role is played by associated Legendre functions. As a consequence, it is possible to obtain conditions in terms of the model parameters for which the homoclinic pulse is stable. Moreover, numerical analysis of the resulting Hopf bifurcations reveals rich nonlinear behaviour such as stable standing localised pulses that bifurcate from the pulses considered here and of which the maximum oscillates up and down in a complex –periodic, quasi-periodic, chaotic– fashion, see Figure 3.1. This novel and intriguing behaviour has not been observed in the literature on GS/GM-type models. In the fourth chapter of this thesis, the nature of the Hopf bifurcation of pulses in system (3.2) is studied. It is established that this Hopf
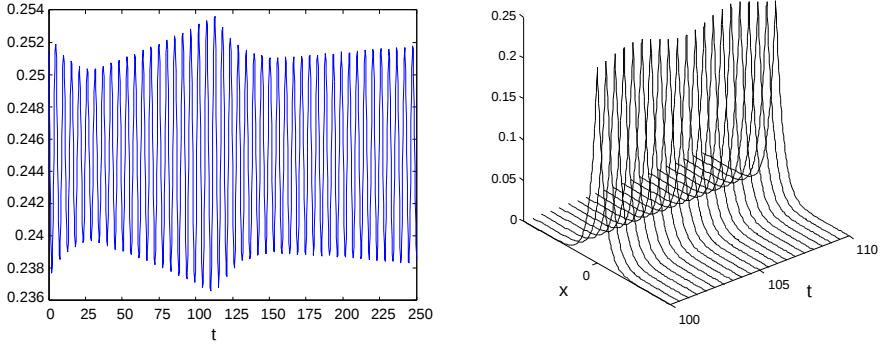
Figure 3.1: A stable oscillating pulse, as observed in the slowly nonlinear Gierer-Meinhardt system (3.2), studied in chapter 2 (see also Remark 3.1). The left figure shows the position of the tip of the pulse as a function of time. In the right picture, the *u*-component of the pulse is shown in a space-time plot. These results were obtained by direct numerical simulation of the PDE system, for $(\mu, \nu_1, \nu_2, d) = (0.9, 1, 2, 2)$ and $\varepsilon = 0.02$.

bifurcation can be both sub- and supercritical, as is expected in the generic setting of system (3.1). The Hopf bifurcation in GM-type models is always subcritical, as is confirmed analytically in chapter 4.

Remark 3.2. In this thesis, we only consider pulse solutions for which the fast *V*-component makes one homoclinic excursion away from the stable rest state. Thus, we do not consider localised multi-pulse patterns that are also very common to GS/GM-type models [13, 6]. More importantly, we also do not consider pulse solutions of 'mesa' or FitzHugh-Nagumo type. Such pulses can be described as bi-heteroclinic (or multi-heteroclinic), since they consist of (at least) two heteroclinic jumps through the fast spatial field separated by a 'long' plateau in which the pattern evolves slowly (in space); see [53, 25, 28, 31, 35] and the references therein.

Remark 3.3. The Schnakenberg model, the third standard model considered in the literature [46], is very similar to the GS and GM models, in the sense that the slow reduced system also does not contain nonlinearities and that the nonlinearity associated to $G(U, V)$ is again exactly quadratic as function of *V*. Although the Schnakenberg model does not have a trivial stable background state, it can be (and has been) studied by methods that are very similar to those developed for the GS and GM equation [27, 56].

3.1.1   The model

The most general two component reaction-diffusion system on the real line, i.e. for $\hat{x} \in \mathbb{R}$, reads

$$\begin{cases} U_{\hat{t}} & = & d_U U_{\hat{x}\hat{x}} & + & a_{11}U & + & a_{12}V & + & H_1(U,V) \\ V_{\hat{t}} & = & d_V V_{\hat{x}\hat{x}} & + & a_{21}U & + & a_{22}V & + & H_2(U,V) \end{cases} \tag{3.3}$$

in which $H_{1,2}(U,V) : \mathbb{R}^2 \to \mathbb{R}$ are nonlinear terms that do not include linear components in U or V. Stable pulse solutions must be bi-asymptotic to a spectrally stable 'trivial state' $(U,V) \equiv (\bar{U}, \bar{V})$. It can be assumed, by a simple translation of U and V, that $(\bar{U}, \bar{V}) = (0,0)$ –which does not necessarily need to be a solution to (3.3), see Remark 3.6–. This trivial state is stable if $a_{11} + a_{22} < 0$ and $a_{11}a_{22} - a_{12}a_{21} > 0$. The system is assumed to be singularly perturbed, i.e. it is assumed that $U(\hat{x}, \hat{t})$ is slowly varying as function of $\hat{x}$ compared to the (relatively fast) spatial variation of $V(\hat{x}, \hat{t})$ – see also Remark 3.5. In other words, we assume that $0 < d_V \ll d_U$, or, without loss of generality, that $d_V = \varepsilon^2 \ll 1$, with $0 < \varepsilon \ll 1$ asymptotically small, and $d_U = 1$. This introduces the fast spatial variable $\hat{\xi} = \hat{x}/\varepsilon$, in which (3.3) has the form

$$\begin{cases} \varepsilon^2 U_{\hat{t}} & = & U_{\hat{\xi}\hat{\xi}} & + & \varepsilon^2 \left[a_{11}U & + & a_{12}V & + & H_1(U,V)\right] \\ V_{\hat{t}} & = & V_{\hat{\xi}\hat{\xi}} & + & & a_{21}U & + & a_{22}V & + & H_2(U,V). \end{cases} \tag{3.4}$$

Since $\hat{U}(x,t)$ is assumed to be bounded on $\mathbb{R}$, we formally conclude from the first equation in (3.4) that $U(\hat{\xi}, \hat{t})$ must approach a constant value $\bar{U}$ in the limit $\varepsilon \to 0$; in other words, the singularly perturbed nature of (3.4) causes U to be constant in leading order as function of the fast spatial variable $\hat{\xi}$. As a consequence, in the singular limit $\varepsilon \to 0$ the existence problem for stationary patterns reduces to a family of fast reduced existence problems for $V = v_f(\xi)$,

$$v_{f,\hat{\xi}\hat{\xi}} + a_{21}\bar{U} + a_{22}v_f + H_2(\bar{U}, v_f) = 0, \tag{3.5}$$

parameterised by $\bar{U} \in \mathbb{R}$; note that this is an integrable planar system.

In this thesis, we focus on the most simple pulse solutions: stationary solutions that are biasymptotic to the stable background state $(0,0)$ of (3.4), that are symmetric in $\hat{\xi}$ (or $\hat{x}$), and that only make one 'jump' through the fast field (which is to leading order described by (3.5) – see also Remark 3.2. By the above asymptotic arguments, system (3.4) can only have such a pulse solution if there are values of $\bar{U}$ for which (3.5) has a 'fast' homoclinic orbit $v_{f,h}(\hat{\xi}; \bar{U})$. The main codimension 1 assumption underlying the reduction of the most general system (3.3)/(3.4) to the model

problem (3.1) is that this homoclinic solution is biasymptotic to the critical point $(v_f, v_{f,\hat{\xi}}) = (0,0)$ of (3.5), i.e. that $\lim_{\hat{\xi} \to \pm\infty} v_{f,h}(\hat{\xi}; \bar{U}) = \lim_{\hat{\xi} \to \pm\infty} \frac{d}{d\hat{\xi}} v_{f,h}(\hat{\xi}; \bar{U}) = 0$. In principle, this is quite a restrictive condition. Since $\bar{U} \neq 0$ in general, it directly implies that a_{21} must be 0. Nevertheless, the methods developed in this chapter can also be applied to systems for which $\lim_{\hat{\xi} \to \pm\infty} v_{f,h}(\hat{\xi}; \bar{U})$ depends on $\bar{U}$, and only approaches 0 on the slow spatial scale, as $\bar{U} \to 0$. However, the analysis does become more involved for those systems: outside the fast homoclinic jump region described by (3.5), the component V will not be constant, but will evolve slowly (as function of $\hat{x}$), 'slaved' to the slow U-component – see Remark 3.5. To highlight the impact of allowing for fully general nonlinearities in (3.1) compared to the restricted cases of the GM and GS equations, we focus on a class of systems (3.3)/(3.4) with $a_{21} = 0$. In other words, we focus on the general class of two component, singularly perturbed, systems in which the slow component $U(\hat{x}, \hat{t})$ only couples into the fast V-equation through the nonlinear term $H_2(U, V)$.

Since $a_{21} = 0$, the assumption that the trivial state $(U(\hat{\xi}, \hat{t}), V(\hat{\xi}, \hat{t}) \equiv (0,0)$ is spectrally stable reduces to $a_{11} < 0$ and $a_{22} < 0$. By introducing $t = -a_{22}\hat{t}$ and $\xi = \sqrt{-a_{22}}\hat{\xi}$, equation (3.4) can now be written as

$$\begin{cases} \varepsilon^2 U_t &=& U_{\xi\xi} &+& \varepsilon^2 \left[-\mu U &+& F(U,V;\varepsilon)\right] \\ V_t &=& V_{\xi\xi} &-& V &+& G(U,V;\varepsilon) \end{cases}$$

with

$$\mu = \frac{a_{11}}{a_{22}} > 0, \ F(U,V;\varepsilon) = -\frac{1}{a_{22}}\left[a_{12}V + H_1(U,V)\right], \ G(U,V;\varepsilon) = -\frac{1}{a_{22}}H_1(U,V).$$

Next, we decompose $F(U,V;\varepsilon)$ into a part that depends only on U and a part that is 0 if $V = 0$,

$$F(U,V;\varepsilon) = F(U,0;\varepsilon) + [F(U,V;\varepsilon) - F(U,0;\varepsilon)] \overset{\text{def}}{=} \nu_1 F_1(U;\varepsilon) + \frac{\nu_2}{\varepsilon} F_2(U,V;\varepsilon), \tag{3.6}$$

where $\nu_{1,2} \in \mathbb{R}$ (not necessarily $O(1)$ in ε) have been introduced to control the relative impact of the nonlinear, non-GS/GM term $F_1(U)$ and the nonlinear coupling term $F_2(U,V)$. Hence, we arrive at (3.1) written in the fast spatial variable ξ,

$$\begin{cases} \varepsilon^2 U_t &=& U_{\xi\xi} &-& \varepsilon^2[\mu U - \nu_1 F_1(U;\varepsilon)] &+& \varepsilon\nu_2 F_2(U,V;\varepsilon) \\ V_t &=& V_{\xi\xi} &-& V &+& G(U,V;\varepsilon). \end{cases} \tag{3.7}$$

Apart from the condition on the (non)appearance of terms that are linear in U in the V-equation, (Remarks 3.5 and 3.11), the model problem (3.1) can thus be seen as a

general two component, singularly perturbed model, in which $O(1)$ pulses can exist. A priori, one could argue that the term v_2/ε in (3.6) also introduces a further restriction, but this is not the case since v_2 will be allowed to be $O(\varepsilon)$ in the analysis. The F_2-term in (3.1)/(3.7) has been artificially 'blown up' by a factor of $1/\varepsilon$ for clarity of presentation – which can be explained most clearly by looking at (3.1). The fast V component enters into the slow U-equation of (3.1) through an asymptotically large term of $O(1/\varepsilon)$ – as is also the case in the GS, generalised GM and Schnakenberg models. Since $V(x,t)$ is strongly localised to a domain of size $O(\varepsilon)$ in the x-scaling, this is quite natural: if the interaction term in the U-equation would be smaller, then the direct impact of V on the evolution of U would be asymptotically small. As was already remarked, this situation can, and will, be studied by considering $|v_2| \ll 1$ in (3.7), see Corollary 3.37. It will be found that (3.7) may have pulse solutions in this case, but that these pulse must be unstable: (3.7) in essence decouples into two scalar equations, the coupling is not strong enough to counteract the unstable eigenvalues of the scalar U, V-subsystems. In other words, by artificially 'blowing up' the F_2-term in (3.1), we automatically focus on the most relevant region in the parameter space associated to (3.1).

Since we have introduced ambiguities by the introduction of $v_{1,2}$ in (3.6), and since we so far not discussed the precise nature of the nonlinear terms, we now list the basic assumptions we impose on the parameters μ, v_1, v_2 and the nonlinearities F_1, F_2, G in (3.1)/(3.7) in the subsequent analysis (for the use of the symbol "$\rightsquigarrow$", see Definition 2.3):

Assumptions 3.4. *The following is assumed to hold:*

(A1) *$\mu, v_{1,2}$ are real and nonsingular in ε; furthermore, $\mu > 0$.*

(A2) *$F_1(U;\varepsilon) \rightsquigarrow U^{f_1}$ as $U \downarrow 0$ for some $f_1 > 1$;*
      F_1 is smooth both on its domain and as a function of ε.

(A3) *Writing $F_2(U,V;\varepsilon) = F_{2,1}(U;\varepsilon)\,V + F_{2,2}(U,V;\varepsilon)$,*
      $F_{2,1}(U;\varepsilon) \rightsquigarrow \tilde{F}_{2,1}(\varepsilon)\,U^{\gamma_1}$ as $U \downarrow 0$ for some $\gamma_1 \geq 0$ and $\tilde{F}_{2,1}(\varepsilon) \in \mathbb{R}$;
      $F_{2,2}(U,V;\varepsilon) \rightsquigarrow \tilde{F}_{2,2,u}(V;\varepsilon)\,U^{\alpha_1}$ as $U \downarrow 0$ for some $\alpha_1 \in \mathbb{R}$;
      $F_{2,2}(U,V;\varepsilon) \rightsquigarrow \tilde{F}_{2,2,v}(U;\varepsilon)\,V^{\beta_1}$ as $V \to 0$ for some $\beta_1 > 1$;
      F_2 is smooth both on its domain and as a function of ε.

(A4) *$G(U,V;\varepsilon) \rightsquigarrow \tilde{G}_u(V;\varepsilon)\,U^{\alpha_2}$ as $U \downarrow 0$ for some $\alpha_2 \in \mathbb{R}$;*
      $G(U,V;\varepsilon) \rightsquigarrow \tilde{G}_v(U;\varepsilon)\,V^{\beta_2}$ as $V \to 0$ for some $\beta_2 > 1$;
      G is smooth both on its domain and as a function of ε.

Assumption (A2) defines $F_1(U;\varepsilon)$ and ν_1 uniquely, while $F_2(U,V;\varepsilon)$ and ν_2 are not (yet), but will be uniquely defined with assumption (A6). The possibly singular behaviour of the functions $F_{2,2}(U,V;\varepsilon)$ and $G(U,V;\varepsilon)$ for U and/or V small (assumptions (A3) and (A4)) is in accordance with the behaviour of the nonlinearities in the generalised GM model, see also Remark 3.11. In fact, the generalised GM model corresponds to (3.1)/(3.7) with

$$\nu_1 = 0, \ \nu_2 = 1, \ F_{2,1}(U;\varepsilon) \equiv 0,$$
$$F_{2,2}(U,V;\varepsilon) = U^{\alpha_1} V^{\beta_1}, \ G(U,V;\varepsilon) = U^{\alpha_2} V^{\beta_2}, \ \beta_1, \beta_2 > 1. \tag{3.8}$$

Remark 3.5. As was already noted, if $a_{21} \neq 0$, it follows from (3.5) that the fast V-component of the homoclinic pattern $(U_h(\xi), V_h(\xi))$ does not go to 0 as ξ leaves the fast field, but instead will be 'slaved' to the slowly evolving U-component and thus only approaches 0 on the slow spatial scale. It has been shown for a model problem [9] that such a situation can be studied along the lines of the present approach. Thus, letting go of the condition $a_{21} = 0$ a priori mostly introduces additional technicalities (see also Remark 3.11). However, allowing a_{21} to be $\neq 0$ may possibly generate more than just 'additional technicalities'. A linear U-term in the V-equation may introduce the possibility of having homoclinic pulse patterns with spatially oscillating, i.e. non-monotonously, decaying 'tails'. We are not aware of any analytical, or even numerical, study of this type of localised patterns in singularly perturbed reaction diffusion equations. At the introduction of the asymptotically large ν_2/ε pre-factor in (3.6), we argued that the fast V-component must couple in an asymptotically strong fashion into the slow U-equation. If V is slowly varying, and thus no longer at leading order constant (i.e. 0) outside the fast field, one has to think carefully about the magnitude and/or impact of the nonlinear coupling term $F_2(U,V)$ in the U-equation. Thus, our choice to impose the codimension 1 condition $a_{21} = 0$ is motivated by our preference to avoid 'additional technicalities', however, this more technical case may exhibit novel phenomena and/or may eventually ask for the development of a novel theoretical approach.

Remark 3.6. We explicitly allow the nonlinearities F_2 and G to be singular in U as $U \downarrow 0$, see assumptions (A3) and (A4) on the exponents $\alpha_{1,2}$. This implies that $(U,V) = (0,0)$ is not necessarily a solution to (3.1). However, the specific form of (3.1) was derived from (3.3) based on considerations on the stability of the trivial state. While strictly speaking this line of reasoning loses validity for singular F_2 and G, the specific context of the pulse construction (see section 3.2) allows for a more 'loose' notion of stability of the trivial state. Since it will turn out that that $V = 0$ to exponential order long before $U \downarrow 0$ in $\hat{x}$, it is only necessary that

$\lim_{U \to 0} \lim_{V \to 0} H_{1,2}(U, V) = 0$, which follows from assumptions (A3) and (A4). As to questions concerning nonlinear stability, the presence of a singularity as $U \to 0$ does have an important influence on the treatment of the subject; however, these questions fall outside the scope of this chapter and this thesis. A more elaborate discussion on the influence of singular terms on well-posedness and nonlinear stability can be found in [6], Remark 1.3.

3.2 The existence of pulses

In this section, we study the existence of positive, symmetric, stationary pulse solutions $(U(\xi, t), V(\xi, t)) = (U_h(\xi), V_h(\xi))$ to (3.7) (or equivalently (3.1)). In the fast spatial coordinate ξ, the associated ODE takes the form

$$
\begin{cases}
u_\xi &= \sqrt{\varepsilon} p \\
p_\xi &= \sqrt{\varepsilon} \left[-v_2 F_2(u, v; \varepsilon) + \varepsilon [\mu u - v_1 F_1(u; \varepsilon)] \right] \\
v_\xi &= q \\
q_\xi &= v - G(u, v; \varepsilon)
\end{cases}
\tag{3.9}
$$

This equation inherits the reversibility symmetry of (3.7) in the form of

$$
\xi \to -\xi, \quad p \to -p, \quad q \to -q.
\tag{3.10}
$$

Especially since we focus on symmetric pulses, this symmetry will play a crucial role in the forthcoming analysis. The singularly perturbed system (3.9) has a family of integrable planar ODEs as fast reduced limit,

$$
v_{f,\xi\xi} = v_f - G(u_0, v_f; 0) \quad \text{or} \quad
\begin{cases}
v_{f,\xi} &= q_f \\
q_{f,\xi} &= v_f - G(u_0, v_f; 0)
\end{cases}
, \quad u_0 > 0
\tag{3.11}
$$

with integrals

$$
\mathcal{H}_v(u_0) = \frac{1}{2} q_f^2 - \frac{1}{2} v_f^2 + \int_0^{v_f} G(u_0, \tilde{v}; 0) \, d\tilde{v},
\tag{3.12}
$$

parameterised by u_0. Note that by the assumption (A4) on $G(u, v; \varepsilon)$ (section 3.1.1), $(v_f, q_f) = (0, 0)$ is a critical point of saddle type for all u_0. The following additional assumption on $G(u, v; 0)$ will be used throughout this chapter.

(A5) *For all $u_0 > 0$ there exists a positive solution $v_{f,h}(\xi; u_0)$ to (3.11) which is homoclinic to $(v_f, q_f) = (0, 0)$.*

Assumption (A5) implies that, for all for all $u_0 > 0$, the level set $\{\mathcal{H}_v(u_0) = 0\}$ (3.12) through the saddle point $(0, 0)$ must intersect the v-axis at $v_M > 0$. If there are multiple intersections, v_M is defined uniquely as the smallest (positive) solution. Due to the translation invariance, $v_{f,h}(\xi; u_0)$ is not yet determined uniquely as function of ξ. Since we consider symmetric pulses in this thesis, we fix $v_{f,h}(\xi; u_0)$ by assuming that

$$v_{f,h}(0; u_0) = v_M, \quad \frac{\mathrm{d}}{\mathrm{d}\xi} v_{f,h}(0; u_0) = 0. \tag{3.13}$$

It is essential for the existence of (positive, symmetric, stationary) pulse solutions $(U_h(\xi)), V_h(\xi))$ to (3.7) that there are open regions in u_0 for which (3.11) has homoclinic solutions to $(0, 0)$: the fast component $V_h(\xi)$ is to leading order determined by an orbit $v_{f,h}(\xi; u_0)$ for a certain $u_0 = u_*$ (see [6, 13] and the subsequent analysis). It is in principle not necessary that such a u_0-region includes the full positive half line. Therefore (A5) is not a crucial assumption to the fullest extent, in the sense that the theory developed here can be straightforwardly extended to equations of the type (3.7) that do not satisfy this condition for all $u_0 > 0$. However, if (A5) is not satisfied, then especially the bifurcation analysis would become much more involved, since homoclinic orbits will appear and disappear as u_* approaches a boundary of one of these regions. These additional bifurcations are not relevant for the method, but do severely diminish the transparency of presentation.

The structure of this section is as follows: we first present an intuitive sketch of the geometrical procedure by which the existence of pulse can be established (that is strongly based on [6]). Based on this, we then formulate our main existence result (Theorem 3.7).

By assumption (A4) on $G(U, V; \varepsilon)$, system (3.9) has a two-dimensional invariant, normally hyperbolic (slow) manifold $\mathcal{M}$, given by

$$\mathcal{M} = \{(u, p, v, q) : v = q = 0, u > 0\}, \tag{3.14}$$

where we restrict ourselves to the positive u-half space since we have allowed G to be singular at $U = 0$ ((A4), [6]). By Fenichel theory [18, 19], $\mathcal{M}$ must have (three-dimensional) stable and unstable manifolds, $\mathcal{W}^s(\mathcal{M})$ and $\mathcal{W}^u(\mathcal{M})$, that are $O(\sqrt{\varepsilon})$ close to the (three-dimensional) stack of level sets $\{\mathcal{H}_v(u_0) = 0\}$ (3.12) associated to the fast reduced limit (3.11). Note that this also implies that both $\mathcal{W}^s(\mathcal{M})$ and $\mathcal{W}^u(\mathcal{M})$ must intersect the hyperplane $\{q = 0\}$ transversally.

The pulse patterns $(U_h(\xi), V_h(\xi))$ considered here (Remark 3.2) correspond to homoclinic orbits $\Gamma_h(\xi) = (u_h(\xi), p_h(\xi), v_h(\xi), q_h(\xi))$ to the critical point $(0, 0, 0, 0)$ of (3.9). These orbits must be contained in the intersection $\mathcal{W}^s(\mathcal{M}) \cap \mathcal{W}^u(\mathcal{M})$ of the stable and unstable manifolds $\mathcal{W}^s(\mathcal{M})$ and $\mathcal{W}^u(\mathcal{M})$ of $\mathcal{M}$. These manifolds may (and most often will) have countably many (two-dimensional) intersections [6]. Here, we restrict ourselves to the first intersections of $\mathcal{W}^s(\mathcal{M})$ and $\mathcal{W}^u(\mathcal{M})$ on which the most simple, one-circuit, homoclinic orbits lie (Remark 3.2). It can be shown by a straightforward Melnikov calculation that the two-dimensional first intersections $\mathcal{I}^{+1} = \mathcal{W}^u(\mathcal{M}) \cap \{q = 0\}$ and $\mathcal{I}^{-1} = \mathcal{W}^s(\mathcal{M}) \cap \{q = 0\}$ must intersect in a one-dimensional manifold $\mathcal{I}^{+1} \cap \mathcal{I}^{-1} = \{(u_0, 0, v_{f,h}(0; u_0) + \mathcal{O}(\sqrt{\varepsilon}), 0); u_0 > 0\} \subset \{p = q = 0\}$, parametrised by u_0 (see [6]). To each $u_0 > 0$ corresponds a solution $\Gamma(\xi; u_0) = (u(\xi; u_0), p(\xi; u_0), v(\xi; u_0), q(\xi; u_0))$ to (3.9) that is biasymptotic to $\mathcal{M}$ (with $\Gamma(0; u_0) \in \mathcal{I}^{+1} \cap \mathcal{I}^{-1}$). Note that this is a natural result: the intersection corresponds to symmetric solutions $\Gamma(\xi; u_0)$ to (3.10); their components $u(\xi; u_0)$ and $v(\xi; u_0)$ are even as function of ξ and have a local extremum at $\xi = 0$. Moreover, if it exists, the homoclinic orbit $\Gamma_h(\xi)$ must correspond to one of the orbits $\Gamma(\xi; u_0)$, i.e. $\Gamma_h(\xi) = \Gamma(\xi; u_*)$ for a certain $u_* > 0$.

Since the u- and p-coordinates only vary slowly in (3.9), the u- and p-components of each orbit $\Gamma(\xi; u_0) \in \mathcal{W}^s(\mathcal{M}) \cap \mathcal{W}^u(\mathcal{M})$ remain to leading order constant during the passage of $\Gamma(\xi; u_0)$ through the fast field. To determine u_*, it is necessary to compute the accumulated change $\Delta u(u_0)$ in $u(\xi; u_0)$ and $\Delta p(u_0)$ in $p(\xi; u_0)$ during a 'jump' of $\Gamma(\xi; u_0)$ through the fast field. To do so, we first give a more precise definition of the fast field,

$$I_f \overset{\text{def}}{=} \left[-\frac{1}{\varepsilon^{\frac{1}{4}}}, \frac{1}{\varepsilon^{\frac{1}{4}}} \right]. \tag{3.15}$$

The boundary of I_f has been placed at the transition zone in which $|\xi| = \varepsilon^{-\frac{1}{4}} \gg 1$ and $|x| = \varepsilon^{\frac{3}{4}} \ll 1$, the precise location of ∂I_f is not essential [6, 8]. In particular the quantity $\Delta p(u_0)$ plays an important role in the analysis, and can be determined as

$$
\begin{aligned}
\Delta p(u_0) &= \int_{-\varepsilon^{-\frac{1}{4}}}^{\varepsilon^{-\frac{1}{4}}} p_\xi \, \mathrm{d}\xi \\
&= \sqrt{\varepsilon} \int_{-\varepsilon^{-\frac{1}{4}}}^{\varepsilon^{-\frac{1}{4}}} \left[-v_2 F_2(u, v; \varepsilon) + \varepsilon[\mu u - v_1 F_1(u; \varepsilon)] \right] \mathrm{d}\xi \\
&= -v_2 \sqrt{\varepsilon} \int_{-\varepsilon^{-\frac{1}{4}}}^{\varepsilon^{-\frac{1}{4}}} F_2(u(\xi; u_0), v(\xi; u_0); \varepsilon) \, \mathrm{d}\xi + \mathcal{O}(\varepsilon^{\frac{5}{4}}) \\
&= -v_2 \sqrt{\varepsilon} \int_{-\varepsilon^{-\frac{1}{4}}}^{\varepsilon^{-\frac{1}{4}}} F_2(u_0, v_{f,h}(\xi; u_0); 0) \, \mathrm{d}\xi + \mathcal{O}(\varepsilon^{\frac{3}{4}}) \\
&= -v_2 \sqrt{\varepsilon} \int_{-\infty}^{\infty} F_2(u_0, v_{f,h}(\xi; u_0); 0) \, \mathrm{d}\xi + \mathcal{O}(\varepsilon^{\frac{3}{4}}),
\end{aligned}
\tag{3.16}
$$

where we used the regular perturbation result that both $|u(\xi; u_0) - u_0|$ and $|v(\xi; u_0) - v_{f,h}(\xi; u_0)|$ are $\mathcal{O}(\sqrt{\varepsilon})$ for $\xi \in I_f$ with $v_{f,h}(\xi; u_0)$ the homoclinic solution of the fast reduced limit system (3.11); note also that $F_2(u_0, v_{f,h}(\xi; u_0); 0)$ decays exponentially in ξ as $|\xi| \to \infty$ (since $F_2(u, 0; 0) = 0$ (A3) and $v_{f,h}(\xi; u_0)$ decays exponentially). We define

$$D_p(u_0) = \int_{-\infty}^{\infty} F_2(u_0, v_{f,h}(\xi; u_0); 0) \, d\xi, \qquad (3.17)$$

so that $\Delta p(u_0) = -v_2 \sqrt{\varepsilon} D_p(u_0) + o(\varepsilon^{\frac{3}{4}})$. Hence, $p(\xi; u_0) = \mathcal{O}(\sqrt{\varepsilon})$ in I_f, which implies that

$$\Delta u(u_0) = \int_{-\varepsilon^{-\frac{1}{4}}}^{\varepsilon^{-\frac{1}{4}}} u_\xi \, d\xi = \sqrt{\varepsilon} \int_{-\varepsilon^{-\frac{1}{4}}}^{\varepsilon^{-\frac{1}{4}}} p(\xi; u_0) \, d\xi = \mathcal{O}(\varepsilon^{\frac{3}{4}}), \qquad (3.18)$$

i.e. that $u(\xi; u_0)$ does not vary at $\mathcal{O}(\sqrt{\varepsilon})$. We can now remove the remaining ambiguities involving the sign of the product of v_2 and F_2 by determining the leading order behaviour of F_2 by gauging

(A6) $D_p(u) \rightsquigarrow 1 \cdot u^{d_p}$ *as* $u \downarrow 0$ *for some* $d_p \in \mathbb{R}$;

see the discussion immediately below Theorem 3.7 for a motivation of this definition. From the above, it follows that the orbits $\Gamma(\xi; u_0)$ 'take off' from $\mathcal{M}$ $\mathcal{O}(\varepsilon^{\frac{3}{4}})$ close to the curve

$$T_o = \left\{ p = \tfrac{1}{2} v_2 \sqrt{\varepsilon} D_p(u), u > 0 \right\} \subset \mathcal{M} \qquad (3.19)$$

and 'touch down' again on its symmetrical image

$$T_d = \left\{ p = -\tfrac{1}{2} v_2 \sqrt{\varepsilon} D_p(u), u > 0 \right\} \subset \mathcal{M}. \qquad (3.20)$$

The curve T_o, respectively T_d, represents the leading order approximation of the collection of base points of the Fenichel fibres in $\mathcal{W}^u(\mathcal{M})$, resp. $\mathcal{W}^s(\mathcal{M})$, that are elements of $\mathcal{W}^u(\mathcal{M}) \cap \mathcal{W}^s(\mathcal{M})$ – see [6] for more details. Hence, the slow evolution of $\Gamma(\xi; u_0) \subset \mathcal{W}^u(\mathcal{M}) \cap \mathcal{W}^s(\mathcal{M})$ after, respectively before its jump through the fast field, i.e. for $\xi > \varepsilon^{-\frac{1}{4}}$ resp. $\xi < -\varepsilon^{-\frac{1}{4}}$, is to leading order governed by a solution of the flow on (the invariant manifold) $\mathcal{M}$ that has $(u_0, p_0) \in T_d$, resp. $\in T_o$, as boundary (initial, resp. end) conditions. Since $F_2(u, 0; \varepsilon) \equiv 0$ (assumption (A3)), the flow on $\mathcal{M}$ is governed by

$$u_{s,xx} = \mu u_s - v_1 F_1(u_s; \varepsilon), \quad \text{or} \quad \begin{cases} u_{s,x} &= p_s \\ p_{s,x} &= \mu u_s - v_1 F_1(u_s; \varepsilon) \end{cases}, \ u > 0, \qquad (3.21)$$

where x is the original slow spatial coordinate of (3.1) (i.e. $x = \varepsilon\xi$). Equation (3.21) is integrable with integral

$$\mathcal{H}_u(\varepsilon) = \frac{1}{2}p_s^2 - \frac{1}{2}\mu u_s^2 + \nu_1 \int_0^{u_s} F_1(\tilde{u}; \varepsilon)\, d\tilde{u}. \tag{3.22}$$

Since $|x| = \varepsilon^{\frac{3}{4}}$ on ∂I_f, the above boundary conditions can (to leading order) be considered as conditions on $(u_s(x), p_s(x))$ at $x = 0$. Note that (3.21) does still depend on ε, i.e. it is not the slow reduced limit associated (3.9): in the form $(u_s(x), p_s(x), 0, 0)$, the solution of (3.21) also is an exact solution of (3.9), in the slow variable x since $\mathcal{M}$ is invariant for the full system (3.9). In fact, since $u_x = \frac{1}{\varepsilon}u_\xi = \frac{1}{\sqrt{\varepsilon}}p$ in (3.9), p_s in (3.21) corresponds to $\frac{1}{\sqrt{\varepsilon}}p$ in (3.9), so that the boundary conditions on $(u_s(x), p_s(x))$ correspond in leading order to

$$(u_s(0), p_s(0)) = \left(u_0, \pm\frac{1}{2}\nu_2 D_p(u_0)\right). \tag{3.23}$$

By the stability of the background state $(U, V) \equiv (0, 0)$ and assumption (A2), the critical point $(0, 0)$ of (3.21) is a saddle point with (one-dimensional) stable, and unstable, manifolds $\mathcal{W}_s^s((0, 0); \varepsilon)$ and $\mathcal{W}_s^u((0, 0); \varepsilon)$. Near $\mathcal{M}$, the orbits $\Gamma(\xi; u_0) \subset \mathcal{W}^u(\mathcal{M}) \cap \mathcal{W}^s(\mathcal{M})$ are with exponential accuracy governed by solutions $u_s(x)$ of (3.21) that satisfy the boundary conditions $(u_s(0), p_s(0)) \in T_{o,d}$, hence it follows that $\Gamma(\xi; u_0)$ is homoclinic to $(0, 0, 0, 0)$ if $u_0 = u_* > 0$ is such that $\Gamma(\xi; u_*)$ takes off from $\mathcal{W}_s^u((0, 0))$ and touches down at $\mathcal{W}_s^s((0, 0))$. In other words, the homoclinic orbit $\Gamma_h(\xi)$ corresponds to a $\Gamma(\xi; u_*)$ with u_* determined as the u-coordinate of an intersection of T_o and $\mathcal{W}_s^u((0, 0))$; note that $T_o \cap \mathcal{W}_s^u((0, 0))$ and $T_d \cap \mathcal{W}_s^s((0, 0))$ have the same u-coordinates by the symmetry (3.10) – see Figure 3.2.

The manifolds $\mathcal{W}_s^u((0, 0))$ resp. $\mathcal{W}_s^s((0, 0))$ are by definition spanned by the solutions $(u_s^u(x; \varepsilon), p_s^u(x; \varepsilon))$ resp. $(u_s^s(x; \varepsilon), p_s^s(x; \varepsilon))$ of (3.21). Note that $u_s^s(x) = u_s^u(-x)$ and $p_s^s(x) = -p_s^u(-x)$ by the reversibility symmetry. As with the definition of the fast reduced homoclinic orbit $v_{f,h}(\xi; u_0)$ – see (3.13) – we need to be more precise here and eliminate the translational invariance from the orbit $(u_s^u(x; \varepsilon), p_s^u(x; \varepsilon))$. This can be done by fixing the location of the point $x = 0$ as $(u_s^u(0; \varepsilon), p_s^u(0; \varepsilon)) = (u_0^u, p_0^u) \in \mathcal{W}_s^u((0, 0))$; now $(u_s^u(x; \varepsilon), p_s^u(x; \varepsilon))$ and therefore $(u_s^s(x; \varepsilon), p_s^s(x; \varepsilon))$ are uniquely determined as solutions of (3.21). Note that the precise position of the point $(u_0^u, p_0^u) \in \mathcal{W}_s^u((0, 0))$ is in general not relevant. However, in an explicit setting, a natural choice for (u_0^u, p_0^u) often presents itself; see the discussion on the relative configurations of $\mathcal{W}_s^u((0, 0))$ and $\mathcal{W}_s^s((0, 0))$ following the statement of Theorem 3.7.
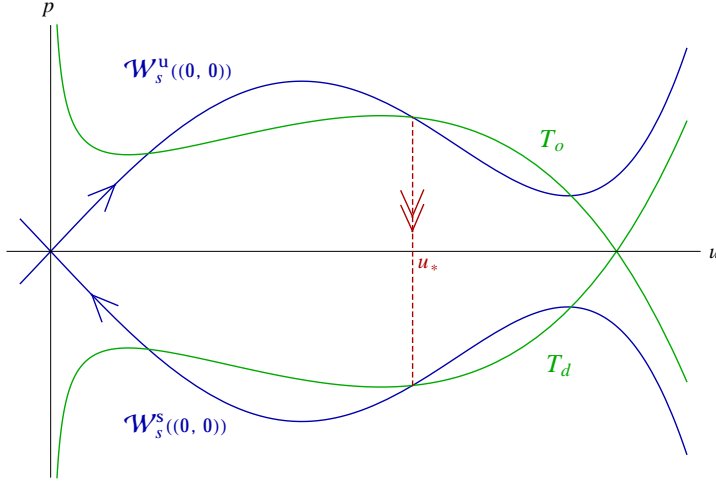
Figure 3.2: The dynamics on the slow manifold $\mathcal{M}$, governed by (3.21). The jump through the fast field is indicated by a red dashed line.

As manifolds $\mathcal{W}_s^u((0,0))$ and $\mathcal{W}_s^s((0,0))$ cannot cross to the negative half-plane (in u), both $\mathcal{W}_s^u((0,0))$ and $\mathcal{W}_s^s((0,0))$ are subsets of $\{\mathcal{H}_u = 0\} \cap \{u \geq 0\}$. A necessary, leading order condition on the critical value(s) u_* for which $\Gamma(\xi; u_*)$ is homoclinic to $(0,0,0,0)$ can be obtained by combining (3.23) with (3.22) and setting ε to 0, i.e. by imposing that $(u_s(0;0), p_s(0;0)) \in \{\mathcal{H}_u(0) = 0\}$, yielding

$$\mu u^2 - 2\nu_1 \int_0^u F_1(\tilde{u}; 0)\, d\tilde{u} = \tfrac{1}{4}\nu_2^2\, D_p^2(u) = \tfrac{1}{4}\nu_2^2 \left[\int_{-\infty}^{\infty} F_2(u, v_{f,h}(\xi; u); 0)\, d\xi \right]^2. \quad (3.24)$$

Since this relation does neither distinguish between T_o and T_d nor between $\mathcal{W}_s^u((0,0))$ and $\mathcal{W}_s^s((0,0))$, there may be solutions $u_{*,j}$ of this equation that do not correspond to homoclinic orbits $\Gamma_h(\xi)$. Using (3.23) we define $p_* = +\tfrac{1}{2}\nu_2 D_p(u_*)$.

As a final prerequisite for the upcoming Theorem, we combine the above defined solutions $(u_s^u(x; \varepsilon), p_s^u(x; \varepsilon))$ which span the slow unstable manifold $\mathcal{W}_s^u((0,0))$ with the (possibly multiple) solution(s) u_* of (3.24) by introducing translational shift(s) x_*, for which the following leading order expression holds:

$$(u_s^u(-x_*; 0), p_s^u(-x_*; 0)) = (u_*, p_*) = (u_s^s(x_*; 0), -p_s^s(x_*; 0)). \quad (3.25)$$

Note that the value of the shift(s) x_* is directly related to the choice of (u_0^u, p_0^u).

Theorem 3.7. *Assume that conditions 3.4 hold and let $\varepsilon > 0$ be small enough. Let K be the number of non-degenerate solutions $u = u_{*,k} > 0$ of (3.24) such that $(u_{*,k}, p_{*,k}) = (u_{*,k}, \frac{1}{2}v_2 D_p(u_{*,k})) \in \mathcal{W}^{\mathrm{u}}_s((0,0); 0)$.*
If $K = 0$ then there are no symmetric, positive, one-circuit homoclinic solutions to $(0, 0, 0, 0)$ in (3.9).
If $K \neq 0$, there are K distinct positive, symmetric, one-circuit homoclinic orbits $\Gamma_{h,k}(\xi) = (u_{h,k}(\xi), p_{h,k}(\xi), v_{h,k}(\xi), q_{h,k}(\xi)) \subset \mathcal{W}^{\mathrm{u}}(\mathcal{M}) \cap \mathcal{W}^{\mathrm{s}}(\mathcal{M})$, $k = 1, 2, ..., K$, in (3.9) with internal reflection point $\xi = 0$, so that $\Gamma_{h,k}(0) = (u_{h,k}(0), 0, v_{h,k}(0), 0)$. In the fast field, $\Gamma_{h,k}(\xi)$ is to leading order determined by the homoclinic solution $v_{f,h}(\xi; u_{*,k})$ of (3.11): there is an $O(1)$ constant $C_1 > 0$ such that

$$
\left| u_{h,k}(\xi) - u_{*,k} \right|, \; \left| p_{h,k}(\xi) \right|, \; \left| v_{h,k}(\xi) - v_{f,h}(\xi; u_{*,k}) \right|,
$$
$$
\left| q_{h,k}(\xi) - \tfrac{\mathrm{d}}{\mathrm{d}\xi} v_{f,h}(\xi; u_{*,k}) \right| \; < C_1 \sqrt{\varepsilon} \; \text{ for } \; \xi \in I_f \quad (3.26)
$$

cf. (3.15). In the slow field, $\Gamma_{h,k}(\xi)$ approaches $\mathcal{W}^{\mathrm{u}}_s((0,0); \varepsilon) \subset \mathcal{M}$, respectively $\mathcal{W}^{\mathrm{s}}_s((0,0); \varepsilon) \subset \mathcal{M}$ exponentially fast for $\xi \to -\infty$, resp. $\xi \to \infty$: there exist $O(1)$ constants $C_{2,3} > 0$ such that

- $\left| v_{h,k}(\xi) \right|, \left| q_{h,k}(\xi) \right| < C_2 e^{-C_3 |\xi|}$ for $\xi \in \mathbb{R} \backslash I_f$;
- *there are shifts $x_{*,k} \in \mathbb{R}$ and solutions $\left(u^{\mathrm{u}}_{*,k}(x), p^{\mathrm{u}}_{*,k}(x) \right) = \left(u^{\mathrm{u}}_s(x - x_{*,k}), p^{\mathrm{u}}_s(x - x_{*,k}) \right)$ of (3.21), such that $\left(u^{\mathrm{u}}_{*,k}(-\varepsilon^{\frac{3}{4}}), p^{\mathrm{u}}_{*,k}(-\varepsilon^{\frac{3}{4}}) \right) = \left(u_{h,k}(-\varepsilon^{-\frac{1}{4}}), \frac{1}{\sqrt{\varepsilon}} p_{h,k}(-\varepsilon^{-\frac{1}{4}}) \right) = \left(u_{*,k} + O(\sqrt{\varepsilon}), p_{*,k} + O(\sqrt{\varepsilon}) \right)$ and*

$$
\left| u_{h,k}(\xi) - u^{\mathrm{u}}_{*,k}(\varepsilon\xi) \right|, \left| \tfrac{1}{\sqrt{\varepsilon}} p_{h,k}(\xi) - p^{\mathrm{u}}_{*,k}(\varepsilon\xi) \right| < C_2 e^{C_3 \xi} \; \text{ for } \; \xi < -\varepsilon^{-\frac{1}{4}}; \quad (3.27)
$$

- $\left(u^{\mathrm{s}}_{*,k}(\varepsilon^{\frac{3}{4}}), p^{\mathrm{s}}_{*,k}(\varepsilon^{\frac{3}{4}}) \right) = \left(u_{h,k}(\varepsilon^{-\frac{1}{4}}), \frac{1}{\sqrt{\varepsilon}} p_{h,k}(\varepsilon^{-\frac{1}{4}}) \right) = \left(u_{*,k} + O(\sqrt{\varepsilon}), -p_{*,k} + O(\sqrt{\varepsilon}) \right)$ with $\left(u^{\mathrm{s}}_{*,k}(x), p^{\mathrm{s}}_{*,k}(x) \right) = \left(u^{\mathrm{u}}_{*,k}(-x), -p^{\mathrm{u}}_{*,k}(-x) \right)$ and

$$
\left| u_{h,k}(\xi) - u^{\mathrm{s}}_{*,k}(\varepsilon\xi) \right|, \left| \tfrac{1}{\sqrt{\varepsilon}} p_{h,k}(\xi) - p^{\mathrm{s}}_{*,k}(\varepsilon\xi) \right| < C_2 e^{-C_3 \xi} \; \text{ for } \; \xi > \varepsilon^{-\frac{1}{4}}. \quad (3.28)
$$

The orbits $\Gamma_{h,k}(\xi)$ correspond to the homoclinic pulse patterns $(U_{h,k}(\xi), V_{h,k}(\xi))$ in (3.7) that are symmetric with respect to $\xi = 0$ through $U_{h,k}(\xi) = u_{h,k}(\xi)$, $V_{h,k}(\xi) = v_{h,k}(\xi)$, $k = 1, ..., K$.

Proof. The essential ingredients of the proof have already been sketched above. The fact that (3.9) concerns a more general class of systems than the generalised GM model does not influence the geometric approach; therefore, we refer to [6] for the full details. □

The (implicit) definition of the signs of $F_2(U, V)$ and ν_2 in assumption (A6) implies that $T_o \subset \{u_s \geq 0, p_s \leq 0\}$ for u_s small enough and $\nu_2 < 0$. In the case that $\mathcal{W}_s^u((0,0)) \subset \{u_s \geq 0, p_s \geq 0\}$ this immediately implies that T_o and $\mathcal{W}_s^u((0,0))$ cannot intersect near the saddle $(0,0)$ if $\nu_2 < 0$. It then follows that, if it is known that expression $D_p(u)$ cannot change sign – which is the case for both the GS and the (generalised) GM models, see [13, 6] and section 3.5.3 – then homoclinic pulse patterns cannot exist. Thus, the definition of the signs of $F_2(U, V)$ and ν_2 through (A6) provides a more direct insight in the relevance of a solution u_* of (3.24), since it gauges the relative positions of T_o and $\mathcal{W}_s^u((0,0))$ as function of ν_2.

Clearly, the condition that $(u_{*,k}, p_{*,k}) \in \mathcal{W}_s^u((0,0); 0)$ is central to the construction of the pulse pattern $(U_{h,k}(\xi), V_{h,k}(\xi))$. Therefore, it is relevant to note that there are two distinct configurations. If $\mathcal{W}_s^u((0,0)) \cap \{p_s = 0\} = \emptyset$, then clearly $\mathcal{W}_s^u((0,0)) \cap \mathcal{W}_s^s((0,0)) = \emptyset$ and $\mathcal{W}_s^u((0,0)) \subset \{u_s \geq 0, p_s \geq 0\}$ (and $\mathcal{W}_s^s((0,0)) \subset \{u_s \geq 0, p_s \leq 0\}$). On the other hand, if $\mathcal{W}_s^u((0,0)) \cap \{p_s = 0\} \neq \emptyset$, then (by the symmetry) $\mathcal{W}_s^u((0,0))$ and $\mathcal{W}_s^s((0,0))$ must have the same, unique, intersection $u_M > 0$ with the u_s-axis and thus merge in a homoclinic orbit to $(0,0)$ – note that this can only happen if $\nu_1 \neq 0$. In this case it is natural to determine $(u_s^u(x; \varepsilon), p_s^u(x; \varepsilon))$ uniquely by choosing $x = 0$ as the location of the internal reflection point of the homoclinic orbit, i.e. to set $(u_s^u(0; \varepsilon), p_s^u(0; \varepsilon)) = (u_0^u, p_0^u) = (u_M, 0)$. Once this gauge choice is made, the sign of x_* determines whether the jump through the fast field occurs before or after the slow component of the pulse passes through the maximum of the slow homoclinic orbit, i.e. whether the jump is downwards ($x_* > 0$) or upwards ($x_* < 0$); see Figure 3.4a resp. 3.4c for an illustration of these two configurations in the context of the model (3.2) studied in chapter 2. It will be shown in section 3.5 (Corollary 3.29) that the second configuration is always unstable. If $\mathcal{W}_s^u((0,0)) \cap \{p_s = 0\} = \emptyset$, there is no natural unique way to gauge the choice of $(u_s^u(0; \varepsilon), p_s^u(0; \varepsilon))$. This is undesirable since in extension the value (and sign) of x_* (3.25) is not fixed. This will turn out to be the cause of technical complications in some parts of the stability analysis, see section 3.5.1. However, the following Lemma allows us to make an unambiguous gauge choice for $(u_s^u(0; \varepsilon), p_s^u(0; \varepsilon)) = (u_0^u, p_0^u)$ in either case. The idea is to alter the vector field defined by $F_{1,2}$ and G beyond a certain u-value, 'bending' the unstable and stable slow manifolds towards each other such that they do intersect.

Lemma 3.8. *Without loss of generality, we may assume that $\mathcal{W}_s^u((0,0)) \cap \{p_s = 0\} \neq \emptyset$ and therefore choose $(u_s^u(0; \varepsilon), p_s^u(0; \varepsilon)) = (u_0^u, p_0^u) = (u_M, 0)$. This fixes the sign of x_* as $\mathrm{sgn}(x_*) = \mathrm{sgn}(p_*)$.*

Proof. Given the functions $F_{1,2}$ and G for which assumptions 3.4 hold, consider an
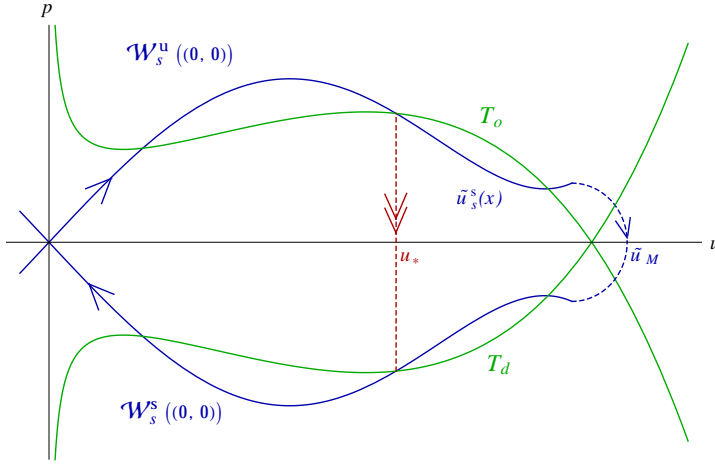
Figure 3.3: The slow manifold with its dynamics as in Figure 3.2, but altered for $u > u_*$ in such a way that the (new) slow stable and unstable manifolds $\tilde{\mathcal{W}}_s^s((0,0))$ and $\tilde{\mathcal{W}}_u^s((0,0))$ intersect at $(\tilde{u}_M, 0)$.

open neighbourhood $\mathcal{U} \in \mathbb{R}^4$ of the set $\left\{(u, p, v, q) \in \mathbb{R}^4 \,|\, u \leq u_{*,K}\right\}$ where $u_{*,K}$ is largest solution to (3.24), see Theorem 3.7. For each function trio $(\tilde{F}_{1,2}, \tilde{G}) \in \Omega$ with

$$\Omega = \left\{\hat{F}_{1,2} \text{ and } \hat{G} \text{ are smooth and } (\tilde{F}_{1,2}(\mathcal{U}), \tilde{G}(\mathcal{U})) = (F_{1,2}(\mathcal{U}), G(\mathcal{U}))\right\},$$

Theorem 3.7 can be applied in the same way and will yield the same results. Now, we alter the original vector field defined by $F_{1,2}$ and G, i.e. pick a suitable function trio $(\tilde{F}_{1,2}, \tilde{G}) \in \Omega$ such that the associated slow stable manifold $\tilde{\mathcal{W}}_s^s((0,0))$ actually does intersect the u-axis beyond $u_{*,K}$ and therefore coincides with $\tilde{\mathcal{W}}_u^s((0,0))$ by symmetry. In the new, altered vector field, the function $\tilde{u}_s^s(x)$ defines a homoclinic orbit, see Figure 3.3. We make the natural choice $(\tilde{u}_0^u, \tilde{p}_0^u) = (\tilde{u}_M, 0)$, see the discussion after Theorem 3.7; this also redefines x_* accordingly as $\tilde{x}_*$. From the choice $\tilde{p}_0^u = \tilde{p}_0^s = 0$ it follows that $\tilde{x}_* > 0$ when $\tilde{p}_* > 0$ and vice versa, see (3.25). $\qquad\square$

Note that the modification of $F_{1,2}$ and G may induce new intersections of $\tilde{W}_s^u((0,0))$ and T_o, see Figure 3.3. These intersections are artificial and –of course– do not correspond to homoclinic orbits in the original system.
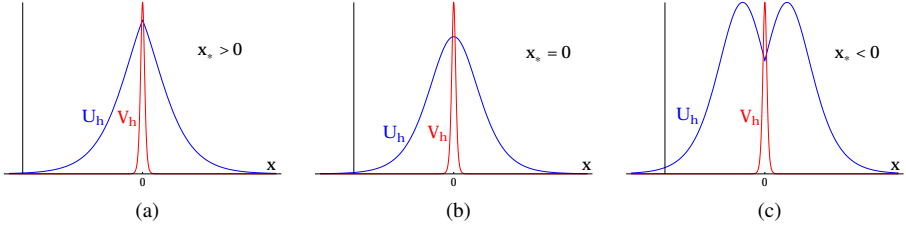
Figure 3.4: The stationary homoclinic pulse $\Gamma_h(x) = (U_h(x), V_h(x))$ as a solution to (3.2) for $x_* > 0$ (3.4a), $x_* = 0$ (3.4b) and $x_* < 0$ (3.4c), as studied in chapter 2.

Finally, we formulate a result on the occurrence of homoclinic saddle node bifurcations, which will especially be relevant in the upcoming stability analysis. We again refer to [6] for (details on the geometry behind) its proof.

Corollary 3.9. *Assume that conditions 3.4 hold and let $\varepsilon > 0$ be small enough. Assume that $u = u_{*,sn} > 0$ is a degenerate solution of (3.24), i.e. that both (3.24) and its u-derivative*

$$2\mu u - 2v_1 F_1(u; 0) = \tfrac{1}{2} v_2^2 D_p(u) \frac{\mathrm{d}}{\mathrm{d}u} D_p(u) \tag{3.29}$$

hold for a certain parameter combination $(\mu_{sn}, v_{1,sn}, v_{2,sn})$ to leading order in ε. Assume furthermore that $(u_{*,sn}, p_{*,sn}) = (u_{*,sn}, \tfrac{1}{2} v_2 D_p(u_{*,sn})) \in \mathcal{W}_s^{\mathrm{u}}((0,0); 0)$ and that $u_{*,sn}$ is a quadratic zero of (3.24). Then the parameter combination $(\mu_{sn}, v_{1,sn}, v_{2,sn})$ determines a saddle node bifurcation of homoclinic orbits: by changing one of the parameters μ, v_1, or v_2 (and keeping the other two fixed), two distinct homoclinic orbits $\Gamma_{h,l}(\xi)$ and $\Gamma_{h,l+1}(\xi)$ of (3.9) merge and annihilate each other.

Remark 3.10. It the forthcoming stability analysis – see especially sections 3.3.2 and 3.5 – it will be necessary to have a measure for the decay rate of $v_{f,h}(\xi; u_*)$ and $v_{f,h}(\xi; u_{*,k})$ as $\xi \to \pm\infty$. It follows from (3.11) in combination with assumption (A4) that $v_{f,h}(\xi; u_*)$ decays like $e^{\mp\xi}$ for $\xi \to \pm\infty$. Therefore, we define $v_{f,\infty}$ by

$$v_{f,h}(\xi; u_*) \rightsquigarrow v_{f,\infty}(u_*) e^{\mp\xi} \quad \text{as} \quad \xi \to \pm\infty. \tag{3.30}$$

Note that $v_{f,\infty} \neq 0$ is determined uniquely, since $v_{f,h}(\xi; u_*)$ has been determined uniquely (3.13) . Likewise, we define $u_{s,\infty}$ by

$$u_s^{\mathrm{s}}(x; \varepsilon) \rightsquigarrow u_{s,\infty} e^{-\sqrt{\mu} x} \quad \text{as} \quad x \to \infty, \tag{3.31}$$

where $u_s^{\mathrm{s}}(x; \varepsilon)$ is the unique nonzero solution to (3.21) that spans the stable manifold $\mathcal{W}_s^{\mathrm{s}}((0,0); \varepsilon)$ – note that the limit exists by assumption (A2).

3.3 Linearization and the reduced problems

In the forthcoming sections we consider the stability of one of the K homoclinic pulse patterns in (3.1) or (3.7) – Theorem 3.7 –, denoted by either $(U_h(x), V_h(x))$ or $(U_h(\xi), V_h(\xi))$.

3.3.1 The linear stability problem

With a small abuse of notation, re-introduce $u(\xi)$ and $v(\xi)$ by

$$U(\xi, t) = U_h(\xi) + u(\xi)e^{\lambda t}, \quad V(\xi, t) = V_h(x) + v(\xi)e^{\lambda t},$$

with $\lambda \in \mathbb{C}$. The linearised stability of $(U_h(\xi), V_h(\xi))$ is thus determined by

$$\varepsilon^2 \lambda u = u_{\xi\xi} - \varepsilon^2 [\mu\, u - v_1 \frac{dF_1}{dU}(U_h)\, u] + \varepsilon v_2 \frac{\partial F_2}{\partial U}(U_h, V_h)\, u + \varepsilon v_2 \frac{\partial F_2}{\partial V}(U_h, V_h)\, v$$

$$\lambda v = v_{\xi\xi} - v + \frac{\partial G}{\partial U}(U_h, V_h) u + \frac{\partial G}{\partial V}(U_h, V_h)\, v \tag{3.32}$$

Introducing the vector $\phi(\xi) = (u(\xi), p(\xi), v(\xi), q(\xi))^T$, with $p = \frac{1}{\sqrt{\varepsilon}} u_\xi$ and $q = v_\xi$, these equations yield the system

$$\dot{\phi} = \mathcal{A}(\xi; \lambda, \varepsilon)\phi, \tag{3.33}$$

where the dot represents $\frac{d}{d\xi}$. Here, $\mathcal{A}(\xi; \lambda, \varepsilon) =$

$$\begin{pmatrix} 0 & \sqrt{\varepsilon} & 0 & 0 \\ \sqrt{\varepsilon}\left(-v_2 \frac{\partial F_2}{\partial U}(U_h, V_h) + \varepsilon\left[\mu + \lambda - v_1 \frac{dF_1}{dU}(U_h)\right]\right) & 0 & \sqrt{\varepsilon}\left(-v_2 \frac{\partial F_2}{\partial V}(U_h, V_h)\right) & 0 \\ 0 & 0 & 0 & 1 \\ -\frac{\partial G}{\partial U}(U_h, V_h) & 0 & \lambda + 1 - \frac{\partial G}{\partial V}(U_h, V_h) & 0 \end{pmatrix}. \tag{3.34}$$

It follows from the smoothness and decay rates in V as $V \to 0$ assumed in (A3) that $\frac{\partial F_2}{\partial V}(U, 0) = F_{2,1}(U) + \frac{\partial F_{2,2}}{\partial V}(U, 0) = F_{2,1}(U)$ and that $\frac{\partial F_2}{\partial U}(U, 0) = 0$. Likewise, by (A4), $\frac{\partial G}{\partial U}(U, 0) = \frac{\partial G}{\partial V}(U, 0) = 0$. Since $V_h(\xi)$ becomes exponentially small as ξ approaches the boundaries $\xi = \pm\varepsilon^{-\frac{1}{4}}$ of the fast field I_f, by the approximation results (3.27), (3.28) on $U_h(\xi)$ for $|\xi| > \varepsilon^{-\frac{1}{4}}$ (Theorem 3.7) and by the reversibility symmetry (3.10), it follows that $\mathcal{A}(\xi; \lambda, \varepsilon)$ approaches the intermediate, slowly varying matrix

$$\mathcal{A}_s(\varepsilon\xi; \lambda, \varepsilon) = \begin{pmatrix} 0 & \sqrt{\varepsilon} & 0 & 0 \\ \varepsilon\sqrt{\varepsilon}\left[(\mu + \lambda) - v_1 \frac{dF_1}{dU}(u_*^s(|\varepsilon\xi|))\right] & 0 & -v_2\sqrt{\varepsilon}F_{2,1}(u_*^s(|\varepsilon\xi|)) & 0 \\ 0 & 0 & 0 & 1 \\ 0 & 0 & \lambda + 1 & 0 \end{pmatrix} \tag{3.35}$$

in the slow field $|\xi| > \varepsilon^{-\frac{1}{4}}$ – see section 3.3.4. It clearly also follows from (3.27), (3.28) (and assumptions (A1 - A4)) that there are positive $O(1)$ constants $\tilde{C}_2$ and $\tilde{C}_3$ such that

$$\|\mathcal{A}(\xi; \lambda, \varepsilon) - \mathcal{A}_s(\varepsilon\xi; \lambda, \varepsilon)\| \le \tilde{C}_2 e^{-\tilde{C}_3|\xi|} \quad \text{for} \quad |\xi| > \varepsilon^{-\frac{1}{4}}. \tag{3.36}$$

Both matrices $\mathcal{A}(\xi; \lambda, \varepsilon)$ and $\mathcal{A}_s(x; \lambda, \varepsilon)$ approach the constant coefficient matrix

$$\mathcal{A}_\infty(\lambda, \varepsilon) = \begin{pmatrix} 0 & \sqrt{\varepsilon} & 0 & 0 \\ \varepsilon\sqrt{\varepsilon}(\lambda + \mu) & 0 & -\nu_2\sqrt{\varepsilon}F_{2,1}(0) & 0 \\ 0 & 0 & 0 & 1 \\ 0 & 0 & \lambda + 1 & 0 \end{pmatrix} \tag{3.37}$$

as $\xi, x \to \pm\infty$ by assumption (A3). Due to the block diagonal, upper triangular structure of $\mathcal{A}_\infty(\lambda)$, its eigenvalues $\{\pm\Lambda_f, \pm\varepsilon\Lambda_s\}$ with

$$\Lambda_f(\lambda) = \sqrt{1 + \lambda}, \quad \Lambda_s(\lambda) = \sqrt{\mu + \lambda}. \tag{3.38}$$

are not influenced by the coupling term $-\nu_2\sqrt{\varepsilon}F_{2,1}(0)$. It follows that $\operatorname{Re}\Lambda_f(\lambda) > \operatorname{Re}\varepsilon\Lambda_s(\lambda)$ outside an $O(\varepsilon)$ neighborhood of the essential spectrum

$$\sigma_e = \{\lambda \in \mathbb{R} : \lambda \le \max(-\mu, -1)\} \subset \mathbb{C} \tag{3.39}$$

associated to the linear stability problem (3.32)/(3.33) – recall that σ_e corresponds to those values of λ for which one of the $\Lambda_{f,s}(\lambda)$'s is purely imaginary [45]. The impact of the coupling term $-\nu_2\sqrt{\varepsilon}F_{2,1}(0)$ on the eigenvectors of $\mathcal{A}_\infty(\lambda)$ is at most of $O(\sqrt{\varepsilon})$ as long as λ is not $O(\sqrt{\varepsilon})$ close to σ_e:

$$\begin{aligned} E_{f,\pm}(\lambda, \varepsilon) &= \left(-\frac{\nu_2\varepsilon F_{2,1}(0;\varepsilon)}{1 + \lambda - \varepsilon^2(\lambda + \mu)}, \mp\frac{\nu_2\sqrt{\varepsilon}F_{2,1}(0;\varepsilon)}{1 + \lambda - \varepsilon^2(\lambda + \mu)}\sqrt{1 + \lambda}, 1, \pm\sqrt{1 + \lambda} \right)^T, \\ E_{s,\pm}(\lambda, \varepsilon) &= \left(1, \pm\sqrt{\varepsilon}\sqrt{\mu + \lambda}, 0, 0 \right)^T. \end{aligned} \tag{3.40}$$

The essential difference between the present stability analysis and the existing literature on the stability of pulses in GS/GM-type models [6, 7, 26, 32, 33] is made explicit by the terms $\nu_1\frac{dF_1}{dU}(u_*^s(|\varepsilon\xi|))$ and $-\nu_2\sqrt{\varepsilon}F_{2,1}(u_*^s(|\varepsilon\xi|))$ of $\mathcal{A}_s(\varepsilon\xi; \lambda)$, i.e. by the fact that there is an intermediate slowly varying matrix between $\mathcal{A}(\xi; \lambda, \varepsilon)$ and $\mathcal{A}_\infty(\lambda\varepsilon)$: in general the matrix $\mathcal{A}(\xi; \lambda, \varepsilon)$ thus does not approach its constant coefficient limit state $\mathcal{A}_\infty(\lambda, \varepsilon)$ exponentially fast on the fast spatial scale. In other words, the GS/GM-type models are (very!) special in the sense that $\nu_1 = 0$ and $F_{2,1}(0) = 0$, so that there is an exponentially accurate estimate like (3.36) on $\|\mathcal{A}(\xi; \lambda, \varepsilon) - \mathcal{A}_\infty(\lambda, \varepsilon)\|$ for $\xi \in \mathbb{R}\backslash I_f$. This fact is crucially used in the stability analysis: it allows one to solve (3.33) outside I_f with an exponential accuracy in terms of simple exponentials (based on (3.38),

(3.40)). Moreover, this behaviour is also central to the construction of an Evans function $\mathcal{D}(\lambda; \varepsilon)$ associated to (3.33) and it subsequent decomposition into a slow and a fast Evans function [3, 6, 7].

In this chapter, the role of $\mathcal{A}_\infty(\lambda, \varepsilon)$ will be taken over by the slow intermediate matrix $\mathcal{A}_s(\varepsilon\xi; \lambda, \varepsilon)$ for $\xi \notin I_f$. The construction of the Evans function $\mathcal{D}(\lambda)$ associated to (3.33) will also be based on the matrix $\mathcal{A}_s(\varepsilon\xi; \lambda, \varepsilon)$. This Evans function will be decomposed in a slow and a fast component using the fast exponential estimate (3.36) – see section 3.4. In the construction of $\mathcal{D}(\lambda)$, the role of the simple exponentials associated to $\mathcal{A}_\infty(\lambda, \varepsilon)$ will be taken over by the fundamental intermediate solutions of the linear system associated to $\mathcal{A}_s(\varepsilon\xi; \lambda, \varepsilon)$. This system will be studied in section 3.3.4. However, we will first study the fast reduced limit systems associated to (3.32)/(3.33).

Remark 3.11. The assumption that $\beta_2 > 1$ in (A4) excludes the possibility of having terms like UV in the V equation, i.e. the nonlinear term $G(U, V)$ of the V-equation is not allowed to be like its counterpart $F_2(U, V)$ in the U-equation (A3). Similar to the effect of a linear term in U in the V-equation for the existence problem – see section 3.1.1 and Remark 3.5 – terms like UV in the V-equation will lead to slowly varying terms in the fast stability equation. Once again (Remark 3.5), this can in principle be handled, see for instance [8] in which an explicit (Ginzburg-Landau type) system with a coupling term the type UV has been analysed along the lines of the present approach. However, since it introduces additional technicalities (and thus obscures the presentation), we refrain from going into the details.

3.3.2 The homogeneous fast reduced Sturm-Liouville problem

It follows from (3.26) in Theorem 3.7 that the linear stability problem (3.32) reduces in the region I_f and in the limit $\varepsilon \to 0$ to the fast reduced limit problem

$$\lambda v = v_{\xi\xi} - v + \frac{\partial G}{\partial U}(u_*, v_{f,h}(\xi; u_*)) \, u(0) + \frac{\partial G}{\partial V}(u_*, v_{f,h}(\xi; u_*)) \, v, \quad \xi \in \mathbb{R}, \qquad (3.41)$$

where we have used that $u(\xi)$ only varies slowly and thus approaches a constant value $u(0)$ in I_f in this limit. Equation (3.41) is an inhomogeneous Sturm-Liouville problem. In this section, we study the associated homogeneous problem

$$(\mathcal{L}_f(\xi) - \lambda) \, w \stackrel{\text{def}}{=} w_{\xi\xi} + \left[\frac{\partial G}{\partial V}(u_*, v_{f,h}(\xi; u_*)) - (1 + \lambda) \right] w = 0, \quad \text{with} \quad \lim_{\xi \to \pm\infty} w(\xi) = 0.$$
$$(3.42)$$

In the NLEP analysis of the Evans function associated to the stability of a pulse in GS/GM-type models [6, 7], the homogeneous fast reduced linearised stability problem (3.42) has a very special form: as function of V, $G(U, V)$ simply behaves as V^{β_1} (with $\beta_2 > 1$ in the (generalised) GM setting (3.8) and $\beta_2 = 2$ for the GS and the standard GM model). As a consequence, (3.42) can be solved exactly (in terms of hypergeometric functions [6, 7] or associated Legendre functions, see chapter 2). This fact is an essential ingredient of the NLEP analysis in this type of models. Of course this is quite a special, and thus a priori restrictive feature of the GS/GM-type models. As was already remarked in the introduction, this restriction forms the second main ingredient of our motivation to develop the present more general (stability) theory.

To do so, we first note that for functions $G(U, V)$ as described by assumption (A4) and $v_{f,h}(\xi; u_*)$ as homoclinic solution to (3.11), equation (3.42) has the form of a classical (singular) Sturm-Liouville eigenvalue problem. The following Lemma summarises results on this type of problems in the literature (see for instance [49]).

Lemma 3.12. *Let $H : \mathbb{R}_{\geq 0} \to \mathbb{R}$ be such that the differential equation $w_{xx} = \rho w - H(w)$, $\rho > 0$ has a solution w_h which is homoclinic to $(w, w_x) = (0, 0)$, and write $h(x) = H'(w_h(x))$. For a differential operator of the form $\mathcal{L}(x) = \frac{d^2}{dx^2} + h(x) - \rho$, consider the eigenvalue problem $[\mathcal{L}(x) - \lambda] w = 0$ with boundary conditions $\lim_{x \to \pm\infty} w(x) = 0$. Moreover, define $\Lambda = \sqrt{\rho + \lambda}$; $arg(\Lambda) \in (-\frac{\pi}{2}, \frac{\pi}{2}]$. Then the following holds:*

(i) There is a finite number of real eigenvalues λ_j, $j = 0, 1, \cdots, J$ for which $\lambda_0 > 0$, $\lambda_1 = 0$ and $0 > \lambda_2 > \cdots > \lambda_J > -\rho$. Equivalently, there is a finite number of real eigenvalues Λ_j for which $\Lambda_0 > \sqrt{\rho}$, $\Lambda_1 = \sqrt{\rho}$ and $\sqrt{\rho} > \Lambda_2 > \cdots > \Lambda_J > 0$.

(ii) The associated eigenfunctions $w_j(x)$ have j distinct zeroes and are even resp. odd as a function of x if j is even resp. odd. Moreover, $\frac{d}{dx} w_h(x)$ is an eigenfunction for $\lambda_1 = 0$ (or $\Lambda_1 = 1$); in other words, $w_1(x) \in span\left\{\frac{d}{dx} w_h(x)\right\}$.

(iii) The eigenfunctions $w_j(x)$, $j = 0, \cdots, J$ form an orthogonal set:

$$\langle w_j, w_k \rangle = \int_{-\infty}^{\infty} w_j(x) w_k(x)\, dx = 0 \quad for \quad j \neq k, \quad and \quad \|w_j\|_2 = \sqrt{\langle w_j, w_j \rangle} \neq 0;$$

these eigenfunctions can be determined uniquely by the condition

$$w_j(x) \rightsquigarrow 1 \cdot e^{-\Lambda_j x} \quad as \quad x \to \infty. \tag{3.43}$$

(iv) The spectrum associated to the eigenvalue problem $[\mathcal{L}(x) - \lambda]\,w = 0$ is given by $\sigma_\lambda = (-\infty, -\rho) \cup \{\lambda_0, \cdots, \lambda_J\}$ or equivalently $\sigma_\Lambda = i\mathbb{R}_{>0} \cup \{\Lambda_0, \cdots, \Lambda_J\}$.

(v) For every $\lambda \notin \sigma_\lambda$, there is a unique solution $w_\lambda^{\mathrm{R}}(x)$ (which depends smoothly on λ) such that

$$w_\lambda^{\mathrm{R}}(x) \rightsquigarrow 1 \cdot e^{-\Lambda x} \quad as \quad x \to \infty. \tag{3.44}$$

Moreover, the pair $\{w_\lambda^{\mathrm{R}}, w_\lambda^{\mathrm{L}}\}$ with $w_\lambda^{\mathrm{L}}(x) = w_\lambda^{\mathrm{R}}(-x)$ spans the solution space of the eigenvalue problem $[\mathcal{L}(x) - \lambda]\,w = 0$.

For (3.42) we can apply the above Lemma with $\rho = 1$, obtaining a set of fast eigenvalues $\lambda_{f,j}$ and their associated eigenfunctions $w_{f,j}(\xi)$. Moreover, we observe that for $\rho = 1$, $\Lambda = \Lambda_f$ (3.38).

Next, we consider the Wronskian

$$\mathcal{W}(\lambda) \stackrel{\mathrm{def}}{=} \det \begin{pmatrix} w_\lambda^{\mathrm{L}}(\xi) & w_\lambda^{\mathrm{R}}(\xi) \\ \frac{\mathrm{d}}{\mathrm{d}\xi} w_\lambda^{\mathrm{L}}(\xi) & \frac{\mathrm{d}}{\mathrm{d}\xi} w_\lambda^{\mathrm{R}}(\xi) \end{pmatrix} \tag{3.45}$$

associated to (3.42). For notational convenience we only consider $\mathcal{W}$ as function of λ here and in the upcoming Lemma. In the forthcoming analysis we will however often switch between the equivalent expressions $\mathcal{W}(\lambda)$ and $\mathcal{W}(\Lambda_f)$. This Wronskian can be defined as a smooth, in fact analytic, function of λ for all $\lambda \in \mathbb{C}$ outside the (closure of the) essential spectrum associated to (3.42), i.e. for $\lambda \notin (-\infty, -1]$, but including the (eigen)values $\lambda = \lambda_{f,j}$ (Lemma 3.12), by setting $\mathcal{W}(\lambda_{f,j}) = 0$, $j = 0, ..., J$ [49]. Note that $\mathcal{W}(\lambda)$ is in fact an Evans function [3]. In combination with Lemma 3.12, the following result on $\mathcal{W}(\lambda)$ enables us to generalise the GS/GM-type hypergeometric functions approach to the present setting.

Lemma 3.13. *Let $\mathcal{W}(\lambda)$ be the Wronskian associated to (3.42) and let $\lambda \notin (-\infty, -1]$, then*

$$\mathcal{W}(\lambda) \rightsquigarrow (-1)^{j+1} \|w_{f,j}\|_2^2 (\lambda - \lambda_{f,j}) \quad as \quad \lambda \to \lambda_{f,j}, \ j = 0, ..., J.$$

See Figure 3.5 for a sketch of a $\mathcal{W}(\lambda)$ for real $\lambda > -1$.

Proof. Since we know that $\mathcal{W}(\lambda)$ is a smooth function of λ near its zeroes $\lambda_{f,j}$, the proof can be based on a (finite) Taylor expansion of $\mathcal{W}(\lambda_{f,j} + \delta)$ for $\delta = \lambda - \lambda_{f,j} \in \mathbb{C}$ small. To do so, we first need to approximate $w_\lambda^{\mathrm{R}}(\xi)$ for $\lambda = \lambda_{f,j} + \delta$. Therefore, we introduce the (regular) approximation

$$w_{\lambda_{f,j}+\delta}^{\mathrm{R}}(\xi) = w_{f,j}(\xi) + \delta w_{1,j}(\xi) + \mathcal{R}(\xi; \delta), \tag{3.46}$$
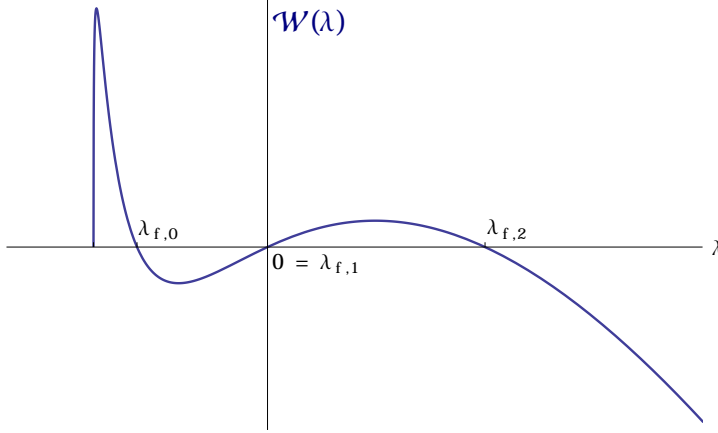
Figure 3.5: A sketch of the Wronskian $\mathcal{W}(\lambda)$ associated to (3.42) in the case of the model problem (3.2), for $\lambda \in \mathbb{R}$.

in which $\mathcal{R}(\xi; \delta)$ represents the error terms. This expansion can in general not give a valid approximation of $w^{\mathrm{R}}_{\lambda_{f,j}+\delta}(\xi)$ for $\xi \to \infty$. However, it follows directly from Poincaré's Expansion Theorem (see for instance [55]) that for every $\rho \in [0, 1)$ there is a positive $O(1)$ constant C_ρ such that

$$|w^{\mathrm{R}}_{\lambda_{f,j}+\delta}(\xi) - (w_{f,j}(\xi) + \delta w_{1,j}(\xi))| = |\mathcal{R}(\xi; \delta)| < C_\rho \delta^{2(1-\rho)}, \tag{3.47}$$

for $|\xi| < O(\delta^{-\rho})$. Note that the standard (and natural) result that $\mathcal{R}(\xi; \delta)| = O(\delta^2)$ on $O(1)$ ξ-intervals corresponds to the case $\rho = 0$ in (3.47). To determine the leading order correction $w_{1,j}(\xi)$, we substitute (3.46) into (3.42) and obtain the inhomogeneous problem

$$(\mathcal{L}_f(\xi) - \lambda_{f,j})\, w_{1,j} = w_{f,j}(\xi) + O\left(\delta^{1-2\rho}\right)$$

(3.42) on the domain $|\xi| < O(\delta^{-\rho})$. It is clear that for the above to be a leading order expression, $\rho < \frac{1}{2}$ must hold. This equation cannot have a solution that is bounded on $\mathbb{R}$, since the operator $\mathcal{L}_f(\xi) - \lambda$ is not invertible at $\lambda = \lambda_{f,j}$ and the inhomogeneous term $b(\xi) = w_{f,j}(\xi)$ clearly does not satisfy the solvability condition $\langle b, w_{f,j} \rangle = \langle w_{f,j}, w_{f,j} \rangle = 0$, see also section 3.3.3. However, this is not a problem: we are constructing an approximation of a solution $w^{\mathrm{R}}_\lambda(\xi)$ and this solution need not be bounded on $\mathbb{R}$ for $\lambda \neq \lambda_{f,j}$ (Lemma 3.12). Since $w_{f,j}(\xi)$ is a solution of the homogeneous problem, we apply the variation of constants method, i.e. we introduce

the unknown function $c_j(\xi)$ by $w_{1,j}(\xi) = c_j(\xi)w_{f,j}(\xi)$ and obtain an equation for c_j:

$$\ddot{c}_j w_{f,j} + 2\dot{c}_j \dot{w}_{f,j} = w_{f,j}.$$

This implies that

$$\dot{c}_j(\xi) = \frac{1}{w_{f,j}^2(\xi)} \left[\int_0^\xi w_{f,j}^2(\eta)\, d\eta + c_{1,j} \right],$$

where $c_{1,j}$ is a constant of integration. Writing $c_{1,j} = \hat{c}_{1,j} - \int_0^\infty w_{f,j}^2(\eta)\, d\eta$, we investigate the behaviour of $\dot{c}_j(\xi)$ as $\xi \to \delta^{-\rho}$. From Lemma 3.12, we know that $w_{f,j}(\xi) \sim e^{-\Lambda_{f,j}\delta^{-\rho}}$ as $\xi \to \delta^{-\rho}$. Therefore,

$$\begin{aligned}
\dot{c}_j(\xi) &\sim e^{2\Lambda_{f,j}\delta^{-\rho}} \left[\int_0^{\delta^{-\rho}} w_{f,j}^2(\eta)\, d\eta - \int_0^\infty w_{f,j}^2(\eta)\, d\eta + \hat{c}_{1,j} \right] \\
&= \left[-\int_{\delta^{-\rho}}^\infty w_{f,j}^2(\eta)\, d\eta + \hat{c}_{1,j} \right] e^{2\Lambda_{f,j}\delta^{-\rho}} \\
&= -\frac{1}{2\Lambda_{f,j}} + \hat{c}_{1,j} e^{2\Lambda_{f,j}\delta^{-\rho}}
\end{aligned} \tag{3.48}$$

as $\xi \to \delta^{-\rho}$. Since the solution $w_{\lambda_{f,j}+\delta}^{R}(\xi)$ (3.46) does not grow exponentially as $\xi \to \delta^{-\rho}$ (3.44), it necessarily follows that $w_{1,j}(\xi)$ does neither. Therefore, $c_j(\xi)$ can at most grow as $\frac{1}{w_{f,j}}$, which is as $e^{\Lambda_{f,j}\xi}$. From this, it follows that $\hat{c}_{1,j} = 0$ and therefore

$$c_{1,j} = -\int_0^\infty w_{f,j}^2(\eta)\, d\eta \quad \text{so that} \quad \dot{c}_j(\xi) = -\frac{1}{w_{f,j}^2(\xi)} \int_\xi^\infty w_{f,j}^2(\eta)\, d\eta. \tag{3.49}$$

We now return to the Wronskian (3.45). Since $w_{\lambda_{f,j}+\delta}^{R}(\xi) = w_{f,j}(\xi)\left(1 + \delta c_j(\xi)\right) + \mathcal{R}(\xi; \delta)$, we can use Lemma 3.12 (ii),(v) to obtain

$$\begin{aligned}
w_{\lambda_{f,j}+\delta}^{R}(\xi) &= w_{f,j}(\xi)\left(1 + \delta c_j(\xi)\right) + \mathcal{R}(\xi; \delta), & (3.50) \\
w_{\lambda_{f,j}+\delta}^{L}(\xi) &= (-1)^j w_{f,j}(\xi)\left(1 + \delta c_j(-\xi)\right) + \mathcal{R}(-\xi; \delta), & (3.51) \\
\frac{d}{d\xi} w_{\lambda_{f,j}+\delta}^{R}(\xi) &= \frac{dw_{f,j}}{d\xi}(\xi)\left(1 + \delta c_j(\xi)\right) + \delta w_{f,j}(\xi)\frac{dc_j}{d\xi}(\xi) + \frac{d\mathcal{R}}{d\xi}(\xi; \delta), & (3.52) \\
\frac{d}{d\xi} w_{\lambda_{f,j}+\delta}^{L}(\xi) &= (-1)^j \left[\frac{dw_{f,j}}{d\xi}(\xi)\left(1 + \delta c_j(-\xi)\right) - \delta w_{f,j}(\xi)\frac{dc_j}{d\xi}(-\xi) \right] - \frac{d\mathcal{R}}{d\xi}(-\xi; \delta). & (3.53)
\end{aligned}$$

Since $w_\lambda^{L/R}(\xi)$ depends smoothly on λ (cf. Lemma 3.12), the Poincaré Expansion Theorem can be applied to $\frac{d}{d\xi} w_{\lambda_{f,j}+\delta}^{R}$ to obtain the result that for every $\hat{\rho} \in [0, 1)$ there is a $C_{\hat{\rho}}$ such that $|\frac{d\mathcal{R}}{d\xi}(\xi; \delta)| < C_{\hat{\rho}} \delta^{2(1-\hat{\rho})}$. Choosing $\hat{\rho} = \rho < \frac{1}{2}$ enables us to treat $\frac{d\mathcal{R}}{d\xi}$ as a higher order term. Using the above expansions for the Wronskian, we obtain

$$\begin{aligned}
\mathcal{W}(\lambda_{f,j} + \delta) &= (-1)^j \left(w_{f,j}\frac{dw_{f,j}}{d\xi} - \frac{dw_{f,j}}{d\xi}w_{f,j} \right)\left(1 + \delta c_j(\xi) + \delta c_j(-\xi)\right) \\
&\quad + \delta(-1)^j w_{f,j}^2(\xi)\left[\frac{dc_j}{d\xi}(\xi) + \frac{dc_j}{d\xi}(-\xi) \right] + \mathcal{O}(\delta^2) \\
&= \delta(-1)^j w_{f,j}^2(\xi)\left[\frac{dc_j}{d\xi}(\xi) + \frac{dc_j}{d\xi}(-\xi) \right] + \mathcal{O}(\delta^2),
\end{aligned} \tag{3.54}$$

in which we refrained from explicitly writing down all $O(\delta^2) = O(|\lambda - \lambda_{f,j}|^2)$ correction terms. Using (3.49), we see that

$$
\begin{aligned}
w_{f,j}^2(\xi) \left[\tfrac{\mathrm{d}c_j}{\mathrm{d}\xi}(\xi) + \tfrac{\mathrm{d}c_j}{\mathrm{d}\xi}(-\xi) \right] &= -\int_\xi^\infty w_{f,j}^2(\eta)\,\mathrm{d}\eta - \int_{-\xi}^\infty w_{f,j}^2(\eta)\,\mathrm{d}\eta \\
&= -\int_{-\infty}^\infty w_{f,j}^2(\eta)\,\mathrm{d}\eta = -\|w_{f,j}\|_2^2
\end{aligned}
$$

using again Lemma 3.12 (ii). $\qquad\square$

Clearly, the Wronskian $\mathcal{W}(\lambda)$ has an extremum for $\lambda \in \mathbb{R}$ between two successive eigenvalues. Based on the previous Lemma it can easily be established that this extremum is a maximum between $\lambda_{2j+1} < \lambda_{2j}$ and a minimum between $\lambda_{2j} < \lambda_{2j-1}$. The following Lemma determines the limit behaviour of $\mathcal{W}(\lambda)$ for $\lambda \in \mathbb{R}$ large, see also Figure 3.5.

Lemma 3.14. *Let $\mathcal{W}(\lambda)$ be the Wronskian associated to (3.42) and let $\lambda \in \mathbb{R}\backslash(-\infty, -1]$, then*

$$
\mathcal{W}(\lambda) \rightsquigarrow -2\sqrt{\lambda} \ \ \text{as} \ \ \lambda \to +\infty.
$$

Proof. Define $\delta = 1/\Lambda_f > 0$ $(\Lambda_f \in \mathbb{R})$. It can be shown by the methods of the above proof that for δ small enough, i.e. $\Lambda_f > 0$ large enough,

$$
w_\lambda^{\mathrm{R}}(\xi) = e^{-\Lambda_f \xi}(1 + O(\delta)), \ \ \text{and} \ \ w_\lambda^{\mathrm{L}}(\xi) = e^{\Lambda_f \xi}(1 + O(\delta)).
$$

on an $O(1)$ ξ-domain $\supset \{\xi = 0\}$. Hence, for Λ_f large enough,

$$
\mathcal{W}(\Lambda_f) = \det \begin{pmatrix} e^{\Lambda_f \xi}(1 + O(\delta)) & e^{-\Lambda_f \xi}(1 + O(\delta)) \\ \Lambda_f e^{\Lambda_f \xi}(1 + O(\delta)) & -\Lambda_f e^{-\Lambda_f \xi}(1 + O(\delta)) \end{pmatrix} = -2\Lambda_f(1 + O(\delta)),
$$

which is equivalent to the statement of the Lemma by the definition of Λ_f (3.38). $\quad\square$

3.3.3 The inhomogeneous fast reduced Sturm-Liouville problem

Since the inhomogeneous problem (3.41) is linear (and can thus be rescaled), we define $v_{\mathrm{in}}(\xi; \lambda)$ as the bounded solution of

$$
(\mathcal{L}_f(\xi) - \lambda)\, v = -\frac{\partial G}{\partial U}(u_*, v_{f,h}(\xi; u_*)). \tag{3.55}
$$

Note that this is only possible if $u(0) \neq 0$; the situation where $u(0) = 0$ will be treated in section 3.5 (which is related to the case $B_-(\lambda) = 0$ there). It follows from

the general theory on Sturm-Liouville problems that $v_{in}(\xi; \lambda)$ is uniquely determined for $\lambda \notin \sigma_f$ [49]. Since $\{w_\lambda^L(\xi), w_\lambda^R(\xi)\} = \{w_\lambda^R(-\xi), w_\lambda^R(\xi)\}$ span the solution space associated to the homogeneous problem (Lemma 3.12), $v_{in}(\xi; \lambda)$ can be determined explicitly (in terms of $w_\lambda^R(\pm\xi)$).

Lemma 3.15. *The bounded solution of (3.55) is given by $v_{in}(\xi; \lambda) = A(\xi)w_\lambda^R(\xi) + A(-\xi)w_\lambda^R(-\xi)$, with*

$$A(\xi) = A(\xi; \lambda) = -\frac{1}{\mathcal{W}(\lambda)} \int_{-\infty}^{\xi} \frac{\partial G}{\partial U}(u_*, v_{f,h}(\tilde{\xi}; u_*)) \, w_\lambda^R(-\tilde{\xi}) \, d\tilde{\xi}. \tag{3.56}$$

Note that it immediately follows from this expression and assumption (A4) in combination with the properties of $v_{f,h}(\xi; u_*)$ that $v_{in}(\xi; \lambda)$ decays exponentially fast to 0 as $\xi \to \pm\infty$ (and as ξ approaches the boundaries of I_f (3.15)).

Proof. By the variation of constants approach, we introduce the unknown functions $A^{L/R}(\xi)$ by $v_{in}(\xi) = A^L(\xi)w_\lambda^L(\xi) + A^R(\xi)w_\lambda^R(\xi)$. Substitution in (3.55) yields

$$\dot{A}^{L/R} = \frac{\mp 1}{\mathcal{W}(\lambda)} \frac{\partial G}{\partial U}(u_*, v_{f,h}(\xi; u_*))w_\lambda^{\mp}(\xi),$$

so that

$$A^{L/R}(\xi) = A^{L/R}(0) \mp \frac{1}{\mathcal{W}(\lambda)} \int_0^{\xi} \frac{\partial G}{\partial U}(u_*, v_{f,h}(\tilde{\xi}; u_*))w_\lambda^{\mp}(\tilde{\xi}) \, d\tilde{\xi}.$$

Both the operator $\mathcal{L}_f(\xi)$ and the inhomogeneous term in (3.55) are even as function of ξ. This implies that also $v_{in}(\xi; \lambda)$ must be even, so that $A^R(\xi) = A^L(-\xi) \stackrel{\text{def}}{=} A(\xi)$ and $A^R(0) = A^L(0)$. A straightforward analysis yields that $v_{in}(\xi)$ can only be bounded if

$$A(0) = -\frac{1}{\mathcal{W}(\lambda)} \int_{-\infty}^{0} \frac{\partial G}{\partial U}(u_*, v_{f,h}(\tilde{\xi}; u_*))w_\lambda^L(\tilde{\xi}) \, d\tilde{\xi},$$

which is a converging integral by assumption (A4). $\qquad\square$

A priori, there is a singularity in the solutions $v_{in}(\xi; \lambda)$ as $\lambda \to \lambda_{f,j}$, due to the fact that $(\mathcal{L}_f(\xi) - \lambda)$ is not invertible at $\lambda_{f,j}$ (and that thus $\mathcal{W}(\lambda_{f,j}) = 0$, Lemma 3.13). However, by the Fredholm alternative, (3.55) will have solutions for $\lambda = \lambda_{f,j}$ with j odd, since $w_{f,j}(\xi)$ is odd as function of ξ (Lemma 3.12) and the (even) inhomogeneity of (3.55) thus satisfies the solvability condition.

Corollary 3.16. *For j even,*

$$v_{\text{in}}(\xi; \lambda) \rightsquigarrow \left(\frac{w_{f,j}(\xi)}{\|w_{f,j}\|_2^2} \int_{-\infty}^{\infty} \frac{\partial G}{\partial U}(u_*, v_{f,h}(\tilde{\xi}; u_*)) \, w_{f,j}(\tilde{\xi}) \, \mathrm{d}\tilde{\xi} \right) \cdot \frac{1}{\lambda - \lambda_{f,j}} \quad as \quad \lambda \to \lambda_{f,j},$$

(3.57)

while $\lim_{\lambda \to \lambda_{f,j}} v_{\text{in}}(\xi; \lambda)$ *exists for j odd.*

Proof. Using the fact that $w_{f,j}(\xi)$ is even/odd as function of ξ for j even/odd, identity (3.57) can be obtained directly by combining Lemma's 3.13 and 3.15, both for j even and for j odd – in the latter case, the integral in (3.57) vanishes. □

It will be necessary to also have an explicit characterization of $v_{\text{in}}(\xi; \lambda)$ for λ near $\lambda_{f,1}$, the crucial (odd) case $j = 1$ for which $\lambda_{f,1} = 0$.

Lemma 3.17. *For $\lambda = \lambda_{f,1} = 0$, $v_{\text{in}}(\xi; \lambda)$ is not uniquely determined: here,*

$$v_{\text{in}}(\xi; 0) = \frac{\partial}{\partial u} v_{f,h}(\xi; u)|_{u=u_*} + C \dot{v}_{f,h}(\xi; u_*),$$

in which $C \in \mathbb{R}$ is a free parameter.

It is also possible to obtain leading order approximations of $v_{\text{in}}(\xi; \lambda)$ for λ near $\lambda_{f,j}$ with $j \geq 3$ odd. However, we refrain from going into these details.

Proof. The fact that $\frac{\partial}{\partial u} v_{f,h}(\xi; u)|_{u=u_*}$ is a solution of (3.55) follows immediately from taking the derivative with respect to the parameter u (or u_0) in (3.11). Uniqueness is lost by adding the kernel $\dot{v}_{f,h}(\xi; u_*)$ associated to the operator $\mathcal{L}_f(\xi)$. □

3.3.4 The intermediate, slowly varying problem

Consider the intermediate (linear) problem

$$\dot{\psi} = A_s(\varepsilon\xi; \lambda, \varepsilon)\psi$$

(3.58)

to the right of I_f, that is for $\xi > \varepsilon^{-\frac{1}{4}}$. Its solution space is four-dimensional. For $\lambda \notin \sigma_e$ (3.39), one can decompose the basis of this space into two fast solutions $\psi_{f,\pm}(\xi; \lambda, \varepsilon)$ that vary with ξ and two slowly varying solutions $\psi_{s,\pm}(\varepsilon\xi; \lambda, \varepsilon)$. The fast solutions $\psi_{f,\pm}(\xi; \lambda, \varepsilon)$ are at leading order determined by the lower diagonal 2×2 block of $A_s(\varepsilon\xi; \lambda, \varepsilon)$ (3.35) and thus at leading order determined by their (v, q)-components: the (u, p)-components are only weakly driven by the asymptotically small coupling term $-v_2 \sqrt{\varepsilon} F_{2,1}(u_{s,*}(\varepsilon\xi))$ in (3.35). The existence of a fast converging solution $\psi_{f,-}$ with an exponential decay that is governed by the most negative eigenvalue $-\Lambda_f$ of

the limiting matrix $\mathcal{A}_\infty(\lambda, \varepsilon)$ (3.38) follows directly by classical methods (see also [3, 21]). Note that $\psi_{f,-}$ is uniquely determined up to a normalization constant (see below). This is not the case for its fast diverging counterpart $\psi_{f,+}$, of which the growth is determined by $+\Lambda_f$ for ξ large enough (one can for instance add a multiple of $\psi_{f,-}$ to $\psi_{f,+}$). However, its existence can be settled by the same methods as for $\psi_{f,-}$. In fact, $\psi_{f,+}$ can be chosen such that for x large, i.e. for $\xi \gg \frac{1}{\varepsilon}$, its decomposition with respect to the four basis solutions of the limiting constant coefficient problem associated to $\mathcal{A}_\infty(\lambda, \varepsilon)$ (section 3.3.1) does not contain 'slow' behaviour (governed by the eigenvalues $\pm\varepsilon\Lambda_s$). Nevertheless $\psi_{f,+}$ needs to be chosen from a family of options, also after normalization. Note that these assertions are all standard within the framework of the Evans function approach – see [3, 21, 6, 7]. Note also that in general $\psi_{f,+}(\xi) \neq \psi_{f,-}(-\xi)$.

In the upcoming analysis, it will be convenient to normalise the fast solutions $\psi_{f,\pm}(\xi; \lambda, \varepsilon)$ as

$$\psi_{f,\pm}(\xi; \lambda, \varepsilon) \rightsquigarrow E_{f,\pm}(\lambda; \varepsilon)\, e^{\pm\Lambda_f \xi} \quad \text{as} \quad \xi \to \infty \tag{3.59}$$

with Λ_f and $E_{f,\pm}(\lambda; \varepsilon)$ as defined in (3.38), (3.40).

It follows from the structure of $A_s(\varepsilon\xi; \lambda, \varepsilon)$ (3.35) that the slow solutions $\psi_{s,\pm}$ have trivial v and q components, so that $\psi_{s,\pm}(\varepsilon\xi; \lambda, \varepsilon) = (u_{s,\pm}(\varepsilon\xi; \lambda, \varepsilon), p_{s,\pm}(\varepsilon\xi; \lambda, \varepsilon), 0, 0)^T$. Note that $\psi_{s,\pm}$ is considered here as function of the slowly varying spatial variable $x = \varepsilon\xi$; more specifically, $p_{s,\pm}$ is defined as $\frac{d}{dx} u_{s,\pm}$. By construction, and by the approximations of Theorem 3.7, $u_{s,\pm}(x; \lambda, \varepsilon)$ is a solution of

$$u_{xx} - \left[(\mu + \lambda) - v_1 \frac{dF_1}{dU}\left(u_*^s(x)\right) \right] u = 0 \quad \text{for} \quad x > \varepsilon^{\frac{3}{4}}. \tag{3.60}$$

Since

$$u_*^s(x) = u_*^u(-x) = u_s^u(-x - x_*) = u_s^s(x + x_*) = u_s^s(y),$$

with $y = x + x_*$ (section 3.2 and Theorem 3.7), (3.60) can be rewritten as

$$(\mathcal{L}_s(y) - \lambda)\, \hat{u} \stackrel{\text{def}}{=} \hat{u}_{yy} + \left[v_1 \frac{dF_1}{dU}(u_s^s(y)) - (\mu + \lambda) \right] \hat{u} = 0 \quad \text{for} \quad y > y_*, \tag{3.61}$$

where $y_* = x_* + \varepsilon^{\frac{3}{4}}$. Except for the condition on y, this is a Sturm-Liouville problem of the type (3.42). As a consequence, Lemma 3.12 can be applied to (3.61) with ρ replaced by μ so that $\Lambda = \Lambda_s$. Hence, for $\lambda \notin \sigma_e$ (3.39) we can define the converging function $\hat{u}_{s,-}(y; \lambda, \varepsilon)$ as the solution of (3.61) that satisfies

$$\hat{u}_{s,-}(y; \lambda, \varepsilon) \rightsquigarrow 1 \cdot e^{-\Lambda_s x} = e^{\Lambda_s x_*} \cdot e^{-\Lambda_s y} \quad \text{as} \quad y \to \infty. \tag{3.62}$$

Note that it is not necessary to exclude the values of λ that are eigenvalues for the full problem, i.e. (3.61) with $y \in \mathbb{R}$: in that case $\hat{u}_{s,-}$ can be defined as the (normalised) eigenfunction. Of course, $u_{s,-}$ is related to $\hat{u}_{s,-}$ through $u_{s,-}(x; \lambda, \varepsilon) = \hat{u}_{s,-}(x + x_*; \lambda, \varepsilon)$. Its diverging counterpart $\hat{u}_{s,+}(y; \lambda, \varepsilon)$ can be obtained by the same methods as above, or as in the proof of Lemma 3.12 (note that the existence of these diverging solutions is not a part of this Lemma). As above, the diverging solution is again not uniquely determined and in general not equal to $\hat{u}_{s,-}(-y; \lambda, \varepsilon)$. In fact, this is impossible at an eigenvalue of the full problem, since in that case $\hat{u}_{s,-}(-y; \lambda, \varepsilon)$ does not grow exponentially as $y \to \infty$. For future reference, we gauge the diverging solution $\hat{u}_{s,+}$ such that

$$\hat{u}_{s,+}(y; \lambda, \varepsilon) \rightsquigarrow 1 \cdot e^{+\Lambda_s x} \quad \text{as} \quad y \to \infty. \tag{3.63}$$

Both basis functions $\psi_{s,\pm}(x; \lambda, \varepsilon)$ can now be defined for $\lambda \notin \sigma_e$; recall that $\psi_{s,\pm}(x; \lambda, \varepsilon)$ are only defined for $x > \varepsilon^{\frac{3}{4}}$. As above, we assume that $\psi_{s,\pm}(x; \lambda, \varepsilon)$ are normalised such that

$$\psi_{s,\pm}(x; \lambda, \varepsilon) \rightsquigarrow E_{s,\pm}(\lambda; \varepsilon) e^{\pm\Lambda_s x} \quad \text{as} \quad x \to \infty \tag{3.64}$$

(3.38), (3.40); note that this is equivalent to (3.62) for $\psi_{-,s}(x; \lambda)$.

Since the matrix A_s is symmetric in $\varepsilon\xi$, the above solutions $\psi_{f,\pm}(\xi; \lambda, \varepsilon)$ and $\psi_{s,\pm}(\varepsilon\xi; \lambda, \varepsilon)$ can be used to define their equivalent counterparts to the left of I_f, i.e. for $\xi < -\varepsilon^{-\frac{1}{4}}$, by using the reflection $\xi \to -\xi$. This fact will be exploited in the next section where the Evans function will be constructed.

3.4 The Evans function and the NLEP procedure

3.4.1 The construction of the Evans function

The Evans function, which is complex analytic outside the essential spectrum – see [45, 3] and the references therein – associated to system (3.33) can be defined by

$$\mathcal{D}(\lambda, \varepsilon) = \det \left[\phi_i(\xi; \lambda, \varepsilon) \right] \tag{3.65}$$

where the functions ϕ_i, $i = 1, 2, 3, 4$ satisfy boundary conditions at $\pm\infty$ (see below) and span the solution space of (3.33). The eigenvalues of (3.34) outside σ_e coincide with the roots of $\mathcal{D}(\lambda, \varepsilon)$, including multiplicities.

Lemma 3.18. *For all $\lambda \in \mathbb{C} \setminus \sigma_e$, there are solutions $\phi_f^{\text{L/R}}(\xi; \lambda, \varepsilon)$ and $\phi_s^{\text{L/R}}(\xi; \lambda, \varepsilon)$ to (3.33) such that the set $\left\{ \phi_f^{\text{L/R}}(\xi; \lambda, \varepsilon), \phi_s^{\text{L/R}}(\xi; \lambda, \varepsilon) \right\}$ spans the solution space of (3.33)*

and

$$\phi_f^{\mathrm{L}}(\xi; \lambda, \varepsilon) \rightsquigarrow E_{f,+}\, e^{\Lambda_f \xi} \quad as \quad \xi \to -\infty \tag{3.66a}$$

$$\phi_f^{\mathrm{R}}(\xi; \lambda, \varepsilon) \rightsquigarrow E_{f,-}\, e^{-\Lambda_f \xi} \quad as \quad \xi \to \infty \tag{3.66b}$$

$$\phi_s^{\mathrm{L}}(\xi; \lambda, \varepsilon) \rightsquigarrow E_{s,+}\, e^{\varepsilon \Lambda_s \xi} \quad as \quad \xi \to -\infty \tag{3.66c}$$

$$\phi_s^{\mathrm{R}}(\xi; \lambda, \varepsilon) \rightsquigarrow E_{s,-}\, e^{-\varepsilon \Lambda_s \xi} \quad as \quad \xi \to \infty \tag{3.66d}$$

Moreover, there exist analytic transmission functions $t_{f,+}(\lambda, \varepsilon)$ and $t_{s,+}(\lambda, \varepsilon)$ such that

$$\phi_f^{\mathrm{L}}(\xi; \lambda, \varepsilon) \rightsquigarrow t_{f,+}(\lambda, \varepsilon)\, E_{f,+}\, e^{\Lambda_f \xi} \quad as \quad \xi \to \infty \tag{3.67a}$$

$$\phi_s^{\mathrm{L}}(\xi; \lambda, \varepsilon) \rightsquigarrow t_{s,+}(\lambda, \varepsilon)\, E_{s,+}\, e^{\varepsilon \Lambda_s \xi} \quad as \quad \xi \to \infty \tag{3.67b}$$

where $t_{s,+}(\lambda, \varepsilon)$ is only defined if $t_{f,+}(\lambda, \varepsilon) \neq 0$. These choices, when possible, determine $\phi_f^{\mathrm{L/R}}$ and ϕ_s^{L} uniquely.

Proof. Although the linearised system (3.33) is not identical to its counterpart in [6], exactly the same arguments as in [6] can be applied here. Therefore, we refer to [6] for the details of the proof. □

The relation between the functions $\phi_{f/s}^{\mathrm{L/R}}$ defined in the above Lemma and the functions $\psi_{f/s,\pm}$ defined in section 3.3.4 will be specified in the next section. Using this relation, an explicit leading order expression for the slow transmission function $t_{s,+}(\lambda)$ will be derived.

The Evans function can be determined by taking the limit $\xi \to \infty$ of the determinant of the functions defined in Lemma 3.18, since the Evans function itself does not depend on ξ; the latter can be established by combining Abel's Theorem with the fact that the trace of $\mathcal{A}(\xi; \lambda, \varepsilon)$ vanishes. This yields using (3.38) and (3.40)

$$
\begin{aligned}
\mathcal{D}(\lambda, \varepsilon) &= \det\left[\left\{\phi_f^{\mathrm{L}}, \phi_f^{\mathrm{R}}, \phi_s^{\mathrm{L}}, \phi_s^{\mathrm{R}}\right\}\right] = \lim_{\xi \to \infty} \det\left[\left\{\phi_f^{\mathrm{L}}, \phi_f^{\mathrm{R}}, \phi_s^{\mathrm{L}}, \phi_s^{\mathrm{R}}\right\}\right] \\
&= \lim_{\xi \to \infty} \det\left[\left\{t_{f,+}(\lambda, \varepsilon)\, E_{f,+}\, e^{\Lambda_f \xi},\; E_{f,-}\, e^{-\Lambda_f \xi},\; t_{s,+}(\lambda, \varepsilon)\, E_{s,+}\, e^{\varepsilon \Lambda_s \xi},\; E_{s,-}\, e^{-\varepsilon \Lambda_s \xi}\right\}\right] \\
&= \lim_{\xi \to \infty} t_{f,+}(\lambda, \varepsilon) t_{s,+}(\lambda, \varepsilon) \det\left[\left\{E_{f,+},\; E_{f,-},\; E_{s,+},\; E_{s,-}\right\}\right] \\
&= 4\varepsilon\, t_{f,+}(\lambda, \varepsilon)\, t_{s,+}(\lambda, \varepsilon)\, \sqrt{1+\lambda}\, \sqrt{\mu + \lambda}. \tag{3.68}
\end{aligned}
$$

Corollary 3.19. *The set of eigenvalues of* (3.34) *is contained in the union of the sets of roots of $t_{f,+}(\lambda, \varepsilon)$ and $t_{s,+}(\lambda, \varepsilon)$.*

Note that, due to the fact that $t_{s,+}(\lambda, \varepsilon)$ only defined when $t_{f,+}(\lambda, \varepsilon) \neq 0$, the Evans function $\mathcal{D}(\lambda, \varepsilon)$ doesn't necessarily vanish when $t_{f,+}(\lambda, \varepsilon) = 0$. This is called the 'resolution to the NLEP paradox' in [6, 7]. Referring to [6], we recall that the roots of $t_{f,+}(\lambda, \varepsilon)$ are to leading order given by the eigenvalues of the homogeneous fast eigenvalue problem (3.42), yielding the following Lemma:

Lemma 3.20. *There are unique $\lambda_j(\varepsilon) \in \mathbb{R}$ such that $\lim_{\varepsilon \to 0} \lambda_j(\varepsilon) = \lambda_{f,j}$ and $t_{f,+}(\lambda_j(\varepsilon), \varepsilon) = 0$ with multiplicity 1 for $j = 0, ..., J$.*

Proof. This statement (and, as a consequence, its proof) is analogous to that of [6], Lemma 4.1. From Lemma 3.13 we know that the Wronksian $\mathcal{W}(\lambda)$ defined there –which is an Evans function itself for the fast problem (3.42)– vanishes at $\lambda = \lambda_{f,j}$ in a nondegenerate way. By construction, $t_{f,+}(\lambda_j(\varepsilon), \varepsilon)$ approaches $\mathcal{W}(\lambda)$ as $\varepsilon \to 0$; see [3, 21, 7] for the technical details. □

Hence, the eigenvalues of (3.42) are to leading order zeroes of the fast component of the Evans function $\mathcal{D}(\lambda, \varepsilon)$ given in (3.68) and thus in principle candidates for being a zero of the full Evans function.

3.4.2 The NLEP procedure

Since in the slow field $\xi > |\varepsilon^{-\frac{1}{4}}|$ the matrix $\mathcal{A}(\xi; \lambda, \varepsilon)$ (3.34) is with exponential accuracy (3.36) given by $\mathcal{A}_s(\varepsilon\xi; \lambda, \varepsilon)$ (3.35), we can conclude that

$$\phi_s^{\text{R}}(\xi; \lambda, \varepsilon) = \psi_{s,-}(\varepsilon\xi; \lambda, \varepsilon) \quad \text{for} \quad \xi > \varepsilon^{-\frac{1}{4}} \tag{3.69}$$

by combining (3.64) with Lemma 3.18. By the reversibility symmetry,

$$\phi_s^{\text{L}}(\xi; \lambda, \varepsilon) = \psi_{s,-}(-\varepsilon\xi; \lambda, \varepsilon) \quad \text{for} \quad \xi < -\varepsilon^{-\frac{1}{4}}. \tag{3.70}$$

Both approximations are valid with exponential accuracy. Moreover, from the second part of Lemma 3.18, we can infer that in the right slow field we can approximate ϕ_s^{L} to exponential accuracy as

$$\phi_s^{\text{L}}(\xi; \lambda, \varepsilon) = t_{s,+}(\lambda, \varepsilon) \psi_{s,+}(\varepsilon\xi; \lambda, \varepsilon) + t_{s,-}(\lambda, \varepsilon) \psi_{s,-}(\varepsilon\xi; \lambda, \varepsilon) \quad \text{for} \quad \xi > \varepsilon^{-\frac{1}{4}}. \tag{3.71}$$

The additional transmission function $t_{s,-}$ needs to be introduced since the asymptotic behaviour of ϕ_s^{L} in the right slow field is only determined by its slow growth, see Lemma 3.18. This normalization choice does not exclude the possibility that $\phi_{s,\text{L}}$ has a slowly decaying component in the right slow field. Since $\{\psi_{f,\pm}, \psi_{s,\pm}\}$ form a basis of the solution space of the right slow field to exponential accuracy, the slowly decaying

component can be represented by $\psi_{s,-}$. Note that since the solution is approximated to exponential accuracy, the possible presence of a fast decaying component is incorporated in this exponential error estimate.

Using the above approximations, an explicit leading order expression for the transmission function $t_{s,+}$ can be determined. Recall that from section 3.4.1 it is known that λ is a zero of the Evans function, and thus an eigenvalue of (3.33), if $t_{s,+}(\lambda, \varepsilon) = 0$. The Theorem below can therefore be considered as the main result of section 3.4 and therefore as one of the main results of this chapter.

Theorem 3.21. *Let $\varepsilon > 0$ be small enough. Define $B_\pm$ and $B'_\pm$ by*

$$B_\pm(\lambda) = \lim_{\varepsilon \to 0} \hat{u}_{s,\pm}(y_*; \lambda, \varepsilon), \;\; B'_\pm(\lambda) = \lim_{\varepsilon \to 0} \frac{\mathrm{d}}{\mathrm{d}y} \hat{u}_{s,\pm}(y; \lambda, \varepsilon)\Big|_{y=y_*}, \qquad (3.72)$$

then, up to corrections of $O(\varepsilon^{\frac{3}{4}})$,

$$t_{s,+}(\lambda) = -\frac{B_-^2}{\Lambda_s} \left\{ \frac{B'_-}{B_-} + \frac{1}{2} \nu_2 \int_{-\infty}^{\infty} \left[\frac{\partial F_2}{\partial U}(u_*, v_{f,h}(\xi; u_*)) + \frac{\partial F_2}{\partial V}(u_*, v_{f,h}(\xi; u_*)) v_{\mathrm{in}}(\xi) \right] \mathrm{d}\xi \right\},$$
$$(3.73)$$

with $v_{\mathrm{in}}(\xi; \lambda)$ as given in Lemma 3.15.

Proof. Let u_s^{L} be the u-component of ϕ_s^{L}. The approximations (3.70) and (3.71) of $u_s^{\mathrm{L}}(\xi; \lambda, \varepsilon)$ are valid outside I_f (3.15). Since I_f has a $O(\varepsilon^{-\frac{1}{4}})$ width in ξ and $u_\xi = \varepsilon p = O(\varepsilon)$, it follows that $u_s^{\mathrm{L}}(\xi; \lambda, \varepsilon)$ can at most change an amount of $O(\varepsilon^{\frac{3}{4}})$ over I_f. Hence, taking the limits $\xi \uparrow -\varepsilon^{-\frac{1}{4}}$ in (3.70) and $\xi \downarrow \varepsilon^{-\frac{1}{4}}$ in (3.71) yields, in combination with de definition of y (section 3.3.4),

$$\hat{u}_{s,-}(y_*; \lambda) = t_{s,+}(\lambda)\hat{u}_{s,+}(y_*; \lambda) + t_{s,-}(\lambda)\hat{u}_{s,-}(y_*; \lambda) + O(\varepsilon^{\frac{3}{4}}).$$

From this, we obtain a first relation between $t_+(\lambda)$ and $t_-(\lambda)$:

$$B_-(\lambda) = t_+(\lambda)B_+(\lambda) + t_-(\lambda)B_-(\lambda) + O(\varepsilon^{\frac{3}{4}}). \qquad (3.74)$$

A second leading order relation between $t_+(\lambda)$ and $t_-(\lambda)$ can be obtained by studying the accumulated change in $\frac{\mathrm{d}}{\mathrm{d}\xi} u_s^{\mathrm{L}}(\xi; \lambda)$ over I_f. According to (3.32) and by Theorem 3.7,

$$
\begin{aligned}
\Delta_f \left(\frac{\mathrm{d}}{\mathrm{d}\xi} u_s^{\mathrm{L}} \right) &= \int_{I_f} \frac{\mathrm{d}^2}{\mathrm{d}\xi^2} u_s^{\mathrm{L}} \, \mathrm{d}\xi \\
&= -\varepsilon \nu_2 \int_{I_f} \left[\frac{\partial F_2}{\partial U}(u_h(\xi), v_h(\xi)) u_s^{\mathrm{L}}(\xi) + \frac{\partial F_2}{\partial V}(u_h(\xi), v_h(\xi)) v_s^{\mathrm{L}}(\xi) + O(\varepsilon) \right] \mathrm{d}\xi \\
&= -\varepsilon \nu_2 \int_{I_f} \left[\frac{\partial F_2}{\partial U}(u_*, v_{f,h}(\xi; u_*)) u_s^{\mathrm{L}}(\xi) + \frac{\partial F_2}{\partial V}(u_*, v_{f,h}(\xi; u_*)) v_s^{\mathrm{L}}(\xi) \right] \mathrm{d}\xi
\end{aligned}
$$

up to $O(\varepsilon^{7/4})$, where v_s^{L} is the v-component of ϕ_s^{L}. For $\xi \in I_f$, we know that u_s^{L} is constant to leading order. Using (3.74), we see that $u_s^{\mathrm{L}}(\xi) = B_- + O(\varepsilon^{\frac{3}{4}})$ for $\xi \in I_f$. The second equation of (3.32) – which describes the evolution of v_s^{L} – can therefore be written as

$$(\mathcal{L}_f(\xi) - \lambda)\, v_s^{\mathrm{L}} = -B_- \frac{\partial G}{\partial U}(u_*, v_{f,h}(\xi; u_*)) + O(\varepsilon^{\frac{3}{4}}),$$

which implies that (see section 3.3.3)

$$v_s^{\mathrm{L}}(\xi; \lambda, \varepsilon) = B_-(\lambda) v_{\mathrm{in}}(\xi; \lambda) + O(\varepsilon^{\frac{3}{4}}),$$

so that $v_{+,s}^{\mathrm{L}}(\xi; \lambda)$ is explicitly known (Lemma 3.15) to leading order. As a consequence,

$$
\begin{aligned}
\Delta_f\!\left(\frac{\mathrm{d}}{\mathrm{d}\xi} u_s^{\mathrm{L}}\right) &= -\varepsilon v_2 B_- \int_{I_f} \left[\frac{\partial F_2}{\partial U}(u_*, v_{f,h}(\xi)) + \frac{\partial F_2}{\partial V}(u_*, v_{f,h}(\xi)) v_{\mathrm{in}}(\xi)\right] \mathrm{d}\xi + O(\varepsilon^{7/4}) \\
&= -\varepsilon v_2 B_- \int_{-\infty}^{\infty} \left[\frac{\partial F_2}{\partial U}(u_*, v_{f,h}(\xi)) + \frac{\partial F_2}{\partial V}(u_*, v_{f,h}(\xi)) v_{\mathrm{in}}(\xi)\right] \mathrm{d}\xi + O(\varepsilon^{7/4})
\end{aligned}
\tag{3.75}
$$

by the convergence properties of $v_{f,h}(\xi; u_*)$ and $v_{\mathrm{in}}(\xi; \lambda)$ in combination with assumption (A3) – note that this same combination also implies that the integral converges. Of course, this accumulated change in $\frac{\mathrm{d}}{\mathrm{d}\xi} u_{+,s}^{\mathrm{L}}(\xi; \lambda)$ must also be reflected by the leading order approximations (3.70) and (3.71) as $\xi \uparrow -\varepsilon^{-\frac{1}{4}}$ respectively $\xi \downarrow \varepsilon^{-\frac{1}{4}}$. Combining (3.75) with (3.70) and (3.71) yields

$$
\begin{aligned}
\Delta_s\!\left(\frac{\mathrm{d}}{\mathrm{d}\xi} u_{+,s}^{\mathrm{L}}\right) &= \lim_{\xi \downarrow \varepsilon^{-\frac{1}{4}}} \frac{\mathrm{d}}{\mathrm{d}\xi}\left[t_{s,+} \hat{u}_{s,+}(\varepsilon\xi + x_*) + t_{s,-} \hat{u}_{s,-}(\varepsilon\xi + x_*)\right] \\
&\quad - \lim_{\xi \uparrow -\varepsilon^{-\frac{1}{4}}} \frac{\mathrm{d}}{\mathrm{d}\xi} \hat{u}_{s,-}(-\varepsilon\xi + x_*) \\
&= \varepsilon \left[t_{s,+}(\lambda) B_+'(\lambda) + t_{s,-}(\lambda) B_-'(\lambda) + B_-'(\lambda)\right] + O(\varepsilon^{7/4}).
\end{aligned}
\tag{3.76}
$$

The second relation between $t_-(\lambda)$ and $t_+(\lambda)$ follows by identifying (3.75) and (3.76). Finally, the term $B_+ B_-' - B_- B_+'$ obtained by combining (3.74) with (3.76) and solving for $t_{s,+}$ can be simplified by recognising it as the Wronksian associated to (3.61) for the solutions $\hat{u}_{s,\pm}$, evaluated at $y = y_*$. Using Abel's Theorem, we see that the Wronskian associated (3.61) is constant in y. Its value can therefore be determined by taking the limit $y \to \infty$, using (3.62) and (3.63). Thus,

$$B_+ B_-' - B_- B_+' = \lim_{y \to \infty} B_+ B_-' - B_- B_+' = -2\Lambda_s.$$

Identity (3.73) can now be obtained by combining relation (3.76) with (3.74), using the above simplification for $B_+ B_-' - B_- B_+'$. $\qquad\square$

The expression for $t_{s,+}$ (3.73) can be studied in the 'linear' limit, yielding the following result:

Corollary 3.22. *Both as $\nu_1 \to 0$ and in the limit of large positive y_*, the roots of $t_{s,+}(\lambda)$ are to leading order given by the solutions to*

$$\frac{\nu_2}{2} \int_{-\infty}^{\infty} \left[\frac{\partial F_2}{\partial U}(u_*, v_{f,h}(\xi; u_*)) + \frac{\partial F_2}{\partial V}(u_*, v_{f,h}(\xi; u_*)) \, v_{\text{in}}(\xi) \right] \mathrm{d}\xi = \sqrt{\mu + \lambda}. \quad (3.77)$$

Note that the 'linear limit' (3.77) indeed coincides with [6], expression (4.11), which determines the (nontrivial) zeroes of an Evans function associated to the stability of pulses in a 'linear' generalised GM-type system (i.e. $F_1(U; \varepsilon) \equiv 0$, $F_2(U, V; \varepsilon) = U^{\alpha_1} V^{\beta_1}$, $G(U, V; \varepsilon) = U^{\alpha_2} V^{\beta_2}$).

Proof. We approximate $B_{\pm}$, $B'_{\pm}$ for large $y_* > 0$ using (3.62) and (3.63), yielding

$$B_-(\lambda) \rightsquigarrow e^{-\Lambda_s y_*} \quad \text{and} \quad B'_-(\lambda) \rightsquigarrow -\Lambda_s \, e^{-\Lambda_s y_*} \quad \text{as} \quad y_* \to \infty. \quad (3.78)$$

From (3.61), it follows that the limit $\nu_1 \to 0$ also yields the 'linear limit', i.e. the solutions $\hat{u}_{s,\pm}$ become pure exponentials. Therefore, any zero of $t_{s,+}$ in either of these limits comes from a solution of equation (3.77). $\qquad \square$

3.5 Implications of Theorem 3.21: (in)stability results

The explicit leading order expression for $t_{s,+}(\lambda)$ established in the previous section and stated in Theorem 3.21 can be interpreted in certain limiting situations, such as near the known fast eigenvalues $\lambda_{f,j}$ of the homogeneous problem (3.42) or for certain parameter limits. In this section, a number of results of this type will be stated, leading to a number of explicit (in)stability results for the full problem (3.33).

Lemma 3.23. *For λ close to $\lambda_{f,0}$, we can describe the leading order behaviour of $t_{s,+}$ as*

$$t_{s,+}(\lambda) \rightsquigarrow -\frac{\nu_2 B_-(\lambda_{f,0})^2}{2\Lambda_s(\lambda_{f,0})} \cdot \frac{T}{\lambda - \lambda_{f,0}} \quad \text{as} \quad \lambda \to \lambda_{f,0}, \quad (3.79)$$

where

$$T = \left(\int_{-\infty}^{\infty} \frac{\partial F_2}{\partial V}(u_*, v_{f,h}(\xi; u_*)) \, \frac{w_{f,0}(\xi)}{\|w_{f,0}\|_2} \mathrm{d}\xi \right) \left(\int_{-\infty}^{\infty} \frac{\partial G}{\partial U}(u_*, v_{f,h}(\xi; u_*)) \, \frac{w_{f,0}(\xi)}{\|w_{f,0}\|_2} \, \mathrm{d}\xi \right). \quad (3.80)$$

Proof. By Corollary 3.16 we see that $v_{in}(\xi; \lambda)$ is singular in λ as $\lambda \to \lambda_{f,0}$. Combining (3.57) with (3.73), we can describe the leading order behaviour of the slow transmission function as (3.79) with the constant T is given by (3.80). $\qquad\square$

Corollary 3.24. *Let $\varepsilon > 0$ be sufficiently small. The nontrivial roots of the Evans function $\mathcal{D}(\lambda, \varepsilon)$ are determined by $t_{s,+}(\lambda, \varepsilon)$ (3.73). In other words, $t_{s,+}$ determines the stability of the pulse Γ_h as defined in Theorem 3.7.*

Proof. By Lemma 3.20, the fast transmission function $t_{f,+}(\lambda, \varepsilon)$ has a single zero at $\lambda = \lambda_{f,0}$ to leading order in ε. Since $t_{f,+}(\lambda)$ is smooth and it approximates the Wronskian $\mathcal{W}(\lambda)$ of Lemma 3.13 (see Lemma 3.20), we can approximate it linearly as $t_{f,+}(\lambda, \varepsilon) \leadsto \hat{t}_{f,+} \cdot (\lambda - \lambda_{f,0}) + O(\varepsilon)$ as $\lambda \to \lambda_{f,0}$, with $\hat{t}_{f,+} = -\|w_{f,0}\|_2^2 \neq 0$. This would suggest that $\lambda_{f,0}$ is a zero of the full Evans function (3.68). However, combining the results of Lemma 3.23 with the fact that $\Lambda_s(\lambda_{f,0}) = \sqrt{\mu + \lambda_{f,0}}$, we see that the Evans function (3.68) behaves to leading order in ε as

$$\mathcal{D}(\lambda, \varepsilon) \leadsto 2\,\varepsilon\,\nu_2\,\|w_{f,0}\|_2^2 T \sqrt{1 + \lambda_{f,0}}\, B_-(\lambda_{f,0})^2 \quad \text{as} \quad \lambda \to \lambda_{f,0}.$$

We see that $\mathcal{D}(\lambda_{f,0}, \varepsilon) = 0$ if and only if $\nu_2 T B_-(\lambda_{f,0})^2 = 0$. Thus, the possibility of an eigenvalue at $\lambda = \lambda_{f,0}$ is determined by $t_{s,+}(\lambda)$, not by $t_{f,+}(\lambda)$. $\qquad\square$

Note that in general $\lambda_{f,0}$ is thus not (close to) an eigenvalue of the full problem. This –again– relates directly to the resolution of the NLEP paradox [6, 7]. The first, positive eigenvalue $\lambda_{f,0}$ of the fast homogeneous problem (3.42) is a zero of the Evans function (3.68) and therefore an eigenvalue of the full problem (3.33) if and only if

$$\nu_2\,T\,B_-(\lambda_{f,0}) = 0, \tag{3.81}$$

where T as defined in (3.80); therefore, (3.81) determines a condition on the parameters of (3.1). Moreover, the relevance of more detailed insight in the behaviour in general and the roots in particular of $B_-(\lambda)$ is apparent.

3.5.1 The structure of $B_-(\lambda)$

Recalling the definition of $B_-(\lambda)$ (3.72), we see that the roots of $B_-(\lambda)$ are directly related to the structure of $\hat{u}_{s,-}$ as a function of λ; also recall that $\hat{u}_{s,-}$ is the solution of (3.61) that decreases exponentially as $y \to \infty$, see (3.62).

Consider the slow eigenvalue problem (3.61). Following the classical approach of [49], we introduce the polar coordinate transformation

$$\hat{u}(y) = r(y) \cos \theta(y), \quad \hat{u}_y(y) = r(y) \sin \theta(y), \tag{3.82}$$

where $r(y) > 0$. Using the consistency condition

$$r(y) \sin \theta(y) = \hat{u}_y = \frac{\mathrm{d}}{\mathrm{d}y} \hat{u} = r'(y) \cos \theta(y) - r(y)\theta'(y) \sin \theta(y), \tag{3.83}$$

the second order equation (3.61) can be transformed into the system

$$r' = \left[1 + \mu + \lambda - \nu_1 \frac{\mathrm{d}F_1}{\mathrm{d}U}(u_s^s(y))\right] r \cos \theta \sin \theta \tag{3.84}$$

$$\theta' = \left[1 + \mu + \lambda - \nu_1 \frac{\mathrm{d}F_1}{\mathrm{d}U}(u_s^s(y))\right] \cos^2 \theta - 1. \tag{3.85}$$

Since r is a strictly positive function, we can identify the zeroes of $\hat{u}(y)$ by studying $\theta(y)$:

$$\hat{u}(y) = 0 \iff \theta(y) = \frac{1}{2}\pi + k\pi, \quad k \in \mathbb{Z}. \tag{3.86}$$

Moreover, we can establish an ordering principle for θ, as stated in the following Lemma:

Lemma 3.25. *Let $\hat{u}_1$, $\hat{u}_2$ be solutions to (3.61) for real λ_1 resp. λ_2 outside the essential spectrum σ_e (3.39). Assume $\theta_2(y_0) < \theta_1(y_0)$ for some $y_0 \in (y_*, \infty)$, where $\theta_{1,2}$ are related to $\hat{u}_{1,2}$ by (3.82). If $\lambda_2 > \lambda_1$, then $\theta_2(y) < \theta_1(y)$ for all $y_* \le y \le y_0$.*

Proof. Introduce $\Delta\lambda = \lambda_2 - \lambda_1 > 0$. Using (3.85), we can deduce a differential equation for the difference $\theta_1 - \theta_2$:

$$(\theta_1 - \theta_2)' = \left[1 + \mu + \lambda_1 - \nu_1 \frac{\mathrm{d}F_1}{\mathrm{d}U}(u_s^s(y))\right] \frac{\left(\cos^2 \theta_1 - \cos^2 \theta_2\right)}{\theta_1 - \theta_2} (\theta_1 - \theta_2) - \Delta\lambda \cos^2 \theta_2 \tag{3.87}$$

This equation has the form $u' = f u - h$, where $u = \theta_1 - \theta_2$ and $h = \Delta\lambda \cos^2 \theta_2 \ge 0$. By introducing $F(y) = \int_y^{y_0} f(\eta)\mathrm{d}\eta$, we see that $e^F (u' - f u) = \frac{\mathrm{d}}{\mathrm{d}y}\left(e^F u\right) = -h\, e^F \le 0$. Since $e^F u$ is decreasing and $e^{F(y_0)}u(y_0) = u(y_0) > 0$ since $\theta_1(y_0) - \theta_2(y_0) > 0$, we can conclude that $e^{F(y)}u(y) > 0$ and hence $u(y) > 0$ for all $y_* \le y \le y_0$. $\qquad\square$

We use Lemma 3.25 to establish a similar ordering result for $\hat{\theta}_{s,-}(y; \lambda, \varepsilon)$, which is the 'angular function' associated to $\hat{u}_{s,-}(y; \lambda, \varepsilon)$ through the polar transformation (3.82). Once again we use the fact that we can approximate $\hat{\theta}_{s,-}$ by an exponential for large values of y (see (3.60)), by taking y_0 arbitrarily large.

Lemma 3.26. *Consider real $\lambda_1, \lambda_2 \notin \sigma_e$ (3.39). If $\lambda_2 > \lambda_1$, then $\theta_{s,-}(y; \lambda_2, \varepsilon) < \theta_{s,-}(y; \lambda_1, \varepsilon)$ for all $y \in (y_*, \infty)$.*

Proof. Since $\hat{u}_{s,-}(y; \lambda, \varepsilon) \rightsquigarrow e^{\Lambda_s x_*} e^{-\Lambda_s y}$ as $y \to \infty$ (3.62) and therefore $\frac{\mathrm{d}}{\mathrm{d}y} \hat{u}_{s,-} \rightsquigarrow -\Lambda_s e^{\Lambda_s x_*} e^{-\Lambda_s y}$ as $y \to \infty$, it follows that

$$r_{s,-} \quad \rightsquigarrow \quad \sqrt{1 + \lambda + \mu} \, e^{\sqrt{\lambda+\mu} x_*} e^{-\sqrt{\lambda+\mu} y} \quad \text{as} \quad y \to \infty,$$

$$\cos\theta_{s,-} \quad \rightsquigarrow \quad \frac{1}{\sqrt{1 + \lambda + \mu}} \quad \text{as} \quad y \to \infty,$$

$$\sin\theta_{s,-} \quad \rightsquigarrow \quad -\frac{\sqrt{\lambda + \mu}}{\sqrt{1 + \lambda + \mu}} \quad \text{as} \quad y \to \infty$$

so $\tan\theta_{s,-} \rightsquigarrow -\sqrt{\lambda + \mu}$ as $y \to \infty$. Since we consider $\lambda \in \mathbb{R}$ outside the essential spectrum (3.39), we know that $0 < \frac{1}{\sqrt{1+\lambda+\mu}} < 1$ so $\theta_{s,-}(\mathrm{mod}\, 2\pi) \in (-\frac{\pi}{2}, \frac{\pi}{2})$ as $y \to \infty$. The angle variable θ is still defined up to a multiple of 2π: we gauge $\theta_{s,-}$ such that $\theta_{s,-} \in (-\frac{\pi}{2}, \frac{\pi}{2})$ as $y \to \infty$. Since the tangent is strictly increasing on $(-\frac{\pi}{2}, \frac{\pi}{2})$, it follows that if $\lambda_2 > \lambda_1$ then $-\sqrt{\lambda_2 + \mu} < -\sqrt{\lambda_1 + \mu}$ and therefore $\tan\theta_{s,-}(y; \lambda_1; \varepsilon) - \tan\theta_{s,-}(y; \lambda_2; \varepsilon) \rightsquigarrow K_1 > 0$ as $y \to \infty$; we can conclude that $\theta_{s,-}(y; \lambda_1, \varepsilon) - \theta_{s,-}(y; \lambda_2, \varepsilon) \rightsquigarrow K_2 > 0$ as $y \to \infty$. Lemma 3.25 can now be used to establish the statement of the Lemma. $\qquad\square$

The ordering principle from Lemma 3.25 can be combined with the eigenfunction hierarchy from Lemma 3.12. This is only possible if the slow eigenvalue problem (3.60) can be extended to the entire real line, i.e. when $u_s^s(x)$ is bounded for $x \to \pm\infty$. Invoking the result of Lemma 3.8, we see that we may assume $\mathcal{W}_s^s((0,0)) \cap \{p_s = 0\} \neq \emptyset$ without loss of generality, and that as a consequence $u_s^s(x)$ may be assumed to be bounded, since the function $u_s^s(x)$ describes a homoclinic orbit on the slow manifold $\mathcal{M}$. This allows us to use Lemma 3.12 on (the extended) eigenvalue problem (3.60), introducing the slow eigenvalues $\lambda_{s,j}$ with their associated eigenfunctions $w_{s,j}$ from Lemma 3.12.

Lemma 3.27. *Assume without loss of generality that $\mathcal{W}_s^s((0,0)) \cap \{p_s = 0\} \neq \emptyset$. If $\lambda_{s,j+1} < \lambda < \lambda_{s,j}$ then the associated function $\hat{u}_{s,-}(y; \lambda; \varepsilon)$ has at least j and at most $j + 1$ zeroes as a function of y. Furthermore, if $0 < \lambda < \lambda_{s,0}$, then $\hat{u}_{s,-}(y; \lambda; \varepsilon) > 0$ if $y > 0$. Secondly, if $\lambda_{s,0} \leq \lambda$, then $\hat{u}_{s,-}(y; \lambda; \varepsilon) > 0$ for all $y \in \mathbb{R}$.*

Proof. Since $\mathcal{W}_s^s((0,0)) \cap \{p_s = 0\} \neq \emptyset$, $u_s^s(x)$ is bounded. This allows us to apply Lemma 3.12 in full, introducing the slow eigenvalues $\lambda_{s,j}$ with associated eigenfunctions $w_{s,j}$. From Lemma 3.12 (ii) and (iii), it follows that $w_{s,1}(y) = -\frac{\mathrm{d}}{\mathrm{d}y} u_s^s(y)$ for

$\lambda_{s,1} = 0$. Moreover, $w_{s,j}(y)$ has j distinct zeroes – in particular, $w_{s,0}(y)$ is positive (Lemma 3.12 (iii)) and never zero. Using the fact that $w_{s,0}(y)$ is even, we can reason analogously to the proof of Lemma 3.26 and conclude that $\theta_{s,0}(y) \in (-\frac{\pi}{2}, \frac{\pi}{2})$ for all y – we use the same gauge for $\theta_{s,j}$ as that for $\theta_{s,-}$ in the proof of Lemma 3.26. Furthermore, evaluating (3.85) at the 'critical' θ-values from (3.86), we see that

$$\theta(y) = \frac{1}{2}\pi + k\pi, \quad k \in \mathbb{Z} \qquad \Longleftrightarrow \qquad \theta'(y) = -1. \qquad (3.88)$$

The function $\theta(y)$ thus crosses each 'critical' value $\theta(y) = \frac{1}{2}\pi + k\pi$, $k \in \mathbb{Z}$ only once, and in a transversal way. Since $w_{s,1}(y)$ is odd, we can infer analogously to the proof of Lemma 3.26 that $\cos\theta_{s,1} \rightsquigarrow -\frac{1}{\sqrt{1+\mu}}$ and $\sin\theta_{s,1} \rightsquigarrow -\frac{\sqrt{\mu}}{\sqrt{1+\mu}}$ as $y \to -\infty$. This means that $\theta_{s,1} \pmod{2\pi} \in (\pi, \frac{3}{2}\pi)$ as $y \to -\infty$. Using the fact that $w_{s,1}(y)$ is has only one zero and therefore $\theta_{s,1}$ crosses the line $\theta = \frac{1}{2}\pi$ only once, we see that the gauge choice allows us to omit the "mod2π", yielding $\theta_{s,1} \in (\pi, \frac{3}{2}\pi)$ as $y \to -\infty$. Using Lemmas 3.25 and 3.26 (extended to the entire real line), we conclude that for all $\lambda_{s,1} = 0 < \lambda < \lambda_{s,0}$, the function $w^{\mathrm{R}}_{s,\lambda}(y)$ has at most one zero, see Figure 3.6. Furthermore, since we know that $\theta_{s,1}$ crosses the line $\theta = \frac{1}{2}\pi$ exactly at $y = 0$ (with slope -1), the aforementioned zero of $w^{\mathrm{R}}_{s,\lambda}(y)$ can only occur for negative values of y. Moreover, analogous reasoning can be applied to every pair $(\lambda_{s,j}, \lambda_{s,j+1})$: if $\lambda_{s,j+1} < \lambda < \lambda_{s,j}$, then $w^{\mathrm{R}}_{s,\lambda}(y)$ has at least j and at most $j + 1$ zeroes. Note that the above also implies that for $\lambda_{s,0} < \lambda$, the function $w^{\mathrm{R}}_{s,\lambda}(y)$ is never zero. Identification of $w^{\mathrm{R}}_{s,\lambda}(y)$ with $\hat{u}_{s,-}(y; \lambda, \varepsilon)$ yields the Lemma. $\qquad\square$

The result of Lemma 3.27 can used to make a statement about $B_-(\lambda)$:

Lemma 3.28. *If $y_* > 0$, then $B_-(\lambda) \neq 0$ for all $\lambda \geq 0$. If $y_* \leq 0$, then there is a $\lambda \geq 0$ for which $B_-(\lambda) = 0$.*

Of course, this has an immediate consequence for pulses for which $x_* < 0$ (see Figure 3.4c).

Corollary 3.29. *Let $F_{1,2}$ and G be such that $\mathcal{W}^{\mathrm{s}}_s((0,0)) \cap \{p_s = 0\} \neq \emptyset$, and assume that $x_* < 0$. Let Γ_h be a pulse solution of (3.7) with $x_* < 0$ (Theorem 3.7). Then Γ_h is unstable.*

Proof of Lemma 3.28. $\mathbf{y_* > 0}$: Since $B_-(\lambda) = \lim_{\varepsilon \to 0} \hat{u}_{s,-}(y_*; \lambda, \varepsilon)$, the last statement of Lemma 3.27 applies for all values of y_* if $\lambda \geq \lambda_{s,0}$. For $0 \leq \lambda < \lambda_{s,0}$, the second statement of Lemma 3.27 makes sure that whenever $y_* > 0$, $\hat{u}_{s,-}(y_*; \lambda, \varepsilon) \neq 0$ and therefore $B_-(\lambda) \neq 0$.
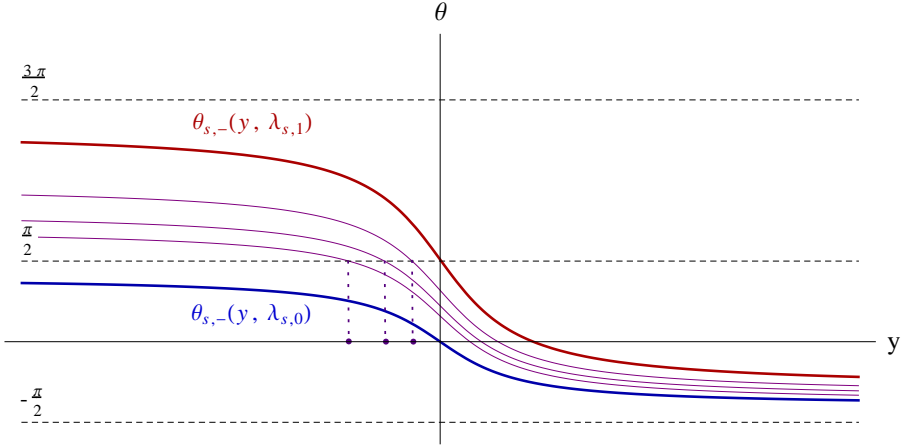
Figure 3.6: The ordering of $\theta_{s,-}(y;\lambda)$, depicted for $\lambda_1 \leq \lambda \leq \lambda_0$. The intersections with the line $\theta = \frac{\pi}{2}$ are also indicated; for these values of λ, each of these intersections is to the left of $y = 0$.

$\mathbf{y_* \leq 0}$: Consider $\lambda \geq 0$; we set out to prove that for every $y_* \leq 0$ there is a $\lambda \geq 0$ such that $\lim_{\varepsilon \to 0} \hat{u}_{s,-}(y_*;\lambda,\varepsilon) = 0$. Define $\mathcal{U}_0 = \{(\lambda,y_0) \,|\, \lim_{\varepsilon \to 0} \hat{u}_{s,-}(y_0;\lambda,\varepsilon) = 0\}$. Using Lemma 3.27 and the previously proven results for $y_* > 0$, we know that $(\mathcal{U}_0 \cap \{(\lambda,y_0) \,|\, \lambda \geq 0\}) \subset [0,\lambda_{s,0}) \times (-\infty, 0]$. By the polar coordinate transformation (3.82), we see that $\mathcal{U}_0 = \Theta_0$, where $\Theta_0 = \left\{(\lambda,y_0) \,|\, \lim_{\varepsilon \to 0} \theta_{s,-}(y_0,\lambda,\varepsilon) = \frac{\pi}{2}\right\}$. Taking the derivative with respect to λ of the defining equation $\lim_{\varepsilon \to 0} \theta_{s,-}(y_0;\lambda,\varepsilon) = \frac{\pi}{2}$ yields $\frac{\partial \theta_{s,-}}{\partial y} \frac{dy_0}{d\lambda} + \frac{\partial \theta_{s,-}}{\partial \lambda} = 0$. For $(\lambda,y_0) \in \Theta_0$ we have $\frac{\partial \theta_{s,-}}{\partial y} = -1$ (3.88), so $\frac{dy_0}{d\lambda} = \frac{\partial \theta_{s,-}}{partial \lambda}$ for $(\lambda,y_0) \in \Theta_0$. Now consider $(\hat{\lambda},\hat{y}_0) \in \Theta_0$ and take $0 < \delta \ll 1$ small enough. Using the smoothness of $\theta_{s,-}$ as a function of λ, we can write $\theta_{s,-}(\hat{y}_0;\hat{\lambda} + \delta,\varepsilon) = \theta_{s,-}(\hat{y}_0;\hat{\lambda},\varepsilon) + \delta \frac{\partial \theta_{s,-}}{\partial \lambda}(\hat{y}_0;\hat{\lambda},\varepsilon) + O(\delta^2)$. Using the extension of Lemma 3.26 to the entire real line, we know that $\theta_{s,-}(\hat{y}_0;\hat{\lambda} + \delta,\varepsilon) < \theta_{s,-}(\hat{y}_0;\hat{\lambda},\varepsilon)$. Taking the limit $\varepsilon \to 0$ yields $\frac{\pi}{2} + \delta \lim_{\varepsilon \to 0} \frac{\partial \theta_{s,-}}{\partial \lambda}(\hat{y}_0;\hat{\lambda},\varepsilon) + O(\delta^2) < \frac{\pi}{2}$ so $\lim_{\varepsilon \to 0} \frac{\partial \theta_{s,-}}{\partial \lambda}(\hat{y}_0;\hat{\lambda},\varepsilon) < 0$ for all $(\hat{\lambda},\hat{y}_0) \in \Theta_0$. This implies that $\frac{dy_0}{d\lambda} < 0$ on Θ_0. Therefore, Θ_0 is a smooth one-dimensional submanifold of the the (λ,y_0)-(half)plane. The continuity of $\hat{u}_{s,-}(y;\lambda,\varepsilon)$ both as a function of y and λ implies that $\mathcal{U}_0 = \Theta_0$ is closed. Since $\frac{\partial \theta_{s,-}}{\partial y}(\lambda,y_0) = -1$ when $\lim_{\varepsilon \to 0} \theta_{s,-}(y_0;\lambda,\varepsilon) = \frac{\pi}{2}$, there is a $\eta > 0$ such that $\lim_{\varepsilon \to 0} \theta_{s,-}(y_0 - \eta;\lambda,\varepsilon) > \frac{\pi}{2}$ and $\lim_{\varepsilon \to 0} \theta_{s,-}(y_0 + \eta;\lambda,\varepsilon) < \frac{\pi}{2}$. The smoothness of $\hat{u}_{s,-}(y;\lambda,\varepsilon)$ as a function of λ implies that these inequalities also hold for an open interval containing λ. This means that Θ_0 is connected and that it does not have singular, i.e. terminal points in the
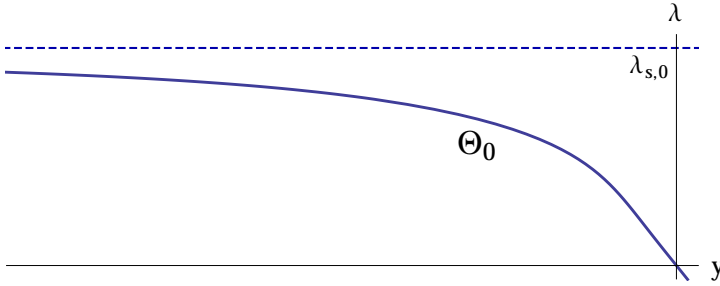
Figure 3.7: The zero set $\Theta_0 = \left\{(\lambda, y_0) \,|\, \lim_{\varepsilon \to 0} \theta_{s,-}(y_0, \lambda, \varepsilon) = \frac{\pi}{2}\right\}$.

interior of the half-plane $\{(\lambda, y_0) \,|\, \lambda \geq 0\}$, except for $(0, 0) \in \Theta_0$ – which also ensures that Θ_0 is nonempty. We conclude that as a graph over λ, the map $\lambda \mapsto y_0(\lambda)$ defines a strictly decreasing function which has the entire negative halfline $(-\infty, 0]$ as its range, see Figure 3.7.

Therefore, for every $y_0 \leq 0$ there is a $\lambda \geq 0$ such that $\lim_{\varepsilon \to 0} \theta_{s,-}(y_0; \lambda, \varepsilon) = \frac{\pi}{2}$, which implies that $B_-(\lambda) = \lim_{\varepsilon \to 0} \hat{u}_{s,-}(y_*; \lambda, \varepsilon) = 0$ if we take $y_* = y_0$. □

The fact that $B_-(\lambda) \neq 0$ for $\lambda \geq 0$ only excludes *real* positive zeroes of $B_-(\lambda)$ if $y_* > 0$. In chapter 2, we have conjectured that $B_-(\lambda) \neq 0$ for all $\lambda \in \mathbb{C}$ with $\mathrm{Im}\,\lambda \neq 0$ for the explicit system (3.2) considered there (Conjecture 2.16). Even for the very simple case in which $\hat{u}_{s,-}$ can be expressed in terms of associated Legendre functions –as is the case in chapter 2–, there is no result in the literature about the (non-)existence of complex zeroes we are aware of. In our (numerical) investigations of $B_-(\lambda)$ we have not found any evidence of the possibility that $B_-(\lambda)$ can be zero for $\lambda \notin \mathbb{R}$.

3.5.2   The trivial eigenvalue $\lambda = 0$

While the explicit expression for $t_{s,+}$ (3.73) is in the general setting hard to analyse explicitly, it is possible to treat some specific situations in detail; in this section, we focus on the trivial eigenvalue $\lambda = 0$. From Lemmas 3.27 and 3.28 we know that $B_-(0) = 0$ if and only if $y_* = 0$ since $\frac{d}{dy} u_s^s(y_*) = 0$ if and only if $y_* = 0$. This situation can be interpreted geometrically as a quadruple intersection of both curves T_o (3.19) and T_d (3.20) with $\mathcal{W}_s^u((0,0)) \cap \mathcal{W}_s^s((0,0))$ at $(u_M, 0)$. This implies that $p_* = 0$ (3.25) and hence $D_p(u_*) = 0$ (3.17), which in turn means that the u-coordinate does not make a jump (3.16). Note that this does not necessarily mean that V-component is

identically zero, only that the U- and V-components decouple to leading order. Since $\lambda = 0$ is always a simple eigenvalue of the pulse, we can conclude the following:

Corollary 3.30. *When $x_* = 0$, the trivial eigenvalue $\lambda = 0$ has multiplicity 2.*

Therefore, the bifurcation which changes the sign of $x_* = y_* + O\left(\varepsilon^{\frac{3}{4}}\right)$, i.e. which changes the qualitative properties of the homoclinic pulse from the situation depicted in Figure 3.4a to Figure 3.4c, (further) destabilises the pulse by sending an eigenvalue through the origin; it is highly likely that there are additional unstable eigenvalues. The fact that the trivial eigenvalue has multiplicity 2 when $x_* = 0$ can also be understood by noticing that in this case there is virtually no coupling between the slow U- and fast V-equation: the fast V-pulse does not have an impact on the U-component since $D_p(u_*) = 0$. The uncoupled U_h- and V_h-components both have a zero (as well as a positive) eigenvalue, since their derivatives are a solution to their respective scalar equations.

The slow transmission function $t_{s,+}$ can be analysed in more detail at $\lambda = 0$, yielding the following Lemma.

Lemma 3.31. *At the trivial eigenvalue $\lambda = 0$, the slow transmission function $t_{s,+}(\lambda)$ can be expressed as*

$$t_{s,+}(0) = \frac{1}{2\sqrt{\mu}} \frac{v_2 D_p(u_*)}{u_{s,\infty}^2} \left\{ \mu u_* - v_1 F_1(u_*; 0) - \frac{1}{4} v_2^2 D_p(u_*) \left.\frac{\mathrm{d}}{\mathrm{d}u}\right|_{u=u_*} D_p(u) \right\}. \qquad (3.89)$$

Proof. First, we recall Lemma 3.17: for $\lambda = 0$, we can write $v_{\mathrm{in}}(\xi; \lambda = 0)$ as

$$v_{\mathrm{in}}(\xi; 0) = \left.\frac{\partial}{\partial u}\right|_{u=u_*} v_{f,h}(\xi; u) + C \dot{v}_{f,h}(\xi; u_*)$$

where $C \in \mathbb{R}$ is a free parameter. Since $v_{f,h}(\xi, u)$ is an even function of ξ, the product

$$\frac{\partial F_2}{\partial V}(u_*, v_{f,h}(\xi; u_*)) \frac{\partial}{\partial \xi} v_{f,h}(\xi; u_*)$$

is odd as a function of ξ, hence its integral vanishes. Therefore we can write the integrand of the integral term occcuring in the expression of $t_{s,+}$ (3.73) as

$$\frac{\partial F_2}{\partial U}(u_*, v_{f,h}(\xi; u_*)) + \frac{\partial F_2}{\partial V}(u_*, v_{f,h}(\xi; u_*)) v_{\mathrm{in}}(\xi) = \left.\frac{\mathrm{d}}{\mathrm{d}u}\right|_{u=u_*} F_2(u, v_{f,h}(\xi; u)).$$

131

Using the notation introduced in (2.9), we can write the integral in (3.73) as

$$\int_{-\infty}^{\infty} \left[\frac{\partial F_2}{\partial U}(u_*, v_{f,h}(\xi; u_*)) + \frac{\partial F_2}{\partial V}(u_*, v_{f,h}(\xi; u_*)) v_{\text{in}}(\xi) \right] d\xi =$$
$$\int_{-\infty}^{\infty} \left[\frac{d}{du}\Big|_{u=u_*} F_2(u, v_{f,h}(\xi; u)) \right] d\xi = \frac{d}{du}\Big|_{u=u_*} D_p(u). \qquad (3.90)$$

As for the expressions B_- and B'_-, we recall Lemma 3.12 (ii): the eigenfunction at $\lambda = 0$ for the problem $(\mathcal{L}_s(y) - \lambda)u = 0$ is (a scalar multiple of) the derivative of the function which is perturbed, in our case

$$\hat{u}_{s,-}(y_*; \lambda = 0) = C_1 \frac{d}{dy}\Big|_{y=y_*} u_s^s(y) = C_1 \frac{d}{dx}\Big|_{x=x_*} u_s^s(x), \quad C_1 \in \mathbb{R}$$

where $u_s^s(x)$ is the solution to (3.21) that spans the stable manifold $W_s^s((0,0))$. Using (3.31), we can determine $C_1 = \frac{1}{u_{s,\infty}}$. Similarly, we can write

$$\frac{d}{dy}\Big|_{y=y_*} \hat{u}_{s,-}(y; \lambda = 0) = \frac{1}{u_{s,\infty}} \frac{d^2}{dx^2}\Big|_{x=x_*} u_s^s(x).$$

As both B_- and B'_- are defined as the limit of the above expressions as $\varepsilon \to 0$ (3.74), we see that

$$B_-(0) = \frac{1}{u_{s,\infty}} \frac{d}{dx}\Big|_{x=x_*} u_s^s(x) \quad \text{and} \quad B'_-(0) = \frac{1}{u_{s,\infty}} \frac{d^2}{dx^2}\Big|_{x=x_*} u_s^s(x). \qquad (3.91)$$

Since the flow on the stable manifold is governed by (3.21), we can write

$$u_{s,\infty} B'_-(0) = \mu u_* - \nu_1 F_1(u_*; 0). \qquad (3.92)$$

Moreover, since the expressions for B_- and B'_- are evaluated at $x = x_*$, we know that at $u(x_*) = u_*$ the slow manifold intersects the touchdown curve T_d. Therefore, by (3.23)

$$u_{s,\infty} B_-(0) = -\frac{1}{2} \nu_2 D_p(u_*). \qquad (3.93)$$

Substitution of (3.90), (3.92) and (3.93) in (3.73) yields the Lemma, using the fact that $u_{s,\infty} \neq 0$. □

When $y_* \neq 0$ and hence $B_-(0) \neq 0$, the trivial eigenvalue is again connected to a bifurcation of the homoclinic pulse (Remark 3.10). Comparison of the saddle-node condition (3.29) from Corollary 3.9 with the expression for $t_{s,+}(0)$ from Lemma 3.31 yields the following Corollary:

Corollary 3.32. *Assume $B_-(0) \neq 0$. The critical eigenvalue $\lambda = 0$ has multiplicity 2 or more – or equivalently $t_{s,+}(0) = 0$ – if and only if the homoclinic orbit $\Gamma_h(\xi)$ of Theorem 3.7 undergoes a saddle node bifurcation (as described in Corollary 3.9).*

This way we may conclude that, apart from the saddle node bifurcation (Corollary 3.9) and the crossing of x_* through 0 (Corollary 3.30), the homoclinic pulse Γ_h can only lose or gain stability when a pair of complex conjugate eigenvalues –with nonzero imaginary parts– crosses the imaginary axis: the associated bifurcation is of Hopf type. In explicit settings, the bifurcation structure of these Hopf bifurcations can be analysed in detail, see chapter 2, section 2.4. The nature of this Hopf bifurcation will be analysed extensively in chapter 4, both in the general setting treated in this chapter and in the applied setting of chapter 2.

3.5.3 Further instability results

The structure of $t_{s,+}(\lambda)$ at $\lambda = 0$ and near $\lambda = \lambda_{f,0}$ can be used to establish explicit conditions for the existence of real positive zeroes of $t_{s,+}(\lambda)$. Note that the line of reasoning is similar to that in [28], where the sign of the Evans function at $\lambda = 0$ and for $\lambda \to \infty$ was combined with counting arguments to establish the (non-)existence of intersections of the (real) Evans function with the positive λ-axis. Compared to [28], we have additional information about the slow component of the Evans function near its pole at $\lambda = \lambda_{f,0}$.

Lemma 3.33. *Consider T as given in (3.80). If $\nu_2 T > 0$, there exists a positive real zero of $t_{s,+}(\lambda)$; therefore, the homoclinic pulse Γ_h unstable when $\nu_2 T > 0$.*

When F_2 is monotonic in V and G is monotonic in U, the coefficient T is nonzero and its sign is known (see (3.80) and recall that $w_{f,0}(\xi) > 0$). In that case –which will often arise in explicit settings such as the generalised GM model– the equation $\nu_2 B_-(\lambda_{f,0}) = 0$ determines a codimension 1 instability condition, see the discussion following Corollary 3.24 on (3.81). Combining this with Lemma 3.33, we see that the homoclinic pulse Γ_h is unstable for either $\nu_2 \in (-\infty, 0]$ or $\nu_2 \in [0, \infty)$, depending on the (fixed) sign of T.

Proof. The idea of the proof is to combine insights on the behaviour of $t_{s,+}(\lambda)$ for real λ as $\lambda \to \infty$ with the behaviour of $t_{s,+}(\lambda)$ as $\lambda \downarrow \lambda_{f,0}$, then use the continuity of $t_{s,+}$. Firstly, as in the proof of Lemma 3.14, define $\delta = \frac{1}{\lambda}$. For δ small enough, i.e. for λ large enough, it can be shown analogous to the proof of Lemma 3.14 that $\hat{u}_{s,\pm}(y; \lambda, \varepsilon) = e^{\pm\sqrt{\lambda}y}(1 + O(\delta))$ on an $O(1)$ y-domain $\supset \{y = 0\}$, using (3.62) and

(3.63). Therefore, we can approximate $B_\pm$ and $B'_\pm$ as

$$B_\pm(\lambda) = e^{\pm\sqrt{\lambda}y_*}(1 + O(\delta)) \quad\text{and}\quad B'_\pm(\lambda) = \pm\sqrt{\lambda}\, e^{\pm\sqrt{\lambda}y_*}(1 + O(\delta)),$$

yielding

$$t_{s,+}(\lambda) = \frac{e^{-2\sqrt{\lambda}y_*}}{\sqrt{\lambda}} \left\{ \sqrt{\lambda} - \frac{v_2}{2} \int_{-\infty}^{\infty} \left[\frac{\partial F_2}{\partial U}(u_*, v_{f,h}(\xi; u_*)) + \frac{\partial F_2}{\partial V}(u_*, v_{f,h}(\xi; u_*))\, v_{\mathrm{in}}(\xi) \right] \mathrm{d}\xi \right\}.$$

Combining Lemma 3.14 and the elements of its proof with the expression for v_{in} from Lemma 3.15, we obtain

$$v_{\mathrm{in}}(\xi; \lambda) = \frac{1}{2\sqrt{\lambda}} \int_{-\infty}^{\infty} \frac{\partial G}{\partial U}(u_*, v_{f,h}(\tilde\xi; u_*))\, e^{-\sqrt{\lambda}|\xi - \tilde\xi|}\mathrm{d}\tilde\xi + O(\delta).$$

From this, we see that $\int_{-\infty}^{\infty} \frac{\partial F_2}{\partial V}(u_*, v_{f,h}(\xi; u_*))\, v_{\mathrm{in}}(\xi)\, \mathrm{d}\xi \to 0$ as $\lambda \to \infty$. Since the integral $\int_{-\infty}^{\infty} \frac{\partial F_2}{\partial U}(u_*, v_{f,h}(\xi; u_*))\, \mathrm{d}\xi$ does not depend on λ, it follows that

$$t_{s,+}(\lambda) \rightsquigarrow e^{-2\lambda y_*} \quad\text{as}\quad \lambda \to \infty.$$

Secondly, we know the behaviour of $t_{s,+}$ in another limit from Lemma 3.23: recall (3.79), with T as in (3.80). Now, when $v_2 T > 0$, then $t_{s,+}$ tends to $-\infty$ as $\lambda \downarrow \lambda_{f,0}$. Since there are no other poles of $t_{s,+}$ for $\lambda > \lambda_{f,0}$, by continuity there must be a $\lambda_* > \lambda_{f,0} > 0$ where $t_{s,+} = 0$ because $t_{s,+}$ approaches zero from above for $\lambda \to \infty$. The existence positive real zero of $t_{s,+}$ establishes the instability of the homoclinic pulse Γ_h. $\qquad\square$

Combining the statement of Corollary 3.29 with the observation that the condition $x_* < 0$ is equivalent with $v_2 D_p(u_*) < 0$ (combining the definition $p_* = +\frac{1}{2}v_2 D_p(u_*)$ with with Lemma 3.8), we see that the homoclinic pulse may only be stable when $v_2 D_p(u_*) > 0$. This observation can be used to obtain another instability criterion:

Lemma 3.34. *Assume $v_2 D_p(u_*) > 0$, and let R be defined by*

$$R = \mu u_* - v_1 F_1(u_*; 0) - \frac{1}{4}v_2^2 D_p(u_*) \left.\frac{\mathrm{d}}{\mathrm{d}u}\right|_{u=u_*} D_p(u). \tag{3.94}$$

If $R > 0$, the homoclinic pulse Γ_h is unstable.

Since R is directly related to the dervative of (3.24) with respect to u (see Corollary 3.9 and Lemma 3.31), it can be interpreted geometrically in the context of the existence problem as the relative slope of T_o with respect to $W^u_s((0,0))$ at their intersection (u_*, p_*). In Figure 3.8, we have indicated the signs of R related to the three possible homoclinic pulses associated to the configuration depicted in Figure 3.2. Lemma 3.34 directly yields the instability of the first and third intersection.
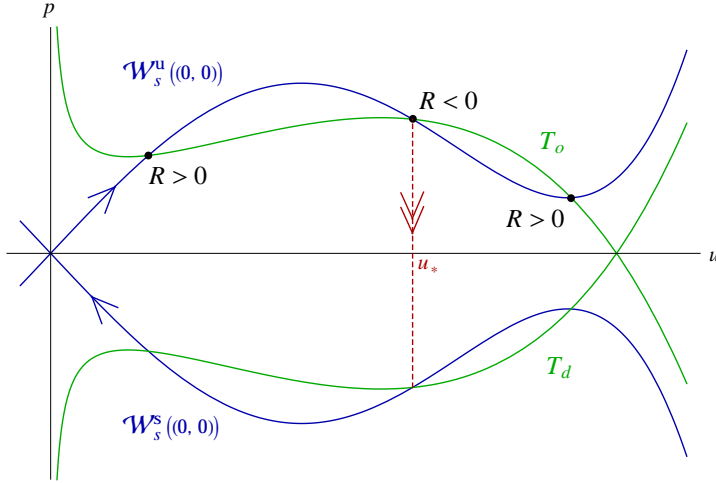
Figure 3.8: The coefficient R (3.94) interpreted geometrically as the relative slope of T_o with respect to $\mathcal{W}_s^u((0,0))$ at their intersection point. Only the homoclinic pulse associated to the second intersection can be stable (Lemma 3.34).

Proof. Since Lemma 3.33 ensures that the pulse is unstable when $\nu_2 T > 0$, we assume $\nu_2 T < 0$ without loss of generality. Using Lemma 3.31, we see that $t_{s,+}(0) = \frac{1}{2\sqrt{\mu}} \frac{\nu_2 D_p(u_*)}{u_{s,\infty}^2} R$, so $\operatorname{sgn}(t_{s,+}(0)) = \operatorname{sgn}(R)$ since $\nu_2 D_p(u_*) > 0$. Since $\nu_2 T < 0$, we can use Lemma 3.23 to conclude that $t_{s,+} \to -\infty$ as $\lambda \uparrow \lambda_{f,0}$. If $R > 0$, i.e. $t_{s,+}(0) > 0$, it follows that there is a $\lambda_0 \in (0, \lambda_{f,0})$ for which $t_{s,+}(\lambda_0) = 0$ since $t_{s,+}(\lambda)$ is continuous for $\lambda \in [0, \lambda_{f,0})$. Since $\lambda_0 > 0$ is a positive zero of $t_{s,+}(\lambda)$, the homoclinic pulse Γ_h is unstable. □

We refer to Figure 3.9 for an illustration of the necessary existence of unstable eigenvalues in the case $\nu_2 T > 0$ (Lemma 3.33) and the case $R > 0$, $\nu_2 T < 0$ (Lemma 3.34). Note that $R < 0$ for the only existing pulse in the explicit model (3.2), see Figure 2.6a in chapter 2.

Combining Corollary 3.29, Lemma 3.33 and Lemma 3.34, we may conclude:

Theorem 3.35. *Let Γ_h be a homoclinic pulse whose existence is established by Theorem 3.7. Γ_h can only be stable if $\nu_2 D_p(u_*) > 0$, $\nu_2 T < 0$ and $R < 0$, where $D_p(u_*)$, T and R are explicitly computable expressions given in (3.17), (3.80) and (3.94).*

Finally, we formulate another instability result that is again based on the fact that we know $t_{s,+}$ has a pole at $\lambda = \lambda_{f,0}$.
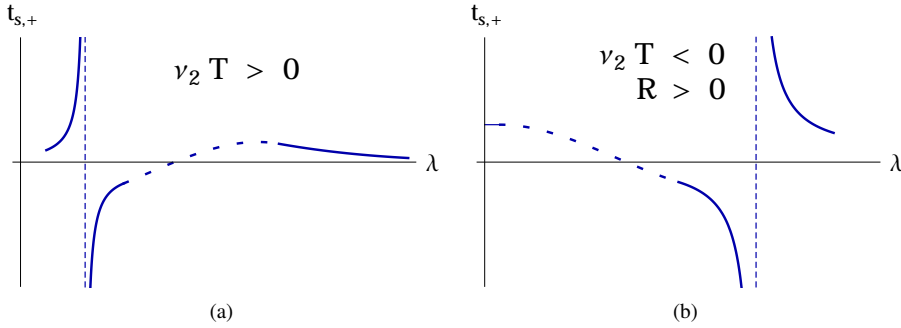
Figure 3.9: An illustration of the proof of Lemma 3.33 (3.9a) and Lemma 3.34 (3.9b). The (singular) behaviour of $t_{s,+}$ near $\lambda = \lambda_{f,0}$ is determined by the sign of $v_2 T$ (Lemma 3.23). In (a), this leads to at least one root of $t_{s,+}$ to the right of $\lambda_{f,0} > 0$ since $t_{s,+} \rightsquigarrow e^{-2y_*\lambda}$ as $\lambda \to \infty$. In (b), $t_{s,+}$ has to cross the horizontal axis in the interval $\lambda \in (0, \lambda_{f,0})$ at least once if $R > 0$.

Lemma 3.36. *Assume $v_2 \neq 0$ and $B_-(\lambda_{f,0}) \neq 0$. Let S be defined by*

$$S = \frac{2}{v_2} \frac{B_-'(\lambda_{f,0})}{B_-(\lambda_{f,0})} + \int_{-\infty}^{\infty} \frac{\partial F_2}{\partial U}(u_*, v_{f,h}(\xi; u_*)) \, d\xi. \tag{3.95}$$

If $|S|$ is large enough, then $t_{s,+}(\lambda)$ has a zero near $\lambda_{f,0}$, rendering the homoclinic pulse unstable.

Proof. Take the interval $I(\lambda_{f,0}, \delta)$ to be a (symmetric) δ-neighbourhood of $\lambda_{f,0}$ in $\mathbb{R}$ with $0 < \delta \ll 1$ small enough. We can rewrite the equation $t_{s,+}(\lambda) = 0$ using (3.73) as

$$\int_{-\infty}^{\infty} \frac{\partial F_2}{\partial V}(u_*, v_{f,h}(\xi; u_*)) \, v_{\mathrm{in}}(\xi) \, d\xi = -\frac{2}{v_2} \frac{B_-'}{B_-} - \int_{-\infty}^{\infty} \frac{\partial F_2}{\partial U}(u_*, v_{f,h}(\xi; u_*)) \, d\xi \tag{3.96}$$

From Corollary 3.16 we know that the lefthand side of (3.96) behaves as $\frac{1}{\lambda - \lambda_{f,0}}$ in $I(\lambda_{f,0}, \delta)$, while the righthand side of (3.96), given by S to leading order in δ, is continuous –and to leading order constant– in λ on the same interval. Therefore, a solution to (3.96) in the interval $I(\lambda_{f,0}, \delta)$ can be found if $|S|$ is large enough; see also Figure 3.10. □

This Lemma can be used to clarify the scaling of the F_2 term in (3.1) / (3.7), as argued in the introductory section 3.1:
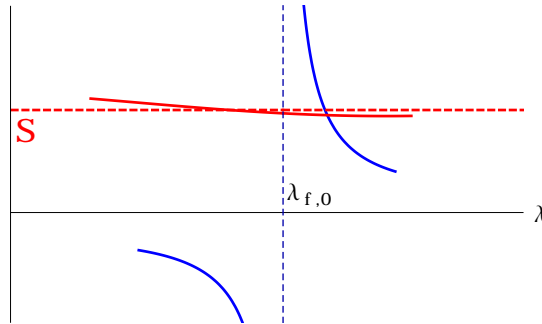
Figure 3.10: The statement of Lemma 3.36 graphically explained. The lefthand side of (3.96), which is singular at $\lambda = \lambda_{f,0}$, is indicated in blue, the righthand side of (3.96) is indicated in red and its approximation S (3.95) by the dashed line.

Corollary 3.37. *When ν_2 is small enough, in particular when $\nu_2 = O(\varepsilon)$, the homoclinic pulse is unstable.*

3.6 Discussion

The existence and stability theory for localised homoclinic pulses in the general setting of equation (3.1) presented in this chapter can be seen as the first fundamental step in the analysis of the dynamics of interacting localised structures. Based on this work, some next steps can now be taken. Several of these steps have already been made in the context of GS/GM-type models – see [5, 12, 14, 26, 32, 33, 34, 47, 51, 58] and the references therein. The present chapter and its predecessor, chapter 2, show that there will be fundamental analytical challenges in further developing the theory in the general setting of (3.1). Moreover, it is clear that the 'slow nonlinearity' of (3.1) will generate pulse dynamics that is much richer than that of 'slowly linear' models – see Remark 3.1 for the case of one localised homoclinic pulse.

A first next step –one that in fact largely inspired the present work– is the stability analysis of localised spatially periodic patterns to systems of type (3.1) on bounded and/or unbounded domains. Based on [51], it was found in the recent work [14] that the nature of the destabilization of spatially periodic multi-pulse patterns with long wavelength is quite complex. It is shown in [14] in the context of GM-type models that such patterns can be destabilised by two distinct types of Hopf bifurcations:

one in which the destabilization makes the pulses of the periodic pattern oscillate exactly in phase with their neighbouring pulses, and one in which each destabilised pulse starts to oscillate exactly out of phase with its neighbours. Moreover, on the unbounded domain $x \in \mathbb{R}$, the character of the destabilization alternates countably many times between these two types of Hopf bifurcation as the wavelength of the underlying pattern grows, i.e. as the spatially periodic pattern approaches the homoclinic limit. This so-called 'Hopf dance' has also been found numerically by AUTO-simulations in generalised Gray-Scott models – models that even include nonlinear diffusion in the slow U-component [14, 52]. The analysis of [14] clearly shows that the Hopf dance, and especially the associated higher order 'belly dance', has its origins in the 'slowly linear' character of GM/GS-type models. It can be expected that the destabilization of long wavelength periodic patterns in system (3.1) has an even richer structure. This is the subject of work in progress, and falls outside the scope of this thesis.

Already in the case of GS/GM-type models, interacting pulses may exhibit complicated, even chaotic, behaviour [41, 42]. However, in the parameter regimes in which the pulse dynamics can be studied in full analytical detail –i.e. the regime in which pulse self-replication does not occur– the pulse interactions are of a much more simple nature, see [5, 12, 32, 33, 34, 47] and the references therein. Nevertheless, the semi-strong pulse dynamics exhibited by GS/GM-type models are much richer than in the weakly interacting case. Weak pulse interactions are only driven by exponentially small tail interactions [17, 44, 45]. The semi-strong GS/GM-type dynamics are largely determined by the slow U-component that does not approach its background state in between the fast V-pulses. However, in the GS/GM-type models studied in the literature, the slow U-dynamics are linear, and –exactly as in the stability analysis for homoclinic pulses– this linearity plays a crucial role in the analysis. In the general system (3.1), also the slow U-dynamics between localised V-pulses will be nonlinear. In combination with the observations of chapter 2 –especially the possibility of stably oscillating pulses (see Remark 3.1)– this implies that even in the semi-strong regime, the pulse dynamics generated by systems of the type (3.1) will be much more rich and complex than encountered so far in the literature. A first step towards the analysis of such rich and complex behaviour is presented in the next and last chapter of this thesis, chapter 4.

4

Hopf bifurcations for localised pulses

4.1 Introduction

The study of localised patterns in systems of reaction-diffusion equations has been a very active field of research for the last couple of decades. In canonical model systems such as the Gray-Scott [23] or Gierer-Meinhardt [22] model, far-from-equilibrium patterns were constructed and analysed in the presence of an asymptotically small parameter, giving the system under consideration a singularly perturbed nature [11, 26]. This singularly perturbed structure induces a spatial scale separation, which can be used to obtain explicit leading order expressions for the pattern under consideration (e.g. [6]). These techniques were applied in full generality in chapter 3 in the context of single pulse patterns, going beyond the existing analysis in the context of the canonical Gray-Scott and Gierer-Meinhardt models. In chapter 2, this extended theory was applied in the context of an explicit model, exhibiting new, previously unobserved behaviour.

In chapters 2 and 3, the stability analysis of the pulse solutions under consideration led to observation that, under certain general conditions, the most general pulse destabilisation scenario corresponds to a Hopf bifurcation of the pulse eigenvalues, an observation that is also known from the extensive literature on Gray-Scott/Gierer-Meinhardt models [5, 6, 7, 14, 17, 26, 32, 47, 52, 57]. This Hopf bifurcation, and in particular its unfolding, is the main topic of this last chapter. The aim of this chapter

is to develop a mechanism for the weakly nonlinear analysis of the aforementioned Hopf destabilisation scenario, through local analysis of the associated centre manifold.

The chapter is structured as follows. In section 4.2, relevant results from chapter 3 on the existence and stability of pulse solutions are summarised, (re)introducing notation which will be used throughout the text. In section 4.3, the Hopf centre manifold is introduced. Also, the issue of the translational eigenmode is addressed. Since the systems of reaction-diffusion equations studied in the field of pattern formation – and in extension localised pattern solutions thereof – exhibit translational invariance, the translational eigenmode with corresponding (central) eigenvalue $\lambda = 0$ is always present when the stability of the pattern under consideration is assessed. However, the centre manifold can be foliated along the direction spanned by the translational mode (Theorem 4.8), and it follows that the dynamics along the translational direction are trivial.

Section 4.4 is dedicated to the explicit local expansion of the centre manifold established in section 4.3, using direct expansions in the Hopf eigenmodes. The main result is an explicit, albeit elaborate, expression for the first Lyapunov coefficient of the (normal form of) the Hopf bifurcation (Corollary 4.12 and equation (4.58)). Leading order expressions for the pulse and its eigenmodes as developed in chapter 3 (summarised in Theorem 4.2 resp. Theorem 4.3), combined with a specific choice for the inner product, are then used to obtain an explicit leading order expression for this first Lyapunov coefficient, which is used to decide whether the Hopf bifurcation under consideration is subcritical or supercritical. Given the intricate nature of the problem, this result is quite remarkable: the formal centre manifold expansion leads to concrete, explicitly computable results, based on explicit leading order expressions for the Hopf eigenfunctions.

In section 4.5, an alternative method for the calculation of the first Lyapunov coefficient is presented, based on the analysis in [24]. While the algebraic manipulations leading to the explicit expression of the first Lyapunov coefficient are less cumbersome than those in section 4.4, this method introduces a number of new inverse problems to be solved, along with the analysis of the adjoint linear operator associated to the linearisation of the pulse solution. It is argued that, while both methods are in essence equivalent, either one of the two approaches can be preferable in terms of algebraic and analytic tractability, depending on the specific choice of (nonlinear) reaction terms in the system under consideration.

The developed theory is in section 4.6 applied to a model example, the slowly nonlinear Gierer-Meinhardt equation (4.109), which was considered in chapter 2. The explicit leading order expressions available for the pulse and its eigenfunctions allow one to obtain directly computable eigenvalues, and in extension directly computable values of the associated first Lyapunov coefficients. For this example, it is shown that the extension of the canonical Gierer-Meinhardt model with a slowly nonlinear term introduces a Hopf bifurcation which can change its nature from sub- to supercritical, depending on the parameter values (Theorem 4.16). As an aside, a relatively old observation from the literature, based on numerical simulations, is confirmed analytically [11, 57], namely that Hopf bifurcation associated with the pulse in the canonical Gierer-Meinhardt equation is always subcritical (Corollary 4.17).

4.2 Preliminaries

In chapter 3, a general theory for establishing the existence and stability of stationary single pulses was presented in a general setting of a singularly perturbed, two component system of reaction-diffusion equations on the real line, with asymptotically small parameter $0 < \varepsilon \ll 1$. It was shown that the most general context in which these pulse solutions could be constructed led to the following system:

$$
\begin{cases}
U_t = U_{xx} - (\mu U - \nu_1 F_1(U; \varepsilon)) + \frac{\nu_2}{\varepsilon} F_2(U, V; \varepsilon) \\
V_t = \varepsilon^2 V_{xx} - V + G(U, V; \varepsilon)
\end{cases}.
\tag{4.1}
$$

System (4.1) is considered on the unbounded domain such that $U, V : \mathbb{R} \times \mathbb{R}_{>0} \to \mathbb{R}$; moreover, we restrict ourselves to positive solutions. A stable homogeneous trivial background state is assumed. The range of the model parameters $\mu, \nu_{1,2}$ and mild regularity assumptions on the nonlinear reaction terms $F_{1,2}$ and G are specified in (A1 - A4) of Assumptions 4.1. In the following subsections 4.2.1 and 4.2.2, a very concise overview of the results obtained in chapter 3 are given. The necessary ingredients for establishing localised pulses and their eigenfunctions are given, in order to be able to set up the theory for a Hopf bifurcation of such a localised pulse, which is the main subject of this chapter. By nature, this overview is far from complete and very brief: the reader is encouraged to consider chapter 3 for a complete exposition.

4.2.1 Existence

Introducing the 'fast' (or short scale) coordinate $\xi = \frac{x}{\varepsilon}$, (4.1) can be transformed into

$$
\begin{cases}
U_t &=& \frac{1}{\varepsilon^2} U_{\xi\xi} &-& (\mu U - \nu_1 F_1(U;\varepsilon)) &+& \frac{\nu_2}{\varepsilon} F_2(U,V;\varepsilon) \\
V_t &=& V_{\xi\xi} &-& V &+& G(U,V;\varepsilon)
\end{cases}
. \tag{4.2}
$$

Establishing the existence of a stationary pulse solution in (4.2) (or equivalently (4.1)) which is asymptotic to the (stable) trivial background state of (4.2) is equivalent to constructing a homoclinic orbit in the associated ODE system

$$
\begin{cases}
u_\xi &=& \sqrt{\varepsilon} p \\
p_\xi &=& \sqrt{\varepsilon} \left(-\nu_2 F_2(u,v;\varepsilon) + \varepsilon \left(\mu u - \nu_1 F_1(u;\varepsilon) \right) \right) \\
v_\xi &=& q \\
q_\xi &=& v - G(u,v;\varepsilon)
\end{cases}
. \tag{4.3}
$$

Since ε is taken to be asymptotically small, (4.3) can be analysed using geometric singular perturbation (or Fenichel) theory [18, 19]. Taking the limit $\varepsilon \to 0$ in (4.3) yields the fast reduced system

$$
v_{f,\xi\xi} = v_f - G(u_0, v_f; 0) \quad \text{or} \quad
\begin{cases}
v_{f,\xi} &=& q_f \\
q_{f,\xi} &=& v_f - G(u_0, v_f; 0)
\end{cases}
, \quad u_0 > 0 \text{ constant,} \tag{4.4}
$$

together with the normally hyperbolic invariant manifold

$$
\mathcal{M} = \{(u, p, v, q) \,|\, v = q = 0, u > 0\}.
$$

Note that, by Assumptions 4.1, (A4), $\mathcal{M}$ is also invariant for the full system (4.3); there, its unstable and stable manifolds are denoted by $\mathcal{W}^{u/s}(\mathcal{M})$.

On $\mathcal{M}$, the slow dynamics can be represented to leading order by the slow reduced system

$$
u_{s,xx} = \mu u_s - \nu_1 F_1(u_s;\varepsilon), \quad \text{or} \quad
\begin{cases}
u_{s,x} &=& p_s \\
p_{s,x} &=& \mu u_s - \nu_1 F_1(u_s;\varepsilon)
\end{cases}
, \quad u > 0. \tag{4.5}
$$

For this slow reduced system, the unstable and stable manifolds of the origin are denoted by $\mathcal{W}_s^{u/s}((0,0);\varepsilon)$. These manifolds are by definition spanned by the solutions $(u_s^u(x;\varepsilon), p_s^u(x;\varepsilon))$ resp. $(u_s^s(x;\varepsilon), p_s^s(x;\varepsilon))$ of (4.5). Note that $u_s^s(x) = u_s^u(-x)$ and $p_s^s(x) = -p_s^u(-x)$ by the reversibility symmetry of (4.5).

The existence of a symmetric stationary pulse solution of (4.2) was established in chapter 3 under certain conditions; first, Assumptions 4.1, (A5) below ensures the existence of a homoclinic orbit in the fast reduced system (4.4). Second, introducing

$$D_p(u_0) = \int_{-\infty}^{\infty} F_2(u_0, v_{f,h}(\xi; u_0); 0) \, d\xi, \qquad (4.6)$$

it was seen that the solutions to the equation

$$\mu u^2 - 2\nu_1 \int_0^u F_1(\tilde{u}; 0) \, d\tilde{u} = \tfrac{1}{4} \nu_2^2 \, D_p^2(u) = \tfrac{1}{4} \nu_2^2 \left[\int_{-\infty}^{\infty} F_2(u, v_{f,h}(\xi; u); 0) \, d\xi \right]^2 \qquad (4.7)$$

play a central role in the pulse construction process. To remove a number of sign ambiguities, it is necessary to gauge F_2 such that the function D_p obeys Assumptions 4.1, (A6). For a more detailed and extended presentation of the above, see chapter 3, section 3.2. We restate the assumptions from chapter 3; see also Definition 2.3.

Assumptions 4.1. *The following is assumed to hold:*

(A1) μ, $\nu_{1,2}$ *are real and nonsingular in ε; furthermore, $\mu > 0$.*

(A2) $F_1(U; \varepsilon) \rightsquigarrow U^{f_1}$ *as $U \downarrow 0$ for some $f_1 > 1$;*
F_1 is smooth both on its domain and as a function of ε.

(A3) *Writing $F_2(U, V; \varepsilon) = F_{2,1}(U; \varepsilon) \, V + F_{2,2}(U, V; \varepsilon)$,*
$F_{2,1}(U; \varepsilon) \rightsquigarrow \tilde{F}_{2,1}(\varepsilon) \, U^{\gamma_1}$ as $U \downarrow 0$ for some $\gamma_1 \geq 0$ and $\tilde{F}_{2,1}(\varepsilon) \in \mathbb{R}$;
$F_{2,2}(U, V; \varepsilon) \rightsquigarrow \tilde{F}_{2,2,u}(V; \varepsilon) \, U^{\alpha_1}$ as $U \downarrow 0$ for some $\alpha_1 \in \mathbb{R}$;
$F_{2,2}(U, V; \varepsilon) \rightsquigarrow \tilde{F}_{2,2,v}(U; \varepsilon) \, V^{\beta_1}$ as $V \to 0$ for some $\beta_1 > 1$;
F_2 is smooth both on its domain and as a function of ε.

(A4) $G(U, V; \varepsilon) \rightsquigarrow \tilde{G}_u(V; \varepsilon) \, U^{\alpha_2}$ *as $U \downarrow 0$ for some $\alpha_2 \in \mathbb{R}$;*
$G(U, V; \varepsilon) \rightsquigarrow \tilde{G}_v(U; \varepsilon) \, V^{\beta_2}$ as $V \to 0$ for some $\beta_2 > 1$;
G is smooth both on its domain and as a function of ε.

(A5) *For all $u_0 > 0$ there exists a positive solution $v_{f,h}(\xi; u_0)$ to (4.4) which is homoclinic to $(v_f, q_f) = (0, 0)$.*

(A6) $D_p(u) \rightsquigarrow 1 \cdot u^{d_p}$ *as $u \downarrow 0$ for some $d_p \in \mathbb{R}$, c.f. (4.6).*

The Gray-Scott and Gierer-Meinhardt models are examples of systems obeying these assumptions. However, the full class of systems described in this way is far more encompassing.
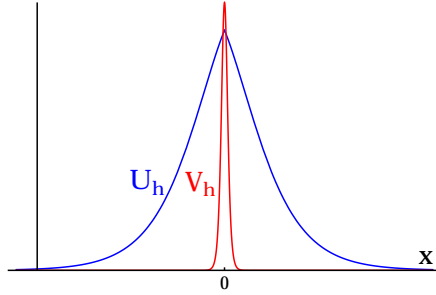
Figure 4.1: A sketch of the stationary, symmetric pulse solution to (4.2), whose existence and structure is established in Theorem 4.2.

The slow-fast structure present in the ODE system (4.3) leads to a scale separation between the U- and V-components of the pulse. Loosely speaking, one can within the unbounded domain define an inner, 'fast' region

$$I_f = \left[-\frac{1}{\varepsilon^{\frac{1}{4}}}, \frac{1}{\varepsilon^{\frac{1}{4}}} \right] \tag{4.8}$$

where the U-component of the pulse is constant to leading order in ε, while outside I_f the V-component of the pulse is exponentially small; see Figure 4.1. The exact leading order pulse structure and existence conditions were stated in chapter 3, Theorem 3.7, reformulated here for reference purposes:

Theorem 4.2. *Assume that conditions 4.1 hold and let $\varepsilon > 0$ be small enough. Let K be the number of non-degenerate solutions $u = u_{*,k} > 0$ of (4.7) such that $(u_{*,k}, p_{*,k}) = (u_{*,k}, \frac{1}{2} v_2 D_p(u_{*,k})) \in \mathcal{W}^u_s((0,0);0)$.*

1. *If $K = 0$ then there are no symmetric, positive, one-circuit homoclinic solutions to $(0,0,0,0)$ in (4.3).*

2. *If $K \neq 0$, there are K distinct positive, symmetric, one-circuit homoclinic orbits $\Gamma_{h,k}(\xi) = (u_{h,k}(\xi), p_{h,k}(\xi), v_{h,k}(\xi), q_{h,k}(\xi)) \subset \mathcal{W}^u(\mathcal{M}) \cap \mathcal{W}^s(\mathcal{M})$, $k = 1, 2, ..., K$, with internal reflection point $\xi = 0$, so that $\Gamma_{h,k}(0) = (u_{h,k}(0), 0, v_{h,k}(0), 0)$ in (4.3). In the fast field (4.8), $\Gamma_{h,k}(\xi)$ is to leading order determined by the homoclinic solution $v_{f,h}(\xi; u_{*,k})$ of (4.4):*

$$\Gamma_{h,k}(\xi) = \left(u_{*,k}, 0, v_{f,h}(\xi; u_{*,k}), \frac{\mathrm{d}}{\mathrm{d}\xi} v_{f,h}(\xi; u_{*,k}) \right) + O(\sqrt{\varepsilon}) \quad \text{for } \xi \in I_f.$$

In the slow field, $\Gamma_{h,k}(\xi)$ approaches $\mathcal{W}^u_s((0,0);\varepsilon) \subset \mathcal{M}$, resp. $\mathcal{W}^s_s((0,0);\varepsilon) \subset \mathcal{M}$ exponentially fast for $\xi \to \pm\infty$: there are $O(1)$ constants $C_{1,2}$ such that

- $v_{h,k}(\xi) \rightsquigarrow C_1 e^{-|\xi|}$ and $q_{h,k}(\xi) \rightsquigarrow \mp C_1 e^{-|\xi|}$ as $\xi \to \pm\infty$;

- there are shifts $x_{*,k} \in \mathbb{R}$ and solutions $u_{*,k}^{\mathrm{u}}(x) = u_s^{\mathrm{u}}(x - x_{*,k})$, $p_{*,k}^{\mathrm{u}}(x) = p_s^{\mathrm{u}}(x - x_{*,k})$ of (4.5), such that $\left(u_{*,k}^{\mathrm{u}}(-\varepsilon^{\frac{3}{4}}), p_{*,k}^{\mathrm{u}}(-\varepsilon^{\frac{3}{4}}) \right) = \left(u_{h,k}(-\varepsilon^{-\frac{1}{4}}), \frac{1}{\sqrt{\varepsilon}} p_{h,k}(-\varepsilon^{-\frac{1}{4}}) \right) = \left(u_{*,k}, p_{*,k} \right) + O(\sqrt{\varepsilon})$ and

$$\left(u_{h,k}(\xi), \frac{1}{\sqrt{\varepsilon}} p_{h,k}(\xi) \right) = \left(u_{*,k}^{\mathrm{u}}(\varepsilon\xi), p_{*,k}^{\mathrm{u}}(\varepsilon\xi) \right) + O\left(e^{C_2\xi} \right) \quad \text{for } \xi < -\varepsilon^{-\frac{1}{4}};$$

- similarly, $\left(u_{*,k}^{\mathrm{s}}(\varepsilon^{\frac{3}{4}}), p_{*,k}^{\mathrm{s}}(\varepsilon^{\frac{3}{4}}) \right) = \left(u_{h,k}(\varepsilon^{-\frac{1}{4}}), \frac{1}{\sqrt{\varepsilon}} p_{h,k}(\varepsilon^{-\frac{1}{4}}) \right) = \left(u_{*,k}, -p_{*,k} \right) + O(\sqrt{\varepsilon})$ with $\left(u_{*,k}^{\mathrm{s}}(x), p_{*,k}^{\mathrm{s}}(x) \right) = \left(u_{*,k}^{\mathrm{u}}(-x), -p_{*,k}^{\mathrm{u}}(-x) \right)$ and

$$\left(u_{h,k}(\xi), \frac{1}{\sqrt{\varepsilon}} p_{h,k}(\xi) \right) = \left(u_{*,k}^{\mathrm{s}}(\varepsilon\xi), p_{*,k}^{\mathrm{s}}(\varepsilon\xi) \right) + O\left(e^{-C_2\xi} \right) \quad \text{for } \xi > \varepsilon^{-\frac{1}{4}}.$$

The orbits $\Gamma_{h,k}(\xi)$ correspond to the homoclinic pulse patterns $(U_{h,k}(\xi), V_{h,k}(\xi))$ in (4.2) that are symmetric with respect to $\xi = 0$ through $U_{h,k}(\xi) = u_{h,k}(\xi)$, $V_{h,k}(\xi) = v_{h,k}(\xi)$.

The situation described in the theorem is illustrated in chapter 3, Figure 3.2.

4.2.2 Linearisation and eigenfunctions

In order to set up an analysis of Hopf bifurcations of the localised pulses considered in the previous section, it is necessary to highlight some aspects of the stability analysis of the pulse, as carried out in chapter 3, section 3.3. The main purpose of the current section is to obtain a leading order expression for the eigenfunctions of such a localised pulse.

In the following, assume that $K \geq 1$ and fix k (see Theorem 4.2); the associated homoclinic pulse pattern is denoted by $\Gamma_h(\xi) = (U_h(\xi), V_h(\xi))$. The stability analysis of this pulse is closely related to the study of the linear operator

$$\mathcal{L}(\xi; \varepsilon) = \begin{pmatrix} \varepsilon^{-2} & 0 \\ 0 & 1 \end{pmatrix} \frac{\mathrm{d}^2}{\mathrm{d}\xi^2} - \mathcal{A}(\xi; \varepsilon), \tag{4.9}$$

where

$$\mathcal{A}(\xi; \varepsilon) = \begin{pmatrix} \mu - \nu_1 \frac{\mathrm{d}F_1}{\mathrm{d}U} - \frac{\nu_2}{\varepsilon} \frac{\partial F_2}{\partial U} & -\frac{\nu_2}{\varepsilon} \frac{\partial F_2}{\partial V} \\ -\frac{\partial G}{\partial U} & 1 - \frac{\partial G}{\partial V} \end{pmatrix} \Bigg|_{(U,V)=(U_h(\xi),V_h(\xi))}. \tag{4.10}$$

Since $\lim_{\xi \to \pm\infty} \Gamma_h(\xi) = (0,0)$, the matrix $\mathcal{A}(\xi; \varepsilon)$ is asymptotically constant as $\xi \to \pm\infty$: $\lim_{\xi \to \pm\infty} \mathcal{A}(\xi; \varepsilon) = A_\infty(\varepsilon)$. The eigenvalues of this constant matrix determine the essential spectrum σ_e of the operator $\mathcal{L}$, which is given by

$$\sigma_e = \{\lambda \in \mathbb{R} : \lambda \le \ \max\,(-\mu, -1)\} \subset \mathbb{C}. \qquad (4.11)$$

The slow-fast structure of the homoclinic pulse Γ_h, made explicit in Theorem 4.2, is inherited by the linear operator $\mathcal{L}$; this operator is the linearisation of (4.2) around Γ_h. One can therefore introduce the 'fast' linear operator

$$\mathcal{L}_f(\xi) = \frac{\mathrm{d}^2}{\mathrm{d}\xi^2} - \left[1 - \frac{\partial G}{\partial V}(u_*, v_{f,h}(\xi; u_*))\right], \quad \xi \in \mathbb{R}, \qquad (4.12)$$

with $u_* = u_{*,1}$ and $v_{f,h}$ as in Theorem 4.2, and determine its spectrum. The associated eigenvalue problem $\left(\mathcal{L}_f - \lambda\right)v = 0$ is of Sturm-Liouville type; relevant results from the literature are summarised in chapter 3, Lemma 3.12. Based on those results, let $\lambda_{f,j}$, $j \in \mathbb{Z}_{\ge 0}$ be the eigenvalues of the linear operator $\mathcal{L}_f$ acting on the space of bounded integrable functions on the entire real line.
Similarly, the 'slow' linear operator

$$\mathcal{L}_s(x) = \frac{\mathrm{d}^2}{\mathrm{d}x^2} - \left[\mu - v_1 \frac{\partial F_1}{\partial U}(u_*^s(x), 0)\right], \quad x \ge 0, \qquad (4.13)$$

with $u_*^s = u_{*,1}^s$ as in Theorem 4.2, plays a central role in the spectral analysis of $\mathcal{L}$. The eigenvalue problem $(\mathcal{L}_s - \lambda)u = 0$ is again of Sturm-Liouville type, albeit on the positive halfline. Let $u_{s,-}(x; \lambda, \varepsilon)$ be the solution to the eigenvalue problem $\mathcal{L}_s u = \lambda u$ that is bounded as $x \to \infty$, such that $u_{s,-}(x; \lambda, \varepsilon) \rightsquigarrow 1 \cdot e^{-\sqrt{\mu+\lambda}\,x}$ as $x \to \infty$.

The coupling between the U- and V-components of the pulse (apparent in the off-diagonal entries of $\mathcal{A}$) manifests itself in the spectral analysis of $\mathcal{L}$ through the nonhomogeneous problem

$$\left(\mathcal{L}_f - \lambda\right)v = -\frac{\partial G}{\partial U}(u_*, v_{f,h}(\xi; u_*)), \quad \xi \in \mathbb{R}. \qquad (4.14)$$

For $\lambda \ne \lambda_{f,j}$ and $\lambda \notin \sigma_e$, let $v_{\mathrm{in}}(\xi; \lambda, \varepsilon)$ be the unique bounded solution to (4.14). The existence and uniqueness of v_{in} follows from the analysis in chapter 3, section 3.3.3, which is based on the Fredholm alternative. Note that it immediately follows that v_{in} is even as a function of ξ, i.e. $v_{\mathrm{in}}(\xi; \lambda, \varepsilon) = v_{\mathrm{in}}(-\xi; \lambda, \varepsilon)$.

The actual spectral analysis of $\mathcal{L}$ (4.9) does not need to be summarised here: for an overview of this spectral analysis, using an Evans function approach, see chapter 3, sections 3.4 and 3.5. There, a leading order expression for the Evans function was derived (Theorem 3.21), enabling direct calculation of the pulse eigenvalues. It was shown (as a result of Corollary 3.32) that the most general destabilisation scenario for a localised pulse in (4.2) is through a Hopf bifurcation. That observation will be the starting point of the analysis presented in this chapter. However, some comments on the trivial eigenvalue are in order; they can be found in section 4.2.3.

The following theorem, which summarises results from section 3.4.2 in chapter 3, characterises the leading order behaviour of eigenfunctions of the linear operator $\mathcal{L}$ (4.9). This leading order behaviour will be very instrumental in the upcoming analysis.

Theorem 4.3. *Let $\varepsilon > 0$ be small enough. Assume that $\lambda \notin \sigma_e$ and $\lambda \neq \lambda_{f,j}$. If there is a $\lambda \in \mathbb{C}$ for which there is a bounded integrable function $\phi : \mathbb{R} \to \mathbb{C}^2$ such that $\mathcal{L}(\xi; \varepsilon) \phi(\xi; \lambda, \varepsilon) = \lambda \phi(\xi; \lambda, \varepsilon)$, then $\phi(\xi; \lambda, \varepsilon)$ is determined uniquely. Furthermore, there are $\mathcal{O}(1)$ constants $C_{1,2}$ such that the following holds:*

- $\phi(\xi; \lambda, \varepsilon) = \begin{pmatrix} u_{s,-}(\varepsilon\xi; \lambda, \varepsilon) \\ 0 \end{pmatrix} + C_1 e^{-C_2 \xi}$ *for $\xi > \varepsilon^{-\frac{1}{4}}$;*

- $\phi(\xi; \lambda, \varepsilon) = \phi(-\xi; \lambda, \varepsilon)$ *for $\xi < -\varepsilon^{-\frac{1}{4}}$;*

- $\phi(\xi; \lambda, \varepsilon) = u_{s,-}(0; \lambda, \varepsilon) \begin{pmatrix} 1 \\ v_{\mathrm{in}}(\xi; \lambda, \varepsilon) \end{pmatrix} + \mathcal{O}(\varepsilon^{\frac{3}{4}})$ *for $\xi \in I_f$.*

Proof. The leading order expressions for the eigenfunction of $\mathcal{L}$ are based on the proof of Theorem 3.21 in chapter 3. $\qquad \square$

Remark 4.4. From Lemma 3.20 in chapter 3, we know that the 'true' fast eigenvalues of the full linear operator $\mathcal{L}$ (4.9) are only to leading order in ε determined by the fast eigenvalues $\lambda_{f,j}$ of the fast operator $\mathcal{L}_f$ (4.12): these 'true' fast eigenvalues $\lambda_j(\varepsilon)$ of $\mathcal{L}$ obey $\lim_{\varepsilon \to 0} \lambda_j(\varepsilon) = \lambda_{f,j}$. Since the above Theorem 4.3 only determines the leading order expression for the eigenfunction ϕ, it is sufficient to exclude the λ-values for which v_{in}, the unique bounded solution to the inhomogeneous problem (4.14), is not defined. We therefore assume $\lambda \neq \lambda_{f,j}$ instead of $\lambda \neq \lambda_j(\varepsilon)$.

4.2.3 Translational symmetry and the trivial eigenvalue

A general n-component reaction-diffusion equation

$$\tilde{u}_t = D\tilde{u}_{xx} + f(\tilde{u}), \quad \tilde{u} \in \mathbb{R}^n, \ D \in \text{Mat}(n, \mathbb{R}), \ f : \mathbb{R}^n \to \mathbb{R}^n \tag{4.15}$$

is equivariant under the continuous one-parameter group of isometries $(T_\alpha)_{\alpha \in \mathbb{R}}$ which acts as

$$T_\alpha \tilde{u}(x) = \tilde{u}(x + \alpha). \tag{4.16}$$

Every stationary solution $\tilde{u}_0$ to (4.15), for which

$$D\tilde{u}_{0,xx} + f(\tilde{u}_0) = 0, \tag{4.17}$$

can therefore be thought of as representing a continuous family of stationary solutions $(T_\alpha \tilde{u}_0)_{\alpha \in \mathbb{R}}$, obtained under the group action T_α. Since the infinitesimal generator of this underlying translational symmetry group (4.16) is $\tau = \frac{\partial}{\partial x}$, it follows from (4.17) that $\tau \tilde{u}_0$ obeys the linear equation

$$\left[D\frac{\partial^2}{\partial x^2} + \frac{\mathrm{d}f}{\mathrm{d}\tilde{u}}(\tilde{u}_0) \right] \tau \tilde{u}_0 = 0. \tag{4.18}$$

The above considerations apply to the PDE system (4.1)/(4.2); in particular, for the homoclinic pulse solution whose existence was established in Theorem 4.2. In this context, (4.18) takes the form

$$\mathcal{L} \frac{\mathrm{d}}{\mathrm{d}\xi} \Gamma_h = 0,$$

from which follows that $\lambda = 0$ is always an eigenvalue of the operator $\mathcal{L}$ (4.9), with eigenfunction $\frac{\mathrm{d}}{\mathrm{d}\xi}\Gamma_h$. Note that Theorem 4.3 does not apply for this eigenvalue, since $\lambda_{f,1} = 0$ (see chapter 3; also, the above argument can be applied to (4.4) with its linearisation (4.12) around the orbit $v_{f,h}$, Assumptions 4.1 (A5)). However, the eigenfunction $\frac{\mathrm{d}}{\mathrm{d}\xi}\Gamma_h$ does have the same scale separated structure as the eigenfunctions described by Theorem 4.3, see Theorem 4.2. Both considerations will be of importance in the next section.

4.3 The Hopf centre manifold

We will focus on the situation where the pulse Γ_h undergoes a Hopf bifurcation. In other words, let $(\mu, \nu_1, \nu_2) = (\mu_H, \nu_{1,H}, \nu_{2,H})$ be such that there is a bounded integrable function $\phi_H : \mathbb{R} \to \mathbb{C}^2$ as in Theorem 4.3 for which

$$\mathcal{L}\phi_H = i\omega_H \phi_H, \tag{4.19}$$

with $\omega_H > 0$. Since the operator $\mathcal{L}$ is real, it immediately follows that the Hopf bifurcation (4.19) yields a complex conjugate pair of eigenvalues $\pm i\,\omega_H$ with associated eigenfunction pair $\left\{\phi_H, \overline{\phi_H}\right\}$ – here and henceforth, complex conjugation will be denoted by an overline.

Since the linear operator $\mathcal{L}$ (4.9) is sectorial and its continuous spectrum is completely determined by the essential spectrum σ_e (4.11), we can infer that its central spectrum

$$\sigma_0 = \{\lambda \in \mathbb{C} : \lambda \text{ is in the spectrum of } \mathcal{L}, \text{ Re}(\lambda) = 0\}$$

consists of finitely many eigenvalues. Moreover, $\lambda = 0 \in \sigma_0$ (see subsection 4.2.3); we assume that this trivial eigenvalue is nondegenerate. As mentioned before, it was argued in chapter 3 that this is the most general destabilisation scenario for a given pulse whose existence is ensured by Theorem 4.2. Indeed, this destabilisation through a Hopf bifurcation is typical for pulses in both the Gierer-Meinhardt equation [6] and its slowly nonlinear counterpart, see chapter 2, sections 2.4 and 2.5. The associated Hopf bifurcation has codimension 1.

Henceforth, we assume $\pm i\,\omega_H$ are the only nontrivial central eigenvalues, i.e. that the central spectrum of $\mathcal{L}$ is given by

$$\sigma_{0,H} = \{\pm i\,\omega_H, 0\}. \tag{4.20}$$

Moreover, based our insight in the general pulse destabilisation mechanisms from chapter 3, we assume that the Hopf bifurcation under consideration is of codimension 1, such that the Hopf eigenvalues are simple.

To carry out a centre manifold analysis for this central spectrum, one would naively aim for an expansion in the three associated eigenvectors. However, the translational symmetry (4.16) of (4.1)/(4.2), being the source of the trivial central eigenvalue $\lambda = 0$, induces a transversal structure for the centre manifold, enabling one to effectively ignore the translational eigenmode in the local centre manifold expansion (see upcoming Theorem 4.8). To set the stage, we first focus on the ambient function space where the centre manifold will be embedded in.

4.3.1 Choosing a function space

In order to properly set up the centre manifold theory for the pulse Γ_h at the Hopf bifurcation (4.19), we need choose an appropriate function space to work in. Since both components of the eigenfunction ϕ_H are eventually exponentially decreasing (see

Theorem 4.3), bounded and thus certainly (square) integrable, the space $(L_2(\mathbb{R}, \mathbb{C}))^2$ seems a natural choice. The scale separation between the two eigenfunction components forces us to make a choice for the integration variable, be it ξ or $x = \varepsilon\xi$. However, this choice cannot be made in a uniform way, as can be seen if we try to establish the norm of ϕ_H by integrating the sum of squares of its components. If we would choose ξ, the integral over the square of the first component $(\phi_H)_1$ is

$$\int_{\mathbb{R}} [(\phi_H)_1(\xi)]^2 \, \mathrm{d}\xi = 2 \int_{\varepsilon^{-\frac{1}{4}}}^{\infty} [(\phi_H)_1(\varepsilon\xi)]^2 \, \mathrm{d}\xi + \int_{-\varepsilon^{-\frac{1}{4}}}^{\varepsilon^{-\frac{1}{4}}} [(\phi_H)_1(\xi)]^2 \, \mathrm{d}\xi$$

The second term of the above expression will cause the integral to become unbounded as $\varepsilon \to 0$, since in particular, the value of $(\phi_H)_1$ at the boundaries of the fast interval I_f will not vanish.

On the other hand, if we would choose x as our integration variable, the integral over the square of the second component of ϕ_H is

$$\int_{\mathbb{R}} [(\phi_H)_1(x)]^2 \, \mathrm{d}x = 2 \int_{\varepsilon^{\frac{3}{4}}}^{\infty} [(\phi_H)_2(x)]^2 \, \mathrm{d}x + \int_{-\varepsilon^{\frac{3}{4}}}^{\varepsilon^{\frac{3}{4}}} \left[(\phi_H)_2 \left(\frac{x}{\varepsilon} \right) \right]^2 \varepsilon \mathrm{d}\frac{x}{\varepsilon},$$

which will vanish in the limit $\varepsilon \to 0$. This would eliminate the contribution of the second component of ϕ_H to the inner product. Therefore, one would be unable to use this inner product to succesfully project onto the finite-dimensional subspace spanned by ϕ_H.

To circumvent this problem, we introduce the function space

$$\mathcal{X} = L_2(\mathbb{R}, \mathbb{C}^2; \mu_\varepsilon) \tag{4.21}$$

with the partly scaled Lebesgue measure μ_ε defined such that the associated inner product $\langle \cdot, \cdot \rangle$ can be defined as

$$\langle \phi, \psi \rangle = \int_{\mathbb{R}} \phi^T S \, \overline{\psi} \, \mathrm{d}\xi \quad \text{with} \quad S = \begin{pmatrix} \varepsilon & 0 \\ 0 & 1 \end{pmatrix} \tag{4.22}$$

for $\phi, \psi \in \mathcal{X}$. In other words: the product of the first components is integrated over $x = \varepsilon\xi$, the product of the second components over ξ. Note that the norm induced by the inner product (4.22) is for all $\varepsilon > 0$ equivalent to the 'standard' norm on $(L_2(\mathbb{R}, \mathbb{C}))^2$, making $\mathcal{X}$ and $(L_2(\mathbb{R}, \mathbb{C}))^2$ isometrically isomorphic as metric spaces. A similar norm was introduced in [12].

4.3.2 Foliation of the centre manifold along the translational eigenmode

In this section, we show that the influence of the translational eigenmode can be separated completely from the other eigendirections. We follow the general approach in [24], section 2.3.3 therein. To make full use of the translational symmetry of (4.2), we choose local tubular coordinates to separate the perturbation of the stationary pulse solution Γ_h into a perturbation along resp. perpendicular to the orbits of the translation group $(T_\alpha)_{\alpha \in \mathbb{R}}$, as follows:

$$\begin{pmatrix} U(\xi, t) \\ V(\xi, t) \end{pmatrix} = \Gamma(\xi, t) = T_{\alpha(t)} \left(\Gamma_h(\xi) + \rho(\xi, t) \right), \tag{4.23}$$

where

$$\langle \rho, \frac{\mathrm{d}}{\mathrm{d}\xi} \Gamma_h \rangle = 0. \tag{4.24}$$

In the tubular coordinates (4.23), the left-hand side of (4.2) yields

$$\begin{pmatrix} U_t \\ V_t \end{pmatrix} = \frac{\partial}{\partial t} \Gamma = \frac{\mathrm{d}\alpha}{\mathrm{d}t} T_{\alpha(t)} \left(\frac{\mathrm{d}}{\mathrm{d}\xi} \Gamma_h(\xi) + \frac{\partial}{\partial \xi} \rho(\xi, t) \right) + T_{\alpha(t)} \frac{\partial}{\partial t} \rho(\xi, t); \tag{4.25}$$

multiplication with $T_{-\alpha(t)}$ gives

$$T_{-\alpha(t)} \begin{pmatrix} U_t \\ V_t \end{pmatrix} = \frac{\mathrm{d}\alpha}{\mathrm{d}t} \left(\frac{\mathrm{d}}{\mathrm{d}\xi} \Gamma_h(\xi) + \frac{\partial}{\partial \xi} \rho(\xi, t) \right) + \frac{\partial}{\partial t} \rho(\xi, t). \tag{4.26}$$

Since the right-hand side of (4.2) is equivariant under the translation $T_{\alpha(t)}$, using the tubular coordinates (4.23) and subsequently multiplying with the inverse translation $T_{-\alpha(t)}$ is equivalent to substitution of $\Gamma_h(\xi) + \rho(\xi, t)$:

$$T_{-\alpha(t)} \begin{pmatrix} U_t \\ V_t \end{pmatrix} = \mathrm{RHS}(\Gamma_h(\xi) + \rho(\xi, t)) \tag{4.27}$$

with

$$\mathrm{RHS}(U, V) = \begin{pmatrix} \frac{1}{\varepsilon^2} U_{\xi\xi} & - & (\mu U - \nu_1 F_1(U; \varepsilon)) & + & \frac{\nu_2}{\varepsilon} F_2(U, V; \varepsilon) \\ V_{\xi\xi} & - & V & + & G(U, V; \varepsilon) \end{pmatrix}. \tag{4.28}$$

Based on the orthogonality condition (4.24), we can project both sides of (4.27) onto the subspace spanned by $\frac{\mathrm{d}}{\mathrm{d}\xi} \Gamma_h$ to obtain separate dynamical equations for $\frac{\mathrm{d}\alpha}{\mathrm{d}t}$ and $\frac{\partial}{\partial t} \rho(\xi, t)$. Introducing the projection

$$\Pi_0 = \frac{\langle \cdot, \frac{\mathrm{d}}{\mathrm{d}\xi} \Gamma_h \rangle}{\langle \frac{\mathrm{d}}{\mathrm{d}\xi} \Gamma_h, \frac{\mathrm{d}}{\mathrm{d}\xi} \Gamma_h \rangle} \frac{\mathrm{d}}{\mathrm{d}\xi} \Gamma_h, \tag{4.29}$$

we see that projecting (4.26) onto the subspace spanned by $\frac{d}{d\xi}\Gamma_h$ yields

$$\Pi_0\, T_{-\alpha(t)} \begin{pmatrix} U_t \\ V_t \end{pmatrix} = \frac{d\alpha}{dt}\left(1 + \langle \frac{\partial}{\partial\xi}\rho, \frac{d}{d\xi}\Gamma_h\rangle \frac{d}{d\xi}\Gamma_h\right). \tag{4.30}$$

Combining this with (4.27), we can express $\frac{d\alpha}{dt}$ as

$$\frac{d\alpha}{dt} = \left(1 + \langle \frac{\partial}{\partial\xi}\rho, \frac{d}{d\xi}\Gamma_h\rangle\right)^{-1} \langle \text{RHS}(\Gamma_h(\xi) + \rho(\xi,t)), \frac{d}{d\xi}\Gamma_h\rangle. \tag{4.31}$$

Note that (4.31) does not depend explicitly on $\alpha(t)$: this is a direct consequence of the equivariance of (4.2) under the translation group $(T_\alpha)_{\alpha\in\mathbb{R}}$.

The projection onto the orthogonal complement of the subspace spanned by $\frac{d}{d\xi}\Gamma_h$, given by $\mathbb{I} - \Pi_0$, can be used to obtain a dynamical equation for $\rho(\xi,t)$. Applying $\mathbb{I} - \Pi_0$ on (4.27) and using (4.31) yields

$$\begin{aligned}
\frac{\partial}{\partial t}\rho(\xi,t) &= (\mathbb{I} - \Pi_0)\,\text{RHS}(\Gamma_h(\xi) + \rho(\xi,t)) - \frac{d\alpha}{dt}\,(\mathbb{I} - \Pi_0)\,\frac{\partial}{\partial\xi}\rho \tag{4.32}\\
&= \text{RHS}(\Gamma_h(\xi) + \rho(\xi,t)) - \left(\frac{d}{d\xi}\Gamma_h + \frac{\partial}{\partial\xi}\rho\right) \frac{\langle \text{RHS}(\Gamma_h(\xi) + \rho(\xi,t)), \frac{d}{d\xi}\Gamma_h\rangle}{1 + \langle \frac{\partial}{\partial\xi}\rho, \frac{d}{d\xi}\Gamma_h\rangle}.
\end{aligned}$$

Up to this point, our analysis only used the translational equivariance of (4.2). It will become clear that the results on the (specific form of) the eigenfunctions of $\mathcal{L}$ (4.9) as stated in Theorem 4.3 will enable us to drastically simplify (4.31). The following observation will be important enough in the following to state it as a Lemma:

Lemma 4.5. *Let the conditions of Theorem 4.3 be fulfilled, and let λ be an eigenvalue of $\mathcal{L}$ with eigenfunction $\phi(\xi; \lambda, \varepsilon)$. Then*

$$\langle \phi, \frac{d}{d\xi}\Gamma_h\rangle = 0. \tag{4.33}$$

Proof. Since the stationary pulse solution Γ_h is symmetric, it is even as a function of ξ, see Theorem 4.2. Therefore $\frac{d}{d\xi}\Gamma_h$ is odd as a function of ξ. Now, from the definition of $\mathcal{L}$ (4.9) it is clear that $\mathcal{L}(\xi)$ is invariant under reflection: $\mathcal{L}(-\xi) = \mathcal{L}(\xi)$. This means that, if $\phi(\xi; \lambda, \varepsilon)$ is an eigenfunction of $\mathcal{L}$ with eigenvalue λ, then $\phi(-\xi; \lambda, \varepsilon)$ must also be an eigenfunction of $\mathcal{L}$ for that same eigenvalue; furthermore, $\phi(-\xi; \lambda, \varepsilon)$ is also bounded. Since the eigenfunction $\phi(\xi; \lambda, \varepsilon)$ is determined uniquely (see Theorem 4.3), it follows that $\phi(-\xi; \lambda, \varepsilon) = \phi(\xi; \lambda, \varepsilon)$. From the observation that the product of an even function and an odd function is odd, and that the integral of an odd function vanishes identically, the statement (4.33) follows from the definition of the inner product (4.22). □

From Lemma 4.5, we see that every eigenfunction ϕ as in Theorem 4.3 fulfills the orthogonality condition (4.24). This motivates us to use the local Ansatz

$$\rho(\xi, t) = A(t)\,\phi(\xi; \lambda, \varepsilon), \tag{4.34}$$

with $A(t) \in \mathbb{C}$, keeping in mind that we will specify the eigenfunction ϕ to be the Hopf eigenfunction ϕ_H at a later stage.

Corollary 4.6. *For any perturbation of the form* (4.34), *equation* (4.31) *simplifies to* $\frac{d\alpha}{dt} = 0$.

Proof. Since ϕ is even as a function of ξ (see the proof of Lemma 4.5), ρ is even as a function of ξ. The pulse Γ_h is symmetric (Theorem 4.2), so $\Gamma_h(\xi) + \rho(\xi, t)$ is even as a function of ξ. That means that $\mathrm{RHS}(\Gamma_h(\xi) + \rho(\xi, t))$ (4.28) is even as a function of ξ. Subsequently, the inner product $\langle \mathrm{RHS}(\Gamma_h(\xi) + \rho(\xi, t)), \frac{d}{d\xi}\Gamma_h \rangle$ vanishes identically, since the translational eigenmode $\frac{d}{d\xi}\Gamma_h$ is odd in ξ, see the proof of Lemma 4.5. Hence, the right-hand side of (4.31) vanishes. $\qquad\square$

Since for the Ansatz (4.34) the expression $\mathrm{RHS}(\Gamma_h(\xi) + \rho(\xi, t))$ (4.28) lies in the orthogonal complement of the span of $\frac{d}{d\xi}\Gamma_h$, equation (4.32) drastically simplifies to

$$\frac{\partial}{\partial t}\rho(\xi, t) = \mathrm{RHS}(\Gamma_h(\xi) + \rho(\xi, t)), \tag{4.35}$$

or equivalently

$$\frac{dA}{dt}\,\phi = \mathrm{RHS}(\Gamma_h(\xi) + A\,\phi). \tag{4.36}$$

To state the main result of this subsection, we invoke Theorem 3.19 from chapter 2 in [24], reformulated here:

Theorem 4.7 (**Centre manifolds in presence of continuous symmetry**). *Let* $\mathcal{X} = \Pi_0\mathcal{X} \oplus \mathcal{X}' = \mathrm{span}\left\{\frac{d}{d\xi}\Gamma_h\right\} \oplus \mathcal{X}'$, $\mathcal{L}' = (\mathbb{I} - \Pi_0)\,\mathcal{L}$ *and let* σ_0' *be the central spectrum of* $\mathcal{L}'$. *Assume that* σ_0' *is finite, and let* $\mathcal{E}_0' \subset \mathcal{X}'$ *be the associated spectral subspace. Let* $\mathcal{U}' \subset \mathcal{X}'$ *be a neighbourhood of the origin in* $\mathcal{X}'$. *Consider the tubular neighbourhood*

$$\mathcal{U} = \{T_\alpha(\Gamma_h + \rho); \rho \in \mathcal{U}', \alpha \in \mathbb{R}\} \subset \mathcal{X}$$

of the line of equilibria $\{T_\alpha \Gamma_h, \alpha \in \mathbb{R}\}$.
There exists a map Ψ *which has the same degree of smoothness as the right-hand side of* (4.2), $\Psi : \mathcal{E}_0' \to \mathcal{X}' - \mathcal{E}_0'$, *with* $\Psi(0) = 0$, $D\Psi(0) = 0$ *such that the manifold*

$$\mathcal{M}_0 = \left\{T_\alpha\left(\Gamma_h + \rho + \Psi(\rho)\right); \rho \in \mathcal{E}_0', \alpha \in \mathbb{R}\right\} \subset \mathcal{X}$$

has the following properties:

1. *The manifold $\mathcal{M}_0$ is locally invariant under (4.2), in other words, if $\Gamma(\xi, t) = (U(\xi, t), V(\xi, t))$ is a solution of (4.2) satisfying $\Gamma(\xi, 0) \in \mathcal{M}_0 \cap \mathcal{U}$ and $\Gamma(\xi, t) \in \mathcal{U}$ for all $t \in [0, T]$, then $\Gamma(\xi, t) \in \mathcal{M}_0$ for all $t \in [0, T]$.*

2. *$\mathcal{M}_0$ contains the set of solutions of (4.2) staying in $\mathcal{U}$ for all $t > 0$, in other words, if Γ is a solution of (4.2) satisfying $\Gamma(\xi, t) \in \mathcal{U}$ for all $t > 0$, then $\Gamma(\xi, 0) \in \mathcal{M}_0$.*

The solutions to (4.2) which stay close to the line of equilibria for all $t > 0$ are of the form (4.23), with $\alpha(t)$ satisfying (4.31) and $\rho(\xi, t)$ satisfying (4.32).

Based on the above results (which in particular hold for our codimension 1 central spectrum (4.20)), we can formulate a theorem on the local structure of the centre manifold associated to the Hopf bifurcation (4.19) and the associated central spectrum (4.20).

Theorem 4.8. *Let the central spectrum of $\mathcal{L}$ be given by (4.20). The associated centre manifold $\mathcal{M}_{0,H}$ can be foliated along the line of equilibria $\{T_\alpha \Gamma_h, \ \alpha \in \mathbb{R}\}$, and has a locally trivial product structure:*

$$\mathcal{M}_{0,H} = \mathbb{R} \times \mathcal{M}'_{0,H}.$$

Moreover, the full dynamics on $\mathcal{M}_{0,H}$ can be represented by the reduced dynamics on $\mathcal{M}'_{0,H}$, given by (4.35).

Proof. We adopt the notation of Theorem 4.7. For the central spectrum (4.20), the reduced spectral subspace $\mathcal{E}'_0$ is spanned by the eigenvectors of the Hopf eigenvalues $\pm i\,\omega_H$, i.e. $\mathcal{E}'_0 = \text{span}\left\{\phi_H, \overline{\phi_H}\right\}$. Therefore, any $\rho(\xi, t) \in \mathcal{E}'_0$ can be written as $\rho(\xi, t) = A(t)\,\phi_H(\xi) + \overline{A(t)}\,\overline{\phi_H(\xi)}$. By Corollary 4.6, we see that (4.31) reduces to $\frac{d\alpha}{dt} = 0$, so $\alpha(t) = \alpha_0$. That means that the full dynamics on $\mathcal{M}_{0,H}$ are represented by (4.32), which in turn can be reduced to (4.35). □

Remark 4.9. Although one would expect, based on the central spectrum (4.20), that the translational eigenmode $\frac{d}{d\xi}\Gamma_h$ in general is excitable, Theorem 4.8 shows that this is not the case. In other words, the pulse Γ_h does not move when perturbed under Hopf bifurcation conditions. Theorem 4.8 therefore enables us to 'neglect' the translational eigenmode in the centre manifold expansion. Moreover, this Theorem analytically confirms the numerical results on the 'pinning' of a periodically oscillating pulse in chapter 2, section 2.5.

4.4 Unfolding the Hopf bifurcation

In this section, we use the results of the previous section, to perform a direct centre manifold expansion around the Hopf bifurcation (4.19). Based on Theorem 4.8, we can choose local coordinates such that a perturbation of the pulse Γ_h can be written as

$$\begin{pmatrix} U(\xi,t) \\ V(\xi,t) \end{pmatrix} = \begin{pmatrix} U_h(\xi) \\ V_h(\xi) \end{pmatrix} + A(t)\,\phi_H(\xi) + \overline{A(t)}\,\overline{\phi_H(\xi)} \tag{4.37}$$

with $A(t) \in \mathbb{C}$ acting as a (small) order parameter, and where ϕ_H is the Hopf eigenfunction as in Theorem 4.3, obeying (4.19). It is worthwhile to emphasise that, choosing local coordinates as in (4.37), we indeed not take the 'irrelevant' $\frac{d}{d\xi}\Gamma_h$ direction into account in the upcoming weakly nonlinear analysis. Substitution of (4.37) in (4.2) yields

$$\begin{aligned} \frac{dA}{dt}\phi_H + \frac{\overline{dA}}{dt}\overline{\phi_H} &= \mathcal{L}\left(A\,\phi_H + \overline{A}\,\overline{\phi_H}\right) + \mathcal{R}\left(\Gamma_h|A,\phi_H\right) \\ &= i\,\omega_H\left(A\,\phi_H - \overline{A}\,\overline{\phi_H}\right) + \mathcal{R}\left(\Gamma_h|A,\phi_H\right) \end{aligned} \tag{4.38}$$

where the remainder terms $\mathcal{R}\left(\Gamma_h|A,\phi_H\right)$ are specified as

$$\mathcal{R}\left(\Gamma_h|A,\phi_H\right) = \begin{pmatrix} \nu_1\mathcal{N}F_1\left(U_h|A,\phi_H;\varepsilon\right) + \frac{\nu_2}{\varepsilon}\mathcal{N}F_2\left(U_h,V_h|A,\phi_H;\varepsilon\right) \\ \mathcal{N}G\left(U_h,V_h|A,\phi_H;\varepsilon\right) \end{pmatrix}. \tag{4.39}$$

Here, $\mathcal{N}$ selects the nonlinear part of the function it is acting on, as follows:

$$\begin{aligned} \mathcal{N}F_1\left(U_h|A,\phi_H;\varepsilon\right) =\ & F_1\left(U_h + A\left(\phi_H\right)_1 + \overline{A}\left(\overline{\phi_H}\right)_1;\varepsilon\right) - F_1\left(U_h;\varepsilon\right) \\ & - \frac{dF_1}{dU}\left(U_h;\varepsilon\right)\left(A\left(\phi_H\right)_1 + \overline{A}\left(\overline{\phi_H}\right)_1\right); \tag{4.40a} \\ \mathcal{N}F_2\left(U_h,V_h|A,\phi_H;\varepsilon\right) =\ & F_2\left(U_h + A\left(\phi_H\right)_1 + \overline{A}\left(\overline{\phi_H}\right)_1, V_h + A\left(\phi_H\right)_2 + \overline{A}\left(\overline{\phi_H}\right)_2;\varepsilon\right) \\ & - F_2\left(U_h,V_h;\varepsilon\right) - \frac{\partial F_2}{\partial U}\left(U_h,V_h;\varepsilon\right)\left(A\left(\phi_H\right)_1 + \overline{A}\left(\overline{\phi_H}\right)_1\right) \\ & - \frac{\partial F_2}{\partial V}\left(U_h,V_h;\varepsilon\right)\left(A\left(\phi_H\right)_2 + \overline{A}\left(\overline{\phi_H}\right)_2\right); \tag{4.40b} \\ \mathcal{N}G\left(U_h,V_h|A,\phi_H;\varepsilon\right) =\ & G\left(U_h + A\left(\phi_H\right)_1 + \overline{A}\left(\overline{\phi_H}\right)_1, V_h + A\left(\phi_H\right)_2 + \overline{A}\left(\overline{\phi_H}\right)_2;\varepsilon\right) \\ & - G\left(U_h,V_h;\varepsilon\right) - \frac{\partial G}{\partial U}\left(U_h,V_h;\varepsilon\right)\left(A\left(\phi_H\right)_1 + \overline{A}\left(\overline{\phi_H}\right)_1\right) \\ & - \frac{\partial G}{\partial V}\left(U_h,V_h;\varepsilon\right)\left(A\left(\phi_H\right)_2 + \overline{A}\left(\overline{\phi_H}\right)_2\right). \tag{4.40c} \end{aligned}$$

155

The next step is to introduce a projection onto the linear subspace spanned by the eigenfunction ϕ_H, using the inner product (4.22). This projection, or rather the component along the span of ϕ_H, is given by

$$\Pi_H = \frac{\langle \phi_H, \phi_H \rangle \langle \cdot, \phi_H \rangle - \langle \overline{\phi_H}, \phi_H \rangle \langle \cdot, \overline{\phi_H} \rangle}{\langle \phi_H, \phi_H \rangle^2 - |\langle \phi_H, \overline{\phi_H} \rangle|^2}, \tag{4.41}$$

and is chosen such that $\Pi_H \phi_H = 1$ and $\Pi_H \overline{\phi_H} = 0$. Applying Π_H on (4.38) yields a first order ODE for the order parameter $A(t)$:

$$\frac{\mathrm{d}A}{\mathrm{d}t} = i\,\omega_H A + \Pi_H \mathcal{R}\left(\Gamma_h, A, \phi_H\right). \tag{4.42}$$

To study the nonlinear behaviour of $A(t)$ in detail, we need to expand the nonlinear component of (4.42), $\Pi_H \mathcal{R}\left(\Gamma_h | A, \phi_H\right)$, in the order parameter A. This –quite elaborate– enterprise will be carried out in the following subsection.

4.4.1 Normal form reduction

For ease of notation, we specify the (two component) Hopf eigenfunction ϕ_H as

$$\phi_H = \begin{pmatrix} (\phi_H)_1 \\ (\phi_H)_2 \end{pmatrix} = \begin{pmatrix} u_H \\ v_H \end{pmatrix}. \tag{4.43}$$

By Assumptions 4.1 (A2 - A4), the nonlinear functions $F_{1,2}$ and G are smooth as a function of positive U, V. We can therefore use a regular Taylor expansion in the order parameter A. For the single variable function F_1, this yields

$$\begin{aligned} F_1(U_h + Au_H + \overline{A}\,\overline{u_H}) &= \sum_{j=0}^{N} \frac{\mathrm{d}^j F_1}{\mathrm{d}U^j}(U_h)\left(Au_H + \overline{A}\,\overline{u_H}\right)^j \\ &= \sum_{k+l \geq 0} \frac{1}{k!l!} f_{1,kl} A^k \overline{A}^l \end{aligned} \tag{4.44}$$

with

$$f_{1,kl} = \frac{\mathrm{d}^{k+l} F_1}{\mathrm{d}U^{k+l}}(U_h)\,(u_H)^k\,(\overline{u_H})^l. \tag{4.45}$$

Using this expansion, the nonlinear component $\mathcal{N}F_1\left(U_h | A, \phi_H; \varepsilon\right)$ (4.40a) can now readily be expressed as

$$\mathcal{N}F_1\left(U_h | A, \phi_H; \varepsilon\right) = \sum_{k+l \geq 2} \frac{1}{k!l!} f_{1,kl} A^k \overline{A}^l. \tag{4.46}$$

For the multivariate functions F_2 and G, we would like to obtain a similar expression (here applied to F_2):

$$
\begin{aligned}
F_2(U_h + Au_H + \overline{A}\overline{u_H}, V_h + Av_H + \overline{A}\overline{v_H}) &= \sum_{j=1}^{N} \sum_{k=0}^{j} \frac{\partial^j F_2}{\partial U^k \partial V^{j-k}}(U_h, V_h)(Au_H + \overline{A}\overline{u_H})^k \\
&\qquad \times (Av_H + \overline{A}\overline{v_H})^{j-k} \\
&= \sum_{k+l \geq 0} \frac{1}{k!l!} f_{2,kl} A^k \overline{A}^l.
\end{aligned}
\tag{4.47}
$$

In order to express the expansion coefficients $f_{2,kl}$ in terms of the components of Γ_h and ϕ_H, we introduce the following tensor definition:

Definition 4.10. *Given a two component function $F(U,V)$, consider the total derivative of F of order k, $D^k F$, as a linear mapping from $\left(\mathbb{C}^2\right)^k$ to $\mathbb{C}$. For every pair of nonnegative integers (m,n) for which $m + n = k$, we can define the (m,n)-tensor $(D^{m+n}F) : \left(\mathbb{C}^2\right)^m \times \left(\left(\mathbb{C}^2\right)^n\right)^* \to \mathbb{C}$ as*

$$
(D^{m+n}F)^{j_1 \cdots j_m}_{i_1 \cdots i_n} = \frac{\partial^{m+n} F}{\partial X_{i_1} \cdots \partial X_{i_m} \partial X_{j_1} \partial X_{j_n}}(U_h, V_h),
$$

where $X = (U,V)$ and $i_1 \ldots i_m, j_1 \ldots j_n \in \{1, 2\}$. We have

$$
(D^{m+n}F) : (z_1, \ldots, z_m, w^1, \ldots, w^n) \mapsto (D^{m+n}F)^{j_1 \cdots j_m}_{i_1 \cdots i_n} (z_1)_{i_1} \ldots (z_m)_{i_m} (w^1)_{j_1} \ldots (w^m)_{j_m};
$$

where the repeated indices are summed over.

Using Definition 4.10, we can express the coefficients $f_{2,kl}$ in (4.47) as

$$
f_{2,kl} = \left(D^{k+l}F_2\right)^{j_1 \cdots j_l}_{i_1 \cdots i_k} (\phi_H)_{i_1} \cdots (\phi_H)_{i_k} (\overline{\phi_H})_{j_1} \cdots (\overline{\phi_H})_{j_l}
\tag{4.48}
$$

where $(\phi_H)_1 = u_H$, $(\phi_H)_2 = v_H$, see (4.43). Analogously, we can expand G as

$$
\begin{aligned}
G(U_h + Au_H + \overline{A}\overline{u_H}, V_h + Av_H + \overline{A}\overline{v_H}) &= \sum_{j=1}^{N} \sum_{k=0}^{j} \frac{\partial^j G}{\partial U^k \partial V^{j-k}}(U_h, V_h)(Au_H + \overline{A}\overline{u_H})^k \\
&\qquad \times (Av_H + \overline{A}\overline{v_H})^{j-k} \\
&= \sum_{k+l \geq 0} \frac{1}{k!l!} g_{kl} A^k \overline{A}^l,
\end{aligned}
\tag{4.49}
$$

where

$$
g_{kl} = \left(D^{k+l}G\right)^{j_1 \cdots j_l}_{i_1 \cdots i_k} (\phi_H)_{i_1} \cdots (\phi_H)_{i_k} (\overline{\phi_H})_{j_1} \cdots (\overline{\phi_H})_{j_l}.
\tag{4.50}
$$

Now, the remaining (multivariate) nonlinear components $\mathcal{N}F_2\left(U_h, V_h | A, \phi_H; \varepsilon\right)$ and $\mathcal{N}G\left(U_h, V_h | A, \phi_H; \varepsilon\right)$ ((4.40b) resp. (4.40c)) can be expressed as

$$\mathcal{N}F_2\left(U_h, V_h | A, \phi_H; \varepsilon\right) \quad = \quad \sum_{k+l\geq 2} \frac{1}{k!l!} f_{2,kl} A^k \overline{A}^l \tag{4.51}$$

$$\mathcal{N}G\left(U_h, V_h | A, \phi_H; \varepsilon\right) \quad = \quad \sum_{k+l\geq 2} \frac{1}{k!l!} g_{kl} A^k \overline{A}^l \tag{4.52}$$

with the coefficients $f_{2,kl}$ and g_{kl} specified in (4.48) resp. (4.50). The remainder terms $\mathcal{R}\left(\Gamma_h | A, \phi_H\right)$ (4.39) can now be expanded in A as

$$\mathcal{R}\left(\Gamma_h | A, \phi_H\right) = \sum_{k+l\geq 2} \frac{1}{k!l!} R_{kl} A^k \overline{A}^l, \tag{4.53}$$

with

$$R_{kl} = \begin{pmatrix} \nu_1 f_{1,kl} + \frac{\nu_2}{\varepsilon} f_{2,kl} \\ g_{kl} \end{pmatrix}. \tag{4.54}$$

Finally, we can expand (4.42) as

$$\frac{\mathrm{d}A}{\mathrm{d}t} = i\,\omega_H A + \sum_{k+l\geq 2} \frac{1}{k!l!} \Pi_H R_{kl}\, A^k \overline{A}^l. \tag{4.55}$$

Equation (4.55) can be brought into normal form via a series of locally invertible complex coordinate changes. We follow [36] and use Lemma 3.6 therein, restated here:

Lemma 4.11 (**Poincaré normal form for the Hopf bifurcation**). *The equation*

$$\dot{z} = i\,\omega\,z + \sum_{2\leq k+l\leq 3} g'_{kl} z^k \overline{z}^l + O\left(|z|^4\right),$$

can be transformed into an equation with only the resonant cubic term:

$$\dot{w} = i\,\omega\,w + c_1 w^2 \overline{w} + O\left(|w|^4\right)$$

where

$$c_1 = \frac{i}{2\omega}\left(g'_{20} g'_{11} - 2\left|g'_{11}\right|^2 - \frac{1}{3}\left|g'_{02}\right|^2\right) + \frac{1}{2} g'_{21}. \tag{4.56}$$

Corollary 4.12. *The nonlinear behaviour of z resp. w is determined by the sign of the first Lyapunov, or Landau, coefficient*

$$\ell_1 = \frac{1}{\omega}\mathrm{Re}\, c_1 = \frac{1}{2\omega^2}\mathrm{Re}\left(i\, g'_{20} g'_{11} + \omega\, g'_{21}\right). \tag{4.57}$$

The Hopf bifurcation is supercritical if $\ell_1 < 0$ and subcritical if $\ell_1 > 0$.

Using Lemma 4.11 and Corollary 4.12, we see that the nonlinear behaviour of $A(t)$ determined by (4.55) can be characterised by the sign of the associated (first) Lyapunov coefficient

$$\ell_1 = \frac{1}{2\omega^2} \text{Re}\left(i\left(\Pi_H R_{20}\right)\left(\Pi_H R_{11}\right) + \omega\,\Pi_H R_{21}\right) \tag{4.58}$$

with R_{kl} as in (4.54).

4.4.2   Calculating the first Lyapunov coefficient to leading order

The scale separated structure of the eigenfunctions ϕ_H as given in Theorem 4.3, combined with the inner product adapted to this scale separation (4.22), can be used to obtain leading order expressions for $\Pi_H R_{kl}$, yielding an explicit leading order expression for the first Lyapunov coefficient ℓ_1 (4.58). This is the key to making the preceding general approach work in the context of the localised pulse solution of (4.2), for which we have a leading order expression (see Theorem 4.2). More importantly, having a leading order expression for the (Hopf) eigenfunctions (see Theorem 4.3), we are able to come to concrete conclusions about the nature of the Hopf bifurcation. The way the leading order eigenfunction expressions can be used to obtain explicit results on the coefficients of the centre manifold expansion is demonstrated below.

Recalling the definition of Π_H (4.41), the first step is to obtain leading order expressions for the inner products $\langle \phi_H, \phi_H \rangle$ and $\langle \phi_H, \overline{\phi_H} \rangle$. Using (4.22), we see that

$$\langle \phi, \psi \rangle = \int_{\mathbb{R}} \phi^T S\, \overline{\psi}\, \mathrm{d}\xi = \int_{\mathbb{R}} (\phi)_1 (\overline{\psi})_1\, \mathrm{d}(\varepsilon\xi) + \int_{\mathbb{R}} (\phi)_2 (\overline{\psi})_2\, \mathrm{d}\xi \tag{4.59}$$

so that, see (4.43),

$$\langle \phi_H, \phi_H \rangle = \int_{\mathbb{R}} |u_H|^2\, \mathrm{d}(\varepsilon\xi) + \int_{\mathbb{R}} |v_H|^2\, \mathrm{d}\xi. \tag{4.60}$$

Using the leading order expression for ϕ_H from Theorem 4.3, we can specify the

above as

$$
\begin{aligned}
\int_{\mathbb{R}} |u_H|^2 \, \mathrm{d}(\varepsilon\xi) \;=\; & \int_{-\infty}^{-\varepsilon^{-\frac{1}{4}}} |u_{s,-}(-\varepsilon\xi; i\,\omega_H, \varepsilon)|^2 \mathrm{d}(\varepsilon\xi) + \int_{-\varepsilon^{-\frac{1}{4}}}^{\varepsilon^{-\frac{1}{4}}} |u_{s,-}(0; i\,\omega_H, \varepsilon)|^2 + O(\varepsilon^{\frac{3}{4}}) \, \mathrm{d}(\varepsilon\xi) \\
& + \int_{\varepsilon^{-\frac{1}{4}}}^{\infty} |u_{s,-}(\varepsilon\xi; i\,\omega_H, \varepsilon)|^2 \mathrm{d}(\varepsilon\xi) \\
=\; & \int_{-\infty}^{-\varepsilon^{\frac{3}{4}}} |u_{s,-}(-x; i\,\omega_H, \varepsilon)|^2 \mathrm{d}x + \int_{-\varepsilon^{\frac{3}{4}}}^{\varepsilon^{\frac{3}{4}}} |u_{s,-}(0; i\,\omega_H, \varepsilon)|^2 + O(\varepsilon^{\frac{3}{4}}) \, \mathrm{d}x \\
& + \int_{\varepsilon^{\frac{3}{4}}}^{\infty} |u_{s,-}(x; i\,\omega_H, \varepsilon)|^2 \mathrm{d}x \\
=\; & 2 \int_0^{\infty} |u_{s,-}(x; i\,\omega_H, \varepsilon)|^2 \mathrm{d}x + O(\varepsilon^{\frac{3}{4}}), \quad\quad (4.61)
\end{aligned}
$$

while

$$
\begin{aligned}
\int_{\mathbb{R}} |v_H|^2 \, \mathrm{d}\xi \;=\; & \int_{-\infty}^{-\varepsilon^{-\frac{1}{4}}} \left| C_1 e^{C_1 \xi} \right|^2 \mathrm{d}\xi + \int_{-\varepsilon^{-\frac{1}{4}}}^{\varepsilon^{-\frac{1}{4}}} |u_{s,-}(0; i\,\omega_H, \varepsilon) v_{\mathrm{in}}(\xi; i\,\omega_H, \varepsilon)|^2 + O(\varepsilon^{\frac{3}{4}}) \, \mathrm{d}\xi \\
& + \int_{\varepsilon^{-\frac{1}{4}}}^{\infty} \left| C_1 e^{-C_1 \xi} \right|^2 \mathrm{d}\xi \\
=\; & |u_{s,-}(0; i\,\omega_H, \varepsilon)|^2 \int_{-\infty}^{\infty} |v_{\mathrm{in}}(\xi; i\,\omega_H, \varepsilon)|^2 \, \mathrm{d}\xi + O(\varepsilon^{\frac{1}{2}}), \quad\quad (4.62)
\end{aligned}
$$

so that

$$
\langle \phi_H, \phi_H \rangle = 2 \int_0^{\infty} |u_{s,-}(x; i\,\omega_H, \varepsilon)|^2 \mathrm{d}x + |u_{s,-}(0; i\,\omega_H, \varepsilon)|^2 \int_{-\infty}^{\infty} |v_{\mathrm{in}}(\xi; i\,\omega_H, \varepsilon)|^2 \, \mathrm{d}\xi + O(\varepsilon^{\frac{1}{2}}).
$$
$$(4.63)$$

Similarly,

$$
\langle \phi_H, \overline{\phi_H} \rangle = 2 \int_0^{\infty} u_{s,-}(x; i\,\omega_H, \varepsilon)^2 \mathrm{d}x + u_{s,-}(0; i\,\omega_H, \varepsilon)^2 \int_{-\infty}^{\infty} v_{\mathrm{in}}(\xi; i\,\omega_H, \varepsilon)^2 \, \mathrm{d}\xi + O(\varepsilon^{\frac{1}{2}}).
$$
$$(4.64)$$

The inner product of R_{kl} with ϕ_H resp. $\overline{\phi_H}$ can be made explicit as well. Using (4.54), we see that

$$\langle R_{kl}, \phi_H \rangle = \int_\mathbb{R} \nu_1 f_{1,kl} \, \overline{u_H} \, \mathrm{d}(\varepsilon\xi) + \int_\mathbb{R} \frac{\nu_2}{\varepsilon} f_{2,kl} \, \overline{u_H} \, \mathrm{d}(\varepsilon\xi) + \int_\mathbb{R} g_{kl} \, \overline{v_H} \, \mathrm{d}\xi, \quad (4.65)$$

$$\langle R_{kl}, \overline{\phi_H} \rangle = \int_\mathbb{R} \nu_1 f_{1,kl} \, u_H \, \mathrm{d}(\varepsilon\xi) + \int_\mathbb{R} \frac{\nu_2}{\varepsilon} f_{2,kl} \, u_H \, \mathrm{d}(\varepsilon\xi) + \int_\mathbb{R} g_{kl} \, v_H \, \mathrm{d}\xi. \quad (4.66)$$

Now, using (4.45), Theorem 4.2 and Theorem 4.3,

$$
\begin{aligned}
\int_\mathbb{R} f_{1,kl} \, \overline{u_H} \, \mathrm{d}(\varepsilon\xi) &= \int_\mathbb{R} \frac{\mathrm{d}^{k+l} F_1}{\mathrm{d} U^{k+l}}(U_h)\,(u_H)^k (\overline{u_H})^{l+1} \, \mathrm{d}(\varepsilon\xi) \\
&= 2 \int_0^\infty \frac{\mathrm{d}^{k+l} F_1}{\mathrm{d} U^{k+l}}(u_s^*(x)) \Big(u_{s,-}(x; i\,\omega_H, \varepsilon)\Big)^k \Big(\overline{u_{s,-}(x; i\,\omega_H, \varepsilon)}\Big)^{l+1} \mathrm{d}x \\
&\quad + O(\varepsilon^{\frac{1}{2}}).
\end{aligned}
\tag{4.67}
$$

Similarly,

$$\int_\mathbb{R} f_{1,kl} \, u_H \, \mathrm{d}(\varepsilon\xi) = 2 \int_0^\infty \frac{\mathrm{d}^{k+l} F_1}{\mathrm{d} U^{k+l}}(u_s^*(x)) \Big(u_{s,-}(x; i\,\omega_H, \varepsilon)\Big)^{k+1} \Big(\overline{u_{s,-}(x; i\,\omega_H, \varepsilon)}\Big)^{l} \mathrm{d}x \quad (4.68)$$

up to $O(\varepsilon^{\frac{1}{2}})$.

The expressions for $f_{2,kl}$ (4.48) and g_{kl} (4.50) are substantially more involved than that for $f_{1,kl}$ (4.45). However, based on their initial definition as expansion coefficients (4.47) resp. (4.49), we can determine their behaviour inside and outside the fast region I_f (4.8).

Lemma 4.13. *For $\xi \notin I_f$, both $f_{2,kl}$ and g_{kl} are exponentially small in ξ, i.e. for all $k, l \geq 0$ there are $C_{1,2} > 0$ such that*

$$\max \big\{\big|f_{2,kl}\big|, |g_{kl}|\big\} \leq C_1 \, e^{-C_2 \xi} \quad \text{for all } \xi \notin I_f. \quad (4.69)$$

Proof. Based on Theorem 4.2 and Theorem 4.3, we see that outside I_f, $V_h + A\,v_H + \overline{A}\,\overline{v_H}$ is exponentially small in ξ. By Assumptions 4.1, (A3) resp. (A4), we can infer that both $F_2(U_h + Au_H + \overline{A}\,\overline{u_H}, V_h + Av_H + \overline{A}\,\overline{v_H})$ and $G(U_h + Au_H + \overline{A}\,\overline{u_H}, V_h + Av_H + \overline{A}\,\overline{v_H})$ must be exponentially small as well for $\xi \notin I_f$. By (4.47) and (4.49), it follows that both $f_{2,kl}$ and g_{kl} are exponentially small in ξ. $\qquad \square$

From Lemma 4.13, it follows that an integral of the form $\int_{\mathbb{R}} \frac{1}{\varepsilon} f_{2,kl} \, \overline{u_H} \, \mathrm{d}(\varepsilon\xi) = \int_{\mathbb{R}} f_{2,kl} \, \overline{u_H} \, \mathrm{d}\xi$ converges, even though both U_h and u_H decay asymptotically slowly outside I_f. Therefore, we can conclude that

$$\frac{1}{\varepsilon} \int_{\mathbb{R}} f_{2,kl} \, \overline{u_H} \, \mathrm{d}(\varepsilon\xi) = \int_{\mathbb{R}} f_{2,kl} \, \overline{u_H} \, \mathrm{d}\xi \tag{4.70}$$

$$= \int_{-\infty}^{\infty} \left(D^{k+l} F_{2,f} \right)_{i_1 \cdots i_k}^{j_1 \cdots j_l} (\phi_{H,f})_{i_1} \cdots (\phi_{H,f})_{i_k} (\overline{\phi_{H,f}})_{j_1} \cdots (\overline{\phi_{H,f}})_{j_l} \cdot (\overline{\phi_{H,f}})_1 \, \mathrm{d}\xi$$

up to $O(\varepsilon^{\frac{1}{2}})$, where $\phi_{H,f} = \phi_H|_{\xi \in I_f}$, i.e. (see Theorem 4.3)

$$\phi_{H,f} = \begin{pmatrix} u_{H,f} \\ v_{H,f} \end{pmatrix} = u_{s,-}(0; i\,\omega_H, \varepsilon) \begin{pmatrix} 1 \\ v_{\mathrm{in}}(\xi; i\,\omega_H, \varepsilon) \end{pmatrix} \tag{4.71}$$

and $D^{k+l} F_{2,f}$ is the equal to the tensor defined in 4.10 applied to F_2, evaluated in $(U_h, V_h) = \left(u_*, v_{f,h}(\xi, u_*) \right)$, see Theorem 4.2. For the same reason,

$$\int_{\mathbb{R}} g_{kl} \, \overline{v_H} \, \mathrm{d}\xi = \int_{-\infty}^{\infty} \left(D^{k+l} G_f \right)_{i_1 \cdots i_k}^{j_1 \cdots j_l} (\phi_{H,f})_{i_1} \cdots (\phi_{H,f})_{i_k} (\overline{\phi_{H,f}})_{j_1} \cdots (\overline{\phi_{H,f}})_{j_l} \cdot (\overline{\phi_{H,f}})_2 \, \mathrm{d}\xi, \tag{4.72}$$

where $\phi_{H,f}$ is as in (4.71) and again $D^{k+l} G_f$ is the equal to the tensor defined in 4.10 applied to G, evaluated in $(U_h, V_h) = \left(u_*, v_{f,h}(\xi, u_*) \right)$. For completeness, we state

$$\frac{1}{\varepsilon} \int_{\mathbb{R}} f_{2,kl} \, u_H \, \mathrm{d}(\varepsilon\xi) = \int_{-\infty}^{\infty} \left(D^{k+l} F_{2,f} \right)_{i_1 \cdots i_k}^{j_1 \cdots j_l} (\phi_{H,f})_{i_1} \cdots (\phi_{H,f})_{i_k} \tag{4.73}$$

$$\times (\overline{\phi_{H,f}})_{j_1} \cdots (\overline{\phi_{H,f}})_{j_l} \cdot (\phi_{H,f})_1 \, \mathrm{d}\xi + O(\varepsilon^{\frac{1}{2}}),$$

$$\int_{\mathbb{R}} g_{kl} \, v_H \, \mathrm{d}\xi = \int_{-\infty}^{\infty} \left(D^{k+l} G_f \right)_{i_1 \cdots i_k}^{j_1 \cdots j_l} (\phi_{H,f})_{i_1} \cdots (\phi_{H,f})_{i_k} \tag{4.74}$$

$$\times (\overline{\phi_{H,f}})_{j_1} \cdots (\overline{\phi_{H,f}})_{j_l} \cdot (\phi_{H,f})_2 \, \mathrm{d}\xi + O(\varepsilon^{\frac{1}{2}}).$$

The expressions derived above can be used to calculate the first Lyapunov coefficient ℓ_1 (4.58) explicitly. A systematic approach to obtain all the necessary terms yields

expressions such as

$$\int_{\mathbb{R}} g_{20}\, \overline{v_H}\, \mathrm{d}\xi \;=\; \int_{-\infty}^{\infty} \left(D^{2+0}G_f\right)_{i_1\, i_2} (\phi_{H,f})_{i_1}(\phi_{H,f})_{i_2} \cdot (\overline{\phi_{H,f}})_2 \, \mathrm{d}\xi$$

$$= \int_{-\infty}^{\infty} \left[\frac{\partial^2 G}{\partial U^2}(U,V)\, u_{H,f}^2 + 2\frac{\partial^2 G}{\partial U \partial V}(U,V)\, u_{H,f}\, v_{H,f} \right.$$

$$\left. + \frac{\partial^2 G}{\partial V^2}(U,V) v_{H,f}^2 \right]_{(U,V)=\left(u_*,\, v_{f,h}(\xi, u_*)\right)} \times \quad \overline{v_{H,f}}\, \mathrm{d}\xi \qquad (4.75)$$

and

$$\int_{\mathbb{R}} f_{2,11}\, \overline{u_H}\, \mathrm{d}\xi \;=\; \int_{-\infty}^{\infty} \left(D^{1+1}F_{2,f}\right)_i^j (\phi_{H,f})_i(\overline{\phi_{H,f}})_j \cdot (\overline{\phi_{H,f}})_1 \, \mathrm{d}\xi$$

$$= \int_{-\infty}^{\infty} \left[\frac{\partial^2 F_2}{\partial U^2}(U,V)\, |u_{H,f}|^2 + \frac{\partial^2 F_2}{\partial U \partial V}(U,V)\left(u_{H,f}\, \overline{v_{H,f}} + \overline{u_{H,f}}\, v_{H,f} \right) \right.$$

$$\left. + \frac{\partial^2 F_2}{\partial V^2}(U,V)|v_{H,f}|^2 \right]_{(U,V)=\left(u_*,\, v_{f,h}(\xi, u_*)\right)} \times \quad \overline{u_{H,f}}\, \mathrm{d}\xi. \qquad (4.76)$$

The above concretisations of the formal expressions from the first part of section 4.4 are summarised in the following key Lemma.

Lemma 4.14. *The leading order expression for the first Lyapunov coefficient ℓ_1 associated to the normal form of Hopf bifurcation (4.19), as given in (4.58), is obtained by combining (4.67), (4.70) and (4.72) with (4.65), resp. (4.68), (4.73) and (4.74) with (4.66), and subsequently using the resulting expression combined with (4.63) and (4.64) in the projection $\Pi_H R_{kl}$ (4.41) for the integer pairs $(k,l) = (2,0)$, $(k,l) = (1,1)$ and $(k,l) = (2,1)$.*

Although the expressions thus obtained may not be quite insightful in their full generality, for specific choices of the model functions $F_{1,2}$ and G, the above approach yields explicit quantities which can be evaluated directly for a specific Hopf bifurcation. This will the subject of section 4.6, where the explicit eigenfunction expressions derived in chapter 2, section 2.3 for the slowly nonlinear Gierer-Meinhardt equation will enable us to obtain (parameter dependent) values for the first Lyapunov coefficient.

4.5   An alternative approach

In the 'direct' approach followed in section 4.4, which was based on the normal form transformation referred to in Lemma 4.11, we used the fact that the local coordinates (4.37) could be used to describe the associated centre manifold. The actual 'shape' of the manifold however was never made explicit: the information contained in Ψ (Theorem 4.7) was hidden in the transformation $z \mapsto w(z)$ indicated in Lemma 4.11. In this section, we again derive an expression for c_1 (for its definition, see Lemma 4.11). We follow a less explicit approach compared to that of the previous section: this upcoming, alternative approach is based on [24], section 3.4.2 therein. The relative elegance of the obtained expressions (see upcoming Lemma 4.15) comes with a cost, however: we will need extra information on the adjoint of $\mathcal{L}$. Depending on the specific choice of the model functions $F_{1,2}$ and G (4.1), this alternative approach might be less or more cumbersome to carry out, compared with the previous, direct approach presented in section 4.4.

4.5.1   Expanding the centre manifold

Based on Theorem 4.7 and Theorem 4.8, we restrict ourselves without loss of generality to $\mathcal{X}' = \mathcal{X} - \text{span}\left\{\frac{d}{d\xi}\Gamma_h\right\}$, i.e. we focus on a single leaf of the foliation of the entire centre manifold. Dropping the tildes, we see that solutions on the centre manifold $\mathcal{M}_{0,H}$ can be expressed as

$$\begin{pmatrix} U(\xi, t) \\ V(\xi, t) \end{pmatrix} = \Gamma(\xi, t) = \Gamma_h(\xi) + A(t)\,\phi_H(\xi) + \overline{A(t)}\,\overline{\phi_H(\xi)} + \Psi(A, \overline{A}, \phi_H, \overline{\phi_H}). \quad (4.77)$$

Also, since we analyse a Hopf bifurcation, we know that the dynamics of $A(t)$ should obey the normal form equation

$$\frac{dA}{dt} = i\,\omega_H\,A + c_1\,A\,|A|^2 + O(|A|^4). \quad (4.78)$$

Adapting the notation from section 4.4, we apply (4.2) on a perturbation of the pulse Γ_h. Substitution of $(U, V) = \Gamma_h + \rho$ in (4.2) yields

$$\frac{\partial \rho}{\partial t} = \mathcal{L}\rho + \mathcal{R}(\Gamma_h; \rho) \quad (4.79)$$

with $\mathcal{L}$ as in (4.9), and

$$\mathcal{R}(\Gamma_h;\rho) = \begin{pmatrix} \nu_1\, F_1(U_h + (\rho)_1;\varepsilon) + \frac{\nu_2}{\varepsilon}\, F_2(U_h + (\rho)_1, V_h + (\rho)_2;\varepsilon) \\ G(U_h + (\rho)_1, V_h + (\rho)_2;\varepsilon) \end{pmatrix}$$
$$- \begin{pmatrix} \nu_1\, F_1(U_h;\varepsilon) + \frac{\nu_2}{\varepsilon}\, F_2(U_h, V_h;\varepsilon) \\ G(U_h, V_h;\varepsilon) \end{pmatrix} + \mathcal{A}\rho \qquad (4.80)$$

with $\mathcal{A}$ as in (4.10). Substituting

$$\rho = A\,\phi_H + \overline{A}\,\overline{\phi_H} + \Psi(A, \overline{A}, \phi_H, \overline{\phi_H}) \qquad (4.81)$$

in (4.79), we obtain for its left-hand side

$$\frac{\mathrm{d}A}{\mathrm{d}t}\left(\phi_H + \frac{\partial}{\partial A}\Psi(A, \overline{A}, \phi_H, \overline{\phi_H})\right) + \frac{\mathrm{d}\overline{A}}{\mathrm{d}t}\left(\overline{\phi_H} + \frac{\partial}{\partial \overline{A}}\Psi(A, \overline{A}, \phi_H, \overline{\phi_H})\right) \qquad (4.82)$$

and for its right-hand side

$$i\,\omega_H A\,\phi_H - i\,\omega_H \overline{A}\,\overline{\phi_H} + \mathcal{L}\Psi(A, \overline{A}, \phi_H, \overline{\phi_H})$$
$$+ \mathcal{R}\left(\Gamma_h; A\,\phi_H + \overline{A}\,\overline{\phi_H} + \Psi(A, \overline{A}, \phi_H, \overline{\phi_H})\right). \qquad (4.83)$$

Since (U, V) (4.77) are real, $\Psi(0) = 0$ and $D\Psi(0) = 0$, see Theorem 4.7, we can expand $\Psi(A, \overline{A}, \phi_H, \overline{\phi_H})$ in powers of A and $\overline{A}$ as

$$\Psi(A, \overline{A}, \phi_H, \overline{\phi_H}) = h_{20}A^2 + h_{11}A\overline{A} + \overline{h_{20}A}^2$$
$$+ h_{30}A^3 + h_{21}A^2\overline{A} + \overline{h_{21}A}\,\overline{A}^2 + \overline{h_{30}A}^3 + O(|A|^4). \qquad (4.84)$$

Note that h_{11} is real since $\Psi(A, \overline{A}, \phi_H, \overline{\phi_H})$ is invariant under complex conjugation, see (4.77). Moreover, from (4.80) we see that $\mathcal{R}(\Gamma_h; 0) = 0$ and $D_\rho\mathcal{R}(\Gamma_h; 0) = 0$, so we can expand $\mathcal{R}(\Gamma_h;\rho)$ in powers of ρ in a similar way as Ψ was expanded in powers of A and $\overline{A}$, yielding

$$\mathcal{R}(\Gamma_h;\rho) = \hat{\mathcal{R}}_{(2)}(\rho, \rho) + \hat{\mathcal{R}}_{(3)}(\rho, \rho, \rho) + O(|\rho|^4), \qquad (4.85)$$

where $\hat{\mathcal{R}}_{(2)}(\cdot, \cdot)$ and $\hat{\mathcal{R}}_{(3)}(\cdot, \cdot, \cdot)$ are fully symmetric 2- and 3-tensors.

Using (4.81) and (4.84), we can expand $\mathcal{R}$ in powers of A and $\overline{A}$ as

$$\mathcal{R}\left(\Gamma_h; A\,\phi_H + \overline{A}\,\overline{\phi_H} + \Psi(A,\overline{A},\phi_H,\overline{\phi_H})\right) =$$
$$\hat{\mathcal{R}}_{(2)}(\phi_H,\phi_H)\,A^2 + 2\,\hat{\mathcal{R}}_{(2)}(\phi_H,\overline{\phi_H})\,A\,\overline{A} + \hat{\mathcal{R}}_{(2)}(\overline{\phi_H},\overline{\phi_H})\,\overline{A}^2$$
$$+ \left[2\,\hat{\mathcal{R}}_{(2)}(\phi_H,h_{20}) + \hat{\mathcal{R}}_{(3)}(\phi_H,\phi_H,\phi_H)\right]A^3$$
$$+ \left[2\,\hat{\mathcal{R}}_{(2)}(\phi_H,h_{11}) + 2\,\hat{\mathcal{R}}_{(2)}(\overline{\phi_H},h_{20}) + 3\,\hat{\mathcal{R}}_{(3)}(\phi_H,\phi_H,\overline{\phi_H})\right]A^2\overline{A}$$
$$+ \left[2\,\hat{\mathcal{R}}_{(2)}(\overline{\phi_H},h_{11}) + 2\,\hat{\mathcal{R}}_{(2)}(\phi_H,\overline{h_{20}}) + 3\,\hat{\mathcal{R}}_{(3)}(\phi_H,\overline{\phi_H},\overline{\phi_H})\right]A\,\overline{A}^2$$
$$+ \left[2\,\hat{\mathcal{R}}_{(2)}(\overline{\phi_H},\overline{h_{20}}) + \hat{\mathcal{R}}_{(3)}(\overline{\phi_H},\overline{\phi_H},\overline{\phi_H})\right]\overline{A}^3 + O(|A|^4). \quad (4.86)$$

Using (4.84) and (4.78) in (4.82) yields

$$\left(i\,\omega_H\,A + c_1\,A^2\overline{A}\right)\left(\phi_H + 2h_{20}A + h_{11}\overline{A} + 3h_{30}A^2 + 2h_{21}A\,\overline{A} + \overline{h_{21}}\overline{A}^2\right) + \text{c.c.} + O(|A|^4)$$
$$= i\,\omega_H\,A\,\phi_H + 2i\,\omega_H\,h_{20}A^2 + i\,\omega_H\,h_{11}A\,\overline{A} + 3i\,\omega_H\,h_{30}A^3 + \left[2i\,\omega_H\,h_{21} + c_1\phi_H\right]A^2\overline{A}$$
$$+ i\,\omega_H\,\overline{h_{21}}A\,\overline{A}^2 + \text{c.c.} + O(|A|^4)$$
$$= i\,\omega_H\,A\,\phi_H + 2i\,\omega_H\,h_{20}A^2 + 3i\,\omega_H\,h_{30}A^3 + \left[i\,\omega_H\,h_{21} + c_1\phi_H\right]A^2\overline{A} + \text{c.c.} + O(|A|^4).$$
$$(4.87)$$

Similarly, using (4.84) and (4.86) in (4.83) yields

$$i\,\omega_H\,A\,\phi_H + \mathcal{L}\left(h_{20}A^2 + \frac{1}{2}h_{11}A\,\overline{A} + h_{30}A^3 + h_{21}A^2\overline{A}\right) + \hat{\mathcal{R}}_{(2)}(\phi_H,\phi_H)\,A^2$$
$$+ \hat{\mathcal{R}}_{(2)}(\phi_H,\overline{\phi_H})\,A\,\overline{A} + \left[2\,\hat{\mathcal{R}}_{(2)}(\phi_H,h_{20}) + \hat{\mathcal{R}}_{(3)}(\phi_H,\phi_H,\phi_H)\right]A^3$$
$$+ \left[2\,\hat{\mathcal{R}}_{(2)}(\phi_H,h_{11}) + 2\,\hat{\mathcal{R}}_{(2)}(\overline{\phi_H},h_{20}) + 3\,\hat{\mathcal{R}}_{(3)}(\phi_H,\phi_H,\overline{\phi_H})\right]A^2\overline{A}$$
$$+ \text{c.c} + O(|A|^4)$$
$$= i\,\omega_H\,A\,\phi_H + \left[\mathcal{L}h_{20} + \hat{\mathcal{R}}_{(2)}(\phi_H,\phi_H)\right]A^2 + \left[\frac{1}{2}\mathcal{L}h_{11} + \hat{\mathcal{R}}_{(2)}(\phi_H,\overline{\phi_H})\right]A\,\overline{A}$$
$$+ \left[\mathcal{L}h_{30} + 2\,\hat{\mathcal{R}}_{(2)}(\phi_H,h_{20}) + \hat{\mathcal{R}}_{(3)}(\phi_H,\phi_H,\phi_H)\right]A^3$$
$$+ \left[\mathcal{L}h_{21} + 2\,\hat{\mathcal{R}}_{(2)}(\phi_H,h_{11}) + 2\,\hat{\mathcal{R}}_{(2)}(\overline{\phi_H},h_{20}) + 3\,\hat{\mathcal{R}}_{(3)}(\phi_H,\phi_H,\overline{\phi_H})\right]A^2\overline{A}$$
$$+ \text{c.c} + O(|A|^4). \quad (4.88)$$

Since (4.87) and (4.88) are the expansions of the left-hand side resp. the right-hand side of (4.79) in powers of A and $\overline{A}$, we can compare their expansion coefficients. The

first order terms (for A and $\overline{A}$) coincide; for the second order terms (in A^2, $A\overline{A}$ and $\overline{A}^2$), equating the coefficients yields

$$(\mathcal{L} - 2\,i\,\omega_H)\,h_{20} \;=\; -\hat{\mathcal{R}}_{(2)}(\phi_H, \phi_H), \tag{4.89}$$

$$\mathcal{L}\,h_{11} \;=\; -2\hat{\mathcal{R}}_{(2)}(\phi_H, \overline{\phi_H}). \tag{4.90}$$

The central spectrum of $\mathcal{L}$ on the foliation leaf under consideration is $\{\pm\,i\,\omega_H\}$, so $2\,i\,\omega_H$ nor 0 is an eigenvalue of $\mathcal{L}$. Therefore, the operators $\mathcal{L}$ and $\mathcal{L} - 2\,i\,\omega_H$ are invertible, yielding unique solutions for h_{20} and h_{11}.

To obtain an equation for c_1, the only third order expansion coefficient we need to consider is that of $A^2\overline{A}$. Equating the respective coefficients in (4.87) resp. (4.88) yields

$$(\mathcal{L} - i\,\omega_H)\,h_{21} = c_1\phi_H - 2\,\hat{\mathcal{R}}_{(2)}(\phi_H, h_{11}) - 2\,\hat{\mathcal{R}}_{(2)}(\overline{\phi_H}, h_{20}) - 3\,\hat{\mathcal{R}}_{(3)}(\phi_H, \phi_H, \overline{\phi_H}). \tag{4.91}$$

This allows us to formulate the following Lemma:

Lemma 4.15. *Let ϕ_H^* be the unique bounded solution for which $\mathcal{L}^*\phi_H^* = i\,\omega_H\,\phi_H^*$. Then c_1 (4.78) is given by*

$$c_1 = \frac{1}{\langle\phi_H, \overline{\phi_H^*}\rangle}\langle 2\,\hat{\mathcal{R}}_{(2)}(\phi_H, h_{11}) + 2\,\hat{\mathcal{R}}_{(2)}(\overline{\phi_H}, h_{20}) + 3\,\hat{\mathcal{R}}_{(3)}(\phi_H, \phi_H, \overline{\phi_H}), \overline{\phi_H^*}\rangle. \tag{4.92}$$

Proof. By the Fredholm alternative, (4.91) has a unique solution for h_{21} if and only if the right-hand side is orthogonal to the kernel of the adjoint operator $(\mathcal{L} - i\,\omega_H)^*$. The spectra of $\mathcal{L}$ and $\mathcal{L}^*$ are each others complex conjugates. Since $\mathcal{L}$ is real, its spectrum is invariant under complex conjugation. Therefore, if λ is an eigenvalue of $\mathcal{L}$, then λ is also an eigenvalue of $\mathcal{L}^*$. That means in particular that the central spectrum of $\mathcal{L}^*$ coincides with the central spectrum of $\mathcal{L}$, which is given by the pair $\pm\,i\,\omega_H$. Let the associated adjoint eigenfunctions be denoted as ϕ_H^*, $\overline{\phi_H^*}$. Since the (one-dimensional) kernel of $(\mathcal{L} - i\,\omega_H)^* = (\mathcal{L}^* + i\,\omega_H)$ is spanned by $\overline{\phi_H^*}$, the solvability condition obtained from the Fredholm alternative yields (4.92). $\qquad\square$

While this expression for c_1 is a lot less involved than the expression derived in Lemma 4.11, it cannot be calculated directly using the eigenfunction expressions stated in Theorem 4.3. The expressions for h_{20} (4.89) and h_{11} (4.90) are still implicit; moreover, we have not yet analysed the adjoint operator $\mathcal{L}^*$. Both are the subject of the next section.

4.5.2 The coefficient c_1 (4.92)

First, we study the adjoint operator $\mathcal{L}^*$. Combining the definition of $\mathcal{L}$ (4.9) with that of the scaling matrix S used in the definition of the inner product (4.22), we see that $\mathcal{L}$ can be written as

$$\mathcal{L} = S^{-2}\frac{\mathrm{d}^2}{\mathrm{d}\xi^2} - \mathcal{A}. \tag{4.93}$$

Now,

$$
\begin{aligned}
\langle \phi, \mathcal{L}^*\psi \rangle = \langle \mathcal{L}\phi, \psi \rangle &= \int_{\mathbb{R}} (\mathcal{L}\phi)^T\, S\overline{\psi}\, \mathrm{d}\xi \\
&= \int_{\mathbb{R}} \left(S^{-2}\frac{\mathrm{d}^2}{\mathrm{d}\xi^2}\phi - \mathcal{A}\phi \right)^T S\overline{\psi}\, \mathrm{d}\xi \\
&= \int_{\mathbb{R}} \left(S^{-2}\frac{\mathrm{d}^2}{\mathrm{d}\xi^2}\phi \right)^T S\overline{\psi} - (\mathcal{A}\phi)^T S\overline{\psi}\, \mathrm{d}\xi \\
&= \int_{\mathbb{R}} \left(\frac{\mathrm{d}^2}{\mathrm{d}\xi^2}\phi \right)^T S^{-2}S\overline{\psi} - \phi^T \mathcal{A}^T S\overline{\psi}\, \mathrm{d}\xi \\
&= \int_{\mathbb{R}} \phi^T S^{-2}S\overline{\frac{\mathrm{d}^2}{\mathrm{d}\xi^2}\psi} - \phi^T S\, S^{-1}\mathcal{A}^T S\overline{\psi}\, \mathrm{d}\xi \\
&= \int_{\mathbb{R}} \phi^T S \left[S^{-2}\overline{\frac{\mathrm{d}^2}{\mathrm{d}\xi^2}\psi} - S^{-1}\mathcal{A}^T S\overline{\psi} \right] \mathrm{d}\xi \\
&= \int_{\mathbb{R}} \phi^T S \overline{\left[S^{-2}\frac{\mathrm{d}^2}{\mathrm{d}\xi^2} - S^{-1}\mathcal{A}^T S \right]\psi}\, \mathrm{d}\xi
\end{aligned}
$$

so

$$\mathcal{L}^* = S^{-2}\frac{\mathrm{d}^2}{\mathrm{d}\xi^2} - S^{-1}\mathcal{A}^T S. \tag{4.94}$$

Using (4.10),

$$S^{-1}\mathcal{A}^T S = \left. \begin{pmatrix} \mu - \nu_1\frac{\mathrm{d}F_1}{\mathrm{d}U} - \frac{\nu_2}{\varepsilon}\frac{\partial F_2}{\partial U} & -\frac{1}{\varepsilon}\frac{\partial G}{\partial U} \\ -\nu_2\frac{\partial F_2}{\partial V} & 1 - \frac{\partial G}{\partial V} \end{pmatrix} \right|_{(U,V)=(U_h(\xi),V_h(\xi))}. \tag{4.95}$$

We see that $\mathcal{L}^*$ has the same scale separated structure as $\mathcal{L}$, with only the roles of $\nu_2\frac{\partial F_2}{\partial V}$ and $\frac{\partial G}{\partial U}$ reversed. Therefore, we can treat $\mathcal{L}^*$ in a similar way as $\mathcal{L}$, see subsection 4.2.2. Since the diagonal entries of $\mathcal{A}$ are the same as those of $S^{-1}\mathcal{A}^T S$, the leading order slow and fast linear operators associated to $\mathcal{L}^*$ coincide with those of

$\mathcal{L}$, i.e. $(\mathcal{L}^*)_s(x) = \mathcal{L}_s(x)$ and $(\mathcal{L}^*)_f(\xi) = \mathcal{L}_f(\xi)$, as given in (4.13) resp. (4.12). The leading order fast nonhomogeneous Sturm-Liouville problem for $\mathcal{L}^*$ is

$$\left(\mathcal{L}_f^* - \lambda\right)v = -\nu_2 \frac{\partial F_2}{\partial V}(u_*, v_{f,h}(\xi; u_*)), \quad \xi \in \mathbb{R}. \tag{4.96}$$

compare (4.14). Since F_2 and G obey equivalent conditions, see Assumptions 4.1, (A3) and (A4), the theory developed in chapter 3, section 3.3 can be directly applied to $\mathcal{L}^*$, yielding Hopf eigenfunctions ϕ_H^*, $\overline{\phi_H^*}$ with the scale separated structure as described in Theorem 4.3. Note that outside I_f, the leading order behaviour of ϕ_H^* coincides with that of ϕ_H, since $(\mathcal{L}^*)_s(x) = \mathcal{L}_s(x)$.

Solving (4.89) and (4.90) for h_{20} resp. h_{11} is a lot more cumbersome. In general, one would approach the problem as follows. First, consider (4.89). Since the operator $\mathcal{L} - 2i\omega_H$ is invertible, we know there is no nontrivial bounded solution to the homogeneous problem

$$(\mathcal{L} - 2i\omega_H)\phi = 0. \tag{4.97}$$

The two-component linear second order differential equation (4.97) can be rewritten as a four-dimensional first order differential equation

$$\frac{\mathrm{d}}{\mathrm{d}\xi}\hat{\phi} = \mathcal{B}\hat{\phi}, \tag{4.98}$$

the solution space of which is spanned by four linearly independent solutions $\{\hat{\phi}_i\}$, $i = 1, \ldots, 4$. To solve (4.89), which can be written in first order form as

$$\frac{\mathrm{d}}{\mathrm{d}\xi}\hat{h}_{20} - \mathcal{B}\hat{h}_{20} = \begin{pmatrix} 0 \\ -\varepsilon^2 \left(\hat{\mathcal{R}}_{(2)}(\phi_H, \phi_H)\right)_1 \\ 0 \\ -\left(\hat{\mathcal{R}}_{(2)}(\phi_H, \phi_H)\right)_2 \end{pmatrix} \tag{4.99}$$

with

$$\mathcal{B} = \begin{pmatrix} 0 & 1 & 0 & 0 \\ \varepsilon^2 \mathcal{A}_{11} + 2i\omega_H & 0 & \varepsilon^2 \mathcal{A}_{12} & 0 \\ 0 & 0 & 0 & 1 \\ \mathcal{A}_{21} & 0 & \mathcal{A}_{22} + 2i\omega_H & 0 \end{pmatrix}, \tag{4.100}$$

we use the method of variation of constants and write

$$h_{20} = \sum_{i=1}^{4} c_i(\xi)\hat{\phi}_i, \tag{4.101}$$

such that (4.99) is transformed into

$$
\sum_{i=1}^{4} \frac{\mathrm{d}c_i}{\mathrm{d}\xi} \, \hat{\phi}_i = \begin{pmatrix} 0 \\ -\varepsilon^2 \left(\hat{\mathcal{R}}_{(2)}(\phi_H, \phi_H) \right)_1 \\ 0 \\ -\left(\hat{\mathcal{R}}_{(2)}(\phi_H, \phi_H) \right)_2 \end{pmatrix} \tag{4.102}
$$

or equivalently

$$
\hat{\Phi} \, \frac{\mathrm{d}c}{\mathrm{d}\xi} = \begin{pmatrix} 0 \\ -\varepsilon^2 \left(\hat{\mathcal{R}}_{(2)}(\phi_H, \phi_H) \right)_1 \\ 0 \\ -\left(\hat{\mathcal{R}}_{(2)}(\phi_H, \phi_H) \right)_2 \end{pmatrix}, \tag{4.103}
$$

where $c = (c_1, c_2, c_3, c_4)^T$ and $\hat{\Phi}$ is the matrix whose columns are given by the eigenvectors $\hat{\phi}_i$, i.e.

$$
\hat{\Phi} = \left\{ \hat{\phi}_1, \hat{\phi}_2, \hat{\phi}_3, \hat{\phi}_4 \right\}. \tag{4.104}
$$

Since the trace of $\mathcal{B}$ (4.100) vanishes, the determinant of $\hat{\Phi}$ is constant; moreover, since $\mathcal{L} - 2 i \omega_H$ is invertible, we know that $\det \hat{\Phi} \neq 0$. Therefore, (4.103) can be solved by inverting $\hat{\Phi}$, yielding

$$
\frac{\mathrm{d}c}{\mathrm{d}\xi} = \frac{1}{\det \hat{\Phi}} \, \mathrm{adj} \, \hat{\Phi} \begin{pmatrix} 0 \\ -\varepsilon^2 \left(\hat{\mathcal{R}}_{(2)}(\phi_H, \phi_H) \right)_1 \\ 0 \\ -\left(\hat{\mathcal{R}}_{(2)}(\phi_H, \phi_H) \right)_2 \end{pmatrix}, \tag{4.105}
$$

where $\mathrm{adj} \, \hat{\Phi}$ is the adjugate matrix of $\hat{\Phi}$. Since $h_{20} = \hat{\Phi} c$ (4.101), we can integrate (4.105) to obtain for h_{20}:

$$
h_{20}(\xi) = \hat{\Phi}(\xi) \int^{\xi} \frac{1}{\det \hat{\Phi}} \, \mathrm{adj} \, \hat{\Phi}(\xi') \begin{pmatrix} 0 \\ -\varepsilon^2 \left(\hat{\mathcal{R}}_{(2)}(\phi_H(\xi'), \phi_H(\xi')) \right)_1 \\ 0 \\ -\left(\hat{\mathcal{R}}_{(2)}(\phi_H(\xi'), \phi_H(\xi')) \right)_2 \end{pmatrix} \mathrm{d}\xi'. \tag{4.106}
$$

Solving (4.90) for h_{11} can be done analogously. Solving the four-dimensional first order differential equation associated to $\mathcal{L} \hat{h}_{11} = -2\hat{\mathcal{R}}_{(2)}(\phi_H, \overline{\phi_H})$, the same variation of constants approach ultimately yields

$$
\hat{h}_{11}(\xi) = \hat{\Phi}_0(\xi) \int^{\xi} \frac{1}{\det \hat{\Phi}_0} \, \mathrm{adj} \, \hat{\Phi}_0(\xi') \begin{pmatrix} 0 \\ -2\varepsilon^2 \left(\hat{\mathcal{R}}_{(2)}(\phi_H(\xi'), \overline{\phi_H(\xi')}) \right)_1 \\ 0 \\ -2 \left(\hat{\mathcal{R}}_{(2)}(\phi_H(\xi'), \overline{\phi_H(\xi')}) \right)_2 \end{pmatrix} \mathrm{d}\xi', \tag{4.107}
$$

where $\hat{\Phi}_0$ is the matrix whose columns are given by the four independent solutions to $\mathcal{L}\phi_0 = 0$, when written in its four-dimensional first order form – this would be equivalent to (4.98), with associated $\mathcal{B}_0$ as in (4.99), with $\omega_H = 0$. To obtain a result for the operator $\mathcal{L}$ on the reduced space $\mathcal{X}' = \mathcal{X} - \mathrm{span}\left\{\frac{\mathrm{d}}{\mathrm{d}\xi}\Gamma_h\right\}$, we project $\hat{h}_{11}$ onto the orthogonal complement of $\mathrm{span}\left\{\frac{\mathrm{d}}{\mathrm{d}\xi}\Gamma_h\right\}$ (c.f. (4.29)), yielding

$$h_{11} = (\mathbb{I} - \Pi_0)\,\hat{h}_{11}. \tag{4.108}$$

The expressions for h_{20} (4.106) and h_{11} (4.108), together with an encompassing analysis of the adjoint operator $\mathcal{L}$ (4.94), can now be combined with the result of Lemma 4.15 to obtain an explicit expression for c_1 (4.92).

Comparing the approach advocated in this section with the more direct approach of section 4.4, we see that the (relatively) short expressions culminating in Lemma 4.15 come with a cost of having to analyse three additional equations: one eigenvalue problem for the adjoint operator $\mathcal{L}^* \phi_H^* = i\,\omega_H \phi_H^*$ and two inverse problems (4.89) and (4.90). Depending on model under consideration, i.e. for a specific choice of $F_{1,2}$ and G, either approach might be preferable over the other. In the next section, we apply the theory developed above to such a specific model, the slowly nonlinear Gierer-Meinhardt equation.

4.6 Application: the slowly nonlinear Gierer-Meinhardt equation

In chapter 2, the existence and stability of pulse solutions as considered in section 4.2 was established for the slowly nonlinear Gierer-Meinhardt equation (2.7), restated here:

$$\begin{cases} U_t = U_{xx} - \left(\mu U - \nu_1 U^d\right) + \frac{\nu_2}{\varepsilon} V^2 \\ V_t = \varepsilon^2 V_{xx} - V + \frac{V^2}{U} \end{cases}. \tag{4.109}$$

The original Gierer-Meinhardt equation, a canonical model for morphogenesis which is studied extensively in the context of pattern formation [6, 12, 22, 26, 48, 51], can be recovered from (4.109) by setting $\nu_1 = 0$. The system (4.109) is of the form (4.1) with

$$F_1^{\mathrm{nGM}}(U;\varepsilon) = U^d,\ d > 1, \quad F_2^{\mathrm{GM}}(U,V;\varepsilon) = V^2, \quad G^{\mathrm{GM}}(U,V;\varepsilon) = \frac{V^2}{U}. \tag{4.110}$$

The nonlinearities F_2 and G are chosen according to the 'classical' Gierer-Meinhardt model, and are therefore denoted as F_2^{GM} and G^{GM}. The 'slow' nonlinearty F_1 is

absent in the Gierer-Meinhardt model, but was introduced in chapter 2 as U^d, to study the influence of such a slow nonlinearity on the pulse construction and stability. The slowly nonlinear term F_1 is therefore denoted as F_1^{nGM}.

4.6.1 Analytical preliminaries

This section summarises the analysis on the slowly nonlinear Gierer-Meinhardt model (4.109), as derived in chapter 2, sections 2.2 and 2.3.

It can easily be verified that the above choice for $F_{1,2}$ and G (4.110) satisfies Assumptions 4.1 (A1 - A4). The reduced fast system (4.4) is realised as

$$v_{f,\xi\xi} = v - \frac{1}{u_0} v^2, \tag{4.111}$$

which has a homoclinic solution

$$v_{f,h}^{\text{GM}}(\xi; u_0) = \frac{3u_0}{2} \operatorname{sech}^2 \frac{1}{2} \xi, \tag{4.112}$$

satisfying Assumptions 4.1, (A5). Using this homoclinic solution, $D_p(u_0)$ (4.6) can be calculated as

$$D_p^{\text{GM}}(u_0) = \int_\infty^\infty \left(v_{f,h}^{\text{nGM}}(\xi; u_0) \right)^2 \mathrm{d}\xi = 6u_0^2, \tag{4.113}$$

which means that Assumptions 4.1, (A6) is satisfied once the factor 6 is scaled out by rescaling $v_2 \to \hat{v}_2 = 6v_2$. The choice of F_1 realises the reduced slow system (4.5) as

$$u_{xx} = \mu u - v_1 u^d, \tag{4.114}$$

which also has an orbit homoclinic to the origin. Therefore, the slow unstable and stable manifolds of the origin $\mathcal{W}_s^{\text{u/s}}((0,0;\varepsilon)$ coincide and are both described by the same function

$$u_s^{\text{nGM}}(x) = \left(\frac{\mu(d+1)}{2v_1} \operatorname{sech}^2 \frac{1}{2}(d-1) \sqrt{\mu} x \right)^{\frac{1}{d-1}}. \tag{4.115}$$

The pulse existence condition (4.7) becomes

$$\frac{2v_1}{d+1} u^{d-1} = \mu - \frac{3}{2} \hat{v}_2 u^2, \tag{4.116}$$

which always has precisely one positive solution for $u = u_*$, so Theorem 4.2 is valid for $K = 1$. From Theorem 4.2, it follows that there exists a pulse solution $\Gamma_h^{\text{nGM}}(\xi)$,

which is to leading order given by

$$
\Gamma_h^{\mathrm{nGM}}(\xi) = \begin{cases} \begin{pmatrix} u_s^{\mathrm{nGM}}(\varepsilon\xi - x_*) \\ 0 \end{pmatrix} & \text{for} \quad \xi < \varepsilon^{-\frac{1}{4}}, \\[2em] \begin{pmatrix} u_* \\ v_{f,h}^{\mathrm{GM}}(\xi; u_*) \end{pmatrix} & \text{for} \quad \xi \in I_f, \\[2em] \begin{pmatrix} u_s^{\mathrm{nGM}}(\varepsilon\xi + x_*) \\ 0 \end{pmatrix} & \text{for} \quad \xi > \varepsilon^{-\frac{1}{4}}. \end{cases}
\tag{4.117}
$$

The stability analysis of the pulse Γ_h^{nGM} yields the fast linear operator (cf. (4.12))

$$
\mathcal{L}_f^{\mathrm{GM}}(\xi) = \frac{\mathrm{d}^2}{\mathrm{d}\xi^2} - \left[1 - 3\operatorname{sech}^2 \frac{1}{2}\xi \right], \quad \xi \in \mathbb{R},
\tag{4.118}
$$

which has eigenvalues $\lambda_{f,0}^{\mathrm{GM}} = \frac{5}{4}$, $\lambda_{f,1}^{\mathrm{GM}} = 0$ and $\lambda_{f,2}^{\mathrm{GM}} = -\frac{3}{4}$. The slow linear operator (4.13) is realised as

$$
\mathcal{L}_s^{\mathrm{nGM}}(x) = \frac{\mathrm{d}^2}{\mathrm{d}x^2} - \mu \left[1 - \frac{d(d+1)}{2} \operatorname{sech}^2 \frac{1}{2}(d-1)\sqrt{\mu}\, x \right], \quad x \geq 0.
\tag{4.119}
$$

The solutions of its eigenvalue problem $(\mathcal{L}_s^{\mathrm{nGM}} - \lambda)u = 0$ can be determined explicitly using associated Legendre functions, see chapter 2, section 2.3. For the nonhomogeneous fast problem (4.14), realised as

$$
\frac{\mathrm{d}^2}{\mathrm{d}\xi^2} v - \left[1 + \lambda - 3\operatorname{sech}^2 \frac{1}{2}\xi \right] v = \frac{9}{4}\operatorname{sech}^4 \frac{1}{2}\xi,
\tag{4.120}
$$

the unique bounded solution v_{in} can also be explicitly represented using associated Legendre functions. These explicit expressions manifest themselves in the leading order eigenfunction behaviour described in Theorem 4.3.

4.6.2   Hopf bifurcations

As in the general case chapter 3, the eigenvalues for the pulse (4.117) can be determined using Evans function techniques. In chapter 2, an explicit leading order expression for the Evans function was found in terms of the leading order eigenfunction expressions from Theorem 4.3, see Theorem 2.12. This leading order Evans function can be directly numerically evaluated for different parameter values. In Figure
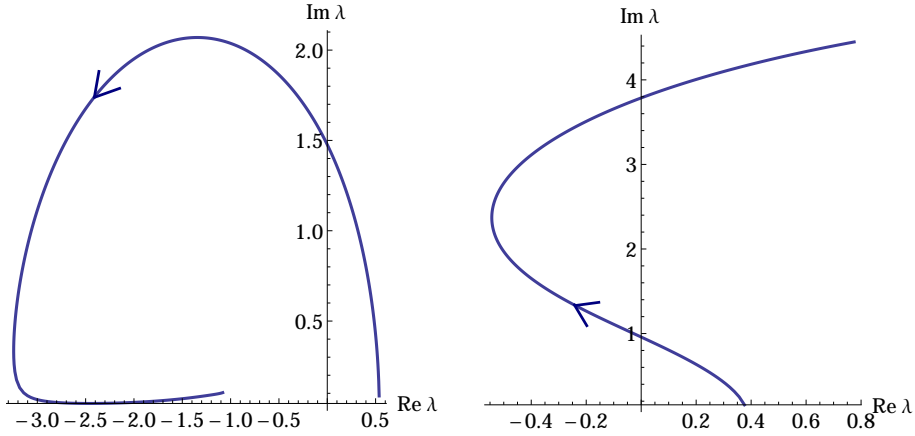
Figure 4.2: The pulse eigenvalues to leading order in ε as a function of increasing μ, indicated by the arrow. Here, $\nu_1 = 2$ and $\nu_2 = \frac{1}{2}$ ($\hat{\nu}_2 = 3$) are fixed. For $d = 2$ (left figure), the pulse undergoes one stabilising Hopf bifurcation for $\mu = \mu_H = 1.47986\ldots$ at $\lambda = i\omega_H = 1.47638\ldots i$. For $d = 5$ (right figure), a second, destabilising Hopf bifurcation takes place for $\mu = \mu_{H,2} = 5.134\ldots$ at $\lambda = i\omega_{H,1} = 3.78646\ldots i$, while the first Hopf bifurcation is at $\mu = \mu_{H,1} = 0.4173\ldots$ with $\lambda = i\omega_{H,1} = 0.958684\ldots i$ for these parameter values.

4.2, the pulse eigenvalues are plotted in the complex plane for fixed $\nu_{1,2}$ and d, while varying μ. Here, the influence of the slow nonlinear term $F_1^{\text{nGM}}(U; \varepsilon) = U^d$ (4.110) can be clearly seen. For $d = 2$, the eigenvalue orbit crosses the imaginary axis for $\mu = \mu_H = 1.47986\ldots$ at $\lambda = i\omega_H = 1.47638\ldots i$, and it becomes clear that the pulse is stable for all $\mu > \mu_H$ (see chapter 2, Theorem 2.18). However, for $d = 5$, the eigenvalue orbit exhibits a different behaviour. After a first stabilising Hopf bifurcation for $\mu = \mu_{H,1} = 0.4173\ldots$ at $\lambda = i\omega_{H,1} = 0.958684\ldots i$, the eigenvalue orbit turns around and undergoes a second, destabilising Hopf bifurcation for $\mu = \mu_{H,2} = 5.134\ldots$ at $\lambda = i\omega_{H,1} = 3.78646\ldots i$.

This turning behaviour is general for $d > 3$, see chapter 2, Theorem 2.19. That means that for all $d > 1$, there is an neighbourhood of $(\nu_1, \nu_2) = (2, \frac{1}{2})$ in parameter space such that there is a (possibly bounded) interval in μ for which the pulse Γ_h^{nGM} is stable. At the boundary of this interval, the pulse destabilises through a Hopf bifurcation. Since our parameter space $\{(\mu, \nu_1, \nu_2, d)\}$ is four-dimensional, we can determine the (boundaries of the) stability region by intersecting it with two-dimensional hy-

perplanes, i.e. by fixing two parameters. In Figure 4.3, the boundary of this stability region is determined for different values of d and ν_1, with μ and ν_2 as free parameters. The two Hopf bifurcation values for $d = 5$, $\nu_1 = 2$, $\nu_2 = \frac{1}{2}$ are indicated on the blue curve in both figures. The Hopf bifurcations merge into a singular Hopf bifurcation where the bifurcation curves fold.

In Figure 4.4, left, the Hopf frequencies for $d = 5$ and $\nu_1 = 2$ are plotted as a function of the parameter ν_2. The merging of Hopf bifurcations can again be observed. For these Hopf eigenvalues, the associated first Lyapunov coefficients ℓ_1 (4.58) were calculated according to Corollary 4.12. It can be seen that the Hopf bifurcations of the lower branch have a positive –even large– first Lyapunov coefficient, and are therefore subcritical (Corollary 4.12). However, for the upper branch of Hopf bifurcations, it is seen that the sign of the first Lyapunov coefficients can change. Note that this upper branch corresponds with the destabilising Hopf bifurcation $\lambda = i\omega_{H,2}$ which is present for all $d > 3$, see Figure 4.2 (right). A collection of such curves of first Lyapunov coefficients is shown in Figure 4.5, based on the associated Hopf curves from Figure 4.3. It is clear that this crossing from sub- to supercriticality is a general phenomenon, and is therefore not restricted to the specific choice of parameters used to produce these Figures.

The direct numerical evaluation of the first Lyapunov coefficient, made possible by the results from Lemma 4.14 and Lemma 4.15, enables us to draw conclusions about the sub- or supercriticality of the Hopf bifurcations of pulses in the slowly nonlinear Gierer-Meinhard model (4.109). Based on the curves shown in Figure 4.5, we can take a well-chosen point in parameter space, e.g. $(\nu_1, \nu_2, d) = (2, \frac{5}{2}, 5)$, such that one of the two Hopf bifurcations for this parameter triplet is subcritical, and the other supercritical. By continuous dependence on parameters, we can then state the following Theorem:

Theorem 4.16. *Let $\varepsilon > 0$ be sufficiently small. There exists an open nonempty neighbourhood $\mathcal{V}$ in (μ, ν_1, ν_2)-parameter space such that the following holds. For any $(\nu_1, \nu_2, d) \in \mathcal{V}$, there are two Hopf bifurcation values $\mu_{H,1}(\nu_1, \nu_2, d)$ and $\mu_{H,2}(\nu_1, \nu_2, d)$ with $\mu_{H,1} < \mu_{H,2}$ for which the associated pulse eigenvalues are given by $\lambda_{H,1} = i\omega_{H,1}$ resp. $\lambda_{H,2} = i\omega_{H,2}$ with $\omega_{H,1}, \omega_{H,2} \in \mathbb{R}$. The Hopf bifurcation $\lambda_{H,1} = i\omega_{H,1}$ is subcritical; the Hopf bifurcation $\lambda_{H,1} = i\omega_{H,1}$ is supercritical.*

With these results in mind, it is quite straightforward to obtain a result which was suggested, but not confirmed, in previous literature on the 'canonical' Gierer-Meinhardt system, i.e. (4.109) with $\nu_1 = 0$. In [6], the existence and stability of
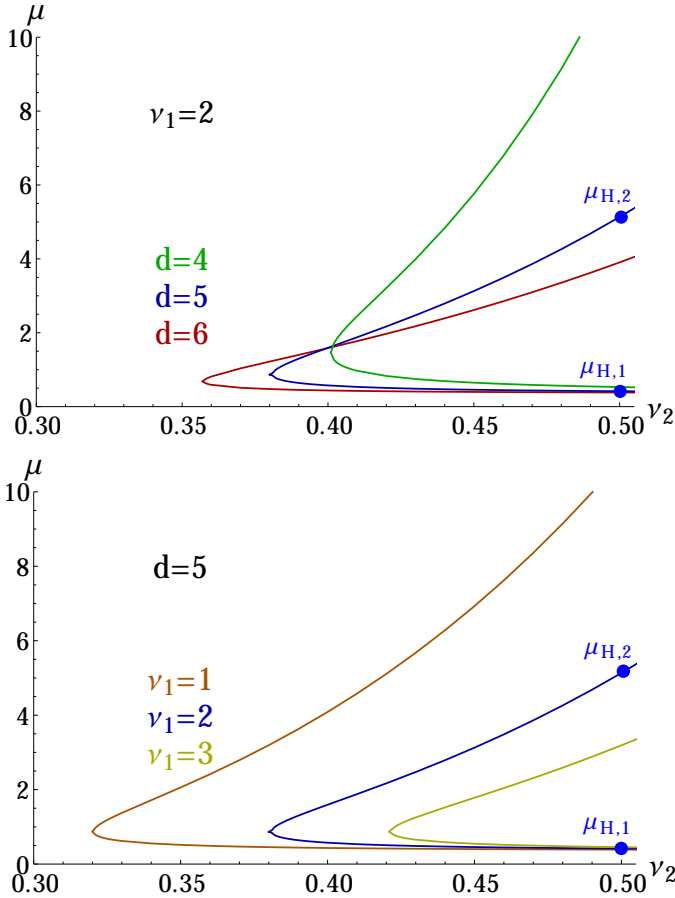
Figure 4.3: Curves of Hopf bifurcation parameter values in the (ν_2, μ)-plane. Left, $\nu_1 = 2$; bifurcation curves are plotted for $d = 4, 5, 6$. Right, $d = 5$; bifurcation curves are plotted for $\nu_1 = 1, 2, 3$. In both figures, the bifurcation values $\mu_{H,1} = 0.4173\ldots$ and $\mu_{H,2} = 5.134\ldots$ for $d = 5, \nu_2 = 2$ are indicated. These curves form the boundary of the region in parameter space for which the pulse Γ_h^{nGM} is stable.

pulse solutions in Gierer-Meinhardt type systems was established using ideas similar to those used in chapters 2 and 3. There, it was shown that for $\mu = \mu_H = 0.36\ldots$, the pulse undergoes a Hopf bifurcation. Numerical simulations [11, 57] suggested that this Hopf bifurcation is subcritical. This observation is confirmed by direct nu-

176

Figure 4.4: In the left figure, the Hopf frequencies are plotted as a function of ν_2, for $d = 5$ and $\nu_1 = 2$. The lower branch, representing $\omega_{H,1}$, is indicated in blue; the upper branch, representing $\omega_{H,2}$, 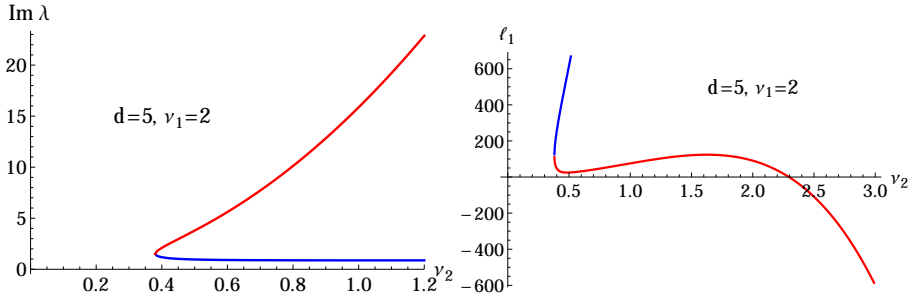is indicated in red. In the right figure, the associated first Lyapunov coefficients ℓ_1 are plotted, using corresponding colors. It can be seen that the first Lyapunov coefficient corresponding to $\omega_{H,2}$ changes sign at $\nu_2 = \nu_2^* = 2.2955\ldots$; there, the nature of this upper branch Hopf bifurcation changes from subcritical to supercritical.

merical evaluation of the associated first Lyapunov coefficient, which has the value $\ell_1 = 2900.91 > 0$. As a consequence, the following Corollary is a direct result from numerical evaluations equivalent to those underlying Theorem 4.16:

Corollary 4.17. *Let $\varepsilon > 0$ be sufficiently small. The Hopf bifurcation associated to the classical Gierer-Meinhardt pulse is subcritical.*

4.7 Discussion

The research presented in this chapter was inspired by the observation of stable oscillating pulses in the slowly nonlinear Gierer-Meinhardt model, see chapter 2, section 2.5. There, it was shown that numerical simulations of the full PDE system suggested the existence of breathing pulses (possibly with a dynamically modulated amplitude) near parameter values for which the stationary pulse undergoes a Hopf bifurcation. The hypothesis that such a Hopf bifurcation could be the 'birthplace' of these breathing pulses is confirmed in the current chapter. A consequence of the supercriticality of the Hopf bifurcation, established in Theorem 4.16, is that stable periodically modulated pulse amplitudes (i.e. breathing pulses) can and do indeed exist.
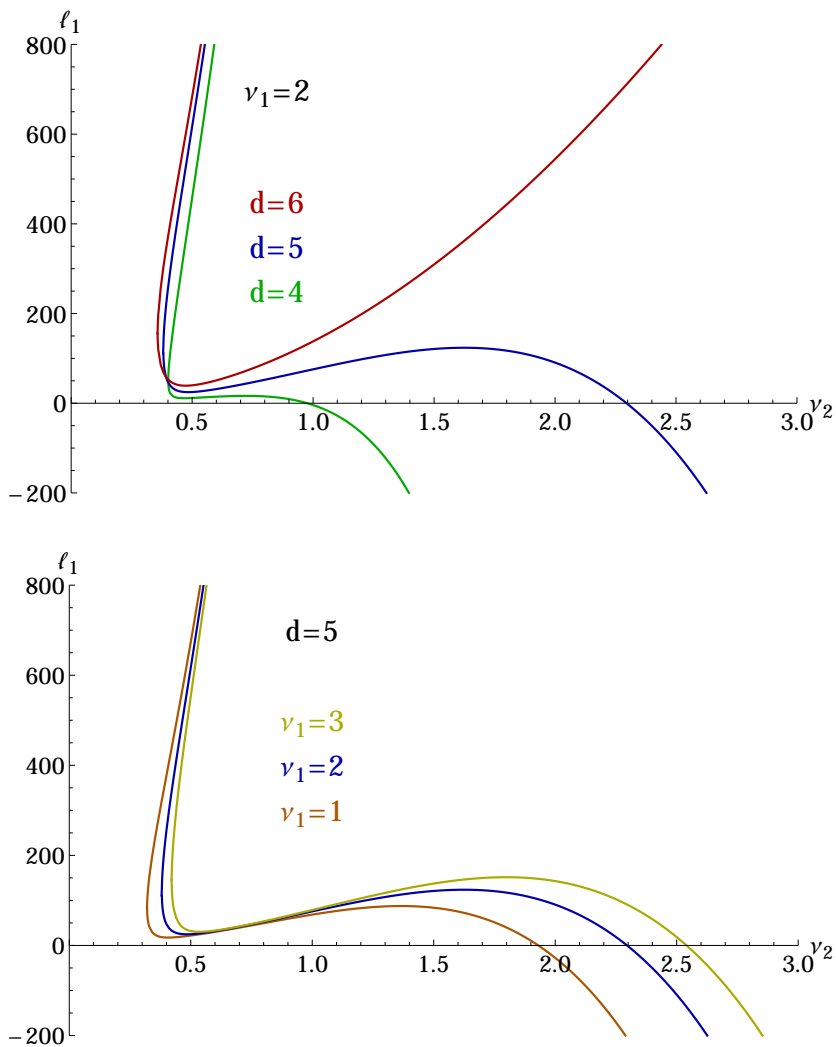
Figure 4.5: An overview of several Lyapunov curves, corresponding to the Hopf bifurcation curves shown in Figure 4.3. The color coding coincides. It can be seen that the transition from sub- to supercriticality is a general phenomenon. However, for $d = 6$, this seems not to occur, at least for values up to $v_2 = 6$ (full range not shown).

However, this is not the end of the story. The centre manifold associated to the Hopf bifurcation has only been expanded up to third order. A fifth order expansion, near the generalised Bautin point where the Hopf bifurcation transgresses from sub- to supercriticality (i.e. where the first Lyapunov coefficient ℓ_1 vanishes), can in principle be done. This would entail performing an analysis analogous to that presented in section 4.4 or 4.5, to the extended fifth order normal form

$$\frac{\mathrm{d}A}{\mathrm{d}t} = i\,\omega_H\,A + c_1\,A\,|A|^2 + c_2\,A\,|A|^4 + \mathcal{O}(|A|^6), \tag{4.121}$$

compare (4.78) / Lemma 4.11. This way, the first steps towards a more encompassing description of the dynamically modulated pulse amplitude near Hopf bifurcations can be taken. Numerical results from chapter 2, section 2.5 suggest that this amplitude can be quasiperiodically or even chaotically modulated.

It is worthwhile to note that the procedure to obtain explicit expressions for the Hopf normal form, as presented in this chapter, is not restricted to the stationary pulse solution, which was analysed in chapters 2 and 3. The procedure is in principle valid for (multi)pulses and fronts in singularly perturbed reaction-diffusion systems: as long as one is able to obtain an explicit expression for the stationary pattern (and, more importantly, for its eigenfunctions), the techniques presented in this chapter can be used to obtain an explicit expression for the normal form expansion coefficients, which can be directly numerically evaluated, allowing one to gain more insight in the dynamical properties of the pattern under consideration.

References

[1] NIST Digital Library of Mathematical Functions: Legendre and Related Functions. `http://dlmf.nist.gov/14`, 2012.

[2] The Wolfram Functions Site: Associated Legendre function of the first kind type 2. `http://functions.wolfram.com/HypergeometricFunctions/ LegendreP2General/`, 2012.

[3] J. Alexander, R.A. Gardner, and C.K.R.T. Jones. A topological invariant arising in the stability analysis of traveling waves. 1990.

[4] W. Chen, D. Iron, J. Rumsey, and M.J. Ward. The stability and dynamics of two-spot patterns for a class of reaction-diffusion systems in $\mathbb{R}^2$. *In preparation*, 2012.

[5] W. Chen and M.J. Ward. Oscillatory instabilities of multi-spike patterns for the one-dimensional Gray-Scott model. *European Journal of Applied Mathematics*, 20(2):187 – 214, 2009.

[6] A. Doelman, R.A. Gardner, and T.J. Kaper. Large Stable Pulse Solutions in Reaction-diffusion Equations. *Indiana University Mathematics Journal*, 50:443 – 507, 2001.

[7] A. Doelman, R.A. Gardner, and T.J. Kaper. *A stability index analysis of 1-D patterns of the Gray-Scott model*, volume 155 of *Memoirs of the Americal Mathematical Society*. American Mathematical Society, 2002.

[8] A. Doelman, G.M. Hek, and N. Valkhoff. Algebraically decaying pulses in a Ginzburg-Landau system with a neutrally stable mode. *Nonlinearity*, 20(2):357 – 389, 2007.

[9] A. Doelman, D. Iron, and Y. Nishiura. Destabilization of fronts in a class of bi-stable systems. *SIAM Journal on Mathematical Analysis*, 35(6):1420–1450, 2004.

[10] A. Doelman and T.J. Kaper. Semi-strong pulse interactions in a class of coupled reaction-diffusion equations. *SIAM Journal on Applied Dynamical Systems*, 2(1):53 – 96, 2003.

[11] A. Doelman, T.J. Kaper, and R.A. Gardner. Stability analysis of singular patterns in the 1D Gray-Scott model: a matched asymptotics approach. *Physica D*, 122:1–36, 1998.

[12] A. Doelman, T.J. Kaper, and K. Promislow. Nonlinear asymptotic stability of the semi-strong pulse dynamics in a regularized Gierer-Meinhardt model. *SIAM Journal on Mathematical Analysis*, 38(6):1760 – 1787, 2007.

[13] A. Doelman, T.J. Kaper, and P.A. Zegeling. Pattern formation in the one-dimensional Gray-Scott model. *Nonlinearity*, 10(2):523 – 563, 1997.

[14] A. Doelman, J. Rademacher, and S. van der Stelt. Hopf dances near the tips of busse balloons. *Discrete and Continuous Dynamical Systems*, 5:61–92, 2012.

[15] A. Doelman and H. van der Ploeg. Homoclinic stripe patterns. *SIAM Journal on Applied Dynamical Systems*, 1(1):65 – 104, 2002.

[16] A. Doelman and F. Veerman. An explicit theory for pulses in two component, singularly perturbed, reaction-diffusion equations. *Journal of Dynamics and Differential Equations*, 2013.

[17] S. Ei. The motion of weakly-interacting pulses in reaction-diffusion systems. *Journal of Dynamics and Differential Equations*, 14:85–137, 2002.

[18] N. Fenichel. Persistence and smoothness of invariant manifolds for flows. *Indiana University Mathematics Journal*, 21:193–226, 1971.

[19] N. Fenichel. Geometrical singular perturbation theory for ordinary differential equations. *Journal of Differential Equations*, 31:53–98, 1979.

[20] R. Fitzhugh. Impulses and physiological states in theoretical models of nerve membrane. *Biophysical Journal*, 1:445–466, 1961.

[21] R.A. Gardner and C.K.R.T. Jones. Stability of travelling wave solutions of diffusive predator-prey systems. *Transactions of the American Mathematical Society*, 327(2):465–524, 1991.

[22] A. Gierer and H. Meinhardt. A theory of biological pattern formation. *Kybernetik*, 12:30–39, 1972.

[23] P. Gray and S.K. Scott. Autocatalytic reactions in the isothermal, continuous stirred tank reactor: isolas and other forms of multistability. *Chemical Engineering Science*, 38:29–43, 1983.

[24] M. Haragus and G. Iooss. *Local Bifurcations, Center Manifolds, and Normal Forms in Infinite-Dimensional Dynamical Systems*. Springer, 2011.

[25] H. Ikeda, Y. Nishiura, and H. Suzuki. Stability of traveling waves and a relation between the Evans function and the SLEP equation. *Journal für die reine und angewandte Mathematik*, 475:1–37, 1996.

[26] D. Iron, M.J. Ward, and J. Wei. The stability of spike solutions to the one-dimensional Gierer-Meinhardt model. *Physica D*, 150:25 – 62, 2001.

[27] D. Iron, J. Wei, and M. Winter. Stability analysis of Turing patterns generated by the Schnakenberg model. *Journal of Mathematical Biology*, 49:358–390, 2004.

[28] C.K.R.T. Jones. Stability of the travelling wave solution of the Fitzhugh-Nagumo system. *Transactions of the Americal Mathematical Society*, 286:431–469, 1984.

[29] C.K.R.T. Jones. Geometric Singular Perturbation Theory. In A. Dold and F. Takens, editors, *Dynamical Systems (Montecatini Terme, Italy, 1994)*, Lecture Notes in Mathematics, vol. 1609, pages 44–118. C.I.M.E., Springer, Berlin, 1995.

[30] T.J. Kaper. An Introduction to Geometric Methods and Dynamical Systems Theory for Singular Perturbation Problems. In J. Cronin and R.E. O'Malley Jr., editors, *Analyzing multiscale phenomena using singular perturbation methods*, Proceedings of Symposia in Applied Mathematics, vol. 56, pages 85–131. American Mathematical Society, 1999.

[31] T. Kolokolnikov, T. Erneux, and J. Wei. Mesa-type patterns in the one-dimensional Brusselator and their stability. *Physica D*, 214:63–77, 2006.

[32] T. Kolokolnikov, M.J. Ward, and J. Wei. The existence and stability of spike equilibria in the one-dimensional Gray-Scott model: the low feed rate regime. *Studies in Applied Mathematics*, 115(1):21 – 71, 2005.

[33] T. Kolokolnikov, M.J. Ward, and J. Wei. The existence and stability of spike equilibria in the one-dimensional Gray-Scott model: the pulse-splitting regime. *Physica D*, 202(3-4):258 – 293, 2005.

[34] T. Kolokolnikov, M.J. Ward, and J. Wei. Pulse-splitting for some reaction-diffusion systems in one-space dimension. *Studies in Applied Mathematics*, 114(2):115 – 165, 2005.

[35] T. Kolokolnikov, M.J. Ward, and J. Wei. Self-replication of mesa patterns in reaction-diffusion models. *Physica D*, 236(2):104–122, 2007.

[36] K. Kuznetsov. *Elements of Applied Bifurcation Theory*. Springer, 3rd edition, 2004.

[37] J.M. Lee, T. Hillen, and M.A. Lewis. Pattern formation in prey-taxis systems. *Journal of Biological Dynamics*, 3(6):551 – 573, 2009.

[38] K.-J. Lin, W.D. McCormick, J.E. Pearson, and H.L. Swinney. Experimental observation of self-replicating spots in a reaction-diffusion system. *Nature*, 369:215 – 218, 1994.

[39] K. Morimoto. Construction of multi-peak solutions to the Gierer-Meinhardt system with saturation and source term. *Nonlinear Analysis*, 71:2532–2557, 2009.

[40] J. Nagumo, S. Arimoto, and S. Yoshizawa. An active pulse transmission line simulating nerve axon. *Proceedings of the IRE*, 50:2061–2070, 1962.

[41] Y. Nishiura and D. Ueyama. A skeleton structure of self-replicating dynamics. *Physica D*, 130:73 – 104, 1999.

[42] Y. Nishiura and D. Ueyama. Spatio-temporal chaos for the Gray-Scott model. *Physica D*, 150:137 – 162, 2001.

[43] J.E. Pearson. Complex patterns in a simple system. *Science*, 261:189–192, 1993.

[44] K. Promislow. A renormalization method for modulational stability of quasi-steady patterns in dispersive systems. *SIAM Journal on Mathematical Analysis*, 33(6):1455–1482, 2002.

[45] B. Sandstede. Stability of travelling waves. In B. Fiedler, editor, *Handbook of Dynamical Systems,*, volume II, pages 983 – 1055. Elsevier, 2002.

[46] J. Schnakenberg. Simple chemical reaction systems with limit cycle behavior. *Journal of Theoretical Biology*, 81:389 – 400, 1979.

[47] W. Sun, M.J. Ward, and R. Russell. The slow dynamics of two-spike solutions for the Gray-Scott and Gierer-Meinhardt systems: competition and oscillatory instabilities. *SIAM Journal on Applied Dynamical Systems*, 4(4):904 – 953, 2005.

[48] I. Takagi. Point-condensation for a reaction-diffusion system. *Journal of Differential Equations*, 61:208 – 249, 1986.

[49] E.C. Titchmarsh. *Eigenfunction Expansions Associated with Second-order Differential Equations*. 1962.

[50] A.M. Turing. The chemical basis of morphogenesis. *Philosophical Transactions of the Royal Society of London*, 237:37–72, 1952.

[51] H. van der Ploeg and A. Doelman. Stability of spatially periodic pulse patterns in a class of singularly perturbed reaction-diffusion equations. *Indiana University Mathematics Journal*, 54(5):1219 – 1301, 2005.

[52] S. van der Stelt, A. Doelman, G.M. Hek, and J. Rademacher. Rise and fall of periodic patterns for a generalized Klausmeier-Gray-Scott model. *Journal of Nonlinear Science*, 23(1):39 – 95, 2013.

[53] P. van Heijster, A. Doelman, T.J. Kaper, and K. Promislow. Front interactions in a three-component system. *SIAM Journal on Applied Dynamical Systems*, 9(2):292–332, 2010.

[54] F. Veerman and A. Doelman. Pulses in a Gierer-Meinhardt equation with a slow nonlinearity. *SIAM Journal on Applied Dynamical Systems*, 12(1):28–60, 2013.

[55] F. Verhulst. *Nonlinear Differential Equations and Dynamical Systems*. Springer, 2nd edition, 1996.

[56] M.J. Ward and J. Wei. The existence and stability of asymmetric spike patterns in the Schnakenberg model. *Studies in Applied Mathematics*, 109:229 – 264, 2002.

[57] M.J. Ward and J. Wei. Hopf bifurcation and oscillatory instabilities of spike solutions for the one-dimensional Gierer-Meinhardt model. *Journal of Nonlinear Science*, 13:209–264, 2003.

[58] J. Wei. Existence, stability and metastability of point condensation patterns generated by the Gray-Scott system. *Nonlinearity*, 12:593 – 616, 1999.

[59] J. Wei and M. Winter. On the Gierer-Meinhardt equation with saturation. *Communications in Contemporary Mathematics*, 6(2):259–277, 2004.

Samenvatting

Deze samenvatting is een Nederlandse versie van het eerste deel van de inleiding, hoofdstuk 1. Net zoals de inleiding is deze samenvatting geschreven voor niet-wetenschappers: het doel van deze samenvatting is een zo groot mogelijk lezers-publiek duidelijk te maken waar dit proefschrift over gaat.
De afbeeldingen waarnaar verwezen wordt zijn te vinden in hoofdstuk 1.

Hoe moet ik dit proefschrift lezen?

Een wiskundeproefschrift is voor niet-wiskundigen moeilijk te lezen, om verschillende redenen. Als eerste, natuurlijk, de formules. Een wiskundige brengt een groot deel van zijn boodschap over door gebruik te maken van symbolen, en de verbanden tussen die symbolen door formules. Als je niet zo veel ervaring hebt met het gebruik van symbolen en formules, is het doorworstelen van teksten die daarmee doordrenkt zijn onbegonnen werk.

Het gebruik van symbolen om wiskunde over te brengen is echter niet alleen handig, het is ook noodzakelijk. Het stelt de onderzoeker in staat om bepaalde (af en toe heel abstracte) ideeën over te brengen met maar een paar symbolen, waardoor zijn redenering goed te volgen blijft – voor medewiskundigen. Als je alle symbolen in dit proefschrift in woorden zou omzetten, zou de tekst binnen de korste keren on-leesbaar worden: de zinnen zouden pagina's lang zijn, het zou onmogelijk worden een duidelijke zinsbouw te gebruiken, en daarmee zou alle hoop vervliegen op het begrijpelijk overbrengen van ideeën op de lezer. De beknoptheid en helderheid van symbolen bewijzen in de wiskunde al eeuwenlang hun nut. Symbolen en formules stellen je in staat nieuwe verbanden te ontdekken, wat het vervolgens weer mogelijk maakt om op abstracter niveau over je onderwerp na te denken, wat leidt tot dieper inzicht – en dat geldt niet alleen voor wiskundigen, maar ook voor alle andere weten-schappers die de 'taal van de wiskunde' gebruiken om hun resultaten samen te vatten.

187

Als je symbolen en formules begint te gebruiken, en gaandeweg ervaren wordt in het lezen ervan, zul je merken dat de symbolen (en de ideeën die ze symboliseren) tastbaarder worden. Je krijgt meer en meer het gevoel waar het symbool eigenlijk voor staat, hoe het zich gedraagt, hoe het reageert op andere symbolen, wat het doet. Vervolgens kun je de symbolen heen en weer gaan schuiven, ze manipuleren, en ondertussen nieuwe symbolen introduceren omdat dat de handigste manier is om weer te geven wat je wil zeggen – en plotseling ben je wiskunde aan het doen.

De tweede reden waarom wiskunde moeilijk te lezen is, is de taal die wordt gebezigd. Als wiskundige is het je doel om objectieve waarheden over te brengen, om een samenhangend en logisch kloppend verhaal te vertellen. Dat betekent onherroepelijk dat de taal ook objectief wordt: in de wiskunde is er voor 'ik' of 'jij' geen plaats, hoogstens voor 'wij'. In een wiskundetekst word je door de auteur stap voor stap meegenomen langs de weg die leidt tot inzicht in een wiskundig onderwerp. Het is een breed gedragen opvatting dat alles wat maar in de buurt van subjectiviteit komt, te allen tijde moet worden vermeden. Wiskundige waarheden hangen immers niet af van degene die ze verkondigt (tenminste, dat zou zo moeten zijn). Bovendien maakt het formuleren van zinnen in subjectieve vorm je ook vatbaarder voor kritiek: *jij* zegt wel dat het zo is, maar dat betekent niet dat *ik* dat zou moeten geloven.

Hoewel deze aanpak vaak noodzakelijk wordt geacht, doet het de leesbaarheid van een wiskundige tekst weinig goeds. Zoals je misschien al hebt gemerkt, heb ik voor deze samenvatting (en voor hoofdstuk 1) gekozen voor een andere stijl. Ik denk dat het noodzakelijk is om, als je wilt dat je ideeën kunnen worden begrepen door een groter publiek, deze ideeën over te brengen in een tekst die toegankelijk is voor de niet-wiskundige, niet-wetenschappelijke lezer – het gevaar 'niet wetenschappelijk genoeg' te zijn, neem ik op de koop toe.

Soms is het onvermijdelijk een objectieve stijl te gebruiken, vanwege het onderwerp dat wordt behandeld. Dit is vooral het geval in het tweede deel van hoofdstuk 1, 'Methoden' (sectie 1.3), waarvan alleen een Engelse versie bestaat. Op het moment dat in hoofdstuk 2 de 'echte' inhoud begint, wordt het pas echt aanpoten: op dat moment verandert de stijl van de directe, subjectieve stijl van het inleidende hoofdstuk 1 naar een objectieve en wat indirecte 'wiskundige' stijl. Dit is dus een noodzakelijke eigenschap van wiskundige teksten op onderzoeksniveau.

Tekst is niet alles. Ik heb als wiskundige gemerkt dat dieper inzicht in een fenomeen door middel van symboolmanipulatie samengaat met de vorming van een bepaald beeld, een bepaalde voorstelling. Omdat de objecten waarmee je werkt vaak abstract zijn, kan deze voorstelling hoogstens ongeveer kloppen.

Ik prijs mezelf in dat opzicht gelukkig dat ik een toegepast wiskundige ben. Ik ben vaker dan in onderzoekers andere, meer fundamentele takken van de wiskunde in de gelegenheid om de objecten die ik onderzoek daadwerkelijk te laten zien zoals ze zijn. Waar in het overmatig gebruik van symbolen het gevaar schuilt dat de analyse onoverzichtelijk wordt, komt het gebruik van afbeeldingen het begrip ten goede. Een van mijn doelen is daarom de lezer een idee geven wat de afbeeldingen in dit proefschrift betekenen. Als je bij het doorbladeren van de wiskunde-hoofdstukken een afbeelding tegenkomt en denkt 'Hee! Ik heb zoiets eerder gezien, zou het met elkaar te maken kunnen hebben?', dan is dat doel bereikt.

Deze samenvatting is hoofdzakelijk geschreven op basis van de gedachte dat, als je een proefschrift in de kast hebt staan, je ten minste in staat moet zijn de titel te begrijpen. Daarvoor moeten eerst een paar concepten worden uitgelegd: dit is het onderwerp van de nu volgende sectie. De woorden waaruit de titel bestaat worden gaandeweg geïntroduceerd. Zoals gezegd is deze samenvatting, die qua inhoud samenvalt met sectie 1.2, speciaal bedoeld voor niet-wiskundigen, zelfs voor niet-wetenschappers. Zoals je kunt zien als je door deze samenvatting bladert, zijn er niet zoveel formules als je in een wiskundeproefschrift zou verwachten, in het bijzonder ten opzichte van de hoofdstukken 2, 3 en 4, waar de 'echte' wiskunde te vinden is. Mocht je na het lezen van de samenvatting de smaak te pakken hebben en benieuwd zijn naar het onderzoek in dit proefschrift, lees dan vooral hoofdstuk 1, in het bijzonder sectie 1.3. Daar ga ik wat verder in op wat het onderzoek dat heeft geleid tot dit proefschrift eigenlijk inhoudt, en wat de resultaten zijn. Ook maak ik duidelijk wat er nieuw is aan deze resultaten, en waarom ze van belang zijn. Tenslotte geef ik in sectie 1.4 een overzicht van de inhoud van dit proefschrift.

Wat betekent de titel?

Patronen

Wat is een patroon? Je zou, in de ruimste zin van het woord, een patroon kunnen kenschetsen als een 'waarneembare regelmaat'. In de natuur struikel je bijna over de patronen. De meest voor de hand liggende patronen zijn vlekken en strepen op dierenvacht, zoals op zebra's, luipaarden, katten en jonge everzwijnen; ingewikkelder patronen komen ook voor, zoals vingerafdrukken, zeeschelpen of slakkenhuizen. Wanneer je op zoek gaat naar patronen, 'daar is iets, dan niets meer, dan weer iets, etc.', vind je ze overal. Neem een boom: zijn takken, de twijgen aan de takken,

bladeren aan de twijgen hebben allemaal min of meer dezelfde onderlinge afstand – zelfs de nerven in de bladeren hebben een vertakkingsstructuur. Op grotere schaal zijn patronen ook alomtegenwoordig, zelfs op dorre plaatsen als de woestijn: denk aan golfpatronen in het zand, of zelfs zandduinen die zelf patronen vormen. Aan de rand van de woestijn groeit de daar aanwezige vegetatie in streep- en vlekpatronen. Zulke patronen kun je ook zien in de lucht, gevormd door wolken; zie Figuur 1.1 voor voorbeelden van patronen in de natuur.

In al deze patronen wordt iets herhaald: ze worden gekarakteriseerd door de herhaling van een bepaald element. De natuur staat bol van zichzelf herhalende processen: de dagelijkse opkomst en ondergang van de zon, de getijden, de fasen van de maan, de seizoenswisselingen. Hoewel je geneigd bent deze fenomenen ook 'patronen' te noemen (en dat zijn ze in een bepaalde zin natuurlijk ook), heeft de regelmaat in deze gevallen betrekking tot iets in de *tijd* en niet zozeer tot iets in de *plaats*. Dit is wat ze onderscheidt van de eerder genoemde patronen: wat wiskundigen een 'patroon' noemen is dan ook een *ruimtelijk* patroon, en daartoe zullen we ons vanaf nu beperken. Dat betekent natuurlijk niet dat verandering (in de tijd) geen rol speelt – integendeel. De 'dynamica van patronen' is een belangrijk onderwerp, waarop in sectie 1.3, hoofdstuk 1 verder wordt ingegaan.

Een patroon kan, zoals al eerder genoemd, worden gekarakteriseerd door de regelmatige terugkeer van een bepaald basiselement, zoals een vlek, een streep, een twijg, een golf, een blad, enzovoort. Dit proefschrift gaat over precies zo'n basiselement, namelijk een '***puls***'. Deze puls kan gezien worden als bouwsteen voor ingewikkelder patronen, zie Figuur 1.2. Het ligt voor de hand om, als eerste stap, de bouwstenen van een patroon te bestuderen. Op het moment dat je dingen te weten bent gekomen over deze bouwsteen kun je vragen over het totale patroon proberen te beantwoorden, door te kijken hoe dit basiselement zichzelf herhaalt. Dit laatste valt echter buiten het bestek van dit proefschrift.

Bij het bestuderen van een patroon zijn er een paar 'natuurlijke' vragen die je zou willen beantwoorden: Wat is het zichzelf herhalende basiselement? En hoe wordt het herhaald? Beide vragen zijn relevant binnen het meer overkoepelende vraagstuk over hoe een patroon wordt gevormd. Het onderzoek dat heeft geleid tot dit proefschrift valt daarom natuurlijkerwijs binnen het wiskundig onderzoeksgebied van 'patroonvorming', en daarbinnen in het onderzoek naar 'gelokaliseerde structuren'. De eerder genoemde puls is een voorbeeld van zo'n gelokaliseerde structuur.
Het basiselement, of de gelokaliseerde structuur, kan afhankelijk van het patroon in

kwestie meer of minder interessant zijn. Bij een vingerafdruk is het spiraalvormige patroon veel belangrijker dan de kanaaltjes die het patroon vormen, in het bijzonder in forensisch onderzoek. In plantgroei zijn de basiselementen (bladeren, twijgen) veel interessanter. Een voorbeeld dat daarmee te maken heeft is de ontwikkeling van ledematen in een embryo, die bestudeerd kan worden in de context van patroonvorming: hier staan de gelokaliseerde structuren (een arm, vingers) centraal. Het proces dat een groeiend organisme zijn vorm laat ontwikkelen, morphogenese, kan daarom in de wiskundige context van patroonvorming bestudeerd worden – en dit is slechts één van de vele toepassingen van patroonvorming als wiskundig onderzoeksgebied.

Dynamische systemen

De wiskundige technieken die in dit proefschrift zijn gebruikt vinden hun oorsprong in het vakgebied van dynamische systemen, in het bijzonder dat van differentiaalvergelijkingen. Het is goed mogelijk om, zonder direct in de wiskunde te duiken, een idee te geven hoe dynamische systemen werken, en welke ideeën in het onderzoek naar patroonvorming gebruikt kunnen worden.

Een dynamisch systeem beschrijft hoe een bepaalde grootheid verandert, waarbij die verandering wordt gestuurd door een aantal voorschriften. Denk bijvoorbeeld aan de positie van de aarde terwijl zij om de zon cirkelt, de concentratie van chemicaliën als je deze samenvoegt en met elkaar laat reageren, of de massa van een groeiende bacteriekolonie. De regels die hier de verandering sturen zijn respectievelijk de wetten van de zwaartekracht, de chemische reacties tussen de chemicaliën en de manier waarop bacteriën voedsel en/of zuurstof gebruiken om te groeien. Dit soort regels kunnen worden gegeven in de vorm van zogenaamde evolutievergelijkingen. Een evolutievergelijking omschrijft hoe een gegeven begintoestand (een beginpositie, een beginconcentratie) evolueert naarmate de tijd verstrijkt. Hoe zoiets er 'in abstracto' uit zou kunnen zien, is te zien in Figuur 1.3.

Zo'n evolutievergelijking is wiskundig gezien een differentiaalvergelijking. Een evolutievergelijking voor een bepaalde grootheid ϕ is daarom een vergelijking voor zijn tijdsafgeleide $\frac{d}{dt}\phi$, ofwel de verandering van ϕ op een bepaald moment in de tijd:

$$\frac{d}{dt}\phi = \text{iets (dat afhangt van } \phi \text{ en/of } t\text{).}$$

Het symbool ϕ staat hier voor wat het ook is dat de evolutievergelijking zou moeten omschrijven, bijvoorbeeld temperatuur, een populatie van een bepaalde diersoort, of de concentratie van een chemische stof.

Het 'iets'-gedeelte is natuurlijk waar al de interessante informatie zit. Op het moment dat je een keuze maakt wat je precies op de 'iets'-plaats invult, kies je ervoor een bepaald gedrag voor te schrijven, en op die manier leg je de evolutie van ϕ vast. Als je iets anders invult, ofwel andere evolutieregels voorschrijft, zal ϕ ook ander dynamisch gedrag gaan vertonen – het is zelfs zo dat kleine veranderingen in dit opzicht grote gevolgen kunnen hebben, zoals we zullen zien in de sectie 'Verstoringen'.

Evolutievergelijkingen worden gebruikt om bepaalde natuurlijke fenomenen waar de tijdsevolutie van bepaalde grootheden een rol speelt te modelleren, bijvoorbeeld om de groei en afname van populaties te omschrijven. Vaak is het nodig om in het model te kunnen beschrijven hoe de grootheid in kwestie is verspreid, in ruimtelijke zin. Als de evolutie van een grootheid ook afhangt van de manier waarop deze is verspreid, dan speelt de ruimtelijke variabele x een belangrijke rol in de evolutievergelijking die zo'n proces beschrijft. De tijdsevolutie van zo'n grootheid ϕ zal van x afhangen, en op zijn ruimtelijke afgeleiden $\frac{d}{dx}\phi$ en $\frac{d^2}{dx^2}\phi$. Zo'n model ziet er daarom als volgt uit:

$$\frac{\partial}{\partial t}\phi = \text{iets dat afhangt van } \phi, \frac{\partial}{\partial x}\phi, \frac{\partial^2}{\partial x^2}\phi, \text{x en/of t.}$$

Het is je misschien opgevallen dat er iets veranderd is aan de manier waarop de afgeleiden worden weergeven: we gebruiken hier '∂' in plaats van 'd'. Deze notatie wordt over het algemeen gebruikt om te benadrukken dat de grootheid ϕ van twee variabelen afhangt, in dit geval van zowel x als van t: je kunt ook zeggen dat ϕ een functie is van x en t. Om het overzichtelijk te houden beperken we ons hier tot één ruimtelijke variabele x: je hebt er meer nodig als het voor het fenomeen in kwestie handig is om te omschrijven hoe de grootheid ϕ zich verspreidt in de lengte, breedte en/of hoogte. De gekozen aanpak is vaak volledig hetzelfde als in het geval van één ruimtelijke variabele.

Reactie-diffusievergelijkingen vormen een belangrijke klasse evolutievergelijkingen waar de ruimtelijke spreiding de evolutie beïnvloedt. In deze reactie-diffusievergelijkingen is er een duidelijk onderscheid tussen de rol van de ruimtelijke afgeleiden van ϕ ($\frac{\partial}{\partial x}\phi$, $\frac{\partial^2}{\partial x^2}\phi$, enz.) en die van de andere termen. Reactie-diffusievergelijkingen zien er (daarom) als volgt uit:

$$\frac{\partial}{\partial t}\phi = \frac{\partial^2}{\partial x^2}\phi + \text{iets dat afhangt van } \phi.$$

Aan de hand van deze structuur kan duidelijk worden gemaakt waar de naam 'reactie-diffusie' vandaan komt. De term 'diffusie' betekent 'het verspreiden door de ruimte':

denk aan een scheutje melk in een kop koffie, waarbij de melk zich (ook zonder te roeren) door de koffie verspreidt. Een ander alledaags voorbeeld is warmtegeleiding: als je een pan op het vuur zet, verspreidt de warmte zich door de pan (en, niet onbelangrijk, door de inhoud van de pan) door middel van diffusie (zie Figuur 1.4). Wiskundig gezien kun je diffusie het meest recht-toe-recht-aan modelleren met de tweede ruimtelijke afgeleide, in dit geval $\frac{\partial^2}{\partial x^2}\phi$. Deze term in de reactie-diffusievergelijking schrijft voor hoe de grootheid ϕ zich verspreidt door de ruimte terwijl zij evolueert in de tijd.

De overige termen, 'iets dat afhangt van ϕ', worden de reactietermen genoemd. De reden voor het gebruik van deze term is het duidelijkst als we niet één, maar twee reactie-diffusievergelijkingen bekijken – met andere woorden, een 'reactie-diffusiesysteem'. Een voorbeeld hiervan is het Gierer-Meinhardtsysteem [22], dat de evolutie van de grootheden U en V beschrijft:

$$\frac{\partial}{\partial t}U = \frac{\partial^2}{\partial x^2}U + V^2 - U$$

$$\frac{\partial}{\partial t}V = \frac{\partial^2}{\partial x^2}V + \frac{V^2}{U} - V$$

Het is duidelijk te zien dat de evolutie van U, beschreven in de bovenste vergelijking, wordt beïnvloed door de waarde van V door de aanwezigheid van de term V^2. Vice versa heeft de onderste vergelijking, waar de evolutie van V wordt beschreven, een term die afhangt van U, namelijk $\frac{V^2}{U}$. Deze wederzijdse afhankelijkheid kun je interpreteren als een reactie tussen U en V, wat de terminologie 'reactietermen' verklaart.

Reactie-diffusievergelijkingen kunnen daarom worden gekarakteriseerd als evolutievergelijkingen die de ruimtelijke spreiding van, en de interactie tussen verschillende grootheden omschrijven.

Patronen in reactie-diffusiesystemen

In fenomenen die beschreven worden door reactie-diffusievergelijkingen komen regelmatig allerlei soorten patronen voor. Dit is geen toeval: het verschijnen van iets dat op een patroon lijkt is voor onderzoekers vaak de aanleiding om te proberen het fenomeen in kwestie te modelleren met reactie-diffusievergelijkingen. Alan Turing –wereldberoemd door onder andere zijn bijdrage aan het ontcijferen van de Enigmacode, zie Figuur 1.5– was de eerste die liet zien hoe en waarom patronen op een natuurlijke manier kunnen ontstaan in systemen van reactie-diffusievergelijkingen. Pa-

tronen die op deze manier ontstaan worden dan ook vaak Turingpatronen genoemd. Het mechanisme dat zorgt voor het ontstaan van een Turingpatroon wordt meestal beschreven aan de hand van een zogenaamd activator-inhibitorpaar. Dit is een paar (chemische) stoffen waarvan de één (de activator) beide laat groeien, terwijl de ander (de inhibitor) de groei van beide stoffen probeert af te remmen. Deze beschrijving van groei en afremming kan door de reactietermen in een reactie-diffusievergelijking worden gemodelleerd. Turing ontdekte dat als de inhibitor zichzelf veel makkelijker door de ruimte verspreidt dan de activator, er een soort terugkoppelingsmechanisme ontstaat. Dit terugkoppelingsmechanisme zorgt ervoor dat de activator en de inhibitor zich niet gelijkmatig verspreiden: hun concentratie fluctueert op een regelmatige manier van plaats tot plaats, en op die manier vormt zich een patroon.

Over het algemeen wordt aangenomen dat dit activator-inhibitormechanisme, dat gemodelleerd kan worden door een reactie-diffusiesysteem, de oorzaak is van een groot aantal patronen die voorkomen in de natuur, zoals vlekken en strepen op dierenvacht of vegetatiepatronen aan de rand van de woestijn. In Figuur 1.6 zie je een aantal voorbeelden van mogelijke patronen in een specifiek reactie-diffusiesysteem (het Gray-Scottmodel).

Wat is een patroon? In de context van reactie-diffusievergelijkingen zou je kunnen zeggen dat een patroon iets is met een duidelijke ruimtelijke structuur, iets wat dus op een specifieke manier van de ruimtelijke variabele x afhangt. Bovendien ligt het voor de hand om te eisen dat een patroon niet of nauwelijks zou moeten veranderen in de tijd. Deze laatste eis is echter nogal beperkend. Er zijn genoeg voorbeelden van dingen die je zeker een 'patroon' zou willen noemen, maar die toch bewegen. Denk bijvoorbeeld aan lopende golven, zoals watergolven, radiogolven, of licht: deze hebben een duidelijke (ruimtelijk) periodieke structuur, maar ze bewegen ook in een bepaalde richting. Je kunt natuurlijk zeggen dat, als je meebeweegt met de golf, dat deze stil lijkt te staan –en dat is precies hoe zulke lopende golven in het algemeen worden beschreven– maar dat verandert niets aan het feit dat deze golven bewegen.

Er zitten een paar belangrijke voordelen aan je beperken tot stationaire, stilstaande patronen: omdat het patroon dat je zoekt niet afhangt van de tijd, kun je je voorstellen dat de analyse in de context van reactie-diffusievergelijkingen een stuk eenvoudiger wordt. Er is geen wederzijdse beïnvloeding tussen de ruimtelijke en tijdelijke variatie van het patroon: het patroon evolueert niet. Je kunt dit ook zien als startpunt van de analyse van patronen die wél veranderen als de tijd verstrijkt. Je kunt vragen gaan stellen als 'Als ik de omstandigheden verander, zal het patroon dat ik gevonden heb ook gaan veranderen? Zal het gaan bewegen? Zal de vorm veranderen?' Op dit soort vragen wordt in sectie 1.3.3 verder ingegaan.

Kort samengevat kan de zoektocht naar een patroon in een reactie-diffusiemodel beginnen met het vinden van een stationaire, tijdsonafhankelijke oplossing van het reactie-diffusiesysteem, met een specifieke ruimtelijke structuur. En dat is precies waar een deel van dit proefschrift over gaat: het vinden van patronen (in het bijzonder, pulsen) in reactie-diffusiesystemen.

Verstoringen

We gaan een experimentje doen. We zijn benieuwd wat er gebeurt met een bal die we laten vallen vanaf een bepaalde hoogte, zeg 2 meter. We kunnen bijvoorbeeld meten hoe lang het duurt voordat de bal de grond raakt. Je kunt je voorstellen dat, als je dit experiment meerdere keren uitvoert, je niet iedere keer hetzelfde antwoord krijgt. Deze variatie in meetresultaten kan meerdere oorzaken hebben: misschien liet je de bal niet iedere keer vanaf precies dezelfde hoogte vallen, misschien was je niet iedere keer even op tijd met je stopwatch. Deze dingen hebben te maken met de feilbaarheid van degene die het experiment uitvoert: natuurlijk heeft jouw eigen onnauwkeurigheid geen invloed op het daadwerkelijke fenomeen van het vallen van de bal. Omdat dit tot nu toe toch een gedachtenexperiment is, nemen we vanaf nu aan dat je in staat bent om de valtijd van de bal precies te meten.

Dan nog zul je niet steeds dezelfde meetresultaten krijgen. Misschien werd de bal een beetje opzij geblazen door de wind, misschien was de grond niet helemaal vlak, misschien is de luchtdruk ondertussen een beetje veranderd, of de luchtvochtigheid, waardoor de luchtweerstand is veranderd; misschien is er een klein stofje aan de bal gaan kleven, waardoor zijn gewicht is veranderd, misschien kruiste de bal op weg naar beneden het pad van een nietsvermoedende vlieg, waardoor de bal iets afremde. Dit zijn oorzaken die je niet kunt controleren, maar die wel invloed kunnen hebben op de meetresultaten. Natuurlijk kun je daar tegenin brengen dat als je hetzelfde experiment vaak herhaalt in een goed beschermde en gecontroleerde omgeving, je de invloed van zulke verstoringen minimaliseert en hun netto effect uit zal middelen. Uiteindelijk zou het, om het fenomeen van de vallende bal te beschrijven, niet uit moeten maken wie het experiment uitvoert, of hoe laat het is, of het regent of niet, of ik het experiment uitvoer in Oslo of in Jakarta – maar wacht eens even. Dat laatste maakt *wel* uit, al is het maar een beetje. Sinds Newton weten we dat de bal valt door de wederzijdse aantrekkingskracht tussen de bal en de aarde. Als je de gravitationele versnelling op verschillende plaatsen op aarde meet (bijvoorbeeld door een bal te laten vallen), zul je zien dat deze gravitationele versnelling g van plaats tot plaats verschilt. Bij benadering is $g = 9.8$ m/s^2; in Oslo geldt dat $g_{\text{Oslo}} = 9.825$ m/s^2, terwijl in Jakarta $g_{\text{Jakarta}} = 9.777$ m/s^2. Alle andere dingen die de vallende bal beïnvloedden

waren willekeurig en hadden niets te maken met de natuurkundige achtergrond van het fenomeen van de vallende bal. Met de plaats op aarde waar het experiment wordt uitgevoerd introduceren we een kleine, maar systematische verandering in de meetgegevens.

Als een onderzoeker een natuurlijk fenomeen bestudeert probeert hij of zij vast te stellen welke processen of wetten werkelijk ten grondslag liggen aan het fenomeen, en welke processen ruis introduceren en zo de metingen alleen maar verstoren. Als je een model voor de vallende bal op zou schrijven in de vorm van een vergelijking, zou je dingen als hoe laat het is of welke kleur je ogen hebben niet in het model stoppen, omdat je weet dat dit soort dingen geen invloed hebben. Je zou ook de aanwezigheid van wind of de luchtvochtigheid niet mee laten wegen, omdat je weet dat die niet te maken hebben met de fundamentele oorzaken van de vallende bal. Hoewel ze de beweging van de bal een beetje kunnen beïnvloeden, is dat niet waarin je uiteindelijk geïnteresseerd bent. Met andere woorden, je wil je model (je vergelijking, je natuurwet) zo eenvoudig, zo zuiver mogelijk hebben. Dat is één van de redenen waarom het zo moeilijk is als wetenschapper een goed model op te schrijven: je hebt een hoop kennis over en ervaring met het te bestuderen fenomeen nodig om te kunnen beoordelen welke processen werkelijk invloed hebben op het fenomeen dat je wilt beschrijven.

In het geval van de vallende bal kunnen we met behulp van de tweede wet van Newton een formule opschrijven, die alleen maar afhangt van de zwaartekracht. Als we de valtijd t noemen en de gravitationele versnelling g, dan krijgen we (voor een valhoogte van 2 meter, waarbij we de eenheden even vergeten):

$$t = \frac{2}{\sqrt{g}}$$

Omdat de waarde van de gravitationele versnelling van plaats tot plaats verandert, verschilt de valtijd ook van plaats tot plaats. Als we alleen maar de valtijd ongeveer zouden willen weten, zouden we altijd de 'benaderde' waarde van g kunnen gebruiken; zelfs al is dit niet de 'echte' waarde van g (en geeft daarom niet de echte waarde van t), het zit er toch niet ver vanaf. Als we de gemiddelde waarde $g_{\text{gemiddeld}} = 9.81$ m/s^2 gebruiken, krijgen we $t_{\text{gemiddeld}} = 0.64$s. Nu kunnen we de daadwerkelijke waarden van de gravitationele acceleratie in Oslo en Jakarta vergelijkigen met de gemiddelde waarde: $g_{\text{Oslo}} = g_{\text{gemiddeld}} + 0.015$ m/s^2 en $g_{\text{Jakarta}} = g_{\text{gemiddeld}} - 0.033$ m/s^2. Op deze manier kunnen we de gravitationele acceleratie waar dan ook op aarde schrijven als $g = g_{\text{gemiddeld}} + \varepsilon$, waar de waarde van ε afhangt van waar je bent. Bovendien is ε behoorlijk klein ten opzichte van $g_{\text{gemiddeld}}$, zoals we hebben gezien. Als we dit nieuwe

gegeven invullen in onze formule voor de valtijd, krijgen we

$$t = \frac{2}{\sqrt{g_{\text{gemiddeld}} + \varepsilon}}$$

Deze formule, die de valtijd van een bal losgelaten op 2 meter hoogte waar dan ook op aarde beschrijft, is een voorbeeld van een model met een **verstoring**. Op deze manier kun je direct een aantal karakteristieke aspecten van het vallende bal-fenomeen aflezen. Als je bijvoorbeeld de kleine variaties in de waarde van g verwaarloost door $\varepsilon = 0$ te kiezen, kun je direct zien hoe je de benaderde, gemiddelde valtijd $t_{\text{gemiddeld}}$ uitrekent, namelijk als

$$t_{\text{gemiddeld}} = \frac{2}{\sqrt{g_{\text{gemiddeld}}}}$$

Bovendien kun je afleiden dat, zolang de verstoring ε klein blijft, de valtijd niet veel van de gemiddelde valtijd zal verschillen, zie Figuur 1.7. Deze laatste eigenschap, dat kleine veranderingen in het model een kleine invloed op de uitkomsten hebben, is de definiërende eigenschap van zogenaamde *reguliere* verstoringen.

Voor ***singuliere verstoringen*** geldt het tegenovergestelde: hier kunnen kleine verstoringen in het model een grote invloed hebben op de groothe den die door het model worden beschreven. Dit klinkt tegenstrijdig, maar er zijn alledaagse voorbeelden waar singuliere verstoringen een belangrijke rol spelen.
Singuliere verstoringen hebben bijna altijd te maken met plotselinge veranderingen, of snelle overgangen. Warmtegeleiding is een goed voorbeeld hiervan: we zijn warmtegeleiding al eerder tegengekomen, als illustratie van de term 'diffusie'.
Als je een pan op het vuur zet, verspreidt de warmte van het fornuis zich heel snel door metaal van de pan: dit metaal is een goed warmtegeleider. Als de pan van porselein zou zijn, zou er iets compleet anders gebeuren: omdat keramische materialen goede hitte-isolatoren zijn, zou de pan erg langzaam opwarmen, omdat de warmte van het fornuis zich nauwelijks door de pan zou verspreiden. Het verschil tussen een metalen en een porseleinen pan in termen van warmtegeleiding is duidelijk zichtbaar als je Figuren 1.8 en 1.9 met elkaar vergelijkt. In het porselein is de verwarmde plek in het midden niet zo uitgespreid als in het metaal. Er is daarom een scherpe overgang zichtbaar tussen de verwarmde plek en zijn omgeving: aan de rand van de plek die wordt verwarmd is er een plotselinge temperatuurdaling. Als we het model dat warmtegeleiding in verschillende materialen beschrijft beter bekijken, wordt duidelijk waarom dit fenomeen alles te maken heeft met singuliere verstoringen.

Warmte verspreidt zich door materialen door middel van diffusie. De manier waarop warmte zich door een materiaal verspreidt kan worden beschreven door een heel eenvoudige evolutievergelijking, beter bekend als de 'warmtevergelijking':

$$\frac{\partial}{\partial t}\phi = \alpha \, \frac{\partial^2}{\partial x^2}\phi$$

In dit geval is ϕ de temperatuur op een bepaalde plaats in het materiaal, op een bepaald moment. De warmtevergelijking is een hele basale reactie-diffusievergelijking, of eigenlijk alleen maar een diffusievergelijking omdat er geen reactietermen in voorkomen (zie de vorige sectie). De letter α is de warmtegeleidingscoëfficiënt: het is een constante die afhangt van het materiaal dat je bekijkt. Een materiaal dat warmte slecht geleidt heeft een heel kleine warmtegeleidingscoëfficiënt.

Laten we, om aan te sluiten bij het vorige voorbeeld, deze kleine warmtegeleidingscoëfficiënt 'ε' noemen, zodat de warmtevergelijking voor een heel goed isolerend materiaal er als volgt uitziet:

$$\frac{\partial}{\partial t}\phi = \varepsilon \, \frac{\partial^2}{\partial x^2}\phi$$

Net zoals in het voorbeeld van de vallende bal kun je je afvragen wat er gebeurt als we de kleine ε-term verwaarlozen, ofwel $\varepsilon = 0$ kiezen. In dit geval leidt dit tot een drastische versimpeling van de warmtevergelijking. We houden de volgende vergelijking over:

$$\frac{\partial}{\partial t}\phi = 0$$

Met andere woorden: de temperatuur verandert niet. Dat betekent dat de overgang van de verwarmde plek naar zijn omgeving echt een abrupte overgang is: de verwarmde plek blijft warm, omdat het omringende isolerende materiaal de warmte op haar plek houdt. Het materiaal in de omgeving warmt niet op, en blijft dus koud. Natuurlijk is dit niet helemaal realistisch: in het echt zal de warmte zich langzaam verspreiden, en de verwarmde plek zal langzaam afkoelen. Toch geeft deze zogenaamde 'singuliere limiet' een behoorlijk goede omschrijving van wat er in het echt zal gebeuren – zolang je er even niet over nadenkt of een perfect isolerend materiaal wel zou kunnen bestaan.

De limiet $\varepsilon = 0$ wordt 'singulier' genoemd omdat het een onderdeel van het model weggooit dat cruciaal is voor de beschrijving van het fenomeen in kwestie, in dit geval warmtediffusie. Deze neiging van singuliere limieten om zich te ontdoen van termen die een belangrijke rol spelen, is iets dat zich regelmatig voordoet in het onderzoek naar singuliere verstoringen. De onderzoeker kan hier vaak zijn of haar voordeel mee doen, omdat het tot gevolg heeft dat het model een stuk eenvoudiger

wordt. Je kunt het zien als een soort compromis: in de singuliere limiet, als je $\varepsilon = 0$ kiest, wordt het opeens mogelijk om bepaalde vergelijkingen op te lossen omdat het aanvankelijk complexe systeem behoorlijk is versimpeld. Aan de andere kant heb je ook een hoop informatie weggegooid: het is vaak onduidelijk hoe je de resultaten die behaald zijn in de singuliere limiet kunt vertalen naar het geval dat ε niet nul is (maar wel heel klein). In het bovenstaande voorbeeld over warmtegeleiding wisten we al hoe de 'volledige' vergelijking zich gedroeg, omdat we het fenomeen dat werd beschreven snapten: op basis daarvan konden we de resultaten van de singuliere limiet interpreteren. In andere toepassingen is dit vaak niet zo eenvoudig.

We hebben gezien dat er, in het geval van zeer trage warmtegeleiding, een scherpe overgang in temperatuur is tussen de verwarmde plek en zijn omgeving. In het echt is deze overgang niet zo plotseling als in de singuliere limiet, maar de overgang is wel heel snel. Om beter te begrijpen wat er in deze overgang gebeurt is het een goed idee om in te zoomen op het gebied waar de overgang plaatsvindt. Als je dat doet, zul je een geleidelijke overgang zien van hoge naar lage temperatuur – maar wel geleidelijk op een erg kleine lengteschaal. Je zou de temperatuurverdeling in een porseleinen pan het best als volgt kunnen beschrijven:

1. Begin ver weg van de verwarmde plek, waar de temperatuur laag is. Als je in de richting van de verwarmde plek begint te 'lopen', verandert er weinig: de temperatuur blijft hetzelfde.

2. Plotseling maakt de temperatuur een grote sprong: je bent nu aan de rand van de verwarmde plek. Als je nauwkeuriger wil zien wat hier gebeurt, zul je even pas op de plaats moeten maken en moeten inzoomen op het overgangsgebied. Je zult zien dat de temperatuur op deze kleine lengteschaal geleidelijk toeneemt.

3. Na de sprong ben je beland in het verwarmde gebied. Hier verandert er weer weinig: overal is min of meer dezelfde (hoge) temperatuur.

Een situatie waarin er een schaalverschil optreedt, en waar het dus het handigste is om sommige gebieden op een andere (kleinere) schaal te bekijken dan andere gebieden, is typisch voor een model met singuliere verstoringen. In zulke situaties is de algemene aanpak dus om het probleem op verschillende schalen te bekijken, en de resultaten van deze afzonderlijke analyses aan elkaar te plakken om zo een totaalbeeld te krijgen. Deze aanpak wordt in sectie 1.3.1 in meer detail toegelicht.

Waar gaat dit proefschrift over?

Inmiddels zijn we genoeg te weten gekomen om de titel van dit proefschrift te begrijpen: 'Pulsen in singulier verstoorde reactie-diffusiesystemen'. Dit proefschrift gaat over de analyse van een bepaald specifiek patroon, namelijk een puls, in de context van een bepaalde klasse modellen, namelijk reactie-diffusiesystemen. Bovendien hebben deze reactie-diffusiesystemen een belangrijke, zeer bruikbare eigenschap: ze zijn singulier verstoord. Wat deze afzonderlijke termen betekenen, is uitgelegd in de voorgaande secties.

Zoals ik al heb gezegd aan het begin van deze samenvatting: mocht je benieuwd zijn naar de onderzoekstechnieken die zijn gebruikt in dit proefschrift, en vraag je je af hoe je de analyse van zo'n puls eigenlijk aanpakt, lees dan verder in hoofdstuk 1. De inhoud van het eerste deel komt overeen met deze samenvatting, maar vanaf sectie 1.3 begint er iets nieuws. Als de overgang van Nederlands naar Engels een probleem is, zal het ongetwijfeld helpen af en toe terug te bladeren naar deze samenvatting.

Dankwoord

Een proefschrift schrijf je grotendeels alleen. Het (overgrote) resterende deel van een promotietraject is gelukkig een stuk minder solistisch. Het was de afgelopen vier jaar een plezier om naar de faculteit te gaan, en dat is te danken aan de aanwezigheid van een aantal collega's en vrienden. Björn, Corine, Eric, Lotte, Martin, Stefanie, Stephanie, en natuurlijk Miek en René, bedankt voor alle momenten tijdens en ver na werktijd, waar zeker niet alleen de gedeelde aspecten van het AIO-schap ter sprake kwamen. Ik ben blij dat ik de afgelopen vier jaar in jullie gezelschap heb kunnen doorbrengen: tijdens koffiepauzes, in de Salon, met etentjes, op conferenties, tijdens pubquizzen.

De vreugde van het promoveren kon ik ook delen met Aron, Jan, Ted en Ties: bedankt voor de gedeelde ervaringen, de tips, en in het bijzonder jullie gezelschap. Ook zou de opmaak van dit proefschrift veel, veel meer moeite hebben gekost zonder jullie voorwerk. Adelheid en natuurlijk Dorien, bedankt voor het lezen van de inleiding: dankzij jullie commentaar heb ik deze nog goed kunnen bijschaven. Dimitris, I'm glad that you were willing to share your gifts and make an outstanding cover design for this thesis. Ook dank ik Nico Temme voor zijn hulp met betrekking tot de eigenschappen van geassocieerde Legendrefuncties, die een grote rol spelen in het tweede hoofdstuk van dit proefschrift.

De belangrijkste rol in een promotietraject is weggelegd voor de begeleiders, en daar heb ik het de afgelopen vier jaar bijzonder mee getroffen.
Vivi, heel erg bedankt voor je grote inzet en je hulp bij vrijwel alle aspecten van het AIO-schap: je was betrokken bij mijn onderwijsverplichtingen, je gaf feedback op mijn presentaties, je bevorderde een actieve rol in de Studiegroep Wiskunde met de Industrie. Je hield in de gaten hoe het ging. Ik kijk met heel veel plezier terug op een goede samenwerking.

Arjen, ik heb de afgelopen vier jaar als bijzonder stimulerend, zinvol en vrucht-baar ervaren. Onze gesprekken waren altijd zowel zeer nuttig als gezellig. Ik heb dankzij jou veel geleerd over wiskunde, het schrijven van artikelen en het doen van onderzoek. Het was erg prettig om een begeleider te hebben die me inhoudelijk – zowel in de details als in de grote lijn– goed kon sturen, terwijl ik toch alle vrijheid hield om dingen op mijn eigen manier aan te pakken. Bedankt voor je inzet voor en achter de schermen, het gebruik van je contacten, je adviezen, je belangstelling. Ik hoop dat we onze samenwerking nog lang zullen voortzetten.

Curriculum vitae

Frits Veerman was born on the 19th of May, 1984 in Huizen, the Netherlands. He completed his pre-university education at the Erfgooiers College, Huizen in 2002 and started his studies at Utrecht University the same year. In 2005, he obtained his Bachelor's degree in Physics and Astronomy and his Bachelor's degree in Mathematics. In 2009, he obtained his Master's degree in Theoretical Physics and his Master's degree in Mathematics at the same university; both were awarded the judicum cum laude. His Master's thesis treated quasiperiodic phenomena in the Van der Pol - Mathieu equation, inspired by and applied to the dynamics of charged dust in plasma.

He started his PhD research at the Mathematical Institute of Leiden University in 2009 under supervision of prof. Arjen Doelman and dr. Vivi Rottschäfer; the results are presented in this thesis. He will continue his research career at the Mathematical Institute of the University of Oxford.